Optimal trajectory management for aircraft descent operations subject to time constraints

RAMON DALMAU CODINA
Aeronautical Engineer

Advisor
DR. XAVIER PRATS I MENÉNDEZ

Doctorate program in Aerospace Science and Technology
Department of Physics – Aeronautics Division
Technical University of Catalonia – BarcelonaTech

A dissertation submitted for the degree of
International Doctor of Philosophy
May 2019

Optimal trajectory management for aircraft descent operations subject to time constraints

Author
Ramon Dalmau Codina

Advisor
Dr. Xavier Prats i Menéndez

Reviewers
Dr. Daniel Delahaye
Dr. Erik-Jan van Kampen

Thesis committee
Dr. Daniel Delahaye
Dr. Erik-Jan van Kampen
Dr. Manuel Soler

Doctorate program in Aerospace Science and Technology
Technical University of Catalonia – BarcelonaTech
May 2019

PhD. Thesis made in:
Department of Physics – Aeronautics Division
Esteve Terradas, 5.
08860 Castelldefels
Catalonia (Spain)

Als meus pares i al meu germà
Olga, Ramon i Ferran

Contents

List of Figures

List of Tables

List of Publications

The list of publications resulting from this PhD. work is given in inverse chronological order as follows:

Journal Papers

- DALMAU, RAMON, BAXLEY, BRIAN & PRATS, XAVIER. Sensitivity-based model predictive control for descent operations subject to time constraints. *Journal of Guidance, Control, and Dynamics*. Submitted to Journal.
- DALMAU, RAMON, VERHOEVEN, RONALD, PRATS, XAVIER, BUSSINK, FRANK & HEESBEEN, BART. Comparison of various guidance strategies to achieve time constraints in optimal descents. *Journal of Guidance, Control, and Dynamics*. In Press.
- DALMAU, RAMON & PRATS, XAVIER. 2017. Controlled time of arrival windows for already initiated energy-neutral continuous descent operations. *Journal of Transportation Research - Part C*. D.O.I: 10.1016/j.trc.2017.09.024. **85**, 334–347.

Conference Proceedings

- DALMAU, RAMON, BAXLEY, BRIAN & PRATS, XAVIER. 2019 (Jun.). Using wind observations from nearby aircraft to update the optimal descent trajectory in real-time. *In: Proceedings of the 13th ATM R&D Seminar (ATMS2019)*. Eurocontrol/FAA, Vienna, Austria.
- DALMAU, RAMON, BAXLEY, BRIAN & PRATS, XAVIER. 2018 (Sept.). Fast sensitivity-based optimal trajectory updates for descent operations subject to time constraints. *In: Proceedings of the 37th Digital Avionics Systems Conference (DASC)*. IEEE/AIAA, London, UK. **Best paper in track award.**
- DALMAU, RAMON, VERHOEVEN, RONALD, PRATS, XAVIER, BUSSINK, FRANK & HEESBEEN, BART . 2017 (Sept.). Performance comparison of guidance strategies to accomplish CTA during a CDO. *In: Proceedings of the 36th Digital Avionics Systems Conference (DASC)*. IEEE/AIAA, Saint Petersburg, FL. **Best student paper of the conference.**
- DALMAU, RAMON, PEREZ-BATLLE, MARC & PRATS, XAVIER . 2017 (Sept.). Estimation and prediction of weather variables from surveillance data using spatio-temporal Kriging. *In: Proceedings of the 36th Digital Avionics Systems Conference (DASC)*. IEEE/AIAA, Saint Petersburg, FL. **Best paper in track award.**
- DALMAU, RAMON & PRATS, XAVIER . 2016 (Jun.). Assessment of the feasible CTA windows for efficient spacing with energy-neutral CDO. *In: Proceedings of the 7th International Conference on Research in Air Transportation (ICRAT)*. EUROCONTROL/FAA, Philadelphia, PA.

Agraïments

Els orígens d'aquesta tesi es remunten al 2014, quan el grup de recerca ICARUS de la UPC començava el FASTOP (FAST OPtimiser for continuous descent approaches). L'objectiu d'aquest projecte era desenvolupar algoritmes capaços d'optimitzar trajectòries en temps real per reduir l'impacte ambiental del descensos. El Dr. Xavier Prats va donar-me la oportunitat de participar activament en aquest projecte, en el marc de les meves pràctiques de grau. La meva tesi no és res més que la continuació d'aquest projecte, d'on van sortir tantes idees per al futur. Així doncs, el primer agraïment és per en Xevi, ja que sense la seva confiança quan encara era un estudiant de grau aquesta tesi no s'hauria materialitzat. A part de tot el que he aprés d'optimització i operacions, que espero que quedi plasmat a continuació, amb en Xevi he descobert el poder del Linux i les seves comandes. Però el més important no és res d'això: en Xevi m'ha ensenyat a ser una persona una mica més organitzada i ordenada, i això podré aplicar-ho a altres àmbits de la vida.

També vull donar les gràcies al coordinador del programa de doctorat, el Dr. David Pino, que m'ha guiat de forma excel·lent per superar totes les fites administratives del doctorat, i sempre ha respost amb rapidesa quan he necessitat alguna firma urgent. Una feina de coordinació impecable!

I would also like to thank Dr. Daniel Delahaye from Ecole Nationale de l'Aviation Civile (ENAC), and Dr.-Ing. Erik-Jan van Kampen from Delft University of Technology (TU Delft) for agreeing to review this PhD dissertation and being members of the committee. I really appreciate your time and commitment, which resulted in valuable comments to improve the quality of the final document. I must also acknowledge Dr. Manuel Soler, from Universidad Rey Juan Carlos (URJC), for agreeing to be part of the committee.

Els meus companys de despatx, el 121, també han estat pilars fonamentals d'aquesta tesi. Vaig tenir la sort de compartir despatx amb en Leonardo Camargo, el *parcero* més *bacano* de Colombia. Gracias a Leo ahora soy un fiel i orgulloso *pythonista* (no lo confundan con pitonista). Al 121 també vaig establir un gran vincle amb el Dr. Yan Xu, la persona amb qui he passat més dies i nits al despatx. I am still impressed how well Yan manages to solve any kind problem he faces, including those related to bureaucracy, no matter how difficult it is. L'últim en instal·lar-se al despatx va ser en Marc Melgosa. En Marc sempre m'ha donat un cop de mà quan més ho he necessitat durant aquests anys de tesi, tant en l'àmbit tècnic com en el personal, i per aquesta raó li estic infinitament agraït. A l'Empordà esperem sempre la seva família amb els braços ben oberts, ja sigui per una *kayakada* a les Coves d'en Gispert o per un dinar a *Cala Bruta*. També ha estat un plaer compartir aquests anys amb tots els altres *aeros* de la UPC: Raúl Saez, Adeline de Villardi, Pep Rojas, Santi Arias, Cristina Barrado, Enric Pastor, Marc Pérez-Batlle, Fernando Melibowski i Jordi Pons-Prats.

La vida al 121 no podria haver estat més fantàstica, però fora també és molt bonica! Part d'aquesta tesi s'ha dut a terme durant una estada de 4 mesos a l'agència espacial Holandesa (NLR). I must aknowledge Baart Heesbeen, Nico De Gelder, Michiel Valens, Frank Bussink and Ronald Verhoeven for being so kind with me. I have no words to describe how *perfect* was my short yet intense time at NLR. I really miss eating a sandwich of *haring* while walking with them in a windy and rainy Amsterdam. I also learned to be more critical with myself and, last but not least, I learned FORTRAN!

La segona estada va ser a l'altra banda de l'Atlàntic, a Vriginia (VA). I must acknowledge the administrative team of the National Insitute of Aerospace (NIA) for the excellent work upon my arrival and the fast preparation of my visa. I am wondering who is preparing the coffee after me and Sabine left. Danke auch an Max Friedrich und Becket Zou, ich werde die Ausflüge mit Ihnen, die Biere, die *slackline* nachmittags in Fort Monroe und das Einschlafen im *beattle* nach fünf Minuten nie vergessen. Ich vermisse dich. Finally, Brian Baxley deserves a warm and sincere acknowledgement for giving me the opportunity of working at NASA. In spite of being at 4,097 mi from my home town, thanks to Brian I always felt accompanied. My life at VA was the most exciting experience of my life, and I would repeat without any doubt!

Sorprenentment, també hi ha gent amb qui no he tingut l'oportunitat de coincidir personalment però que també han posat el seu granet de sorra. I must acknowledge the technical support during the development of the algorithms presented in this PhD thesis of Dr. Joel Andersson and Dr. Joris Grills. Much appreciation goes out also to Prof. Dr.-Ing. Wolfgang Marquardt and Dr. Ralf Hannemann-Tamás for their expertise in the nonlinear model predictive control field and valuable advice.

Ja fora de l'àmbit acadèmic, estic especialment agraït a l'Estel, la persona amb qui probablement he passat més estones escrivint i programant els algoritmes d'aquesta tesi. La seva càlida companyia ha fet molt més amè tot aquest llarg camí. Gràcies també a la família Ferrer Torres per estimar-me tant i fer-me sentir sempre un més de família. Tampoc em puc deixar a la Ivette i a la família Bas Sànchez, per escoltar-me, preocupar-se per mi animar-me en els moments més difícils. Les seves empentes i les nadades de desconnexió per les *Vies Braves* durant la recta final d'aquesta tesi han estat peces claus.

També vull agrair als amics de tota la vida, els de Sant Antoni de Mar (i també a tots aquells de Calonge), tot el suport moral i optimisme des del dia que vaig marxar del poble per començar els estudis. Ells sempre han estat disposats a escoltat els meus rotllos, tot i tenir *zerut* interès o no entendre ben bé del que parlava. Espero que aquest document expliqui amb prou detall que es cou darrera la famosa *pantalla negre de Matrix amb números verds que no paren de caure*. No em perdonaria mai deixar-me'n cap, així que moltes gràcies companys de *Can Tududut* i a la colla de carnaval *Els Gambats*!

Pel que fa a la família, estic molt agraït a tots els Codina, ja siguin de Premià, de Rimini o de La Roca. Em sento molt afortunat de tenir uns avis i uns tiets tant fantàstics. També he d'agrair a la família Dalmau, especialment a la tia Laura, estar sempre tant interessada per com evolucionava la meva tesi i com anaven les conferències. Òbviament, també estic immensament agraït als meus pares, en Ramon i l'Olga, per la seva confiança i consells; per deixar-me gaudir quan era un nen (i quan ja no ho era tant); i per posar sempre la meva felicitat per davant de qualsevol altra cosa. Sense uns pares com ells n'estic segur que no ho hauria aconseguit. Finalment, he d'agrair al meu germà Ferran haver-me acompanyat a tot arreu quan necessitava un descans, per molt sonat que semblés el pla. No us podeu imaginar com d'afortunat em sento de ser el seu germà!

Brétigny-Sur-Orge, Maig de 2019
Ramon Dalmau Codina

Resum

El creixement del trànsit ha augmentat la pressió sobre la sostenibilitat ambiental del transport aeri. En aquest àmbit s'han dedicat molts esforços en recerca per reduir l'impacte ambiental en les diferents fases del vol. Les operacions de descens continu, en les quals l'aeronau descendeix amb els motors a ralentí des de l'altitud de creuer fins just abans d'aterrar, han demostrat ser una solució atractiva per reduir el combustible, el soroll i les emissions en la fase de descens. Desafortunadament, aquest tipus d'operacions tenen un inconvenient molt important: la pèrdua de predictibilitat des del punt de vista dels controladors de trànsit aeri, en termes de temps de sobrevol als diferents punts de pas de la ruta. Per aquesta raó, els controladors necessiten aplicar més separació entre aeronaus, reduint així la capacitat de l'aeroport.

Treballs anteriors han demostrat que si les aeronaus fossin capaces de satisfer restriccions de temps de sobrevol a un o més punts de pas, seria possible implementar operacions de descens continu sense degradar la capacitat de l'aeroport. Malauradament, avui en dia existeixen pocs sistemes de gestió de vol capaços de generar trajectòries òptimes que satisfacin restriccions de temps, principalment perquè l'optimització de trajectòries en temps real continua sent una tasca difícil. A més, la resolució espacial i temporal dels models de vent utilitzats per els planificadors de trajectòria no son suficients per generar prediccions de temps de sobrevol prou fiables. Finalment, les estratègies de guiatge que fins i tot avui en dia permetrien satisfer amb exactitud restriccions de temps de sobrevol, no estan dissenyades específicament per minimitzar l'impacte ambiental.

Aquesta tesi té com a objectiu explorar algoritmes de d'optimització ràpids i robustos que permetin actualitzar la trajectòria òptima en temps real durant l'execució del descens, satisfent al mateix temps restriccions de temps de sobrevol; també s'investigaran nous conceptes de que permetin generar models de vent molt exactes a partir d'observacions emeses per aeronaus veïnes; i estratègies de guiatge més intel·ligents que minimitzin l'impacte ambiental de les operacions de descens continu subjectes a restriccions de temps de sobrevol.

En primer lloc, es quantifica la finestra de temps disponible al punt on s'aplica la restricció de temps de sobrevol, en funció dels estats de l'aeronau (altitud, velocitat i distància al punt) i assumint que els motors es mantenen ralentí i que no s'utilitzen aerofrens durant tot el descens. Els resultats de l'experiment indiquen que es podrien utilitzar estratègies de guiatge que gestionessin l'energia cinètica i potencial de l'aeronau per satisfer restriccions de temps sense necessitat de gastar més combustible. A continuació, es compararen quatre d'aquestes estratègies. Els resultats d'aquests segon experiment indiquen que el control predictiu, una estratègia que actualitza regularment la trajectòria òptima durant el descens, és molt robusta en termes d'errors de temps i energia, i alhora redueix l'impacte ambiental. Malauradament, es tarda massa a calcular la trajectòria òptima cada cop que s'ha d´actualitzar, fet que limita la implementació d'aquesta estratègia per operacions reals. Per tal d'afrontar aquesta limitació, es proposa una variant que utilitza sensitivitats paramètriques per reduir el temps d'execució a l'hora d'actualitzar la trajectòria òptima, sense degradar significativament la seva exactitud. Finalment, s'investiguen els possibles beneficis d'aprofitar observacions de vent enviades per les aeronaus veïnes per millorar el model de vent i, conseqüentment,

l'exactitud de la trajectòria calculada. Els resultats d'aquest últim experiment demostren que si s'implementés model predictiu com a estratègia de guiatge i les aeronaus cooperessin per compartir observacions de vent, es reduiria l'impacte ambiental sense degradar la capacitat de l'aeroport.

Abstract

The growth in traffic increased the pressure on the environmental sustainability of air transport. In this context, many research effort has been devoted to minimise the environmental impact in the different phases of flight. Continuous descent operations, ideally performed with the engines at idle from the cruise altitude to right before landing, have shown to reduce fuel, noise nuisance and gaseous emissions if compared to conventional descents. However, this type of operations suffer from a well known drawback: the loss of predictability from the air traffic control point of view in terms of overfly times at the different waypoints of the route. Due to this loss of predictability, air traffic controllers require large separation buffers, thus reducing the capacity of the airport.

Previous works investigating this issue showed that the ability to meet a controlled time of arrival at a metering fix could enable continuous descent operations while simultaneously maintaining airport throughput. In this context, the planning and guidance functions of state-of-the-art flight management systems need to be modernised. On-board trajectory planners capable to generate an optimal trajectory plan satisfying time constraints introduced during the flight are seldom, mainly because the real-time optimisation of aircraft trajectories is still elusive. Furthermore, the time scale and spatial resolution of the wind forecasts used by these trajectory planners are far from being adequate to generate accurate flight time predictions. Finally, there exist guidance strategies capable to accurately comply with time constraints enforced at a certain fix in the trajectory plan, yet they are not specifically designed to minimise the environmental impact.

This PhD thesis aims at investigating fast optimisation techniques to enable real-time updates of the optimal trajectory plan subject to time constraints during the descent; wind networking concepts to generate more accurate and up-to-date wind forecasts and, consequently, time predictions; and more robust an efficient guidance strategies to reduce the environmental impact at the maximum extent while complying with the time constraints of the trajectory plan.

First, the feasible time window at a metering fix that could be achieved during a descent requiring neither thrust nor speed brakes usage is quantified as a function of the aircraft states (altitude, distance to the metering fix and airspeed), aiming to assess the feasibility of guidance strategies that take advantage of time and energy management concepts. Then, the performance of four of these guidance strategies is compared in terms of environmental impact mitigation and ability to satisfy operational constraints. Results from the comparison reveal that model predictive control, a strategy based on a frequent re-calculation of the optimal trajectory plan during the execution of the descent, is the most robust in terms of energy and time deviation at the metering fix, providing at the same time excellent environmental impact mitigation figures. However, the execution time required to solve a rigorous trajectory optimisation problem at each re-calculation instant remains a critical limitation for practical applications. In order to address this issue, a variant of the model predictive control strategy that allows for fast updates of the optimal trajectory plan based on parametric sensitivities is proposed, which shows analogous results yet halving the time needed to update the optimal trajectory plan. Finally, the potential benefits of using wind observations broadcast

by nearby aircraft to reconstruct the wind profile downstream right before updating the optimal trajectory plan when using model predictive control is also investigated. Promising results show that the combination of model predictive control with wind networking concepts could enable optimal descents without degrading the capacity of the airport.

Notation

Throughout this PhD thesis and as a general rule, scalars and vectors are denoted either with lower or upper case letters. Vectors are noted with the conventional overhead arrow, like for example $\vec{a}$ or $\vec{\psi}$. Sets are denoted using caligraphic fonts, like for example $\mathcal{A}$, $\mathcal{B}$ or $\mathcal{X}$, while matrices use the same font but in bold series, like $\boldsymbol{\mathcal{R}}$. The derivative of magnitude $a(t)$ with respect to t is expressed by $\frac{\mathrm{d}a(t)}{\mathrm{d}t} = \dot{a}$. Furthermore, if not otherwise noted, all vectors are column vectors and a transposed vector is denoted by $[\cdot]^T$. For an ordered set or a vector, for example $\mathcal{A}$, the element at the i^{th} position is denoted by $\mathcal{A}_i$. Similarly, $\mathcal{A}_{i:j}$ is the subset of $\mathcal{A}$ that includes the elements whose position ranges from i to j (inclusive). Being consistent with this notation, $\mathcal{A}_{i:}$ is the subset of $\mathcal{A}$ that includes the elements with position greater or equal than i. Note that $\mathcal{A}_{1:} = \mathcal{A}$. Furthermore, $(\cdot)^*$ indicates *optimal*. Finally, for a scalar function $(\cdot)^+ = max((\cdot), 0)$, and for a vector-valued function of n elements, $(\cdot)^+ = \left[(\cdot)_1^+, (\cdot)_2^+, \ldots, (\cdot)_n^+\right]$.

Next, the principal symbols that are used throughout this dissertation are shown along with their meaning. The reader should note that this list is not exhaustive.

B	B-Spline basis function
C_D	drag coefficient
C_L	lift coefficient
$C_{D,BADA}$	drag coefficient of the BADA v4 model
$C_{D,sim}$	drag coefficient of the simulator
$C'_{D,sim}$	drag coefficient of the simulator increased by a factor of K_{C_D}
C_{D0}	parasite drag coefficient
C_{D2}	induced drag coefficient
$C_{D\beta}$	coefficient that represents the increase in drag coefficient when speed brakes are deployed
D	aerodynamic drag
E_k	kinetic energy of the aircraft
E_p	potential energy of the aircraft
E_s	specific energy of the aircraft
E_t	total energy of the aircraft
J	cost function of the optimal control problem
K_{C_D}	factor to increase or decrease the nominal drag coefficient
$K_{T_{idle}}$	factor to increase or decrease the nominal thrust idle
K_β	weighting parameter that determines howmuch the use of speed brakes is penalised
L	aerodynamic lift force
M	Mach number
N	number of discretisation intervals in the whole time horizon
$N1$	revolutions of the engine fan
$N1_{idle}$	minimum revolutions of the engine fan

$N1_{max}$	maximum revolutions of the engine fan
P	number of phases of the optimal control problem
R	perfect gas constant
S	wing surface area
T	engine thrust
$T_{idle,sim}$	idle thrust of the simulator
$T'_{idle,sim}$	idle thrust of the simulator increased by a factor of $K_{T_{idle}}$
T_{idle}	idle thrust
T_{max}	maximum thrust
ΔE_s	difference of specific energy
$\Delta\tau$	discretisation step
Λ	forgetting factor
Π	quadrature function of the running cost
$\Re$	set of real numbers
α	Hellman exponent
β	speed brakes deflection
χ_g	ground track angle
δ	normalised pressure of the air
δ_{11}	normalised pressure of the air at the tropopause
ϵ_{inf}	infeasibility criteria
ϵ_{opt}	optimality criteria
η	landing gear status
γ	aerodynamic flight path angle
γ_a	a specific heat ratio of the air
γ_{min}	minimum aerodynamic flight path angle
π	throttle setting
λ_h	standard temperature lapse rate
$\boldsymbol{\mathcal{W}}^{eq}$	weighting matrix for the slack variables associated with equality constraints
$\boldsymbol{\mathcal{W}}^{in}$	weighting matrix for the slack variables associated with inequality constraints
$\mathcal{E}$	set associating the index of the last time sample to its corresponding phase
$\mathcal{G}_{ac}$	active set of inequality constraints
$\mathcal{G}_{in}$	inactive set of inequality constraints
$\mathcal{I}$	set associating the index of the first and interior time samples to its corresponding phase
$\mathcal{L}$	lagrangian of the nonlinear programming optimisation problem
$\mathcal{N}$	normal distribution
$\mathcal{O}$	set of wind observations
$\mathcal{P}$	algorithm that solves the nonlinear programming optimisation problem
$\mathcal{Q}$	algorithm that solves the quadratic programming optimisation problem
$\mathcal{T}$	set associating the index of each time sample to its corresponding phase
$\mathcal{U}$	uniform distribution
μ	parameter describing the expected number of occurrences in a Poisson distribution
μ_ϵ	expectation of the simulated wind speed error
ω	weight associated to each wind observation
ϕ	end cost or Mayer term
π	running cost or Lagrange term
ρ_{SSL}	SSL density of the air at standard sea level
σ	normalised density of the air
σ_ϵ	standard deviation of the simulated wind speed error
τ	discretised time sample
τ_{SSL}	temperature of the air at standard sea level
τ_{inf}	threshold for the infeasibility criteria
τ_{opt}	threshold for the optimality criteria
Pos	Poisson distribution
θ	normalised temperature of the air
θ_{11}	normalised temperature of the air at the tropopause
$\vec{F}$	evolution function of the state vector
$\vec{X}$	current states vector
$\hat{\vec{X}}$	predicted states vector

$\vec{\lambda}$	dual variables associated with inequality constraints
$\vec{\mu}$	dual variables associated with equality constraints
$\vec{\psi}$	terminal constraints
$\vec{\vartheta}^{eq}$	equality interior-point constraints
$\vec{\vartheta}^{in}$	inequality interior-point constraints
$\vec{b}^{eq}$	equality path constraints
$\vec{b}^{in}$	inequality path constraints
$\vec{c}$	control points of the spline
$\vec{d}$	fixed parameters of the model
$\hat{\vec{d}}$	predicted fixed parameters of the model
$\vec{e}^{eq}$	vector of slack variables for the equality constraints
$\vec{e}^{in}$	vector of slack variables for the inequality constraints
$\vec{f}$	dynamics of the state vector
$\vec{g}$	inequality constraints of the nonlinear programming optimisation
$\vec{h}$	equality constraints of the nonlinear programming optimisation problem
$\vec{p}$	vector of parameters of the nonlinear programming optimisation problem
$\hat{\vec{p}}$	predicted vector of parameters of the nonlinear programming optimisation problem
$\vec{u}$	controls vector
$\vec{w}$	wind vector
$\vec{x}$	states vector
$\vec{z}$	primal variables of the nonlinear programming optimisation problem
ζ	aerodynamic configuration of the aircraft
a	speed of sound
f	cost function of the nonlinear programming optimisation problem
g	gravity acceleration
h	geometric altitude
h_r	reference altitude of the Hellman model
h_{11}	standard altitude of the tropopause
h_{CO}	cross-over altitude
h_{FAP}	altitude at which the FAP has to be intercepted
h_{IF}	altitude at which the IF has to be intercepted
k_{max}	maximum number of QP iterations before triggering a NLP trajectory update
m	mass of the aircraft
n_z	load factor
p	probability
p_{SSL}	pressure of the air at standard sea level
q	nominal fuel flow
q_{idle}	idle fuel flow
s	distance to go
s_{FAP}	distance to go of the FAP
s_{IAF}	distance to go of the IAF
s_{IF}	distance to go of the IF
t	time
t_F	final time of the time horizon
t_I	initial time of the time horizon
v	true airspeed
v_{CAS}	calibrated airspeed
v_{FAP}	calibrated airspeed at which the FAP has to be intercepted
v_{IF}	calibrated airspeed at which the IF has to be intercepted
v_{max}	maximum true airspeed
v_{min}	minimum true airspeed
w_e	east wind component
w_n	north wind component
w_r	reference speed of the Hellman model
w_s	longitudinal wind component
w_x	cross wind component
ϵ	simulated wind speed error

List of Acronyms

3D-PAM	3D-path arrival management
ACARS	aircraft communication and reporting system
ADS-B	automatic dependent surveillance-broadcast
AGL	above ground level
AMAN	arrival manager
AMDAR	aircraft meteorological data relay
ANSP	air navigation service providers
APERO	avionics prototyping environment for research and operations
APM	aircraft performance model
AsNMPC	advanced-step NMPC
ATC	air traffic control
ATFM	air traffic flow management
ATM	air traffic management
BADA	base of aircraft data
CAS	callibrated airspeed
CDA-MP	continuous descent approach for maximum predictability
CDO	continuous descent operation
CI	cost index
CONCORDE	flight operations for novel continuous descents
CTA	controlled time of arrival
DAE	differential algebraic equation
EDA	efficient descent advisor
FAA	Federal Aviation Administration
FAP	final approach point
FASTOP	fast optimizer for continuous descent approaches
FMS	flight management system
GAMS	general algebraic modelling system
GD	green dot speed

GFS	global forecast system
GRACE	generic research aircraft cockpit environment
IAF	initial approach fix
ICAO	International Civil Aviation Organization
IF	intermediate fix
ILS	instrumental landing system
INMPC	ideal NMPC
ISA	international standard atmosphere
KKT	Karush-Kuhn-Tucker conditions
MLM	maximum landing mass
MMO	maximum operative Mach
MPC	model predictive control
NASA	National Aeronautics and Space Administration
NextGen	next generation air transportation system
NLP	nonlinear programming
NLR	Netherlands Aerospace Centre
NMPC	nonlinear model predictive control
NOAA	National Oceanic and Atmospheric Administration
NWP	numerical weather prediction
ODE	ordinary differential equation
OL	open-loop guidance
OPD	optimised profile descent
OPTIMAL	optimised procedures and techniques for improvement of approach and landing
PARTNER	partnership for air transportation noise and emission reduction
PEP	Airbus performance engineering program
PM	particulate matter
QP	quadratic programming
RAP	rapid refresh
RMSE	root-mean-square error
RNAV	area navigation
RTA	required time of arrival
SbNMPC	sensitivity-based NMPC
SESAR	Single European Sky Air traffic management Research
SLQP	sequential linear-quadratic programming
SNOPT	sparse nonlinear optimiser
SQP	sequential quadratic programming
SSL	standard sea level
STAR	standard arrival procedure
STATFOR	statistics and forecast service
SUNDIALS	SUite of Nonlinear and DIfferential/ALgebraic Equation Solvers
TA	tailored arrival
TAAM	total airport and airspace model
TAS	true airspeed
TDDA	three-degrees deceleration approach

TEMO	time and energy managed operations
TMA	terminal maneouvering area
TOD	top of descent
TRL	technology readiness level
UPC	Technical University of Catalonia
UPS	United Parcel Service
VMO	maximum operative CAS
VNAV	vertical navigation
WAFC	world area forecast model

We are trying to prove ourselves wrong as quickly as possible, because only in that way can we find progress.

— Richard P. Feynman

The significant problems we have cannot be solved at the same level of thinking with which we created them.

— Albert Einstein

I

Introduction

According to the most likely scenario of the Eurocontrol's statistics and forecast service (STATFOR), there will be around 14 million flights in Europe in 2035, 1.5 times the level of 2012, with an annual growth around 1.8% (Eurocontrol, 2013). To accommodate the increasing demand for flights from passengers and freighters, more airports will need to operate close to their capacity limits, thus adversely impacting the predictability and punctuality of flights. According to SESAR (2015a), in the reference scenario where no action is taken to increase capacity, alarming predictions estimate that around 12% of the future demand will not be accommodated in 2035. The growth in traffic also implies increased pressure on the environmental sustainability of air transport. In this context, Penner *et al.* (1999) were among the first to assess the environmental impact of aviation, both for (what was then) current-day conditions and future scenarios. Results from the assessment showed that, in 1992, aviation represented roughly 3.5% of total man-made climate change impact, but this could increase by a factor between 2.6 and 11 by 2050 if no measures are taken. Scientific advances since 1992 reduced uncertainties and sharpened the quantitative evaluation, yet the conclusions remain the same. Updated assessments of the climate change impact of aviation since 1999 have been performed, for instance, by Sausen *et al.* (2005), Lee *et al.* (2010) and Phoenix *et al.* (2019).

Through the Single European Sky Air traffic management Research (SESAR) and next generation air transportation system (NextGen) programmes, the SESAR Joint Undertaking and the Federal Aviation Administration (FAA), respectively, are addressing the impact of air traffic growth by implementing new or improved procedures and technologies that aim to increase the capacity and efficiency of the air traffic management (ATM) system, while simultaneously improving safety and reducing the environmental impact.

One of the SESAR ambition is to increase the capacity of the whole ATM system by 80-100% (SESAR, 2015a). Enhancements to conflict and separation management processes and increased automation for both on-board and ground systems will help to safely handle the increasing traffic demand in the terminal maneouvering area (TMA) and en-route environments. At airspace and air traffic flow management (ATFM) level, more dynamic optimisation and allocation of airspace resources (see for instance the study performed by Sergeeva *et al.* (2017)) is foreseen to enable airspace users to access required airspace with minimum constraints. Finally, airport throughput is expected to increase by improving the traffic sequencing and merging techniques and by reducing separation requirements for both arrivals and departures.

Furthermore, another SESAR ambition estimates a total reduction of between 5% and 10% in fuel burn per flight (SESAR, 2015a). Improvements to the design of engines over the past years have greatly reduced fuel consumption and gaseous emissions. Promising procedural solutions, which have the advantage to provide fuel benefits without modifying aircraft engines or airframe, have been also proposed. For instance, in the en-route environment, more direct routes and more efficient vertical profiles (i.e., altitude and speed) are expected to reduce fuel consumption by 2.5%. Optimal vertical profiles for en-route operations, performed by progressively increasing the altitude of the aircraft as fuel is burnt, were investigated, for instance, by Betts & Cramer (1995) and Soler *et al.* (2012). The actual quantitative benefits in terms of fuel and time savings with respect to current profiles, performed at constant cruise altitudes, were assessed by Dalmau & Prats (2015, 2017). Results from a recent study by Prats *et al.* (2018) showed that the en-route inefficiencies of current operations in the vertical domain are similar to those in the lateral domain. In addition, most of these inefficiencies are due to the strategic part of the ATM (the fact that airspace users are still forced to use a structured en-route network). In addition, it was observed that air traffic control (ATC) typically contribute to reduce route extension by short-cutting the planned trajectory.

In the TMA environment, the SESAR target is to enable an average reduction around 10% fuel burn reduction by enabling continuous climb and descent profiles with fewer tactical interventions from ATC. The introduction of more fuel-efficient profiles, however, is achieved at the cost of a reduction on capacity due to the more diverse trajectories that the ATC need to handle. New concepts of operation need to be implemented in order to maintain capacity at acceptable levels, or even increasing it, while simultaneously allowing fuel-efficient profiles. Major challenges involved with the implementation of new concepts of operation include the upgrade of the planning and guidance capabilities of current flight management systems (FMSs), changes in airspace and procedure design, as well as modernisation of current ATC separation, sequencing and merging techniques and their ground decision support tools.

I.1 Environmental impact of descents

In terms of environmental impact, the optimal descent of an aircraft should be performed uninterruptedly, with the engines at idle from the cruise altitude to the stabilisation point, typically at 1,000 ft above ground level (AGL), where the aircraft is configured for landing. This kind of flight operation is commonly referred as continuous descent operation (CDO). It should be noted, however, that there is some controversy in the rigorous definition of CDO. Some authors consider that a CDO is a trajectory performed without segments at constant altitude (also known as *level-offs*) during the whole descent. Yet, this does not ensure a complete engine-idle descent, since additional thrust might be required to maintain certain vertical speeds or flight path angles without decelerating. For this reason, other authors prefer to define a CDO as a trajectory executed with the engines at idle during the whole descent, no matter how many level-offs are performed. In the case of a level-off at idle thrust, the aircraft will nothing but decelerate. In this PhD thesis, the latter definition of CDO has been considered because a level-off at idle thrust could be used as a mechanism to rapidly reduce the energy of the aircraft without deploying drag devices.

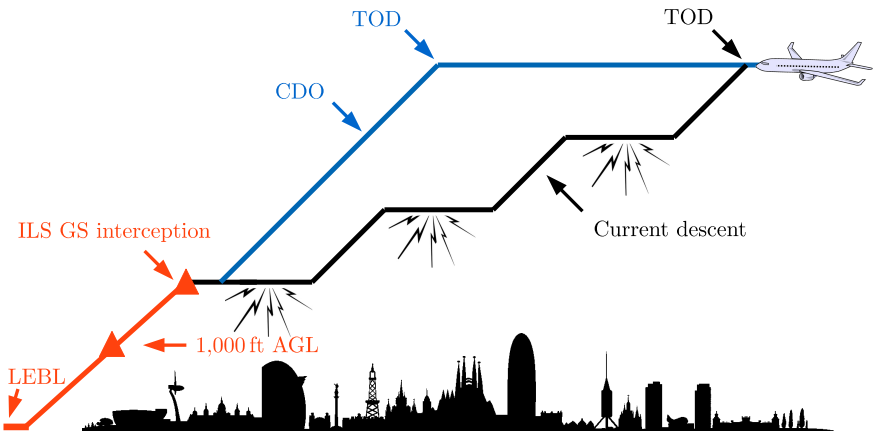

Figure I-1: *Comparison between a CDO and a current descent operation*

Figure I-1 shows an illustrative comparison between the altitude profile of a typical descent in the current concept of operations and that of a CDO. Current descents leave the cruise altitude earlier, typically as a result of an ATC clearance. Then, the aircraft descends stepwise by performing several level-offs caused by tactical ATC instructions (as will be explained in next section) or constraints defined at the waypoints of the particular procedure being flown. During these segments at constant altitude, additional thrust is typically required to maintain the altitude without decelerating too much.

A CDO keeps at the cruise altitude a longer distance, where the fuel consumption is lower. Then, at the optimal top of descent (TOD) computed by the FMS, the point at which the aircraft leaves the cruise altitude, the engines are set to idle and the aircraft starts the CDOs towards the interception of the instrumental landing system (ILS) glide slope. Summing up, a CDO is performed (as far as possible) at higher altitudes, lower thrust settings and lower drag configurations, thus greatly reducing fuel consumption, gaseous emissions and noise nuisance (Erkelens, 2000; Warren & Tong, 2002; Clarke *et al.*, 2004).

Considerable research has been conducted to quantitatively assess the environmental benefits of CDOs. For instance, extensive simulations and field tests were performed within the optimised procedures and techniques for improvement of approach and landing (OPTIMAL) programme initiated by the European Commission in 2004, and the partnership for air transportation noise and emission reduction (PARTNER) programme established by the FAA in support of the NextGen initiative in 2003. It is worth mentioning that these programmes are only two of the many research activities that have been performed to quantify the benefits and to identify the limitations of CDOs.

In the OPTIMAL programme, field tests were performed at two major European airports to assess the trade-off between environmental benefits and operational flexibility of CDOs, including predictability of the descent trajectories, ATC coordination procedures and workload of the flight crew. The results obtained from field tests at London Heathrow airport (LHR) were reported by Reynolds *et al.* (2005), while the main findings obtained at Amsterdam Schiphol airport (AMS) were presented by Wat *et al.* (2006). Similar experiments were performed within the PARTNER project at Louisville international airport (SDF) (Clarke *et al.*, 2004, 2006), Atlanta international airport (ATL) (Clarke *et al.*, 2007) and Los Angeles international airport (LAX) (Clarke *et al.*, 2013).

With no exception, all the aforementioned experiments concluded that CDOs lead to fuel savings, noise nuisance and gaseous emission reduction if compared to current descents. For instance, results from United Parcel Service (UPS) flight tests during night-time operation at SDF reported fuel savings about 200 kg per flight for B767 models (Clarke *et al.*, 2006), while results from flight tests at ATL, which considered flights from two airlines, suggested fuel savings around 460 kg and 600 kg per flight for B757 and B767 models, respectively (Clarke *et al.*, 2007). Later on, analysis over more than 480,000 flights to 25 airports in the national airspace system during four months concluded that fuel savings of CDOs were lower than 25 kg for 45% of the flights, and less than 100 kg for 87% of the flights (Robinson & Kamgarpour, 2010).

Based on this diversity of fuel saving figures, it can be concluded that comparison of results across different experiments is difficult due to the substantial differences in assumptions, types of data, models, and methods being used. Nevertheless, Thompson *et al.* (2013) quantified the benefits of CDOs in Paris and New York regions using similar sources of data, analytical methods and models, and concluded that discrepancies in fuel saving figures across different experiments are also caused by the differences in traffic intensity, as well as the distribution of level-off segments in the current descent trajectories due to the dissimilar ATC practises, procedure designs, traffic patterns and meteorological conditions. These results manifest the tangible trade-off between environmental impact and capacity, which will be further discussed in the next section.

Different from previous works, Jin *et al.* (2013) aimed at explaining the fuel savings observed in field tests found in the literature from an analytical point of view. In order to accomplish that, the relationship between speed, altitude, and fuel consumption during a CDO were analytically derived. Based on their findings, several helpful design guidelines for CDOs were proposed.

I.2 Predictability of descents

Each aircraft performing a CDO will have a different optimal vertical profile (altitude and speed) depending on, e.g, the aircraft type, the mass, the wind field and the cost index (CI)[1]. To give an insight into this fact, Fig. I-2 compares two optimal CDOs, computed with the Airbus performance engineering program (PEP), for the descent of an Airbus A320.

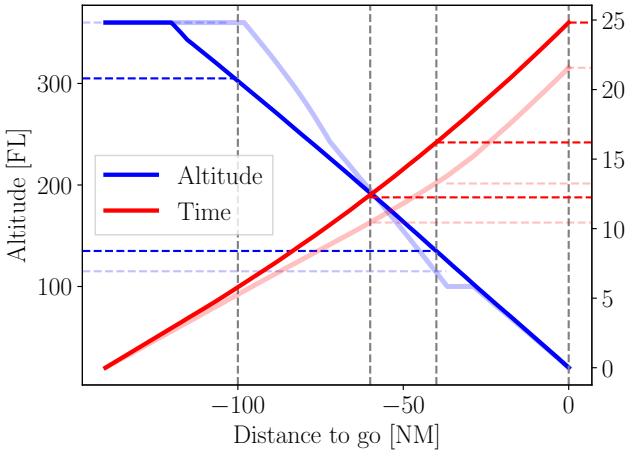

Figure I-2: *Comparison between two CDOs with different mass and CI. Heavy and fast: solid light lines. Light and slow: solid dark lines.*

Despite both descents are performed at idle thrust and for the same weather conditions, they differ on the mass of the aircraft and the selected CI. By observing these dissimilar vertical profiles, the reader could guess the compelling diversity of vertical profiles that ATC needs to manage when considering the wide range of aircraft performance across different aircraft types, weather conditions and airline business models. Due to the heterogeneity of vertical flight profiles and aircraft behaviour, a well-known drawback of CDOs is the loss of predictability of the trajectory from the ATC point of view, in terms of altitude uncertainties and overfly-times at the different fixes.

Table I-1 shows the overfly time with respect to the initial conditions and the altitude of the two CDOs shown in Fig I-2 at four distances to the final approach point (FAP).

Table I-1: *Altitude and overfly time of two CDOs with different mass and CI at various distances to go*

Distance to FAP [NM]	Overfly time		Altitude [FL]	
	Light and slow	Heavy and fast	Light and slow	Heavy and fast
100	5 min 38 s	2 min 46 s	305	360
60	12 min 15 s	10 min 26 s	195	195
20	16 min 12 s	13 min 15 s	135	115
0	24 min 49 s	21 min 34 s	20	20

According to Table I-1, at 100 NM from the FAP the heavy and fast CDO is still in the cruise phase, while the light and slow CDO has started the descent a while ago. As a result, the altitude dispersion at that point is around 5,500 ft. Despite at 60 NM to the FAP both CDOs arrive at the same altitude, the time difference at this distance is 1 minute and 49 seconds. In fact, the time difference increases with the flight distance, reaching 3 minutes and 15 seconds at the FAP.

Due to this low predictability, existing CDO implementations typically require ATC to introduce additional sequencing buffers to ensure safe spacing between aircraft, thus reducing the throughput of the airport. For this reason, in busy airports CDOs are only operational in off-peak hours, when the traffic demand is low (Robinson & Kamgarpour, 2010). In busy TMAs, very few flights are cleared to perform CDO, and even those might be interrupted with ATC tactical instructions after starting the descent to ensure safe spacing with surrounding traffic due to uncertainty.

[1]The cost index is a number representing the ratio of the time-related cost of an aircraft operation and the cost of fuel (Airbus, 1998)

The relationship between target spacing, probability of uninterrupted CDO execution, and airport capacity was investigated by Ren & Clarke (2007b,a) by means of Monte-Carlo simulations. The simulations were used to estimate the number of possible CDOs that could be performed without ATC intervention and thereby determine the minimum target spacing at a metering fix, such that there is a high probability of no separation violations thereafter. Later on, the tool was used to determine the target spacing for CDOs at SDF airport. Results showed that CDOs could be efficiently implemented in TMAs under low to moderate traffic conditions (Ren & Clarke, 2008).

A well-known disadvantage of CDOs with the current ATC sequencing and merging techniques is that, once initiated, it is hardly possible to react on ATC instructions while maintaining the engines at idle for the remainder of the descent. The main reason is that the remaining distance to the runway threshold must be known by the FMS in order to compute the optimal trajectory plan in terms of environmental impact. The remaining distance to go could be computed from the lateral route (i.e., sequence of waypoints) if the aircraft were following it through to completion. The fixed lateral route needed to enable CDOs, however, is seldom used. In busy TMAs, descending aircraft are tactically vectored by ATC, who stretch or shorten the lateral route to maintain and acquire safe separation with other departing and arriving traffic. Unfortunately, with this very common practise it is not known neither the duration of the *open-loop* vector, nor how the aircraft will re-join its initial route. As illustrative example, Fig. I-3 shows the vectoring instructions used by the ATC at Barcelona-El Prat airport during a typical day of operations.

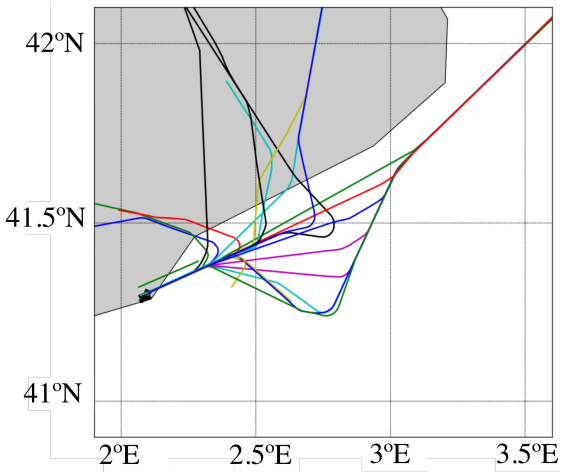

Figure I-3: *Vectoring instructions used by the ATC at Barcelona-El Prat airport during a typical day*

Any lateral path stretching would place the aircraft below the trajectory plan, while any shortcut would place it above. In the first case, more thrust might be required to intercept the planned vertical profile from below at the moment of knowing the remaining distance to go, leading to both increased fuel consumption, gaseous emissions and noise; in the second case, additional drag through the use of drag devices might be required to capture the planned vertical profile, leading to both increased airframe noise and an uncomfortable ride for passengers. Furthermore, since most FMSs do not allow for real-time updates of the trajectory plan once the descent has been initiated (i.e., the trajectory plan is *frozen* at the TOD), the pilot would be in charge of managing the vertical profile, probably not in the most environmentally friendly way due to the lack of automated support in the face of the open-loop vectors. These instructions also increase the workload of both ATC and pilots, and decrease the situational awareness of pilots.

Even when the route is unmodified, other tactical instructions commonly used by ATC to sequence and merge arrival traffic in busy TMAs include segments at constant altitude and speed control. In order to fly at the requested altitude and/or speed, aircraft might need to increase the energy by means of engine thrust or to remove energy by increasing the aerodynamic drag.

Most of the field tests listed in Section I.1 were performed in low traffic demand scenarios. Nevertheless, some studies indicated that the fuel savings expected to result from CDOs could be potentially neutralised by the need to provide separation assurance modifying the aircraft speed, altitude and/or by using vector instructions (Cao *et al.*, 2014). The extent of this reduction on the benefits of CDOs would depend on the target spacing, the traffic demand level and the types of ATC instructions used to absorb the delays due to the additional separation buffers.

Since field tests of CDOs in high traffic scenarios are difficult to conduct, Wilson & Hafner (2005) presented a simulation-based approach to quantify the benefits of CDOs in busy TMAs taking into consideration spacing and sequencing issues. Fast-time simulations at ATL airport were performed with the total airport and airspace model (TAAM) by removing altitude constraints associated to the waypoints of the original procedures, as well as allowing aircraft to directly fly from the initial approach fix (IAF) to the base-leg of the landing runway. Promising results showed significant fuel and time savings with minimum increase on ATC workload. Aiming at assessing safety aspects of CDOs, Park *et al.* (2016) proposed a trajectory-based methodology to estimate the encounter rate of CDOs in high traffic scenarios. The proposed method was validated by comparing to Monte-Carlo simulation results. Khan *et al.* (2009) also performed fast-time simulations in high traffic scenarios to compare current ATC procedures with ATC assisted with various systems of ground automation, in terms of CDO success rate and throughput.

Statistical analysis from the fast-time experiment performed by Robinson & Kamgarpour (2010) revealed that fuel savings of CDOs are marginal for high traffic scenarios due to the tactical instructions required to provide separation assurance, which have negative effects on the fuel-efficiency of CDOs. In particular, fuel savings due to CDOs were reduced by 70-85% if compared to the low traffic scenarios. This work also reported a reduction of 45 kg per CDO due to traffic congestion at ATL airport. A similar experiment at ATL airport reported a sightly different reduction of 23 to 36 kg per CDO (Cao *et al.*, 2014).

In addition to fast-time simulations, human-in-the-loop studies with ATC showed that CDOs would not be feasible at ATL airport during the busiest traffic periods, since too much efficiency would be lost to accommodate the traffic demand (Johnson, 2009). In such traffic conditions, few flights would be issued the CDO clearance and even some flights would likely need to be removed from CDO procedures after being cleared in order to manage the demand. Nevertheless, results also showed that at least 15% of the total environmental benefit would still be achievable for CDOs that are terminated earlier.

I.3 New concepts to enable CDOs in busy TMAs

Results from previous works reveal that the predicted increase in traffic demand will negatively impact the potential benefits of CDOs due to their low predictability if compared to current descent operations. In order to face this issue, several ATM concepts have been proposed that aim to enable CDOs also in high traffic demand scenarios.

I.3.1 Fixed flight path angle descents

The three-degrees deceleration approach (TDDA) (De Prins *et al.*, 2007; Sopjes *et al.*, 2011; De Leege *et al.*, 2009) is a concept in which the descent is performed all along a 3° path from the TOD to the runway threshold. To perform the spacing task, two controls are given to the pilot: the first is the thrust cutback altitude, in which the throttle is set to idle and, consequently, the aircraft starts to decelerate; and the second is the flaps/slats and gear setting, which allows to manage the deceleration after the thrust cutback altitude. Figure I-4 (adapted from De Prins *et al.* (2007)) shows a scheme of this concept.

Pradeep & Wei (2017) investigated the variability and operational feasibility aspect of CDOs with fixed path angle descents, and concluded that this kind of flight operation has higher degree of vertical predictability and lesser variability in terms of altitude and speed profiles if compared to the CDOs performed at idle thrust. This is achieved at the cost of thrust settings different from idle and with higher drag configurations, which implies more environmental impact.

I.3.2 CDOs in vertical corridors

Aiming to allow for more flexible vertical profiles than fixed flight path angle descents, the International Civil Aviation Organization (ICAO) published some CDO guidance material (ICAO, 2010) to support air navigation service providers (ANSP) to design vertical corridors in which all descent trajectories must be contained, helping in this way to strategically separate them from other arrival and departure procedures in the vicinity. As reported by Fricke *et al.* (2015), however, these vertical corridors have been established without explicitly considering the aircraft type, assuming international standard atmosphere (ISA) conditions and with coarse assumptions regarding the aircraft gross mass and aircraft performance models. This leads, in the majority of cases, to too restrictive corridors that limit the CDO adherence in real operations.

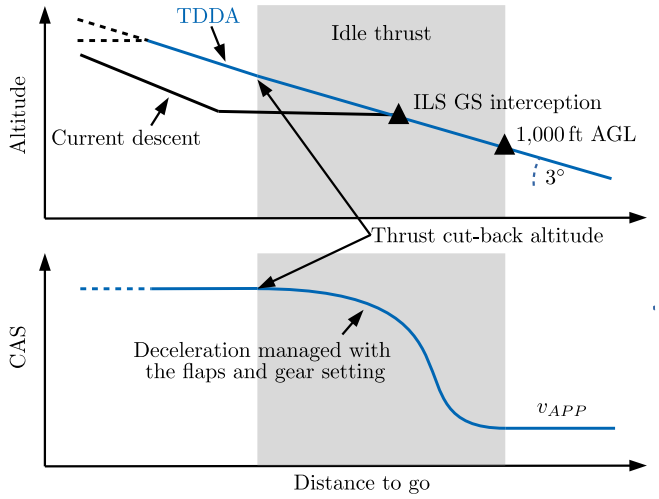

Figure I-4: *Scheme of the three-degrees deceleration approach concept*

I.3.3 Optimised profile descents

Standard arrival procedures (STARs) used in most of the airports have been historically designed to ensure that a wide variety of aircraft can fly the procedure, from those basically equipped to the most modern aircraft. In order to enable the descent to aircraft with various navigation capabilities, current STARs include altitude and speed constraints at various fixes of the route and, generally speaking, are not designed to execute the whole descent with the engines at idle.

An optimised profile descent (OPD) is a procedure, normally associated with a published STAR, designed to allow maximum practical use of CDOs (ICAO, 2010). Accordingly, OPD could be interpreted as one method of facilitating CDOs by using altitude constraints that restrict the vertical profile to a near-idle descent for many of the currently in use commercial aircraft.

Shresta *et al.* (2009) assessed the potential benefits and issues of implementing OPDs at Denver international airport (DEN). Arrival flights descending along CDOs were modelled by transforming the descent trajectories of real flights, taken from radar tracks, into descent trajectories at idle thrust. Several potential conflicts were identified as a result of allowing aircraft to descend along their optimal trajectories. Implementing OPDs only in a certain altitude interval, allowing level-off above and below the delimiting altitudes, demonstrated to greatly reduce conflicts while still offering attractive benefits in terms of fuel consumption. As in previously mentioned studies (Johnson, 2009), a major conclusion of the work performed by Shresta *et al.* (2009) was that CDOs do not need to be implemented from the cruise altitude to the stabilisation point in order to obtain reasonable reductions of fuel consumption and gaseous emissions.

I.3.4 3D-Path arrival management

The working principle of the solutions presented so far consists of removing level-offs to the greatest possible extent, while still supporting ATC to predict the vertical profile of aircraft. In addition, these solutions assume static routes, corresponding to the published STARs of the airport, and therefore not tailored to each individual flight. The next solutions go one step further by controlling the time at which aircraft reach one or several metering fixes along the route.

For instance, using the 3D-path arrival management (3D-PAM) concept (Nagle *et al.*, 2011; Coppenbarger *et al.*, 2010), a ground system computes the arrival schedule of flights at a metering fix. Then, for each flight, it strategically assigns the best route to the metering fix in combination of cruise and speed advisories and (eventually) a path adjustment in the form of point-bearing-distance to meet the schedule. These instructions, which are designed to facilitate the delivery by voice using standard phraseology, are cleared prior the TOD and given to the pilot for manual entry into the FMS. This negotiation prior the TOD allows the FMS to know the remaining distance to go, compute the optimal trajectory plan complying with the cleared instructions, and uninterruptedly execute it. This is generally not feasible today due to the use of open-loop vectors. A system for the integration of this concept is the efficient descent advisor (EDA), developed by the National Aeronautics and Space Administration (NASA) (Coppenbarger *et al.*, 2004).

Figure I-5 shows a scheme of the 3D-PAM concept.

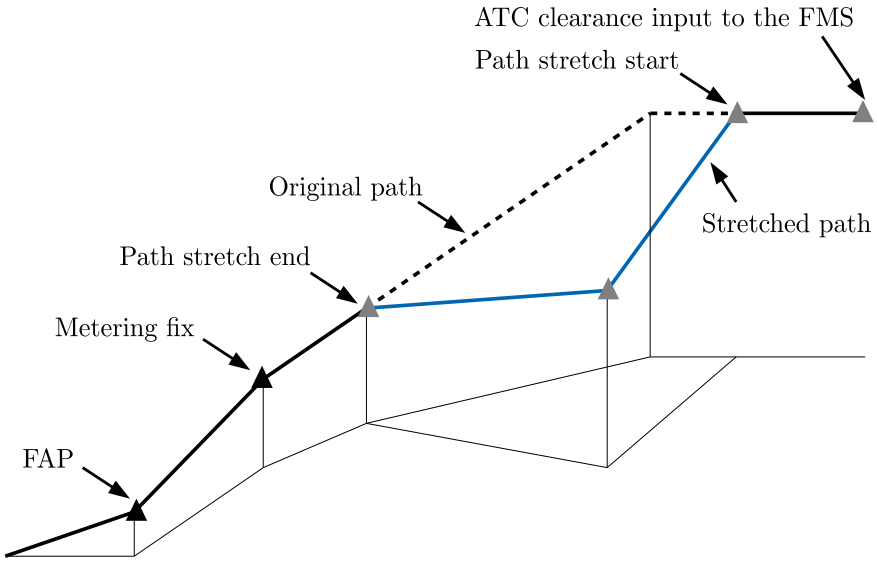

Figure I-5: *Scheme of the 3D-path arrival management concept*

It should be noted that, even if when implementing 3D-PAM some flights are actually travelling a longer distance due to the point-bearing-distance instruction (see blue segment in Fig. I-5), the descent to the metering fix is typically flown at a lower power setting, overall reducing the fuel consumption, gaseous emissions and noise nuisance.

I.3.5 Tailored arrivals

Tailored arrivals (TAs) are a step further of 3D-PAM to enable CDOs. TAs are similar concept to OPDs, but are not restricted to published STARs (Coppenbarger *et al.*, 2009; Elmer, 2008). In the TA concept, a customised, dynamic and conflict-free descent trajectory, tailored by ATC through use of a list of fixes with associated speed and altitude constraints, is uplinked via data-link to the FMS before starting the descent, given as a single clearance well before to TOD. These clearances provide sufficient information for the FMS to compute the trajectory plan from the current aircraft position to the runway threshold. When possible, the clearances should allow to generate a near-idle descent trajectory. It should be noted that even for ATC without data-link support, TAs could be implemented by using a pre-negotiated set of STARs stored in the database of the FMS.

I.3.6 CDOs with controlled times of arrival and fixed routes

A primary challenge of 3D-PAMs and TAs is the design of the route and constraints that are issued to the FMS, which shall be chosen to allow the FMS to generate a trajectory plan that can be flown at idle thrust. Ground systems in charge of computing these constraints, however, use trajectory predictors configured with simplified models to represent the dynamics and performance of the aircraft. These models will rarely reproduce the behaviour of all aircraft types without errors. Any discrepancy between the models used by the on-board and ground trajectory predictors might result in clearances selected by the 3D-PAM or TA ground automation system that, even if supposed to enable an idle descent according to the (inaccurate) ground trajectory predictor, might require the use of additional thrust or drag according to the FMS.

Another promising concept to enable CDOs in busy TMAs consists of enforcing controlled time of arrival (CTA) at one or several metering fixes while keeping the aircraft on a lateral route cleared before the TOD (Muynch *et al.*, 2012). Note that this route could be either a published STAR or a sequence of waypoints uplinked to the FMS by the ground system before the TOD. With this type of flight operations, ATC would assign (using data-link, for instance) at least one CTA to each aircraft, ideally before they reach their TOD, to sequence and merge arrival traffic.

A negotiation process of CTAs via data-link between ATC and FMSs provided with 4D capabilities was proposed by Uebbing-Rumke & Temme (2011) and Oberheid *et al.* (2008). The negotiation process includes the on-board computation (i.e., using accurate models bundled into the FMS) of the earliest and latest achievable CTA at the metering fix (in other words, the feasible time window) for the known lateral route that is to be flown, and the subsequent down-link of this information to the ground automation system. Based on the feasible time window and the surrounding traffic, the ground system replies with the CTA. The received CTA is entered as a required time of arrival (RTA) into the FMS, and then the on-board trajectory planner computes a new (optimal) trajectory plan starting at the current position, while satisfying the RTA and other operational constraints. Then, the resulting trajectory plan is executed by an on-board guidance system with 4D capabilities (De Prins *et al.*, 2007).

Note that, different from TAs and 3D-PAM, the constraints are not in form of altitude and speed instructions at the different waypoints, but purely CTAs. The on-board trajectory planner is who selects the optimal altitude and speed profile such that the applicable CTAs are satisfied. Accordingly, this kind of flight operations are expected to increase the likelihood to generate a trajectory plan at idle thrust that satisfies the CTA requested by ATC, supposed to safely sequence and merge arrival traffic.

Summing up, vertical dispersions of the CDOs trajectories could be mitigated by appropriately selecting the location of the metering fix and conveniently assigning CTAs to each inbound aircraft, while allowing them to follow a pre-negotiated lateral route to completion without ATC interventions. This kind of flight operations, however, require a modernisation of both current ground automation and airborne systems. The focus of this PhD will be in the development of new planning and guidance strategies to accurately and efficiently satisfy CTAs during CDOs.

I.4 Motivation of this PhD

Sections I.4.1 and I.4.2 present the capabilities of current ground automation and on-board trajectory management systems, respectively, and the future needs for the efficient implementation of CDOs subject to CTAs. These future needs drive the motivation of this PhD thesis.

I.4.1 Ground automation

Arrival managers (AMANs) were developed in the late 1990s to provide automated sequencing support for ATC to achieve a smooth, predictable and optimised arrival stream with as few tactical interventions as possible. State-of-the-art AMANs use information from the flight plans, radar tracks, weather data, local airspace structure information, and approximated aircraft performance models to predict trajectories and provide the predicted time of arrival at the different fixes for every flight. Research is currently ongoing into how modern AMANs could also provide support to select appropriate CTAs (Muynch *et al.*, 2012). ATC would be ultimately in charge to provide the CTA to the pilot, who would then use a FMS trajectory management with 4D capabilities to satisfy it.

I.4.2 On-board trajectory management

FMSs were developed in the early 1980s to reduce both workload of the flight crew and flight costs due to their capability to generate trajectory plans minimising fuel and time, as well as to automatically guide the aircraft along that plan by using elevator and throttle commands. In the last decades, a variety of FMSs have been designed to comply with CTAs. Most of these systems, however, have difficulties to satisfy time constraints with an accuracy of 30 s. It should be noted that even this 30 s accuracy is too large for reliable use within the TMA. In 2009, Lenz & Korn (2009) reported that only about 11% of the aircraft flying in the European airspace were equipped with FMS capable of meeting a CTA with an accuracy of 6 s.

Modern FMSs include vertical navigation (VNAV) functions that can compute the optimal trajectory plan for the descent and provide guidance to execute it. Limitations in both planning and guidance capabilities of VNAV, however, have prevented widespread adoption of time-constrained CDOs for operational use (Oseguera-Lohr *et al.*, 2007). For instance, despite modern FMSs have the ability to meet a CTA on cruise, state-of-the-art VNAV functions do not allow pilots to easily perform speed changes during the descent while maintaining the engines at idle.

I.4.2.1 Future needs for on-board trajectory management

An example of concept that overcomes the main issues of current VNAV functionalities is the continuous descent approach for maximum predictability (CDA-MP), developed by Boeing (Garrido-López *et al.*, 2009). This strategy uses a tactical controller to nullify time deviations with the elevator by following a ground speed plan, and operates with the throttle applying small amounts of thrust in order to provide a mean to reduce the energy in the face of disturbances. Since the elevator and the throttle are following, respectively, the ground speed and thrust plans, when the models used by the FMS to generate the trajectory plan do not match the reality (e.g., if the wind forecast is not representative of the actual wind conditions), the aircraft will deviate from the altitude plan. If the aircraft deviates above the plan by more than a predefined threshold, the throttle will revert to idle. Conversely, if the aircraft deviates below the plan by more than a predefined threshold, the thrust will increase to nullify the vertical deviation. This strategy is able to satisfy CTAs while being more fuel-efficient that current VNAV functionalities. If the models used by the FMS were *perfect*, however, the resulting fuel consumption would be higher than that of a CDO performed at idle thrust. In fact, taking into consideration the definition of CDO stated early in this chapter, the trajectory plan computed with the CDA-MP would not be considered a CDO.

The CDA-MP concept assumes that the trajectory plan is computed right after receiving the CTA prior the TOD and that is frozen afterwards, meaning that it is not dynamically updated during the course of the descent. The initial trajectory plan, however, will be actually optimal and its time prediction will be correct only if the models used by the FMS to represent the aircraft dynamics, aircraft performance, and weather are accurate enough. In practise, these models will rarely reproduce the *real world* and are not exempted from errors. In addition, if the deviation from the initial trajectory plan is significant, it might be preferable (in terms of environmental impact) to update the trajectory plan, rather than trying to strictly follow it. Last but not least, in the future trajectory-based ATM paradigm we could envisage ATC updating the CTA once the descent has been initiated, requiring a new trajectory plan after the TOD.

Based on the above discussion, future FMS shall be able to dynamically update the trajectory plan (on-board and in real-time) at any time during the course of the descent, in such a way constraints are satisfied requiring the minimum amount of additional thrust and/or speed-brakes use. For instance, Liu *et al.* (2018) presented a trajectory optimisation algorithm that allows to update the trajectory during the course of a CDO. Similarly, Ramasamy *et al.* (2013) proposed a conceptual design for the next generation of FMSs, which includes 4D trajectory planning and air-to-ground trajectory negotiation functionalities. In this novel prototype of FMS, the optimal trajectory satisfying the negotiated CTAs is computed using direct collocation methods, updating the trajectory with an execution time around 120 seconds, which might not be acceptable for real-time applications considering the typical duration of a descent. Time and energy management concepts have been also investigated in this context, showing very promising results.

I.4.2.2 The time and energy management operations concept

Time and energy managed operations (TEMO) is a trajectory management (planning and guidance) concept that aims to satisfy a CTA at a metering fix by means of only elevator control while keeping, as far as possible, the engines at idle during the whole descent (De Jong, 2014; De Jong *et al.*, 2015). Otherwise, optimal amounts of energy are removed or added by means of thrust or speed brakes, respectively, to satisfy the CTA and applicable operational constraints while minimising the environmental impact. A descent in which the total energy is not increased by means of thrust higher than idle nor removed by using active drag devices is known as *energy-neutral*.

TEMO is a new concept that was developed within the management of trajectory and mission work package of the area of systems for green operations of the Clean Sky European Joint Undertaking research initiative. TEMO is in line with SESAR step 2 capabilities, since it proposes 4D trajectory management and aims to provide significant environmental benefits in the arrival phase without negatively affecting throughput, even in high density and peak-hour operations.

From an ATC point of view, the TEMO concept assumes that the AMAN will use available trajectory information to determine the preferred arrival route, landing sequence, inter-aircraft spacing, and arrival schedule based on the capabilities and constraints of the inbound aircraft, as well as the scheduled airport constraints (such as runway configuration, mixed-use runway use, dependent approaches, and weather conditions). The scheduling process will be coordinated with adjacent ATC centres and, when the schedule is frozen, a fixed area navigation (RNAV) arrival route (to the runway) with CTAs at some metering fixes will be provided. The assigned control times will be entered as RTAs by the on-board TEMO tool-set.

Then, the on-board trajectory planner will compute the optimal trajectory plan such that a given cost function is minimised (typically fuel), while fulfilling the entered RTAs. The trajectory plan is computed by assuming more or less complex models for the aircraft dynamics, aircraft performance and weather conditions. When the models used by the FMS trajectory planning function do not match the reality, the initial trajectory is not longer the most optimal and some operational constraints may even be violated if errors are not nullified by the guidance system.

Several guidance strategies were proposed as a part of the TEMO concept (De Jong *et al.*, 2017, 2015), which working principle will be explained in Section II.3. While all these methods have in common to manage the total energy of the aircraft (altitude and speed) such that CTAs are satisfied in an environmentally friendly way, they differ in the mechanisms implemented to correct time and energy deviations. At present, however, it is still not known which of these guidance strategies is the best in terms of environmental impact mitigation and capability to satisfy operational constraints (of utmost interest CTA).

Initial batch studies of the TEMO concept were done using a conventional laptop to test its feasibility, reaching technology readiness level (TRL)-3 and proving lower fuel consumption and noise levels on ground, if compared with current step-down descents (De Jong *et al.*, 2015). Thereafter, a human-in-the-loop study was performed in a high-fidelity flight simulator to look at human factors aspects, reaching TRL-4 and showing acceptable RTA adherence performance and operational acceptability by qualified pilots (De Jong *et al.*, 2017). Yet, the models used by the trajectory planner were subject to several limitations.

The fast optimizer for continuous descent approaches (FASTOP) project, funded by the CleanSky Joint Undertaking initiative, enhanced that version of the TEMO algorithm in order to test it in more realistic environments, aiming at the TRL-5 gate. The main improvements of the model were the consideration of realistic wind fields, non-standard atmospheres or curved routes. In addition, the TEMO software was redesigned from scratch allowing to use it in real-time on-board applications (Prats *et al.*, 2014, 2015b).

In 2014, a second human in the loop study was performed in the Netherlands Aerospace Centre (NLR) full-motion flight simulator generic research aircraft cockpit environment (GRACE) to test TEMO in a more realistic simulated environment, achieving in this way TRL-5. The design of the experiment and the qualitative assessments gathered from pilots were reported by Bussink *et al.* (2016), while Prats *et al.* (2015a) presented a more detailed description of the trajectory optimisation algorithm and the quantitative results.

In 2015, and aiming at TRL-6, the NLR in cooperation with the Delft university of technology and with the support of the flight operations for novel continuous descents (CONCORDE) consortium, executed some flight trials with a Cessna Citation II research aircraft. Several TEMO guidance variants were tested, including current step-down descents for benchmarking purposes. The preparation of this flight testing campaign was described by Verhoeven *et al.* (2016), and the results were presented by Prats *et al.* (2017).

I.4.2.3 Wind modelling

As mentioned in previous section, the accuracy of the trajectories computed by the FMS, and especially the computation of the estimated time of arrival over a fix in the flight plan, critically depends on the quality of the wind and, to a less extent, temperature data used during the trajectory planning process. Therefore, accurate weather predictions are of utmost importance to generate accurate trajectory plans and minimise the need of corrective actions during the execution of the descent, which typically restrict the accomplishment of energy-neutral descents.

Historically, the flight crew have received the wind forecast prior to the flight from the flight dispatchers, and have manually entered this information into the FMS. At present, in order to simplify operations, wind forecasts can be also up-linked automatically via the aircraft communication and reporting system (ACARS). Typical FMS allow to store these wind data at several waypoints of the flight plan. Yet, at each one of these waypoints, wind data is typically available at only five altitudes. Then, the wind is interpolated between these altitudes and extrapolated beyond the limits when performing FMS trajectory predictions.

The wind data entered to the FMS are primarily based on wind charts from numerical weather prediction (NWP) models. Nowadays, the observations required to initialize NWP models are mainly gathered from radiosondes and aircraft equipped with aircraft meteorological data relay (AMDAR). The spatial distribution of the radiosondes, which are launched only two to four times a day, however, is too coarse, and wind observations gathered through AMDAR are not sufficient because not all aircraft in operation are equipped with such system (Haan, 2010). Due to the relatively low spatio-temporal resolution of the data required to initialize NWP models and the computational burden of running a prediction, wind forecasts are generated over large areas of study only three to eight times per day, and are valid until +6, +12 or +24 hours beyond their issued time. Consequently, the wind forecast for the descent is not tailored for the current as-amended flight plan, and could be several hours old by the time the TOD is reached.

Most flight planning suppliers currently use the world area forecast model (WAFC) that is produced to an ICAO specification by meteorological providers. Other suppliers allow to use higher resolution wind forecasts in the spatial domain, but do not provide a higher update rate due to the time required to uplink the data to the FMS (Bienert & Fricke, 2013). Aiming to increase the update rate of wind forecasts, Boeing developed an advanced weather service that uplinks tailored wind data to the FMS via ACARS (Durham, 2011). This system, however, does not include additional altitudes at which wind data can be stored, but determines the best depending on the prevailing meteorological conditions of the flight plan.

Some studies identified aircraft themselves as a potential network of airborne sensors emitting the sensed wind and temperature to ground receivers (Hollister *et al.*, 1986) or directly to nearby aircraft (De Leege *et al.*, 2013) to provide accurate, high-resolution and up-to-date weather data replacing or complementing the forecasts obtained from NWP models.

I.5 Objectives of this PhD thesis

The optimisation of the trajectory of an aircraft can be formulated as a multi-phase optimal control problem (Bryson & Ho, 1975), which aims at finding the *best* control history (e.g., flight path angle and thrust) such that a given cost function is minimised (e.g., fuel consumption) while satisfying applicable operational constraints (e.g., a CTA). For *real-life* problems, obtaining the analytical solution is seldom. Consequently, most practical implementations transform the continuous optimal control problem into a finite-dimensional nonlinear programming (NLP) optimisation problem (Betts, 2010), which can be solved using standard gradient-based optimisation techniques.

The execution time required to solve the resulting NLP optimisation problem and the robustness of the algorithm, however, are critical aspects that need to be addressed when using these optimisation techniques for on-board applications. A first objective of this PhD thesis is to establish a framework for robust and real-time optimisation of aircraft trajectories, and also to provide guidelines to cope with the most common implementation issues that one's might encounter.

The paradigm of FMS considered in this PhD thesis generates an optimal trajectory plan (on-board and in real-time) whenever either the guidance system requests a trajectory plan update due to, e.g., an excessive time deviation, or the ATC up-links a new CTA. In both cases, the FMS attempts to generate an *energy-neutral* trajectory plan, i.e., correcting eventual deviations and/or adjusting the time of arrival at the metering fix without requiring additional engine thrust and keeping the active drag devices retracted. This might be achieved by using time and energy management concepts, using only elevator control to exchange potential energy by kinetic energy and vice-versa. For instance, if the aircraft had excess of potential energy and needed to arrive earlier than initially planned due to, e.g., a CTA update, altitude could be exchanged by speed by pitching down. The amount of time that can be absorbed or gained by using only elevator control, as a function of the state of the aircraft (i.e., altitude, speed, mass and distance to the metering fix) at the moment of updating the optimal trajectory plan, however, is still unknown. This PhD thesis aims to quantify the performance limits of energy-neutral trajectories.

Any trajectory plan obtained after the optimisation process needs to be executed by the FMS in an uncertain environment, in which the models used to generate the plan are not exempt of errors. Guidance strategies build on time and energy management concepts are very attractive for executing CDOs subject to CTAs in an environmentally-friendly way. To the best of our knowledge, however, a comprehensive comparison of the existing guidance strategies based on time and energy management concepts has not been performed before. An important objective of this PhD is to assess the performance differences across various guidance strategies.

In this PhD thesis, a new guidance strategy is also proposed as a part of the TEMO concept. This strategy is based on an iterative update of the optimal trajectory plan when new measurements of the current state of the aircraft and/or better knowledge of the surrounding environment are available (e.g., an improved wind prediction). This guidance strategy, commonly referred in the literature as model predictive control (MPC) - or nonlinear model predictive control (NMPC) for nonlinear systems - has been in use in the process industries in chemical plants and oil refineries since the 1980s. NMPC guidance strategies typically exploit the fact that the consecutive optimal control problems solved to update the trajectory plan are similar to each other. This allows to initialise the solution procedure efficiently by a suitably shifted guess from the previous trajectory plan, saving considerable amounts of computation time and improving convergence. The similarity of subsequent optimal control problems is even further exploited by strategies that never attempt to iterate the optimisation problem to convergence, and sensitivity-based trajectory updates that use parametric sensitivity information of the previous solution with respect to the uncertain parameters to generate acceptable approximations of the optimal solution quasi-instantaneously. To the best of our knowledge, this is the fist time that NMPC guidance and its sensitivity-based variants are implemented to satisfy time constraints during the descent of an aircraft.

As explained before, one of the most uncertain parameters is the wind that the aircraft will encounter during the execution of the descent. An inaccurate wind forecast will both negatively effect CTA compliance and reduce the environmental benefits of CDO. A lot of research activities on this field are currently conducted, and future air-to-air communications to exchange accurate and up-to-date wind observations are expected to improve the quality of the wind data input to the FMS. The quantitative benefits, in terms of fuel consumption and time and energy deviations at the metering fix, of using wind observations emitted from nearby aircraft to update the trajectory plan in real-time are still unknown. Therefore, this PhD thesis proposes a method to include up-to-date weather observations in the trajectory management process under NMPC guidance, and assesses the benefits of this new concept that combines optimisation and estimation.

Based on the discussions presented so far, the specific objectives of this PhD thesis can be outlined as follows:

- Establish a trajectory management (planning and guidance) framework for the robust optimisation and execution of aircraft descent trajectories, on-board and in real-time.
- Demonstrate the potential applicability of time and energy management concepts by quantifying the feasible time windows at a metering fix of energy-neutral descents subject to last minute CTA updates once the descent has been initiated (i.e., the aircraft has overflown the TOD).
- Perform a comprehensive comparison of guidance strategies build on time and energy management concepts to satisfy CTAs during CDOs flying in an uncertain environment. The set of guidance strategies compared in this PhD thesis includes those already existing in the TEMO concept (i.e., tactical, strategic and hybrid) and the newly proposed NMPC.
- Assess sensitivity-based alternatives to the generic NMPC methodology to overcome its main drawback, namely, the uncertain and in some cases excessive execution time required to update the trajectory plan. These guidance strategies make use parametric sensitivity information from the active optimal trajectory plan to frequently update it quasi-instantaneously.
- Investigate the benefits of combining the NMPC stategy with wind networking concepts (i.e., sharing wind observations between aircraft), in terms of environmental impact and ability to comply with operational constraints. In addition, the sensitivity of the performance metrics to the rate of wind observations received from nearby aircraft will be also quantified.

I.6 Scope and limitations of this PhD thesis

In order to accomplish the objectives of this PhD thesis, the research is subject to several assumptions and limitations that define its scope:

- This PhD thesis only focuses on the on-board systems required to satisfy CTAs during CDOs. Accordingly, it is assumed that the CTAs is provided by an hypothetical ATC through a data-link communications system. Furthermore, the time constraint is computed by an ideal AMAN, which is able to accurately sequence the arrival traffic and ensure sufficient spacing.
- The concept of operations investigated assumes a closed-loop path from the TOD to the runway threshold. Therefore, updates of the optimal trajectory plan due to route changes are not contemplated. Changes of the lateral route, however, could be translated to changes in the distance to go, and use the proposed algorithms with minor modifications.
- All the experiments of this PhD thesis evaluate the best a single aircraft can do given a CTA and route, thus neglecting interaction with surrounding traffic. The potential effectiveness of the proposed planning and guidance algorithms are not investigated through a traffic simulation, and discussions on their benefits in the traffic stream management are not performed.
- Aircraft emissions consist primarily of carbon dioxide (CO_2), nitrogen oxides (NO_x), and methane. Of additional concern are the generation of contrails, the sulphur oxides (SO_x) and the particulate matter (PM). In the recent years, several studies have proposed trajectory optimisation strategies to mitigate the environmental impact of aviation considering some of these factors (see for instance the work performed by Hartjes & Visser (2017)). In this PhD thesis, however, fuel consumption is the only environmental impact metric considered for the optimisation of aircraft trajectories. Yet, airframe noise is indirectly considered in the optimisation algorithm by also minimising the number of speed brakes deployments. In addition, in certain experiments a noise model is used to asses, ad-hoc, the noise footprints of the trajectories.
- The performance assessment of the planning and guidance strategies is done through simulation, which requires an aircraft performance model. All the results presented in this PhD thesis are only valid for the Airbus A320, which represents the vast majority of worldwide narrow-body commercial aircraft. The proposed planning and guidance algorithms, however, are generic enough to consider different aircraft types by adopting the corresponding performance model.
- It it assumed that speed brakes and throttle are the only mechanisms to remove and add energy from the system to correct disturbances, respectively. Despite flaps and gear might be more efficient than deploying speed brakes or decreasing the thrust, they have not been considered in this PhD thesis as means to control the energy rate of the aircraft. In spite of that, they have been modelled in some experiments to represent realistic approaches.
- The trajectory optimisation problem tackled in this PhD involves nonlinear constraints and/or cost function and is, in consequence, a non-convex optimisation problem. This means that several local minima may exist. Since global optimisation algorithms require a high computational burden, they are prohibited for real-time applications such as the on-board generation of optimal trajectory plans when using NMPC guidance. Thus, the proposed trajectory optimisation techniques involve the use of local optimisation algorithms.
- Contingencies, such as downgraded guidance or engine failure, are not considered in the experiments. In other words, normal operations are assumed in all the experiments.

I.7 Outline of this PhD thesis

The present document is organised in seven chapters, which are summarised as follows. It is worth noting that a broad state-of-the-art of the main topics addressed in this PhD thesis has been presented before. A deeper and more specific state-of-the-art for each individual topic is included at the beginning of the chapter that addresses it.

- **Chapter II** presents a detailed framework for trajectory management, which includes optimisation techniques to generate optimal trajectory plans in real-time, and various guidance strategies to execute the resulting plans using time and energy management concepts.
- **Chapter III** quantifies the feasible time window for energy-neutral CDO trajectories as a function of the altitude and distance to go; and analyses the sensitivity of the feasible time window to different winds, metering fix position, aircraft masses, and initial speeds.
- **Chapter IV** compares the performance of four guidance strategies designed to satisfy time constraints during a continuous descent operation: tactical, strategic, hybrid and NMPC.
- **Chapter V** proposes two variants of the generic NMPC guidance strategy that rapidly update the optimal trajectory plan by using parametric sensitivities of the active trajectory plan. Then, the performance of these two variants are compared with those of an ideal NMPC, which updates the optimal trajectory plan instantaneously at each re-calculation instant, as well as those of the open-loop execution of the initial trajectory plan computed before the TOD.
- **Chapter VI** assesses the benefits, in terms of environmental impact and CTA compliance, of combining the NMPC guidance strategy with wind networking concepts to generate accurate and up-to-date wind predictions on-board before updating the optimal trajectory plan.
- **Chapter VII** gives the conclusions that are drawn from this work and points out some future work that could be done in the direction of the presented research.

When everything seems to be going against you, remember that the airplane takes off against the wind, not with it.

— Henry Ford

The proper use of science is not to conquer nature but to live in it.

— Barry Commoner

II

Framework on trajectory management

Flight management systems (FMSs) emerged as a part of the standard avionics suite on Boeing 757 and 767 aircraft in the early 1980s (Liden, 1994). From that point on, FMSs became a standard in all new aircraft. FMSs represented a revolutionary advance in the management of a flight, reducing both workload of the flight crew and cost of flight for the airline due to its capability to generate and automatically execute trajectory plans minimising fuel and time according to certain optimisation criteria. The birth of FMSs also allowed high flexibility in the avionics functionalities and opened the door to design new operational concepts, such as these addressed in this PhD.

One of the main tasks of a FMS is to generate the trajectory plan that is to be subsequently flown. The trajectory plan is decomposed in a lateral route (sequence of waypoints) and a vertical profile (time histories of the altitude and speed). Since this PhD thesis assumes an operational concept in which the lateral route is fixed and only the vertical profile is managed to satisfy controlled time of arrivals (CTAs), the concept of *trajectory plan* will refer only to the vertical profile.

In current FMSs, the trajectory plan is constructed by numerical integration of the differential equations of the mathematical model describing the dynamics of the aircraft. This numerical integration starts at the current state of the aircraft, applying the appropriate flight intents or controls, using certain aircraft performance and weather models, and satisfying the operational constraints entered at the different waypoints of the lateral route. In order to be optimal, the trajectory plan is generated by using *economic* speeds and altitudes stored in pre-computed look-up tables as a function of the cost index (CI) and other flight parameters. Even if some modern FMSs are also able to satisfy CTAs by using brute force (they iterate with the CI to obtain different speed profiles, and therefore times of arrival, until the CTA is satisfied), the trajectory plan for the descent is typically computed and frozen before the top of descent (TOD), meaning that updates of the optimal trajectory plan are not allowed once the descent has started Airbus (1993).

Future FMSs, capable to optimally plan and execute continuous descent operations (CDOs) subject to CTAs, will require on-board trajectory planning algorithms capable to rapidly generate, in real-time, the optimal trajectory plan complying with entered required time of arrivals (RTAs) and typical operational constraints. Future FMSs will also require a guidance system capable to satisfy RTAs in the most environ-

mentally friendly way, even in presence of modelling errors during the planning process.

Section II.1 presents the models considered in the formulation of the trajectory optimisation problem in this PhD thesis. Note that, depending on the specific goal of each experiment conducted in this PhD thesis, these models will be adapted in the following chapters according to appropriate assumptions. Section II.2 formulates the generic optimal control problem, which objective function and constraints will be also particularised later on for each experiment, and then presents a numerical method to solve it. Finally, the working principle of the existing time and energy managed operations (TEMO) guidance strategies, as well as the nonlinear model predictive control (NMPC) variants proposed in this PhD thesis, are described in Section II.3.

II.1 Models needed for trajectory management

An aircraft can be represented as a system composed by several states, which evolve according to a set of nonlinear ordinary differential equations (ODEs) given some control inputs or, more generally, flight intents in the form of algebraic constraints, which transform the ODEs system into a system of differential algebraic equations (DAEs). In turn, this model for the aircraft dynamics must be particularised with certain models for the aircraft performance and the weather, respectively. The aircraft dynamics, performance and weather models are thoroughly described in the following sections.

II.1.1 Aircraft dynamics model

The motion of an aircraft can be described with a six degrees of freedom model (Nelson, 1998), where the derivative equations of the three translations and the three rotations of the aircraft can be integrated along the time. Although this methodology results in the most accurate planning of the aircraft trajectory, it requires an extensive aerodynamic and propulsive model and the knowledge of the inertia tensor of the aircraft. Due to the complexity of this model, many trajectory predictors used in some air traffic management (ATM) applications use basic kinematic models that directly model the path characteristics of the aircraft, without attempting to model the underlying physics (Bilimoria *et al.*, 2000). Somewhere in between these two approaches lie the aircraft point-mass model (Hull, 2007), a kinetic approach that is considered accurate enough for on-board trajectory planning and the majority of ground-based ATM applications.

In a point-mass model, the aircraft motion is reduced to three degrees of freedom (the three translations), assuming that all forces are applied to the centre of gravity of the aircraft. Thus, there is no need to model its inertia tensor or stability control loops (considered as higher order dynamics) and only the aerodynamic, propulsive, and external forces (e.g., due to the gravity) must be modelled. This approach is adopted in all the experiments conducted in this PhD thesis:

$$\frac{\mathrm{d}v}{\mathrm{d}t} = \dot{v} = \frac{T - D(v,h,s,C_L,\beta)}{m} - g\sin\gamma \tag{II.1a}$$

$$\frac{\mathrm{d}\gamma}{\mathrm{d}t} = \dot{\gamma} = \frac{g}{v}\left(\frac{L(v,h,s,C_L)}{mg} - \cos\gamma\right) \tag{II.1b}$$

$$\frac{\mathrm{d}h}{\mathrm{d}t} = \dot{h} = v\sin\gamma \tag{II.1c}$$

$$\frac{\mathrm{d}s}{\mathrm{d}t} = \dot{s} = \sqrt{v^2\cos^2\gamma - w_x^2(h,s)} + w_s(h,s) \tag{II.1d}$$

$$\frac{\mathrm{d}m}{\mathrm{d}t} = \dot{m} = -q(v,h,s,T), \tag{II.1e}$$

where the state vector $\vec{x} = [v, \gamma, h, s, m]^T$ is composed, respectively, by the true airspeed (TAS), the aerodynamic flight path angle, the geometric altitude, the distance to go and the mass of the aircraft; the control vector $\vec{u} = [T, \beta, C_L]^T$ is composed, respectively, by the total thrust force of the engines, the speed brakes deflection and the lift coefficient; D is the aerodynamic drag force; L is the aerodynamic lift force; q is the nominal fuel flow; w_x and w_s are, respectively, the cross and longitudinal wind components; and g is the local gravity acceleration. Remember that in the notation adopted in this PhD thesis, $(\cdot)^T$ represents the transpose of $(\cdot)$.

It should be noted that a flat, non-rotating earth with a constant gravity acceleration has been assumed to derive Eq. (II.1). Moreover, the sideslip angle and angle of attack have been neglected, being the sum of all propulsive forces a single thrust vector along the longitudinal axis of the aircraft. Finally, the vertical component of the wind has been also neglected because it is typically orders of magnitude below that of the horizontal component.

The aerodynamic forces (lift and drag) in Eq. (II.1) are commonly modelled as:

$$L(v,h,s,C_L) = \frac{1}{2}\sigma(s,h)\rho_{SSL}v^2SC_L \tag{II.2a}$$

$$D(v,h,s,C_L,\beta) = \frac{1}{2}\sigma(s,h)\rho_{SSL}v^2SC_D(v,h,s,C_L,\beta), \tag{II.2b}$$

where σ is the normalised density of the air, ρ_{SSL} is the density of the air at standard sea level (SSL), S is the wing surface area, and C_D is the drag coefficient.

For practical reasons (such as requirements to speed up the algorithms) several simplifications can be done in the mathematical representation of the equations describing the aircraft dynamics (Eq. (II.1)). In general, the more complex (and typically accurate) the model is, the larger the number of nonlinearities in the model and the more execution time required to solve the trajectory optimisation problem. As a result, the trade-off between accuracy and execution time must be considered when selecting an appropriate aircraft dynamics model for real-time trajectory optimisation purposes. For this reason, each chapter of this PhD thesis considers a different variant of Eq. (II.1), depending on the specific implementation needs.

The thrust control is typically bounded by the idle (or minimum) thrust (T_{idle}), and maximum thrust (T_{max}) of the particular aircraft type. Similarly, bounds on the remaining controls, C_L and β, are also enforced to ensure that the aircraft remains within its operational limits. Generally speaking, the drag coefficient, the maximum and minimum thrust, the maximum lift coefficient, the nominal fuel flow, and the fuel flow when the engines operate at idle (q_{idle}) are functions of the state and/or control variables. The complexity of these mathematical expressions depends on the adopted aircraft performance model (APM).

II.1.2 Aircraft performance model

An APM particularises the expressions for C_D, T_{max}, T_{idle}, q and q_{idle} as a function of $\vec{x}$ and/or $\vec{u}$. The accuracy of the APM is of crucial importance if one aims at computing realistic trajectories and thus obtain representative results. Without going any further, the fuel flow function will be used to determine the total fuel consumption, which will be used, in turn, to support investment decisions in many assessments of new ATM systems and concepts of operations.

Generally speaking, the drag coefficient depends on C_L (induced drag), Mach number (M) (effects of air compressibility), and to a lesser extent, the altitude (effects of air temperature on the Reynolds Number). The drag coefficient will also change if speed brakes are applied, the gear ($\eta \in \{0,1\}$) is deployed or the aircraft is configured with flaps/slats (ζ). These gear status and flaps/slats configurations could be either considered as additional controls (i.e., $\vec{u} = [T, \beta, C_L, \eta, \zeta]$) or modelled as a function of the state vector.

Another alternative widely used to reduce the nonlinearities of the model consists to split the descent in several phases, where each phase is particularised with a different model for the C_D, q, T_{min} and T_{max}. The formulation of multi-phase optimal control problems, where each phase could have a different aircraft dynamics and/or performance model, will be described in Section II.2.2.

For low subsonic flight (Mach approximately below 0.6) the effects of Mach and altitude in the drag coefficient can be neglected, leading to the well-known drag polar, which is composed by a constant term plus a quadratic term function of the square of the lift coefficient:

$$C_D(C_L,\beta,\eta,\zeta) = C_{D0}(\beta,\eta,\zeta) + C_{D2}(\beta,\eta,\zeta)C_L^2, \tag{II.3}$$

where C_{D0} and C_{D2} are the parasite and induced drag coefficients, respectively, which depend on the status of the landing gear, the flaps/slats configuration and the speed brakes deflection. Typical airliners, however, operate in the range between approximately Mach 0.60-0.85 for most of the flight. Thus, compressibility effects on drag coefficient cannot be neglected and models more elaborated than Eq. (II.3) need to be considered to generate realistic trajectories.

Regarding the idle and maximum thrust, these functions essentially depend on the Mach number and the outside air temperature and pressure conditions. Similarly, nominal fuel flow depends on thrust, Mach number and outside air temperature and pressure.

Several APMs can be used to model these aerodynamic and propulsive functions, from simple linear interpolations with look-up tables coming directly from experimental or simulated data, to more or less sophisticated mathematical approximations that fit these data. For instance, Dalmau & Prats (2015) approximated aerodynamic and propulsive data from the manufacturer with polynomial functions, while Betts (2010) approximated similar kinds of data with tensor product spline functions (de Boor, 1972). Both methods will be used in this PhD thesis.

Another example of APM used in many ATM applications, such as air traffic control (ATC) simulation purposes, is the Eurocontrols's base of aircraft data (BADA) v3. In BADA v3, the drag coefficient is modelled with Eq. (II.3), thus neglecting compressibility effects, the thrust limits are only given as a function of altitude, and the fuel flow depends on the true airspeed and thrust. It is well-known that BADA v3 was designed to model aircraft performance and fuel consumption in nominal flight conditions, and several studies have already revealed that is not accurate enough to derive correct fuel consumption figures in the terminal maneouvering area (TMA) (Senzig *et al.*, 2009; Senzig & Fleming, 2009). In particular, it has been reported that BADA v3 model tends to underestimate fuel flow in idle conditions. The newly developed BADA v4 was designed as a realistic, accurate, and complete APM that overcomes the main limitations of BADA v3 (Poles *et al.*, 2010). BADA v4 will be also used in this PhD thesis.

It is out of the scope of this PhD thesis to review and assess the accuracy of existing APMs. Yet, it is very important to remark the importance of having representative APMs when aiming to compute accurate trajectory plans and time predictions. For instance, Slater (2009) showed the importance to accurately model idle thrust and drag coefficient functions when generating trajectory plans for the descent phase. In the same context, Casado *et al.* (2013) proposed a methodology to assess the impact of uncertainties in the coefficients of parametric models such as BADA (i.e., models defined my mathematical functions which depend on several coefficients) on the accuracy of the computed trajectory plan.

II.1.3 Weather model

The ground speed of the aircraft is greatly influenced by the wind field. Moreover, the performance of the aircraft notably depends on the temperature and pressure of the air. For instance, during a 20 minutes climb, temperature errors of 1.5 K throughout the climb would produce an altitude prediction error around 500 ft (Forester & Dharssi, 1992), and a difference of 12 kt in the ground speed would result in an estimated time of arrival deviation of 5%, assuming an original ground speed of 250 kt (Robert & De Smedt, 2013). Moreover, the ground speed not only depends on the longitudinal and cross winds, as shown in Eq. (II.1d), but also on temperature if the aircraft is flying at a constant Mach number, or on temperature and pressure if it is following a constant callibrated airspeed (CAS). As shown by Chatterji *et al.* (1996), ground speed sensitivity is around 1.1 knot per K for typical cruise conditions, where aircraft operate at constant Mach number. Therefore, an accurate weather model will definitely reduce the number of corrective actions required to nullify altitude, time and/or speed deviations from the trajectory plan. Last but not least, the trajectory plan is optimal only for the weather conditions considered in the weather model. Thus, if the weather model does not accurately reproduce the actual wind, temperature and pressure conditions, the executed trajectory will not be the most optimal achievable.

Typically, trajectory planning tools assume the international standard atmosphere (ISA) model (ICAO, 1993), which is representative of an ideal atmosphere based on the thermodynamic equation, as defined by the International Civil Aviation Organization (ICAO). In the ISA model, the normalised temperature of the air (θ) decreases at a constant lapse rate of $\lambda_h = 6.5\,\mathrm{K\,km^{-1}}$ from standard sea level (where the ISA temperature is $\tau_{SSL} = 288.15$ K) up to the altitude of the tropopause, which ISA value takes $h_{11} = 36,000$ ft. Above the tropopause, the temperature is considered constant with a value of $\theta_{11} = 0.732$ up to 65,600 ft (well above the typical altitudes where commercial aircraft operate):

$$\theta(h) = \begin{cases} 1 - \frac{\lambda_h}{\tau_{SSL}} h & \text{if } h \leq h_{11} \\ \theta_{11} & \text{if } h > h_{11}. \end{cases} \tag{II.4}$$

By combining this linear model with the hydrostatic equation, the expression of the normalised pressure (δ) as a function of the altitude can be easily obtained:

$$\delta(h) = \begin{cases} \theta(h)^{\frac{g}{\lambda_h R}} & \text{if } h \leq h_{11} \\ \delta_{11} e^{\frac{g\tau_{SSL}}{R\theta_{11}}(h_{11}-h)} & \text{if } h > h_{11}, \end{cases} \tag{II.5}$$

where $R = 287.058$ Jkg K^{-1} is the specific gas constant for dry air, $\delta_{11} = 0.224$ is the normalised pressure of the air at the tropopause, and $p_{SSL} = 1013.25$ hPa is the pressure at standard sea level. Finally, given the normalised temperature and normalised pressure values, the normalised air density can be obtained by using the perfect gas law relationship:

$$\sigma(h) = \frac{\delta(h)}{\theta(h)}. \tag{II.6}$$

The ISA model is just a theoretical representation of the atmosphere. In practise, due to temperature inversions, as well as additions or decrease of moisture, the actual atmosphere will have lapse rates and standard conditions at sea level different from those of ISA. Non-standard conditions are often modelled by adding a specified temperature offset to the standard temperature at SSL (the well-known ISA+ΔT). However, pressure is not recalculated at the non-standard temperature because temperature effects on it are considered to be much less important than the effect of altitude. In spite of that, non-standard conditions for the pressure can be also modelled by considering a p_{SSL} different from 1013.25 hPa.

It should be noted that the ISA model is not the only existing reference for temperature and pressure profiles. The United States department of defense standard MIL-STD-210C and its successor standard MIL-HDBK-310 also define temperature models for use as references of hot day, cold day, tropical, and polar temperature profiles. Figure II-1(a) compares different standard temperature profile models.

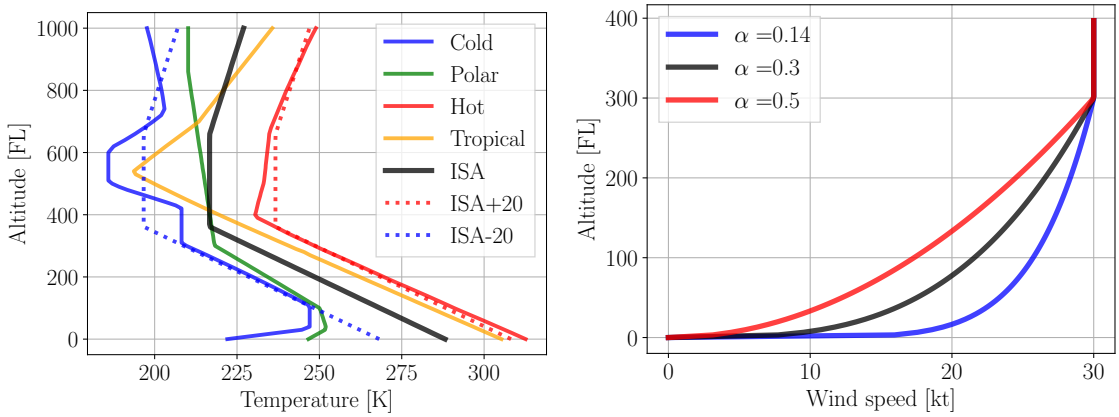

(a) Standard temperature profile models

(b) Empirical wind models (Hellmann model)

Figure II-1: *Theoretical and empirical weather models*

Realistic temperature and pressure data, as a function of the geopotential altitude[1] and geographical location (latitude and longitude) for different time stamps, can be obtained from weather forecasts and analysis generated by numerical weather prediction (NWP) models. At present, there exist several NWP which provide weather forecasts and analysis with a variety of resolutions, accuracies and look-ahead times. To give a couple of examples, the global forecast system (GFS) is a NWP developed and maintained by the National Oceanic and Atmospheric Administration (NOAA) that covers the entire globe with an horizontal resolution of 28 km and look-ahead forecast times up to 192 hours; while the rapid refresh (RAP) covers a limited region (North America), but has an horizontal resolution of 13 km and forecast look-ahead times going out 18 hours. These data in gridded format can be interpolated to obtain the weather information at specific geographical coordinates and altitudes or approximated with continuous functions of various complexity, such as polynomials or splines. The RAP model will be used in this PhD thesis.

[1]For typical aircraft altitudes, the gravity variations at different altitudes can be neglected. Thus geopotential altitudes, which are typically used in weather models, and geometric altitudes are assumed to be the same.

Note that since in the concept of operations tackled in this PhD thesis the lateral route (sequence of waypoints) is known before generating the optimal vertical profile, realistic air temperature and pressure models will be essentially function of the altitude and distance to go.

A similar rationale is adopted to model the wind field. Simple models used for academic purposes assume constant wind speed and direction throughout the descent, independently of the geographical location and altitude. In practise, however, wind speed tends to increase with the altitude. This typical behaviour can be represented using various empirical and theoretical models, from linear functions to more or less complex mathematical expressions. An example of empirical model for the total wind speed ($|\vec{w}|$), which assumes constant longitudinal wind above a reference altitude (h_r) is the well-known Hellmann exponential law:

$$|\vec{w}|(h) = \begin{cases} w_r & \text{if } h > h_r \\ w_r \left(\frac{h}{h_r}\right)^{\alpha} & \text{if } h \leq h_r, \end{cases} \tag{II.7}$$

where w_r is a known wind speed at h_r. The Hellmann exponent (α) depends on many factors, such as the coastal location, the shape of the terrain on the ground, and the stability of the air. Figure II-1(b) shows the Hellmann exponential law for different values of α, fixing w_r to 30 kt and h_r to FL300.

State-of-the-art weather forecasts obtained from NWPs typically provide the wind vector at different altitudes and geographical locations. These forecasts decompose the wind vector in north component (w_n), east component (w_e) and vertical component. Again, since the route is known beforehand in this PhD thesis, the bearing between consecutive waypoints of the route is also known, and the wind field can be projected to along-track and cross-track wind components as a function of the altitude and distance to go:

$$w_s(h,s) = w_n(h,s)\cos\chi_g(s) + w_e(h,s)\sin\chi_g(s) \tag{II.8a}$$
$$w_x(h,s) = -w_n(h,s)\sin\chi_g(s) + w_e(h,s)\cos\chi_g(s), \tag{II.8b}$$

where χ_g is the track angle, a known function of the distance to go.

In should be noted that the temporal variations of temperature, pressure and wind components are neglected in this PhD thesis because the duration of a descent is small if compared with the time scale of typical atmosphere dynamics. In addition, the trade-off between additional complexity (thus execution time) of the model and accuracy of the resulting trajectories is not appealing. Yet, readers interested on the extension of the model that considers temporal variations of the weather variables could consult the model proposed by Prats *et al.* (2014).

For each of the experiments conducted in this PhD thesis, the expressions for δ, θ, w_s and w_x will be particularised as a function of h and s, either with mathematical expressions approximating realistic weather data from NWP forecasts or using empirical or theoretical models.

II.2 Optimal trajectory planning

As mentioned before, the optimisation of the vertical profile of an aircraft trajectory can be formulated as a multi-phase, constrained optimal control problem (Soler *et al.*, 2015). The formulation of a generic optimal control problem is presented in Section II.2.1. Since the trajectory optimisation problem tackled in this PhD thesis cannot be solved analytically due to the nonlinearity and complexity of the constraints and cost function, a discretisation approach is presented in Section II.2.2 to solve it numerically.

II.2.1 Optimal control problem formulation

An optimal control problem for a generic system during a fixed or variable continuous time horizon $[t_I, t_F]$ can be formulated as follows (Bryson & Ho, 1975):

$$
\begin{aligned}
\min_{\vec{u}(t)} \quad & J := \phi\left(\vec{x}(t_F), \vec{d}\right) + \int_{t_I}^{t_F} \pi\left(\vec{x}(t), \vec{u}(t), \vec{d}\right) \mathrm{d}t \\
\text{s.t} \quad & \vec{x}(t_I) = \vec{X} \\
& \dot{\vec{x}} = \vec{f}\left(\vec{x}(t), \vec{u}(t), \vec{d}\right) \\
& \vec{b}^{in}\left(\vec{x}(t), \vec{u}(t), \vec{d}\right) \leq 0 \\
& \vec{b}^{eq}\left(\vec{x}(t), \vec{u}(t), \vec{d}\right) = 0 \\
& \vec{\psi}\left(\vec{x}(t_F), \vec{d}\right) = 0,
\end{aligned}
\tag{II.9}
$$

where $\vec{x} \in \Re^{n_x}$ is the vector of differential states, $\vec{u} \in \Re^{n_u}$ is the vector of controls, and $\vec{d} \in \Re^{n_d}$ is the vector of fixed parameters of the model. The cost function $J : \Re^{n_x} \times \Re^{n_u} \times \Re^{n_d} \to \Re$, which is composed by a running cost (or Lagrange term) $\pi : \Re^{n_x} \times \Re^{n_u} \times \Re^{n_d} \to \Re$ and an end cost (or Mayer term) $\phi : \Re^{n_x} \times \Re^{n_d} \to \Re$, is to be minimised subject to: dynamic constraints $\vec{f} : \Re^{n_x} \times \Re^{n_u} \times \Re^{n_d} \to \Re^{n_x}$ in the form of ODEs with initial conditions $\vec{X} \in \Re^{n_x}$, algebraic constraints $\vec{b}^{eq} : \Re^{n_x} \times \Re^{n_u} \times \Re^{n_d} \to \Re^{n_{b^{eq}}}$, inequality path constraints $\vec{b}^{in} : \Re^{n_x} \times \Re^{n_u} \times \Re^{n_d} \to \Re^{n_{b^{in}}}$, and terminal constraints $\vec{\psi} : \Re^{n_x} \times \Re^{n_d} \to \Re^{n_\psi}$ enforced only at t_F.

In some applications, free parameters that, in contrast to the controls, are constant in time might be also included as a part of the decision variables. For instance, when the final time is fixed, t_F is a known and fixed parameter. For optimal control problems with variable final time, however, t_F becomes a new decision variable to be optimised, in addition to $\vec{u}(t)$.

It should be noted that the vector of fixed parameters of the model ($\vec{d}$), however, is not part of the decision variables and, consequently, must be chosen by the user and remains constant during the whole optimisation process. Yet, it might change for different problems. For instance, parameters that could be included in $\vec{d}$ are the coefficients α, w_r, and h_r of Eq. (II.7) if the Hellmann model were considered.

The optimal control problem described by Eq. (II.9) assumes that the same running cost, dynamic constraints and algebraic and path constraints apply during the whole time horizon. In addition, event constraints can be set only at the very end of the time horizon. Yet, many *real-life* processes can be divided into several phases (or stages), where the dynamics of the system, the running cost and the algebraic and path constraints might change. In addition, in some particular applications it is necessary to formulate interior-point constraints between two consecutive phases. Even in some applications, it could be desirable to define different states and controls vectors for each phase. In this PhD thesis, different phases could have different algebraic, path and interior-point constraints, yet they must have the same number of differential dynamic constraints, because it has been assumed that the state vector is identical in all phases.

In order to extend the optimal control problem of Eq. (II.9) to multiple phases, let the time horizon $[t_I, t_F]$ be divided into P known intervals $[t_j, t_{j+1}]$, with $j = 0, \ldots, P-1$. Note that $t_0 = t_I$ and $t_P = t_F$. Each one of these intervals corresponds to a different phase. The generic multi-phase optimal control problem defined over P phases can be formulated as:

$$
\begin{aligned}
\min_{\vec{u}(t)} \quad & J := \sum_{j=0}^{P-1} \left(\phi_j\left(\vec{x}(t_{j+1}), \vec{d}\right) + \int_{t_j}^{t_{j+1}} \pi_j\left(\vec{x}(t), \vec{u}(t), \vec{d}\right) \mathrm{d}t \right) \\
\text{s.t} \quad & \vec{x}(t_0) = \vec{X} \\
& \dot{\vec{x}} = \vec{f}_j\left(\vec{x}(t), \vec{u}(t), \vec{d}\right);\ j = 0, \ldots, P-1 \\
& \vec{b}_j^{in}\left(\vec{x}(t), \vec{u}(t), \vec{d}\right) \leq 0;\ j = 0, \ldots, P-1 \\
& \vec{b}_j^{eq}\left(\vec{x}(t), \vec{u}(t), \vec{d}\right) = 0;\ j = 0, \ldots, P-1 \\
& \vec{\vartheta}_j^{eq}\left(\vec{x}(t_{j+1}), \vec{d}\right) = 0;\ j = 0, \ldots, P-2 \\
& \vec{\vartheta}_j^{in}\left(\vec{x}(t_{j+1}), \vec{d}\right) \leq 0;\ j = 0, \ldots, P-2 \\
& \vec{\psi}\left(\vec{x}(t_P), \vec{d}\right) = 0,
\end{aligned}
\tag{II.10}
$$

where $\vec{f}_j : \Re^{n_x} \times \Re^{n_u} \times \Re^{n_d} \rightarrow \Re^{n_x}$ and $\pi_j : \Re^{n_x} \times \Re^{n_u} \times \Re^{n_d} \rightarrow \Re$ are the differential dynamic constraints and running cost of the j^{th} phase, respectively. Similarly, $\vec{b}_j^{eq} : \Re^{n_x} \times \Re^{n_u} \times \Re^{n_d} \rightarrow \Re^{n_{b_j^{eq}}}$ and $\vec{b}_j^{in} : \Re^{n_x} \times \Re^{n_u} \times \Re^{n_d} \rightarrow \Re^{n_{b_j^{in}}}$ are the algebraic and path constraints, respectively, of the j^{th} phase; and $\vec{\vartheta}_j^{eq} : \Re^{n_x} \times \Re^{n_d} \rightarrow \Re^{n_{\vartheta_j^{eq}}}$ and $\vec{\vartheta}_j^{in} : \Re^{n_x} \times \Re^{n_d} \rightarrow \Re^{n_{\vartheta_j^{in}}}$ represent applicable equality and inequality interior-point constraints, respectively, applying at the last time of the j^{th} phase.

When dealing with mutli-phase optimal control problems, a new set of constraints is added to link the state variables across two consecutive phases and guarantee continuity in the solution:

$$\vec{x}(t_{j+1}^{+}) - \vec{x}(t_{j+1}^{-}) = 0;\ j = 0, \dots P-2. \tag{II.11}$$

Analogously to the single-phase optimal control problem, for multi-phase optimal control problems the final time of each phase could be either a known parameter or a decision variable to be optimised. For instance, if only the final time of the whole time interval were fixed (e.g., due to a CTA) but the duration of each phase were flexible, t_P would be a known parameter and t_{j+1}, $j = 0, \dots, P-2$, additional decision variables of the optimisation problem, in addition to $\vec{u}(t)$.

Basically, two different methods are available for solving optimal control problems:

- **Indirect methods**: consist of first deriving the necessary conditions for optimality in an analytical way, and then solve them numerically by using root-finding solvers and ODE integrators. These methods are commonly referred in the literature to *optimise-then-discretise*.
- **Direct methods**: consist of first discretising the time history of the controls and/or states to transcribe infinite-dimensional optimal control problem Eq. (II.9) into a finite-dimensional nonlinear programming (NLP) optimisation problem, and then attempt a direct numerical solution. These methods are commonly referred in the literature to *discretise-then-optimise*.

In turn, indirect methods can be further classified into single-shooting and multiple-shooting, while the direct methods can be divided into single-shooting, multiple-shooting and collocation (see Fig. II-2). An excellent review of these methods was performed by Andersson (2013), illustrating the working principle of them by introducing a simple, yet industrially relevant optimal control problem. Prats (2010) also described the main features and the trade-offs of each method, in terms of complexity and computational burden, from a more practical perspective.

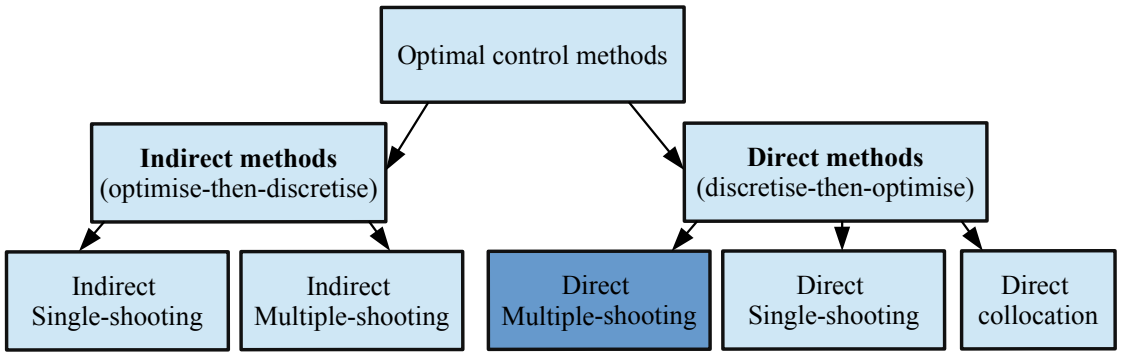

Figure II-2: *Methods to solve optimal control problems*

The major drawback of indirect methods is the requirement for a detailed mathematical analysis of each single optimal control problem. Even small changes in the definition of the constraints can lead to a completely different solution, often requiring a complete derivation of the necessary conditions for optimality. These methods also require a very accurate initial guess for the *adjoint* variables. These variables, however, do not have any physical meaning, and the optimal solution is highly sensitive to even small changes of them (Prats, 2010). Last but not least, including path inequality constrains in the formulation of the optimal control problem can be prohibitely difficult when using indirect methods. For these reasons, they were not implemented in this PhD thesis.

Direct methods are much easier to set up, if compared with the indirect ones, and allow to solve very complex problems with a minimum effort of mathematical analysis. Using direct methods, the whole time horizon is divided into several time intervals, and the control vector is parameterised with a low order polynomial on each interval (e.g., a piecewise constant control).

In direct single-shooting, the initial state vector ($\vec{X}$) is propagated forward in time from t_I to t_F by integrating the differential equations ($\vec{f}$) with ODE/DAE integrators. As a result, the state vector at t_F becomes a function of the parametrised controls on each interval and the initial state vector. The integral of the running cost (π) is also calculated to evaluate the cost incurred during the whole time horizon, which is to be minimised. Then the value of the terminal constraint ($\vec{\psi}$) is evaluated and, by using a NLP optimisation algorithm, the parametrised controls and the initial state vector are adjusted in order to satisfy it. In other words, with the single-shooting approach, only the time history of the controls is parametrised, eliminating the state variables with ODE/DAE integrators. This method is effective for problems that are either simple or have an extremely good initialisation. The main drawback of direct single-shooting is that the objective and constraint are highly nonlinear dependent on $\vec{u}$, thus slowing down the convergence of the NLP solution (Andersson, 2013). In addition, if a *guess* for the state variables is available, e.g., from a previously computed trajectory, it cannot be used to initialise and speed-up the solution.

Multiple-shooting methods address these issues by including the state trajectory in the NLP, essentially breaking the problem into shorter steps. The working principle of multiple-shooting consists on parametrising not only the controls, but also the state vector at the beginning of each interval. On each interval, the initial state vectors can be propagated to the beginning of the next one by integrating the differential equations with ODE/DAE integrators. As a result, the state vector at the end of each interval becomes a (nonlinear) function of the state and control vectors at its beginning. The discretised state vectors could be pieced together to form a continuous trajectory if and only if their values match at the junction points. The discontinuities at the junction points, called *defects*, are included in the constraints vector as a system of nonlinear equations that depend on the parametrised states and controls. Finally, the resulting finite-dimensional optimisation problem is solved by using standard NLP optimisation algorithms. A deep analysis on the proprieties of direct shooting methods was performed by Gath (2002) and Bulirsch *et al.* (1993). In this PhD thesis, this approach was selected to solve the trajectory optimisation problem.

For a detailed explanation of the remaining direct collocation methods, the reader is referred to Betts (2010). The main difference between direct collocation and multiple-shooting methods is that the former perform an implicit integration of the dynamic system on each time interval, while multiple-shooting methods use explicit integration formulas, such as Euler or Runge-Kutta. One of the major advantages of using multiple-shooting methods, if compared to direct collocation, is the possibility of running them with ODE integrators that include step-size control techniques, resulting in an algorithm almost independent of the discretisation grid that will, if it converges, at least deliver a suboptimal solution Gath (2002). A very interesting survey on existing optimal control software packages was performed by Virtanen *et al.* (1999).

II.2.2 Direct multiple-shooting formulation

Let the continuous time horizon $[t_I, t_F]$ of Eq. (II.9) be discretised into $N+1$ equidistant time samples τ_k, with $k = 0, \ldots, N$. Note that $\tau_0 = t_I$, $\tau_N = t_F$ and the discretisation step is $\Delta\tau = {}^{(\tau_N - \tau_0)}/_{N}$. The optimal control problem discretised by using direct multiple-shooting methods and minimising J in a time horizon of N time intervals can be formulated as:

$$
\begin{aligned}
\min_{\substack{\vec{x}_k, k=0,\ldots,N \\ \vec{u}_k, k=0,\ldots,N-1}} \quad & J := \phi\left(\vec{x}_N, \vec{d}\right) + \sum_{k=0}^{N-1} \Pi\left(\vec{x}_k, \vec{u}_k, \vec{d}, \Delta\tau\right) \\
\text{s.t} \quad & \vec{x}_0 = \vec{X} \\
& \vec{x}_{k+1} = \vec{F}\left(\vec{x}_k, \vec{u}_k, \vec{d}, \Delta\tau\right);\ k = 0, \ldots, N-1 \\
& \vec{b}^{in}\left(\vec{x}_k, \vec{u}_k, \vec{d}\right) \leq 0;\ k = 0, \ldots, N-1 \\
& \vec{b}^{eq}\left(\vec{x}_k, \vec{u}_k, \vec{d}\right) = 0;\ k = 0, \ldots, N-1 \\
& \vec{\psi}\left(\vec{x}_N, \vec{d}\right) = 0,
\end{aligned}
\tag{II.12}
$$

where $\vec{x}_k \in \Re^{n_x}$ and $\vec{u}_k \in \Re^{n_u}$ are the state and control vectors discretised at τ_k, respectively, for $k = 0, \ldots, N$. While the algebraic, path and terminal constraints of the continuous optimal control problem Eq. (II.9) can be directly evaluated at the discretised states and controls, the states evolution function $\vec{F} : \Re^{n_x} \times \Re^{n_u} \times \Re^{n_d} \times \Re \to \Re^{n_x}$ must be defined as the result of integrating $\vec{f}$ during a time interval of duration $\Delta\tau$ using an appropriate integration scheme with the discretised states and controls. Similarly, $\Pi : \Re^{n_x} \times \Re^{n_u} \times \Re^{n_d} \times \Re \to \Re$ is a quadrature function resulting from a numerical integration of π during a time interval of duration $\Delta\tau$. For instance, using the Euler method with one integration step these functions would be:

$$\vec{F}(\vec{x}_k, \vec{u}_k, \vec{d}, \Delta\tau) = \vec{x}_k + \vec{f}\left(\vec{x}_k, \vec{u}_k, \vec{d}\right)\Delta\tau;\ k = 0, \ldots, N-1 \tag{II.13a}$$

$$\Pi(\vec{x}_k, \vec{u}_k, \vec{d}, \Delta\tau) = \pi\left(\vec{x}_k, \vec{u}_k, \vec{d}\right)\Delta\tau;\ k = 0, \ldots, N-1. \tag{II.13b}$$

where $\Delta\tau$ could be a known parameter for optimal control problems with fixed final time, or an additional decision variable to be optimised in Eq. (II.12) if the final time were free. It should be noted, however, that Eq. (II.13) represents the most simple method to integrate $\vec{f}$ and π during $\Delta\tau$. In this PhD thesis, more complex and accurate techniques have been used, which will be presented in the following chapters.

Analogously to Eq. (II.10), in the discrete domain the optimal control problem can be also defined over more than one phase. First, let the continuous time horizon $[t_I, t_F]$ be divided into P time intervals $[t_j, t_{j+1}]$ for $j = 0, \ldots, P-1$; each time interval corresponding to a different phase. Again, $t_0 = t_I$ and $t_P = t_F$. Then, each time interval (or phase) is discretised into N_j equidistant time samples $\left[\tau_k, \tau_{k+1}, \ldots, \tau_{k+N_j-1}\right]$, where $\tau_k = t_j$, $\tau_{k+N_j-1} = t_{j+1}$ and $k = \sum_{i<j} N_i$, for all $j = 0, \ldots, P-1$. The discretisation step of the j^{th} phase is denoted by $\Delta\tau_j$. As a result, the whole time horizon is discretised again into $N+1 = \sum_{j=0}^{P-1} N_j$ time samples $[\tau_0, \tau_1, \ldots, \tau_N]$.

Let $\mathcal{T}$ be a multi-dimensional set that relates the index of each phase to the indexes of its corresponding time samples. The subset $\mathcal{E} \subseteq \mathcal{T}$ only includes the index corresponding to the last time sample of each phase; and $\mathcal{I}$ is defined as $\mathcal{T} \backslash \mathcal{E}$. For instance, for a multi-phase optimal control problem with $P = 3$ phases and $N+1 = 12$ time samples equally distributed among them (i.e., $N_j = 4$ for $j = 0, 1, 2$), these subsets would be particularised as:

$$\begin{aligned}
\mathcal{T} &= \{(0,0), (0,1), (0,2), (0,3), (1,4), (1,5), (1,6), (1,7), (2,8), (2,9), (2,10), (2,11)\} \\
\mathcal{E} &= \{(0,3), (1,7), (2,11)\} \\
\mathcal{I} &= \{(0,0), (0,1), (0,2), (1,4), (1,5), (1,6), (2,8), (2,9), (2,10)\}.
\end{aligned}$$

Figure II-3 shows an illustrative scheme of the discretisation process for an arbitrary number of phases and time samples.

Based on the definitions stated above, the discrete multi-phase optimal control problem is:

$$\begin{aligned}
\min_{\substack{\vec{x}_k, k=0,\ldots,N \\ \vec{u}_k, \forall(j,k)\in\mathcal{I}}} \quad & J := \sum_{(j,k)\in\mathcal{E}} \phi_j\left(\vec{x}_k, \vec{d}\right) + \sum_{(j,k)\in\mathcal{I}} \Pi_j\left(\vec{x}_k, \vec{u}_k, \vec{d}, \Delta\tau_j\right) \\
\text{s.t} \quad & \vec{x}_0 = \vec{X} \\
& \vec{x}_{k+1} = \vec{F}_j\left(\vec{x}_k, \vec{u}_k, \vec{d}, \Delta\tau_j\right);\ \forall(j,k) \in \mathcal{I} \\
& \vec{b}_j^{in}\left(\vec{x}_k, \vec{u}_k, \vec{d}\right) \leq 0;\ \forall(j,k) \in \mathcal{I} \\
& \vec{b}_j^{eq}\left(\vec{x}_k, \vec{u}_k, \vec{d}\right) = 0;\ \forall(j,k) \in \mathcal{I} \\
& \vec{\vartheta}_j^{eq}\left(\vec{x}_k, \vec{d}\right) = 0;\ \forall(j,k) \in \mathcal{E}\backslash\{(P-1, N)\} \\
& \vec{\vartheta}_j^{in}\left(\vec{x}_k, \vec{d}\right) \leq 0;\ \forall(j,k) \in \mathcal{E}\backslash\{(P-1, N)\} \\
& \vec{\psi}\left(\vec{x}_N, \vec{d}\right) = 0 \\
& \vec{x}_k - \vec{x}_{k+1} = 0;\ \forall(j,k) \in \mathcal{E}\backslash\{(P-1, N)\}.
\end{aligned} \tag{II.14}$$

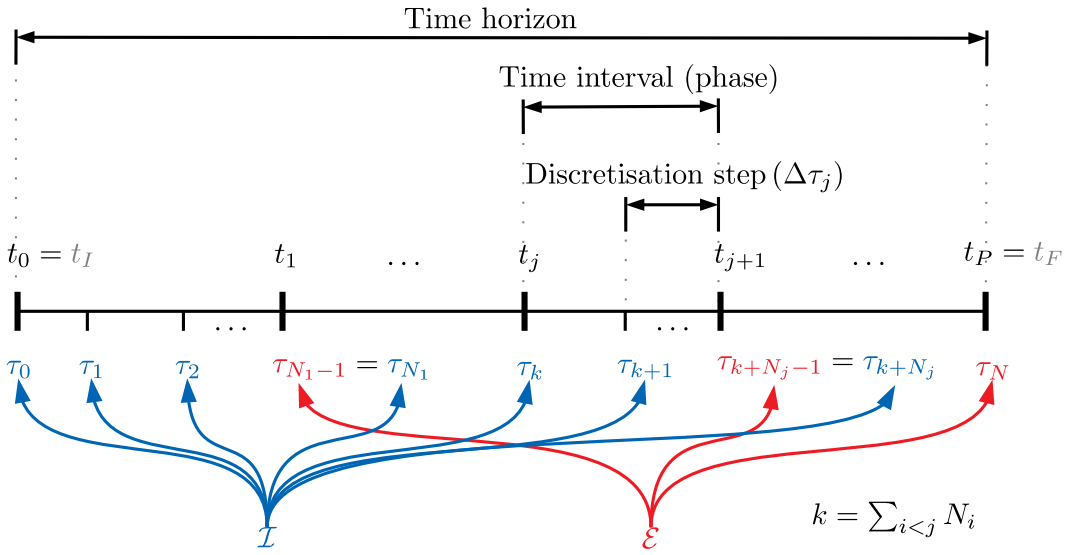

Figure II-3: *Discretisation process for a generic optimal control problem*

In Eq. (II.14), $\Pi_j : \Re^{n_x} \times \Re^{n_u} \times \Re^{n_d} \times \Re \to \Re$ and $\vec{F}_j : \Re^{n_x} \times \Re^{n_u} \times \Re^{n_d} \times \Re \to \Re^{n_x}$ are the quadrature and states evolution functions for the j^{th} phase, respectively.

The discretisation step of each individual phase could be considered either known parameter or variable to be optimised, depending on the problem. For instance, if the duration of the whole time horizon were fixed to a certain parameter, say a CTA, but the duration of each phase were flexible, $\Delta\tau_j$ for $j = 0, \dots, P-1$ would become decision variables subject to:

$$\sum_{j=0}^{P-1} (N_j - 1)\,\Delta\tau_j - \text{CTA} = 0, \tag{II.15}$$

which would be appended as an equality constraints in Eq. (II.14).

II.2.3 Nonlinear programming problem

As mentioned above, direct methods for optimal control compute the optimal trajectory plan by formulating the generic multi-phase optimal control problem Eq. (II.14) as a parametric NLP optimisation problem. This NLP optimisation problem has the following form:

$$\begin{aligned} \min_{\vec{z}} \quad & f(\vec{z}, \vec{p}) \\ \text{s.t} \quad & \vec{h}(\vec{z}, \vec{p}) = 0 \\ & \vec{g}(\vec{z}, \vec{p}) \leq 0, \end{aligned} \tag{II.16}$$

where $\vec{z} \in \Re^{n_z}$ is the vector of primal variables, $\vec{h} : \Re^{n_z} \times \Re^{n_p} \to \Re^{n_h}$ is the vector of equality constraints, $\vec{g} : \Re^{n_z} \times \Re^{n_p} \to \Re^{n_g}$ is the vector of inequality constraints, and $\vec{p} \in \Re^{n_p}$ is the vector of (fixed) parameters of the NLP optimisation problem. In this PhD thesis, the following definitions are considered:

$$\vec{z} := \begin{bmatrix} \vec{z}_0 \\ \vec{z}_1 \\ \dots \\ \vec{z}_N \end{bmatrix}, \vec{h}(\vec{z}, \vec{p}) := \begin{bmatrix} \vec{h}_0(\vec{z}, \vec{p}) \\ \vec{h}_1(\vec{z}, \vec{p}) \\ \dots \\ \vec{h}_N(\vec{z}, \vec{p}) \end{bmatrix}, \vec{g}(\vec{z}, \vec{p}) := \begin{bmatrix} \vec{g}_0(\vec{z}, \vec{p}) \\ \vec{g}_1(\vec{z}, \vec{p}) \\ \dots \\ \vec{g}_N(\vec{z}, \vec{p}) \end{bmatrix}, \tag{II.17}$$

where:

$$
\begin{aligned}
\vec{z}_k &:= \begin{cases} \begin{bmatrix} \vec{u}_k \\ \vec{x}_k \end{bmatrix} & \text{if } (j,k) \in \mathcal{I} \\ \vec{x}_k & \text{if } (j,k) \in \mathcal{E} \end{cases} \\
\vec{h}_k &:= \begin{cases} \begin{bmatrix} \vec{x}_{k+1} - \vec{F}_j\left(\vec{x}_k, \vec{u}_k, \vec{d}, \Delta\tau_j\right) \\ \vec{b}_j^{eq}\left(\vec{x}_k, \vec{u}_k, \vec{d}\right) \end{bmatrix} & \text{if } (j,k) \in \mathcal{I} \\ \begin{bmatrix} \vec{\vartheta}_j^{eq}\left(\vec{x}_k, \vec{d}\right) \\ \vec{x}_k - \vec{x}_{k+1} \end{bmatrix} & \text{if } (j,k) \in \mathcal{E}\backslash\{(P-1,N)\} \\ \vec{\psi}\left(\vec{x}_k, \vec{d}\right) & \text{if } k = N \end{cases} \\
\vec{g}_k &:= \begin{cases} \vec{b}_j^{in}\left(\vec{x}_k, \vec{u}_k, \vec{d}\right) & \text{if } (j,k) \in \mathcal{I} \\ \vec{\vartheta}_j^{in}\left(\vec{x}_k, \vec{d}\right) & \text{if } (j,k) \in \mathcal{E}\backslash\{(P-1,N)\}. \end{cases}
\end{aligned}
\tag{II.18}
$$

According to Eq. (II.18), $\vec{z}_k$ includes both discretised states and controls at the time sample τ_k. Similarly, $\vec{g}_k$ and $\vec{h}_k$ include the inequality and equality constraints applied at τ_k, respectively.

In Eq. (II.16), f is the cost function of the original optimal control problem evaluated at the primal variables and NLP parameters, i.e., $f\left(\vec{z},\vec{p}\right) = J(\vec{z},\vec{p})$. In this PhD thesis, the vector of NLP parameters is composed of both current state of the aircraft and parameters of the model:

$$
\vec{p} = \begin{bmatrix} \vec{X} \\ \vec{d} \end{bmatrix}. \tag{II.19}
$$

Furthermore, in order to reduce the number of NLP variables and constraints, the constraint that fix the initial conditions of the optimal control problem to the current state of the system is eliminated by substituting the variables $\vec{x}_0$ for the vector of fixed initial conditions $\vec{X}$ in the whole NLP optimisation problem (i.e., equality constraints, inequality constraints and cost function). This allows to remove the constraint $\vec{x}_0 = \vec{X}$ and the variable $\vec{x}_0$ from the optimisation problem.

The Lagrangian function associated to the NLP optimization problem (II.16) is:

$$
\mathcal{L}\left(\vec{z},\vec{p},\vec{\lambda},\vec{\mu}\right) := f\left(\vec{z},\vec{p}\right) + \vec{\lambda}^T \vec{g}\left(\vec{z},\vec{p}\right) + \vec{\mu}^T \vec{h}\left(\vec{z},\vec{p}\right), \tag{II.20}
$$

where $\vec{\lambda} \in \Re^{n_g}$ and $\vec{\mu} \in \Re^{n_h}$ are the Lagrange multipliers (dual variables) vectors paired up with the constraints $\vec{g}$ and $\vec{h}$, respectively. An optimal primal-dual pair $\left(\vec{z}^*,\vec{\lambda}^*,\vec{\mu}^*\right)$, where $(\cdot)^*$ indicates *optimal*, satisfies the first-order necessary conditions of optimality, also known as Karush-Kuhn-Tucker conditions (KKT) (Kuhn & Tucker, 1950), if:

$$
\frac{\partial \mathcal{L}}{\partial \vec{z}}\left(\vec{z}^*,\vec{p},\vec{\lambda}^*,\vec{\mu}^*\right) = \frac{\partial f}{\partial \vec{z}}\left(\vec{z}^*,\vec{p}\right) + \vec{\lambda}^{*T} \frac{\partial \vec{g}}{\partial \vec{z}}\left(\vec{z}^*,\vec{p}\right) + \vec{\mu}^{*T} \frac{\partial \vec{h}}{\partial \vec{z}}\left(\vec{z}^*,\vec{p}\right) = 0 \tag{II.21a}
$$

$$
\vec{h}\left(\vec{z}^*,\vec{p}\right) = 0;\ \vec{\mu}^* > 0 \tag{II.21b}
$$

$$
g_i\left(\vec{z}^*,\vec{p}\right) = 0;\ \lambda_i^* > 0;\ \forall (g_i,\lambda_i^*) \in \mathcal{G}_{ac} \tag{II.21c}
$$

$$
g_i\left(\vec{z}^*,\vec{p}\right) < 0;\ \lambda_i^* = 0;\ \forall (g_i,\lambda_i^*) \in \mathcal{G}_{in}, \tag{II.21d}
$$

where the pairs of inequality constraints and associated dual variables have been divided into two complementary sets: the active set ($\mathcal{G}_{ac}$) and the inactive set ($\mathcal{G}_{in}$) (Würth *et al.*, 2009).

Newton methods suitable to solve this kind of optimisation problems try to find a point satisfying Eq. (II.21), by using successive linearisation of the cost function and constraints. The major differences between them are on how to achieve the conditions related with the inequality constraints Eqs. (II.21c) and (II.21d). The two big families are:

- **Interior-point methods**, which typically replace the original NLP optimisation problem by a series of barrier subproblems (Wachter & Biegler, 2006), which are controlled by a barrier parameter. Two representative interior-point methods are the primal-dual method, and the trust-region method.
- **Active-set methods**, which solve in turn a sequence of subproblems based on a quadratic approximation of the original NLP optimisation problem. Representative active-set methods are the sequential quadratic programming (SQP) method (Gill *et al.*, 2005), the sequential linear-quadratic programming (SLQP) method (Byrd *et al.*, 2003), and the gradient projection method (Lin & Moré, 1999).

Let $\mathcal{P}_N$ be the NLP algorithm (either interior-point or active-set) that provides the optimal primal-dual solution (i.e., satisfying Eq. (II.21)) as a function of $\vec{p}$ for the next N time samples:

$$\left(\vec{z}^*, \vec{\lambda}^*, \vec{\mu}^*\right) \leftarrow \mathcal{P}_N\left(\vec{p}\right). \tag{II.22}$$

Remember that the vector of NLP parameters includes both current states and parameters of the model (see Eq. (II.19)). Taking into account that, by definition of Eq. (II.22), the optimal primal-dual solution is an implicit function of $\vec{p}$, any change in $\vec{p}$ would lead to a new optimal primal-dual solution. This fact will be exploited in Section II.3.4.2 when considering parametric sensitivity methods to update the optimal trajectory plan quasi-instantaneously.

II.2.4 Implementation considerations

Several common issues must be considered when dealing with NLP optimisation problems. In particular, how to react in the face of an infeasible solution in which some constraints are not satisfied, how to handle discontinuities present in tabular data, and which mechanisms should be used to speed up the optimisation process when solving a sequence of similar problems. The following sections give a couple of recommendations related to these three topics, respectively.

II.2.4.1 Recovering from infeasible solutions

In practical applications, the solution of the NLP optimisation problem described by Eq. (II.16) may not always be feasible. Accumulated deviations caused by disturbances and modelling errors could eventually lead to the impossibility to satisfy one or several constraints to a given numerical precision. If this were the case, the NLP solver would not provide a valid solution and, consequently, the optimal trajectory plan could not be obtained. Yet, in some circumstances it may be reasonable to allow, to some extent, violations in certain constraints, so that a sub-optimal solution can still be obtained, as long as the safety requirements of the application permit. With this aim, there exist several alternatives to recover the feasibility of the solution.

Constraint relaxation method

An attractive method consists of not defining the admissible range of the constraints to their actual operational limits but to more conservative values. Then, these limits will be systematically relaxed whenever an infeasible solution is obtained. This approach is commonly referred as the constraint relaxation method. It is not always obvious, however, which constraints to relax, nor the amount which they should be relaxed. In order to overcome this issue, some optimisation techniques have been proposed, which determine the constraints that should be relaxed, according to some priority list, and the minimum relaxation required to recover feasibility (Vada *et al.*, 2001). These techniques resort to optimisation problems running in parallel to the original optimal control problem. Accordingly, their algorithmic complexity may be significant.

Transient constraint violation method

A second alternative consists of allowing constraint violations only during a certain period of time, typically at the beginning of the new trajectory, which duration is to be minimized. In some cases, however, the time transient constraints violations could be large (Scokaert & Rawlings, 1999).

Soft-constraint method

Finally, the soft-constraint method consists of defining additional slack variables in the optimisation problem, which allow to violate the path and/or terminal constraints in case of not obtaining a feasible solution to the optimal control problem (Scokaert & Rawlings, 1999). Using this method, the original NLP optimisation problem, Eq. (II.16), is re-formulated as follows:

$$\begin{aligned} \min_{\vec{z},\vec{e}^{eq},\vec{e}^{in}} \quad & f\left(\vec{z},\vec{p}\right) + \vec{e}^{in^T}\boldsymbol{\mathcal{W}}^{in}\vec{e}^{in} + \vec{e}^{eq^T}\boldsymbol{\mathcal{W}}^{eq}\vec{e}^{eq} \\ \text{s.t} \quad & \vec{h}\left(\vec{z},\vec{p}\right) = \vec{e}^{eq} \\ & \vec{g}\left(\vec{z},\vec{p}\right) \leq \vec{e}^{in} \\ & \vec{e}^{in} \geq 0, \end{aligned} \tag{II.23}$$

where $\vec{e}^{in} \in \Re^{n_g}$ and $\vec{e}^{eq} \in \Re^{n_h}$ are the vector of slack variables paired up with the inequality and equality constraints of the original NLP optimisation problem, respectively.

Additional constraints ensure that the slack variables related to inequality constraints do not make the associated constraints more restrictive than their original values.

The positive-definite weighting matrices $\boldsymbol{\mathcal{W}}^{in} \in \Re^{n_g \times n_g}$ and $\boldsymbol{\mathcal{W}}^{eq} \in \Re^{n_h \times n_h}$ determine how much the violation of inequality and equality constraints is penalised, respectively. By educatedly tuning these weights, it is expected that the optimisation algorithm will violate constraints only if necessary. Otherwise, the result shall be equivalent to that obtained from solving (II.16).

The rule of thumb known as *Bryson's rule* (Bryson & Ho, 1975) can be used as a guideline to determine these weighting matrices. This rule states that the weights should be chosen so that the contribution of each slack variable to the cost function is approximately the same. In order to accomplish that, the inverse square of the admissible range of each constraint could be used as weight for the associated slack variable.

Last but not least, it should be noted that using this technique not all the constraints need to be necessarily slacked. For these constraints which cannot be violated under any condition, the corresponding slack variable could be either removed from the set of variables, or the weight associated to the slack variable could be set to a very large value. Yet, the later solution is not recommended for numerical stability reasons.

II.2.4.2 Handling tabular data in NLP algorithms

On optimal control problems such as Eq. (II.9) one often encounters a cost function and/or constraints given in tabular form, as a function of the states and/or controls. For instance, the drag coefficient of the aircraft, which depends on the lift coefficient and Mach number, could be given as a look-up table with performance data obtained from the manufacturer. Similarly, wind data from NWP forecasts, which are required to compute the ground speed, are typically given in tabular form as a function of the latitude, longitude and pressure level.

For use in simulations, the (linear) interpolation between discrete data points is a simple and convenient way to extract information from look-up tables. However, typical NLP solvers require the first and second derivatives of the cost functions and constraints with respect to the primal variables in order to work. The derivatives of a piecewise linear function are undefined at the data points, where two linear functions with different slopes intercept. For this reason, state-of-the-art NLP solvers have difficulties when using tabular data. In this kind of optimisation problems, the data must be approximated off-line in order to generate continuous and twice-differentiable curves by some smooth function fitting techniques.

The easiest way to approximate tabular data is perhaps to use polynomial fittings. Although some of the aircraft performance data could be approximated quite well by polynomial functions, these expressions are not able to accurately approximate sharp change such as the drag rise region due to compressibility effects or complex functions such as the wind field. In these cases, high-order polynomials prone to oscillation due to the Runge's phenomenon would be required, potentially leading to poor convergence, local minima issues and large errors between data points.

In order to deal with tabular data in optimal control problems, Betts (2010) suggested to approximate the data points with tensor product splines. Splines are functions defined piecewise by polynomials of any degree, which keep sufficiently continuity and differentiability at the places where the polynomial pieces connect, called knots (de Boor, 1972).

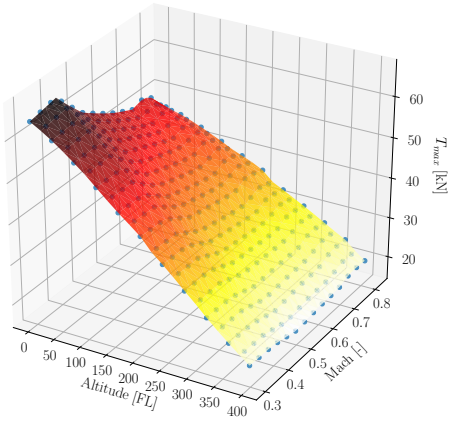

(a) Interpolating spline

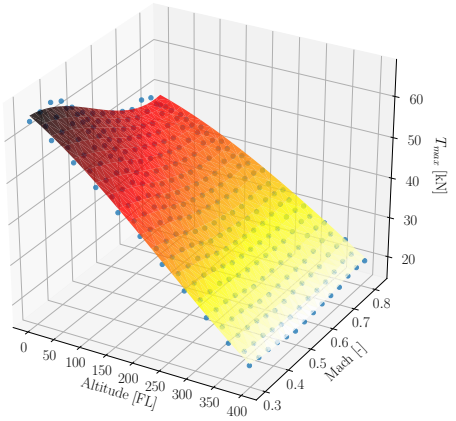

(b) Smoothing spline

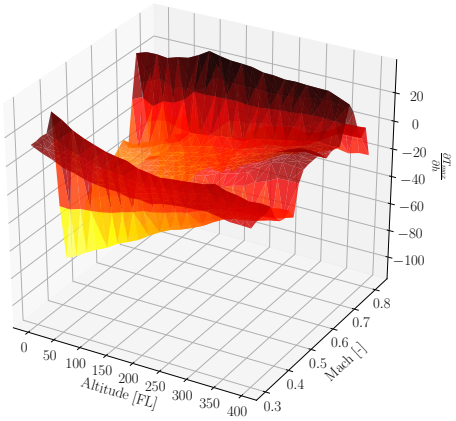

(c) Interpolating spline: first derivative with respect to altitude

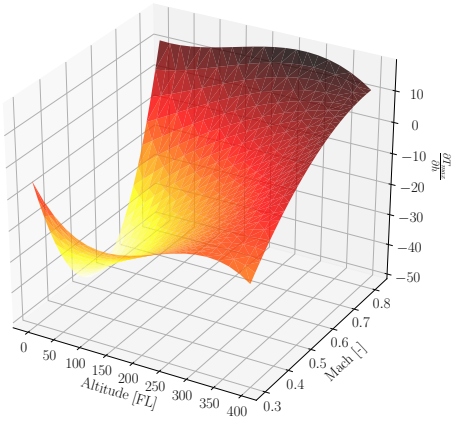

(d) Smoothing spline: first derivative with respect to altitude

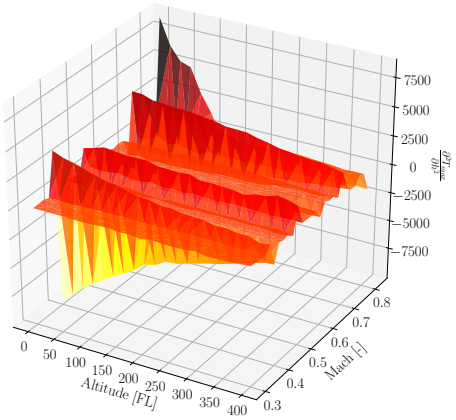

(e) Interpolating spline: second derivative with respect to altitude

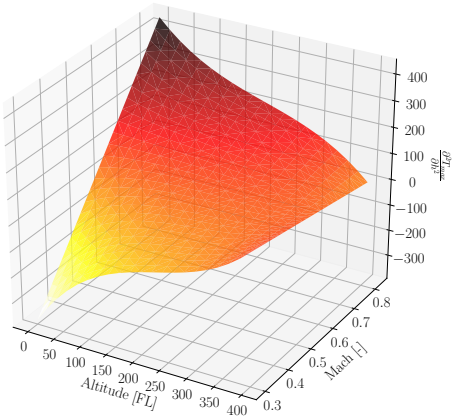

(f) Smoothing spline: second derivative with respect to altitude

Figure II-4: *Comparison between interpolating and smoothing spline approximation for the maximum thrust of an A320*

The simplest way to compute the splines coefficients is by ensuring interpolation to all data points (the interpolating spline). The resulting function provides the continuity and second-order differentiability required by NLP solvers to work. However, it is common for this kind of function to include *wiggles* that are not actually present in the data itself. A technique for eliminating these oscillations is to approximate the data rather than interpolating them. This can be achieved by using smoothing splines, which minimise the *curvature* of the spline whilst ensuring sufficient accuracy through the smoothing factor Betts (2010).

Figure II-4 illustrates the effect of the smoothing factor in the approximation. Figures II-4(a) and II-4(b) show the interpolating and smoothing splines that approximate maximum thrust data for an Airbus A320, respectively. These data was obtained from the Airbus performance engineering program (PEP). According to this figure, the smoothing spline approximates the data and does not pass through all the data points, while the interpolating spline does. However, this excellent interpolation comes at the cost of oscillating first and second derivatives (see Figs. II-4(c) and II-4(e)). The main conclusion is that, by using smoothing splines, a small reduction on the accuracy of the resulting interpolation function could lead to significant benefits in terms of convergence and execution time, due to the smoother first and second derivatives.

II.2.4.3 Solving a sequence of related NLP optimisation problems

Imagine an hypothetical case in which, at τ_0, the algorithm $\mathcal{P}_N$ has provided the optimal primal-dual solution in the time horizon $\tau_0, \tau_1, \ldots, \tau_N$. After implementing the optimal control $\vec{u}_0^*$ during the first time interval $\Delta\tau$, the system would be driven to a new state. If the dynamic model and associated parameters $\vec{d}$ were perfect, the new state would correspond to $\vec{F}\left(\vec{X}, \vec{u}_0^*, \vec{d}, \Delta\tau\right)$.

Assuming a situation in which the optimal primal-dual solution starting at the new state needs to be updated, the structure of the NLP optimisation problem and the old primal-dual solution corresponding to the new time horizon could be used to speed-up the optimisation process. Stated in a more general form, the solution of the NLP optimisation problem at any τ_i, $i = 1, \ldots, N-1$ could take advantage of the NLP optimisation problem structure and the optimal primal-dual solution at any of the preceding time samples.

The rationale behind this statement is that, firstly, the structure of the NLP optimisation problem at τ_i will be a reduced version of that of a preceding τ_k. In particular, the variables and constraints will be:

$$\vec{z}_{i:} := \begin{bmatrix} \vec{z}_i \\ \vec{z}_{i+1} \\ \cdots \\ \vec{z}_N \end{bmatrix}, \; \vec{h}_{i:}\left(\vec{z}_{i:}, \vec{p}\right) := \begin{bmatrix} \vec{h}_i\left(\vec{z}_{i:}, \vec{p}\right) \\ \vec{h}_{i+1}\left(\vec{z}_{i:}, \vec{p}\right) \\ \cdots \\ \vec{h}_N\left(\vec{z}_{i:}, \vec{p}\right) \end{bmatrix}, \; \vec{g}_{i:}\left(\vec{z}_{i:}, \vec{p}\right) := \begin{bmatrix} \vec{g}_i\left(\vec{z}_{i:}, \vec{p}\right) \\ \vec{g}_{i+1}\left(\vec{z}_{i:}, \vec{p}\right) \\ \cdots \\ \vec{g}_N\left(\vec{z}_{i:}, \vec{p}\right) \end{bmatrix}, \tag{II.24}$$

where $(\cdot)_{i:}$ indicates the elements of $(\cdot)$ corresponding to time samples from τ_i to the end of the time horizon. Similarly, $\vec{\lambda}_{i:}$ and $\vec{\mu}_{i:}$ are the dual variables paired up with $\vec{g}_{i:}$ and $\vec{h}_{i:}$, respectively; and the cost function is:

$$f_{i:}\left(\vec{z}_{i:}, \vec{p}\right) = J(\vec{z}_{i:}, \vec{p}). \tag{II.25}$$

According to this definition, the vectors of primal and dual variables, and of equality and inequality constraints for the NLP optimisation problem solved at τ_i, are subvectors of the NLP optimisation problem solved at a preceding time sample. This also implies that the Jacobian and Hessian matrices required by the NLP solver at τ_i are sub-matrices of the Jacobian and Hessian matrices at a preceding time sample. Figure II-5 illustrates this feature, showing the Jacobian matrix of a generic NLP problem solved at τ_0. Note that the columns correspond to the variables, and the rows to the constraints. Each element of this matrix corresponds to the derivative of the n^{th} constraint (row) with respect to the m^{th} variable (column). Non-zero entries, meaning that the derivative of the constraint n^{th} might depend on the variable m^{th}, are filled in black. Figure II-5 also shows, in red, the Jacobian matrix for the NLP problem solved at any τ_i, $i > 0$. As can be observed in this figure, the red matrix is contained in the Jacobian matrix for the NLP problem solved at τ_0, thus it can be obtained by simply eliminating the appropriate rows and columns.

The Lagrangian function of the NLP optimisation problem starting at τ_i is:

$$\mathcal{L}_{i:}\left(\vec{z}_{i:}, \vec{p}, \vec{\lambda}_{i:}, \vec{\mu}_{i:}\right) := f_{i:}\left(\vec{z}_{i:}, \vec{p}\right) + \vec{\lambda}_{i:}^T \vec{g}_{i:}\left(\vec{z}_{i:}, \vec{p}\right) + \vec{\mu}_{i:}^T \vec{h}_{i:}\left(\vec{z}_{i:}, \vec{p}\right), \tag{II.26}$$

and the KKT conditions Eq. (II.21) need to be also satisfied at $\left(\vec{z}_{i:}^*, \vec{\lambda}_{i:}^*, \vec{\mu}_{i:}^*\right)$.

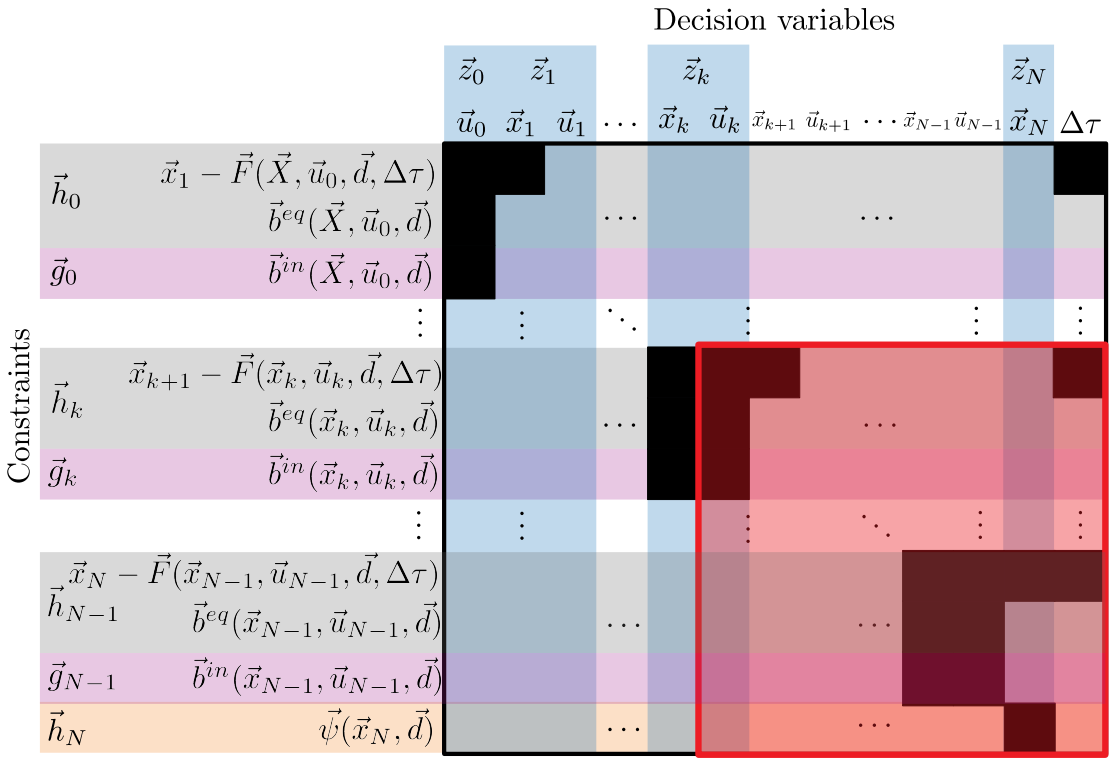

Figure II-5: *Jacobian matrix for a generic NLP optimisation problem*

Let $\mathcal{P}_{N-i}$ be the NLP algorithm that provides the optimal primal-dual solution as a function of $\vec{p}$, starting at τ_i and for the next $N - i$ time intervals:

$$\left(\vec{z}^*_{i:}, \vec{\lambda}^*_{i:}, \vec{\mu}^*_{i:}\right) \leftarrow \mathcal{P}_{N-i}\left(\vec{p}\right). \tag{II.27}$$

Secondly, NLP solvers are always executed from a starting point with all the primal and dual variables of the problem (unknowns of the problem) initialised to some value. Typically, the user can specify these starting values and otherwise, the solver will just set all the unknowns to zero or to another random value. Then, from this starting point, the internal algorithm of the NLP solver aims to find a feasible (i.e., that fulfils all the constraints) and optimal (i.e., that minimises/maximises the cost functional) solution.

An appropriate starting point or initial guess can dramatically reduce the convergence time of the optimisation problem, being for some complex problems, a key aspect influencing the solver's success on convergence too, which cannot even converge if the guess solution is not good enough. It should be noted that, since NLP solvers cannot guarantee a global optimal, different initial guesses could lead to different sub-optimal solutions. Therefore, when solving a sequence of related problems, the solution from the preceding optimisation corresponding to the current time horizon should be used as a guess. This technique, which could significantly reduce the execution time, is commonly known as *warm start*.

Interior-point methods perform a minimisation steps on each barrier subproblem, then decrease the barrier parameter and repeat the process until the original problem has been solved to the desired accuracy. This strategy is powerful for solving large-scale NLP optimisation problems with thousands of variables and inequality constraints. However, a well-known drawback of this strategy is that it might not provide a clear picture of which constraints are active at the solution (i.e., the active set $\mathcal{G}_{ac}$). In addition, they typically return a less exact solution and less exact sensitivity information than active-set methods. Conversely, most active-set NLP solvers implement SQP or SLQP strategies to estimate the active set. This method may be preferable to interior-point algorithms when a good initial point (i.e., guess) can be provided; for example, when solving a sequence of related problems where one problem is a perturbed version of another.

II.3 Trajectory guidance

A trajectory plan computed by solving the problem described in Section II.2 is just that: a plan. In order to materialise it, the FMS uses its guidance system, which continuously generates commands for the elevator and throttle/speed brakes to nullify deviations from certain variables included in (or derived from) the trajectory plan $\vec{z}$. If having two actuators at one's disposal, only two variables can be simultaneously controlled. Accordingly, several guidance strategies can be defined, depending on which variable is controlling the elevator and which variable is controlling the throttle/speed brakes, and which mechanisms these actuators use to correct deviations.

The core principle of the guidance strategies build on the TEMO concept (recall Section I.4.2.2) is that the energy of the aircraft can be managed in such a way that the CTAs are always (or most of the time) satisfied. The total energy of the aircraft in TEMO (E_t) is composed by the sum of its kinetic (E_k) and potential (E_p) energy:

$$E_t(v,h,m) = E_k(v,m) + E_p(h,m) = \frac{1}{2}mv^2 + mgh, \tag{II.28}$$

which can be computed as a function of $\vec{x}$, thus at any point of the trajectory plan $\vec{z}$.

Note that v is the speed of the aircraft relative to the airmass frame in which the aircraft is flying, while h is the geometric altitude with respect to the inertial earth frame. Clearly, these reference frames are different and move with respect to each other dependent on the wind. This implies that the reference frame associated with the total energy as defined in Eq. (II.28) is fictitious, i.e., without any physical meaning.

By differentiating Eq. (II.28) and combining it with Eqs. (II.1a) and (II.1c), the energy rate of the aircraft can be expressed as:

$$\dot{E}_t(v,h,s,T,C_L,\beta) = v\left(T - D(v,h,s,C_L,\beta)\right). \tag{II.29}$$

According to Eq. (II.29), the total energy of an aircraft can be increased by applying engine thrust, and decreased by increasing the aerodynamic drag. In addition, the law of conservation of energy states that potential energy can be exchanged for kinetic energy and vice versa through energy modulation. It is well-known that throttle and active drag devices (such as the speed brakes) are the most effective means to increase and decrease the total energy, respectively, whereas elevator control provides an effective mean to modulate this energy.

Summing up, the elevator could be used to exchange potential energy (altitude) and kinetic energy (speed) at an appropriate rate, while throttle and speed brake would be only applied when energy needs to be added or removed from/to the system, respectively. For instance, if the aircraft is late with respect to the RTAs and at the same time has an excessive potential energy with respect to the plan, altitude should be exchanged by speed with the elevator to accelerate and arrive on time while simultaneously reducing the potential energy deviation.

This section presents several guidance strategies designed to execute a trajectory plan for a CDO subject to a CTA at a metering fix. All of them are build on the TEMO concept. Yet, they differ in the behaviour to react against energy and time deviations.

II.3.1 Tactical guidance

When executing a trajectory plan with tactical guidance, the deviations from the planned time at the current distance to go are continuously nullified by using the elevator to control the speed (speed-on-elevator). That is, if the aircraft is late, the aircraft will pitch down to accelerate; if the aircraft is early, the aircraft will pitch up to decelerate. At the same time, the throttle and the speed brakes act together to maintain the planned energy level all the time. That is, if the aircraft has less energy than planned, the thrust will increase to add energy; if the aircraft has excessive energy, speed-brakes will be deployed to increase the airframe drag and reduce the energy. As a result, using this strategy the aircraft is continuously following the initially computed trajectory plan with minimum energy and time deviations, thus there is no need to update the trajectory plan during the course of the descent, unless reaching the operational limits of the aircraft. However, this kind of guidance strategy typically has a negative impact on the environment (and on engine wear and tear) because the continuous use of thrust to nullify energy deviations.

II.3.2 Strategic re-planning

Using this guidance strategy, both CAS and thrust plans are followed. The thrust plan is obtained directly from $\vec{z}$, while the CAS can be computed at any point of the plan using the following expression:

$$v_{CAS}(v,h) = \sqrt{\frac{2\gamma_a}{\gamma_a - 1}\frac{p_{SSL}}{\rho_{SSL}}\left((\delta(h)B(v,h)+1)^{\frac{\gamma_a-1}{\gamma_a}} - 1\right)}, \tag{II.30}$$

where:

$$B(v,h) := \left(\frac{1}{2}\frac{\gamma_a - 1}{\gamma_a}v^2\left(\frac{\sigma(h)\rho_{SSL}}{\delta(h)p_{SSL}}\right) + 1\right)^{\frac{\gamma_a}{\gamma_a-1}} - 1 \tag{II.31}$$

and γ_a is the specific heat ratio of the air.

On the one hand, the CAS plan is followed by using the elevator. On the other hand, the thrust plan is followed by acting on the throttle. Different from the tactical strategy, time and energy deviations are not continuously nullified. Instead, the guidance system remains passive with respect to time and energy deviations as long as they do not exceed predefined thresholds. When the threshold is exceeded, the FMS optimises again the trajectory, enforcing the initial conditions to the current state of the aircraft. This results in a new CAS and thrust plan that minimises a certain cost function while satisfying all the constraints.

An advantage of this strategy is that the entire remaining time horizon is taken into account when correcting deviations. In addition, being passive with respect to time and energy deviations could lead to positive effects if the errors caused by different sources are counteractive. For instance, Figure II-6 shows an hypothetical scenario in which an aircraft flies a curved approach with an unexpected wind from the north. The aircraft starts the approach without time error. During the leg to B, the unforeseen head wind increases the time error. However, the time error when reaching the point B is not high enough to trigger a re-plan. After point B, the relative wind changes its direction and the unforeseen tail wind reduces the time error, which returns to zero by the end of the procedure. Under these conditions, strategic guidance would perform better (in terms of environmental impact) than tactical guidance, which would require additional thrust in the upwind leg and speed-brakes in the downwind leg in order to nullify time deviations.

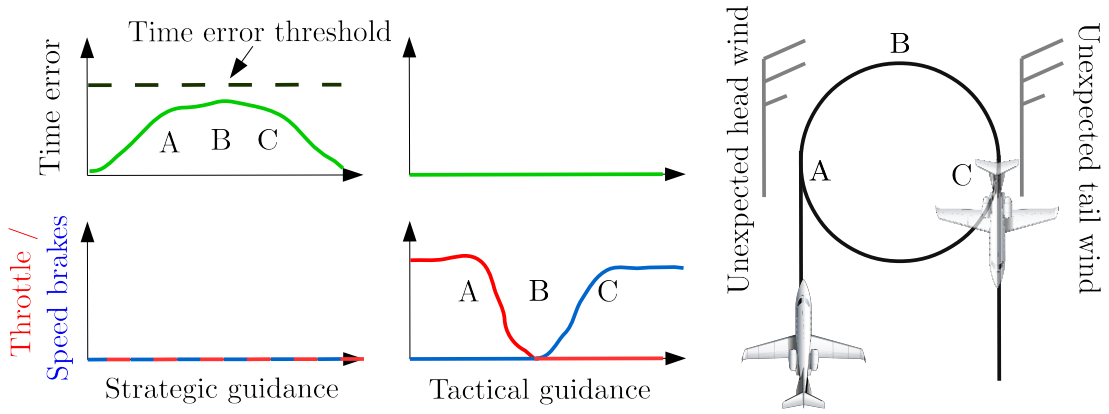

Figure II-6: *Tactical and strategic behaviour in a 180 degree turn*

Nevertheless, using this strategy, one must be cautious when selecting the energy and time error thresholds, a critical design task that is not straightforward. For instance, if the thresholds were too permissive, it could be too late to react and satisfy all applicable constraints when reaching the time and or energy error threshold. In that case, any of the strategies presented in Section II.2.4.1 could be implemented to recover feasibility. Conversely, if the thresholds were too strict, this strategy would result in a continuous re-planning of the trajectory, which behaviour is similar to that of the NMPC guidance.

II.3.3 Hybrid guidance

This guidance strategy is obtained as a result of combining the tactical and the strategic guidances described above. For instance, one possibility consists of using the elevator to tactically nullify sustained time errors, while simultaneously executing the thrust plan with the throttle. In that case, eventual energy deviations from the trajectory plan caused by, e.g., wind uncertainties, are corrected by means of strategic re-planning whenever the pre-defined energy error threshold is exceeded. As a result, the aircraft is no longer affected by time errors, at the expense of being more prone to energy deviations. The analogous configuration consists of a tactical controller nullify sustained energy deviations, and a strategic controller correcting time errors by updating the optimal trajectory plan whenever the pre-defined time error threshold is overpassed. Using this hybrid configuration, the aircraft is continuously following the energy plan, and the trajectory plan is dynamically adapted to satisfy the time constraints.

II.3.4 Nonlinear model predictive control (NMPC)

This guidance strategy is based on the repeated solution of the optimal control problem described in Section II.2.2. Based on the current state of the aircraft, the optimal control problem is solved over a finite time horizon in the future, and the resulting optimal control is executed only until the next time sample. Then, the process is repeated moving forward the time horizon, and so on.

A well-known way of classifying NMPC is according to the size of the optimisation time horizon. Considering this criteria, NMPC can be divided into two major classes: in a receding-horizon NMPC (Almassalkhi, 2013), the size of the optimisation time horizon is constant and relatively small. In a shrinking-horizon NMPC, the entire remaining trajectory is optimised at each re-calculation instant, thus the length of the optimisation time horizon decreases while approaching the terminal state.

For the specific problem of an aircraft (a system with relatively slow dynamics) that needs to achieve a fix in space and time (conditioned by a CTA), the hypothesis of this PhD is that shrinking-horizon NMPC could be an excellent choice based on the execution times required to solve the open-loop optimal control problem with existing NLP algorithms. Depending on whether the optimal trajectory plan is updated at each time sample by solving a rigorous NLP optimisation problem as described by Eq. (II.16) and/or by taking advantage of parametric sensitivities, the following NMPC guidance strategies can be defined.

II.3.4.1 Ideal NMPC (INMPC)

In an ideal case, problem $\mathcal{P}_{N-i}$ is solved at each time sample as soon as the parameter vector is measured or estimated. Then, the resulting optimal control $\vec{u}_i^*$ is applied without delay until τ_{i+1}, where the process is repeated. For achieving optimal performance, however, problem $\mathcal{P}_{N-i}$ needs to be solved instantaneously. We refer to this hypothetical case as the ideal NMPC (INMPC). Algorithm (II.1) details its main steps.

Algorithm II.1: *Working principle of the ideal NMPC (INMPC)*

1: $\left(\vec{z}^*, \vec{\lambda}^*, \vec{\mu}^*\right) \leftarrow \mathcal{P}_N\left(\vec{p}\right)$
2: Build the guess for $\vec{z}^*_{1:}$, $\vec{\lambda}^*_{1:}$ and $\vec{\mu}^*_{1:}$ from $\vec{z}^*$, $\vec{\lambda}^*$ and $\vec{\mu}^*$, respectively
3: **for** $i = 1, \ldots, N-1$ **do**
4: Measure $\vec{X}$ and estimate $\vec{d}$
5: $\vec{p} \leftarrow \begin{bmatrix} \vec{X} \\ \vec{d} \end{bmatrix}$
6: $\left(\vec{z}^*_{i:}, \vec{\lambda}^*_{i:}, \vec{\mu}^*_{i:}\right) \leftarrow \mathcal{P}_{N-i}\left(\vec{p}\right)$ using warm start (see Section II.2.4.3)
7: Build the guess for $\vec{z}^*_{i+1:}$, $\vec{\lambda}^*_{i+1:}$ and $\vec{\mu}^*_{i+1:}$ from $\vec{z}^*_{i:}$, $\vec{\lambda}^*_{i:}$ and $\vec{\mu}^*_{i:}$, respectively
8: Implement $\vec{u}_i^*$ until τ_{i+1}

Unfortunately, in practical applications $\mathcal{P}_{N-i}$ may be computationally expensive to solve. This implies that the control $\vec{u}_i^*$ cannot be applied just after $\vec{p}$ is measured or estimated, but only after $\mathcal{P}_{N-i}$ is solved. The delay in calculating the new solution may lead to sub-optimal trajectories, failure to meet constraints, or in some instances instabilities of the solution (Jäschke *et al.*, 2014). This motivates the introduction of sensitivity-based methods to update the optimal trajectory plan, which are presented below.

II.3.4.2 Sensitivity-based NMPC (SbNMPC)

Sensitivity-based methods are based on the statement that, as long as the differences in the parameters vector $\vec{p}$ are *relatively small* between consecutive time samples, parametric sensitivities at the active optimal solution can be used to rapidly update the optimal trajectory for perturbation in the parameters vector ($\Delta\vec{p}$).

The parametric sensitivities of the primal and dual variables with respect to the parameters vector at τ_i, $i = 0, \dots, N-1$ can be obtained by differentiating the KKT conditions, Eq. (II.21), evaluated at the active optimal primal-dual solution $\left(\vec{z}^*_{i:}, \vec{\lambda}^*_{i:}, \vec{\mu}^*_{i:}\right)$ (Wolf & Marquardt, 2016):

$$\begin{bmatrix} \frac{\partial \vec{z}_{i:}}{\partial \vec{p}} \\ \frac{\partial \vec{\lambda}_{i:}}{\partial \vec{p}} \\ \frac{\partial \vec{\mu}_{i:}}{\partial \vec{p}} \end{bmatrix} = - \begin{bmatrix} \frac{\partial^2 \mathcal{L}^*_{i:}}{\partial \vec{z}^2_{i:}} & \frac{\partial \vec{g}^*_{i:}}{\partial \vec{z}_{i:}}^T & \frac{\partial \vec{h}^*_{i:}}{\partial \vec{z}_{i:}}^T \\ \frac{\partial \vec{g}^*_{i:}}{\partial \vec{z}_{i:}} & 0 & 0 \\ \frac{\partial \vec{h}^*_{i:}}{\partial \vec{z}_{i:}} & 0 & 0 \end{bmatrix}^{-1} \begin{bmatrix} \frac{\partial^2 \mathcal{L}^*_{i:}}{\partial \vec{z}_{i:} \partial \vec{p}} \\ \frac{\partial \vec{g}^*_{i:}}{\partial \vec{p}} \\ \frac{\partial \vec{h}^*_{i:}}{\partial \vec{p}} \end{bmatrix}, \tag{II.32}$$

being consistent with the notation, $(\cdot)^*_{i:} = (\cdot)(\vec{z}^*_{i:}, \vec{\lambda}^*_{i:}, \vec{\mu}^*_{i:}, \vec{p})$. In addition, remember that $(\cdot)_{i:}$ represents the subvector of $(\cdot)$ that includes the elements with position greater or equal than i.

The linear system Eq. (II.32) can be solved for $\frac{\partial \vec{z}_{i:}}{\partial \vec{p}}$, $\frac{\partial \vec{\lambda}_{i:}}{\partial \vec{p}}$ and $\frac{\partial \vec{\mu}_{i:}}{\partial \vec{p}}$, allowing to update the optimal solution using a simple first-order Taylor approximation as follows:

$$\vec{z}^*_{i:}(\vec{p} + \Delta\vec{p}) = \vec{z}^*_{i:}(\vec{p}) + \frac{\partial \vec{z}_{i:}}{\partial \vec{p}} \Delta\vec{p} \tag{II.33a}$$

$$\vec{\lambda}^*_{i:}(\vec{p} + \Delta\vec{p}) = \vec{\lambda}^*_{i:}(\vec{p}) + \frac{\partial \vec{\lambda}_{i:}}{\partial \vec{p}} \Delta\vec{p} \tag{II.33b}$$

$$\vec{\mu}^*_{i:}(\vec{p} + \Delta\vec{p}) = \vec{\mu}^*_{i:}(\vec{p}) + \frac{\partial \vec{\mu}_{i:}}{\partial \vec{p}} \Delta\vec{p}. \tag{II.33c}$$

Unfortunately, this fast and convenient parametric sensitivity update can only be used if the set of active constraints does not change after the perturbation (Würth *et al.*, 2009). In practical NMPC applications, however, constraints in the active set may become inactive, or constraints in the inactive set may become active for the solution corresponding to the perturbed $\vec{p}$.

An interesting approach that accounts for active set changes after a perturbation in the NLP parameters vector was suggested by Kadam & Marquardt (2004). This approach consists of reformulating Eq. (II.32) as a quadratic programming (QP) optimisation problem:

$$\begin{aligned} \min_{\Delta\vec{z}} \quad & \frac{1}{2} \Delta\vec{z}^T_{i:} \frac{\partial^2 \mathcal{L}^*_{i:}}{\partial \vec{z}^2_{i:}} \Delta\vec{z}_{i:} + \Delta\vec{z}^T_{i:} \frac{\partial^2 \mathcal{L}^*_{i:}}{\partial \vec{z}_{i:} \partial \vec{p}} \Delta\vec{p} + \frac{\partial f^*_{i:}}{\partial \vec{z}_{i:}}^T \Delta\vec{z}_{i:} \\ \text{s.t} \quad & \vec{g}^*_{i:} + \frac{\partial \vec{g}^*_{i:}}{\partial \vec{z}_{i:}} \Delta\vec{z}_{i:} + \frac{\partial \vec{g}^*_{i:}}{\partial \vec{p}} \Delta\vec{p} \leq 0 \\ & \vec{h}^*_{i:} + \frac{\partial \vec{h}^*_{i:}}{\partial \vec{z}_{i:}} \Delta\vec{z}_{i:} + \frac{\partial \vec{h}^*_{i:}}{\partial \vec{p}} \Delta\vec{p} = 0. \end{aligned} \tag{II.34}$$

Let $\mathcal{Q}_{N-i}$ represent the QP algorithm that provides optimal primal variables perturbation $\Delta\vec{z}^*_{i:}$ and dual variables $\vec{\lambda}^*_{i:}$, $\vec{\mu}^*_{i:}$as a function of $\Delta\vec{p}$:

$$\left(\Delta\vec{z}^*_{i:}, \vec{\lambda}^*_{i:}, \vec{\mu}^*_{i:}\right) \leftarrow \mathcal{Q}_{N-i}\left(\Delta\vec{p}\right). \tag{II.35}$$

Then, the dual variables of the optimal solution computed with the unperturbed parameters vector (i.e., $\vec{\lambda}^*_{i:}(\vec{p})$ and $\vec{\mu}^*_{i:}(\vec{p})$) are updated with those obtained from solving $\mathcal{Q}_{N-i}$, and:

$$\vec{z}^*_{i:}(\vec{p} + \Delta\vec{p}) = \vec{z}^*_{i:}(\vec{p}) + \Delta\vec{z}^*_{i:}(\Delta\vec{p}). \tag{II.36}$$

The first-order update Eq. (II.36), however, will be accurate only for relatively small $\Delta\vec{p}$. For large perturbations, the new solution must to be analysed to verify that the KKT conditions are still satisfied. This is

accomplished by computing the error in the Lagrange sensitivity (ϵ_{opt}) and the nonlinear constraint infeasibility (ϵ_{infs}) at the updated pair of primal-dual variables (Wolf & Marquardt, 2016):

$$\epsilon_{opt} = \frac{\|\frac{\partial \mathcal{L}^*_{i:}}{\partial \vec{z}}\|_\infty}{\|\vec{\lambda}^*_{i:}\|_2 + \|\vec{\mu}^*_{i:}\|_2 + 1}, \; \epsilon_{infs} = \frac{\|\vec{g}^{*^+}_{i:}\|_\infty + \|\vec{h}^*_{i:}\|_\infty}{\|\vec{z}^*_{i:}\|_2 + 1}. \tag{II.37}$$

If these metrics were higher than pre-defined values, the set of first and second-order sensitivities $\mathcal{F}^*_{i:} := \{\frac{\partial^2 \mathcal{L}^*_{i:}}{\partial \vec{z}^2_{i:}}, \frac{\partial^2 \mathcal{L}^*_{i:}}{\partial \vec{z}_{i:} \partial \vec{p}}, \frac{\partial \vec{f}^*_{i:}}{\partial \vec{z}_{i:}}, \frac{\partial \vec{g}^*_{i:}}{\partial \vec{z}_{i:}}, \frac{\partial \vec{g}^*_{i:}}{\partial \vec{p}}, \frac{\partial \vec{h}^*_{i:}}{\partial \vec{z}_{i:}}, \frac{\partial \vec{h}^*_{i:}}{\partial \vec{p}}\}$ would be updated with the new $\left(\vec{z}^*_{i:}, \vec{\lambda}^*_{i:}, \vec{\mu}^*_{i:}\right)$ solution and $\vec{p}$, and further iterations of $\mathcal{Q}_{N-i}$ would be triggered until satisfying feasibility and optimality criteria.

Summing up, if $\Delta\vec{p}$ is small, it is not really necessary to solve $\mathcal{P}_{N-i}$ at each time sample. In the neighbourhood of the active optimal solution, parametric sensitivities can be calculated to rapidly update the optimal solution at τ_i using a first-order approximation and checking for optimality and feasibility criteria. This fast trajectory update is performed by solving $\mathcal{Q}_{N-i}$, which is expected to be faster than $\mathcal{P}_{N-i}$.

A virtue of this method is that $\mathcal{F}^*_{i:}$ can be evaluated in the background at the preceding optimal solution assuming the estimated parameters $\vec{p}$ (Würth *et al.*, 2008a; Gros *et al.*, 2009). Then, the optimal solution is updated on-line by solving $\mathcal{Q}_{N-i}$ almost instantaneously right after measuring and/or estimating $\vec{p}$. This is why this method is commonly referred as sensitivity-based NMPC (SbNMPC).

Algorithm (II.2) shows the main steps of SbNMPC, where τ_{opt} and τ_{infs} are the pre-defined tolerances for the optimality and feasibility criteria, respectively. The contingency step (line 17 in Algorithm II.2) is optional. An alternative is to not update the trajectory if the optimality and feasibility criteria are not satisfied after k_{max} QP iterations.

Algorithm II.2: *Working principle of the sensitivity-based NMPC (SbNMPC)*

1: $\left(\vec{z}^*, \vec{\lambda}^*, \vec{\mu}^*\right) \leftarrow \mathcal{P}_N\left(\vec{p}\right)$
2: Build $\mathcal{F}^*_{1:}$ from $\mathcal{F}^*$
3: **for** $i = 1, \ldots, N-1$ **do**
4: Measure $\vec{X}$ and estimate $\vec{d}$
5: $\vec{p} \leftarrow \begin{bmatrix} \vec{X} \\ \vec{d} \end{bmatrix}$
6: $\Delta\vec{p} \leftarrow \vec{p} - \vec{p}(\tau_{i-1})$
7: $\left(\Delta\vec{z}^*_{i:}, \vec{\lambda}^*_{i:}, \vec{\mu}^*_{i:}\right) \leftarrow \mathcal{Q}_{N-i}\left(\Delta\vec{p}\right)$
8: $\vec{z}^*_{i:} \leftarrow \vec{z}^*_{i:} + \Delta\vec{z}^*_{i:}$
9: Evaluate $\mathcal{F}^*_{i:}$ at the new $(\vec{z}^*_{i:}, \vec{\lambda}^*_{i:}, \vec{\mu}^*_{i:})$ and $\vec{p}$
10: $k \leftarrow 1$
11: **while** $(\epsilon_{opt} > \tau_{opt} \,|\, \epsilon_{infs} > \tau_{infs})$ & $k <= k_{max}$ **do**
12: $\left(\Delta\vec{z}^*_{i:}, \vec{\lambda}^*_{i:}, \vec{\mu}^*_{i:}\right) \leftarrow \mathcal{Q}_{N-i}\left(0\right)$
13: $\vec{z}^*_{i:} \leftarrow \vec{z}^*_{i:} + \Delta\vec{z}^*_{i:}$
14: Evaluate $\mathcal{F}^*_{i:}$ at the new $(\vec{z}^*_{i:}, \vec{\lambda}^*_{i:}, \vec{\mu}^*_{i:})$ and $\vec{p}$
15: $k \leftarrow k + 1$
16: **if** $k == k_{max}$ **then**
17: $\left(\vec{z}^*_{i:}, \vec{\lambda}^*_{i:}, \vec{\mu}^*_{i:}\right) \leftarrow \mathcal{P}_{N-i}\left(\vec{p}\right)$ using warm start
18: Build $\mathcal{F}^*_{i+1}$ from $\mathcal{F}^*_{i:}$
19: Build the guess for $\vec{z}^*_{i+1:}$, $\vec{\lambda}^*_{i+1:}$ and $\vec{\mu}^*_{i+1:}$ from $\vec{z}^*_{i:}$, $\vec{\lambda}^*_{i:}$ and $\vec{\mu}^*_{i:}$, respectively
20: Implement $\vec{u}^*_i$ until τ_{i+1}

It should be noted that sensitivity-based trajectory updates presented in this section will work only for small perturbations of the parameters vector, since they are based on a linear approximation of the necessary conditions of optimality. For large perturbations, the linear approximation will not be accurate enough, and a large amount of QP iterations might be required to satisfy feasibility and optimality criteria.

II.3.4.3 Advanced-step NMPC (AsNMPC)

Consider that at any τ_i, $i = 0, \ldots, N-1$, the current state vector is $\vec{X}$ and that $\vec{u}_i^*$ is applied to the system. If the model and associated parameters used during the trajectory optimisation process match with the reality, the system will evolve according to $\vec{F}$. Under these circumstances, at τ_i it is possible to predict with high accuracy the future state vector $\hat{\vec{X}}(\tau_{i+1})$ and, using the most recent prediction for $\hat{\vec{d}}$, solve $\mathcal{P}_{N-i+1}$ in advance. If this problem can be solved in background during the discretisation interval $[\tau_i, \tau_{i+1}]$, and under the strong assumption that the models match the reality, then $\vec{u}_{i+1}^*$ will be already available when reaching τ_{i+1}. Accordingly, when using this guidance strategy, the discretisation interval between two consecutive time samples needs to be higher than the expected time required to solve the optimisation problem.

Even if the execution time could be guessed from past experience, in some particular cases the optimisation may not finish before the next time sample. If this were the case, one of the following three contingency actions could be implemented: first, to stop the optimisation and not update the optimal trajectory at the current time sample; second, to wait until the optimisation finishes, and then shift the remaining time sample in such a way that the separation between them keeps unchanged; third, to wait until the optimisation finishes, but keeping the remaining time samples at their original values.

This simple approach allows to remove the computational delay and associated issues of the INMPC. In the presence of errors in the models, however, the real state vector at τ_i will not coincide with that predicted at τ_{i-1}. In this case, the optimal control cannot be computed in advance with accuracy. In order to account for errors in the models used by the FMS planning function, a fast update using parametric sensitivities can be used when measuring the actual state and parameters at τ_i. This strategy, which mixes an advanced full recalculation in background with an on-line sensitivity-based update when receiving measurements, is shown in Algorithm (II.3) (Jäschke *et al.*, 2014; Zavala & Biegler, 2009).

Algorithm II.3: *Working principle of the advanced-step NMPC (AsNMPC)*

1: $\left(\vec{z}^*, \vec{\lambda}^*, \vec{\mu}^*\right) \leftarrow \mathcal{P}_N\left(\vec{p}\right)$
2: Build $\vec{z}_{1:}^*$, $\vec{\lambda}_{1:}^*$ and $\vec{\mu}_{1:}^*$ from $\vec{z}^*$, $\vec{\lambda}^*$ and $\vec{\mu}^*$
3: **for** $i = 1, \ldots, N-1$ **do**
4: Predict $\hat{\vec{X}}$ and $\hat{\vec{d}}$
5: $\hat{\vec{p}} \leftarrow \begin{bmatrix} \hat{\vec{X}} \\ \hat{\vec{d}} \end{bmatrix}$
6: $\left(\vec{z}_{i:}^*, \vec{\lambda}_{i:}^*, \vec{\mu}_{i:}^*\right) \leftarrow \mathcal{P}_{N-i}\left(\hat{\vec{p}}\right)$ using warm start
7: Evaluate $\mathcal{F}_{i:}^*$ at the new $(\vec{z}_{i:}^*, \vec{\lambda}_{i:}^*, \vec{\mu}_{i:}^*)$ and $\hat{\vec{p}}$
8: Measure $\vec{X}$ and estimate $\vec{d}$
9: $\vec{p} \leftarrow \begin{bmatrix} \vec{X} \\ \vec{d} \end{bmatrix}$
10: $\Delta\vec{p} \leftarrow \vec{p} - \hat{\vec{p}}$
11: $\left(\Delta\vec{z}_{i:}^*, \vec{\lambda}_{i:}^*, \vec{\mu}_{i:}^*\right) \leftarrow \mathcal{Q}_{N-i}\left(\Delta\vec{p}\right)$
12: $\vec{z}_{i:}^* \leftarrow \vec{z}_{i:}^* + \Delta\vec{z}_{i:}^*$
13: Same as steps 9 to 20 of Algorithm (II.2)

You may delay, but time will not.

— Benjamin Franklin

I only feel angry when I see waste. When I see people throwing away things we could use.

— Mother Teresa

III

The energy-neutral time window

Arrival managers (AMANs) were designed to provide support for air traffic control (ATC) when sequencing and merging arrival traffic in the terminal maneouvering area (TMA). Existing AMANs use ground-based trajectory predictors to estimate the time of arrival of each inbound flight. These trajectory predictions are used to provide sequence information to the ATC, and also advisories of the required time to loose or gain for each flight in order to achieve the desired landing rate and spacing at the runway. The ATC is then responsible for selecting and notifying appropriate instructions (e.g., vectoring, speed changes) for the aircraft to loose or gain that time.

Future AMANs will also determine the optimum landing sequence based on inbound flight plans and trajectory predictions. Then, a controlled time of arrival (CTA) will be calculated for each inbound aircraft at a specific metering fix such that the required landing rate and spacing are satisfied. When executed with sufficient timing accuracy, the CTAs will help to achieve an orderly arrival sequence of optimum descent profiles without excessive workload to the ATC.

In order to efficiently allocate the CTAs, AMANs should know the earliest and latest time of arrival of each inbound flight (i.e., the feasible time window). An estimation of the feasible time window could be computed by the same ground system based on trajectory predictions. The models used by the ground-based trajectory predictor to represent the aircraft dynamics and performance, however, are typically subject to several simplifications, which limit the accuracy of the trajectory predictions. Furthermore, even if the models used by the ground-based trajectory predictor were perfect, the lack of flight intent information would make difficult to accurately predict the trajectory of the aircraft. A novel concept for synchronisation of ground-based trajectory predictors and flight management systems (FMSs) was proposed by Bronsvoort (2014), in which FMSs provide to the ground system flight intent information to improve their predictions.

An alternative solution consists of using the on-board trajectory planner of the aircraft, which obviously knows the flight intent and has access accurate aircraft dynamics and performance models, to compute both the earliest and latest times of arrival at the metering and report them to the AMAN. Having this valuable information for all aircraft, the AMAN could compute the required CTAs (SESAR, 2015b).

The earliest and latest times of arrival depend on many factors, including aircraft performance, weather conditions and, noticeably, the current aircraft states when computing it (i.e., altitude, speed, mass and remaining distance to the metering fix). If the aircraft were in the cruise phase, the time of arrival at the metering fix could be easily modified by advancing or receding the position of the top of descent (TOD). Therefore, wide feasible time windows are expected for aircraft that have not initiated their descent yet. In some circumstances, however, the aircraft might be required to adapt the time of arrival after initiating the descent (e.g., due to a late CTA update or a large time deviation). In this situation, time and energy management concepts might still be used to efficiently re-plan the trajectory and adjust the time of arrival to the requested CTA with minimum fuel consumption and speed brakes use. The extent for which energy management can be used to adjust the time of arrival in this situation depends on the feasible time window, which, to the best of our knowledge, has not been quantified before.

In this chapter, the feasible time windows for energy-neutral trajectories are quantified, assuming that the descent has been already initiated when the time of arrival at the metering fix needs to be changed by the on-board trajectory planner. In order to accomplish that, the earliest and latest times of arrival at a metering fix are computed for a wide range of aircraft states. This optimisation is restricted in such a way that neither thrust higher than idle nor speed brakes use are allowed along the whole descent. In this way, the entire trajectory is subject to optimisation to minimise or maximise the flight time, and only elevator control is left to modify the speed profile and change the time of arrival of the energy-neutral trajectory. In addition, the CTA window sensitivity to different longitudinal winds, metering fix position and masses is also investigated.

III.1 State of the art

Several studies have dealt with the assignment of CTA and the quantification of the feasible CTA windows when the aircraft is still in cruise, well before reaching the TOD. See for instance the works of Takeichi (2017) and Park & Clarke (2013, 2016), which computed CTA windows at a metering fix by allowing the aircraft to adjust the TOD position (i.e., the duration of the cruise phase) and the descent speed profile, while keeping the thrust at idle during the whole descent. With similar purposes, Takeichi & Inami (2010) also enabled the addition (resp. omission) of waypoints to stretch (resp. shorten) the flight path length in addition to adjust the TOD under a tailored arrivals (TAs) concept. However, in the cruise phase, energy must be added to the system by means of throttle in order to maintain constant altitude and speed. This leads to considerably more fuel consumption and emissions than during an energy-neutral descent.

The robustness of energy-neutral descent trajectories facing late changes to the CTA during the descent was assessed by Lindsay *et al.* (2009). Aiming to minimise the environmental impact of the continuous descent operation (CDO), only elevator control was permitted to adjust the time at which the metering fix was reached, assuming rather simple Mach/callibrated airspeed (CAS) profiles and allowing a single (and instantaneous) modification of the scheduled speed. Furthermore, the assessment was performed for few initial aircraft states, and the method used to generate the energy-neutral descents could not ensure the optimality (in the strict mathematical sense) of the resulting trajectories.

Another important limitation of previous works is that none of them (up to our best knowledge) took into account the remaining descent between the metering fix at which the CTA was assigned and the instrumental landing system (ILS) interception or the runway threshold. Adjusting the descent speed profile to minimise or maximise flight time may result in a change to the altitude at which the metering fix is overflown. If the energy of the aircraft at this fix were too low, additional thrust might be needed after overflying it, interrupting in this way the CDO. Similarly, if the energy were too high, it might be required to use speed brakes and/or to deploy high-lifting devices or the landing gear earlier than initially planned, leading to more airframe noise.

Furthermore, most previous works used the base of aircraft data (BADA) v3 performance model, which has been reported to show significant limitations for accurate trajectory planning tasks in the TMA (Senzig *et al.*, 2009; Hoekstra, 2016). More sophisticated aircraft performance models (APMs) are needed in order to compute realistic descent profiles and to obtain accurate fuel consumption and flight time, in particular time window, figures.

III.2 Setup of the experiment

The goal for the study was to quantify the CTA window (latest arrival time - earliest arrival time) at a certain metering fix as a function of the aircraft state when receiving the CTA after the TOD, and to study the sensitivity of the feasible CTA window to the following parameters: initial speed when receiving the CTA, aircraft mass, position of the metering fix along the route and longitudinal wind speed. In order to accomplish that, thousands of optimal trajectory plans starting at different aircraft states and configured with different values of the listed parameters were generated to minimise and maximise the time of arrival at a single metering fix. The optimisation of these aircraft trajectories was formulated as an optimal control problem as described in Section II.2.1, and was solved by using the numerical optimisation techniques described in Section II.2.3.

This section describes the setup of the experiment performed in this chapter. First, Section III.2.1 presents the scenario. Then, the generic models introduced in Section II.1 are particularised for this experiment in Section III.2.2. Analogously, the generic optimal control problem described in Section II.2.1 is particularised in Section III.2.3 with specific cost function and constraints. Finally, the selected case studies are listed in Section III.2.4.

III.2.1 Scenario

Considering a specific aircraft type, descent procedure with associated constraints, geographical location and realistic weather conditions corresponding to a certain day and time only gives a clue of the feasible CTA window for that particular scenario, and results might not be representative of other scenarios. Since computing the CTA time window for all possible scenarios would be impracticable in combinatorial terms, this study aimed to be as generic as possible.

Based on the discussion above, the following generic scenario was considered in this experiment: an Airbus A320 (one of the mostly used commercial aircraft types nowadays in Europe) attempts to perform an energy-neutral descent along an hypothetical straight-line route from the TOD to the interception of the ILS glide slope at the final approach point (FAP), and somewhere in the descent, before reaching the initial approach fix (IAF), the ATC assigns (or updates) a CTA at this metering fix. The typical speed constraint of 250 kt at FL100, enforced nowadays in most of the TMAs, was also considered in the formulation of the optimal control problem. Figure III-1 shows a schematic representation of this scenario.

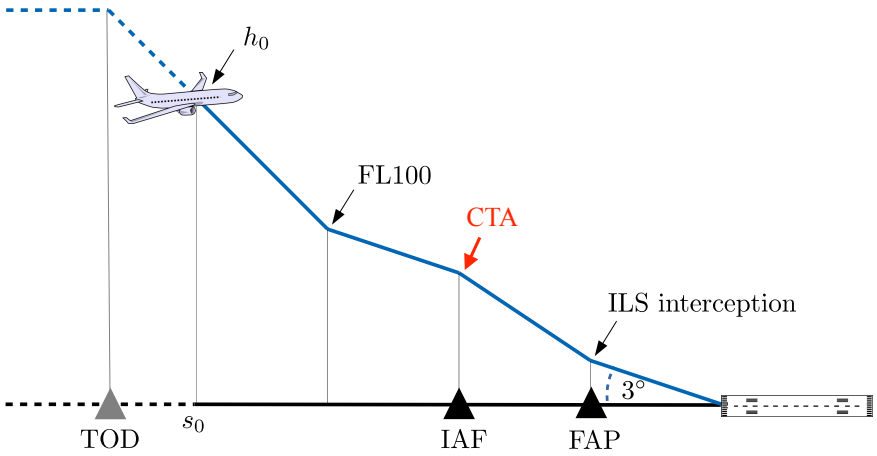

Figure III-1: *Scenario to investigate the feasible time window of energy-neutral descents*

III.2.2 Models

The models required to formulate the optimisation of the aircraft trajectory, which were presented in Section II.1, are particularised below for the experiment conducted in this chapter.

III.2.2.1 Aircraft dynamics model

The point-mass model described by Eq. (II.1) was reduced to a γ-*command* model, which could be considered accurate enough for the objectives of the experiment. The γ-*command* model assumes continuous vertical equilibrium thorough the flight (i.e., lift balances weight):

$$\dot{\gamma} = 0 \rightarrow L = mg\cos\gamma. \tag{III.1}$$

As a result, Eq. (II.1b) is removed from Eq. (II.1) and the aerodynamic flight path angle becomes an input control variable that can change instantaneously.

The following assumptions were also considered:

- The effect of the cross-wind on the ground speed is orders of magnitude below that of the longitudinal wind (i.e., $w_x = 0$).
- The longitudinal wind is a function of only the altitude (i.e., $w_s = w_s(h)$).
- The fuel consumption during an energy-neutral descent is a very small fraction of the total mass (Clarke *et al.*, 2004) and, consequently, the variations in mass m can be neglected (i.e., $\dot{m} = 0$). In spite of that, the idle fuel flow q_{idle} was computed in the model to determine the amount of fuel consumption for each trajectory, which was used as a metric during the assessment of results.

Under the aforementioned assumptions, Eq. (II.1) can be simplified to:

$$\begin{aligned}
\frac{\mathrm{d}v}{\mathrm{d}t} &= \dot{v} = \frac{T_{idle}(v,h) - D(v,h,\gamma,\zeta)}{m} - g\sin\gamma \\
\frac{\mathrm{d}s}{\mathrm{d}t} &= \dot{s} = v\cos\gamma + w_s(h) \\
\frac{\mathrm{d}h}{\mathrm{d}t} &= \dot{h} = v\sin\gamma.
\end{aligned} \tag{III.2}$$

In this widely known γ-*command* model, the state vector is $\vec{x} = [v, s, h]^T$. Furthermore, since neither additional thrust nor speed brakes use is permitted, the control vector is composed by only the aerodynamic flight path angle (i.e., $\vec{u} = [\gamma]$), and the thrust in Eq. (II.1a) is replaced by T_{idle}, which mathematical expression, function of $\vec{x}$, is particularised by the APM described below.

III.2.2.2 Aircraft performance model

Aerodynamic and propulsive data from the Airbus performance engineering program (PEP) were taken to approximate the drag coefficient, idle thrust, and idle fuel flow tables with continuous and twice-differentiable functions suitable for gradient-based nonlinear programming (NLP) optimisation algorithms, as suggested in Section II.2.4.2. Using these accurate data from the manufacturer allowed us to obtain realistic fuel and flight time figures.

The drag coefficient was approximated by a smoothing spline of the form:

$$C_D\left(C_L, M, h\right) = \sum_{i,j,k} c_{i,j,k} B_i(C_L) B_j(M) B_k(h). \tag{III.3}$$

Assuming temperature changes only with altitude, the Mach number can be expressed as a function of the altitude and speed:

$$M(v,h) = \frac{v}{a(h)} = \frac{v}{\sqrt{\gamma_a R \theta(h) \tau_{SSL}}}, \tag{III.4}$$

where a is the speed of sound.

In Eq. (III.3), $B_{(\cdot)}$ (with $(\cdot) \in \{i,j,k\}$) are spline basis functions; $c_{i,j,k}$ are control points of the spline (de Boor, 1972); and C_L is the lift coefficient, which can be obtained by assuming continuous vertical equilibrium (see Eq. (III.1)) and solving Eq. (II.2a) for C_L:

$$C_L(v,h,\gamma) = \frac{2mg\cos\gamma}{S\rho_{SSL}\sigma(h)v^2}. \tag{III.5}$$

Following the same methodology, T_{idle} and q_{idle} were expressed as a function of h and M:

$$T_{idle}\left(h,M\right) = \sum_{i,j} c_{i,j} B_i\left(h\right) B_j\left(M\right), \tag{III.6a}$$

$$q_{idle}\left(h,M\right) = \sum_{i,j} c_{i,j} B_i\left(h\right) B_j\left(M\right). \tag{III.6b}$$

The control points and knots of the splines appearing in Eqs. (III.3) and (III.6) were obtained by fitting the aircraft performance data from the manufacturer using the FITPACK library (Dierckx, 1993). Figure III-2 shows the smoothing splines functions approximating the aircraft performance data obtained from PEP.

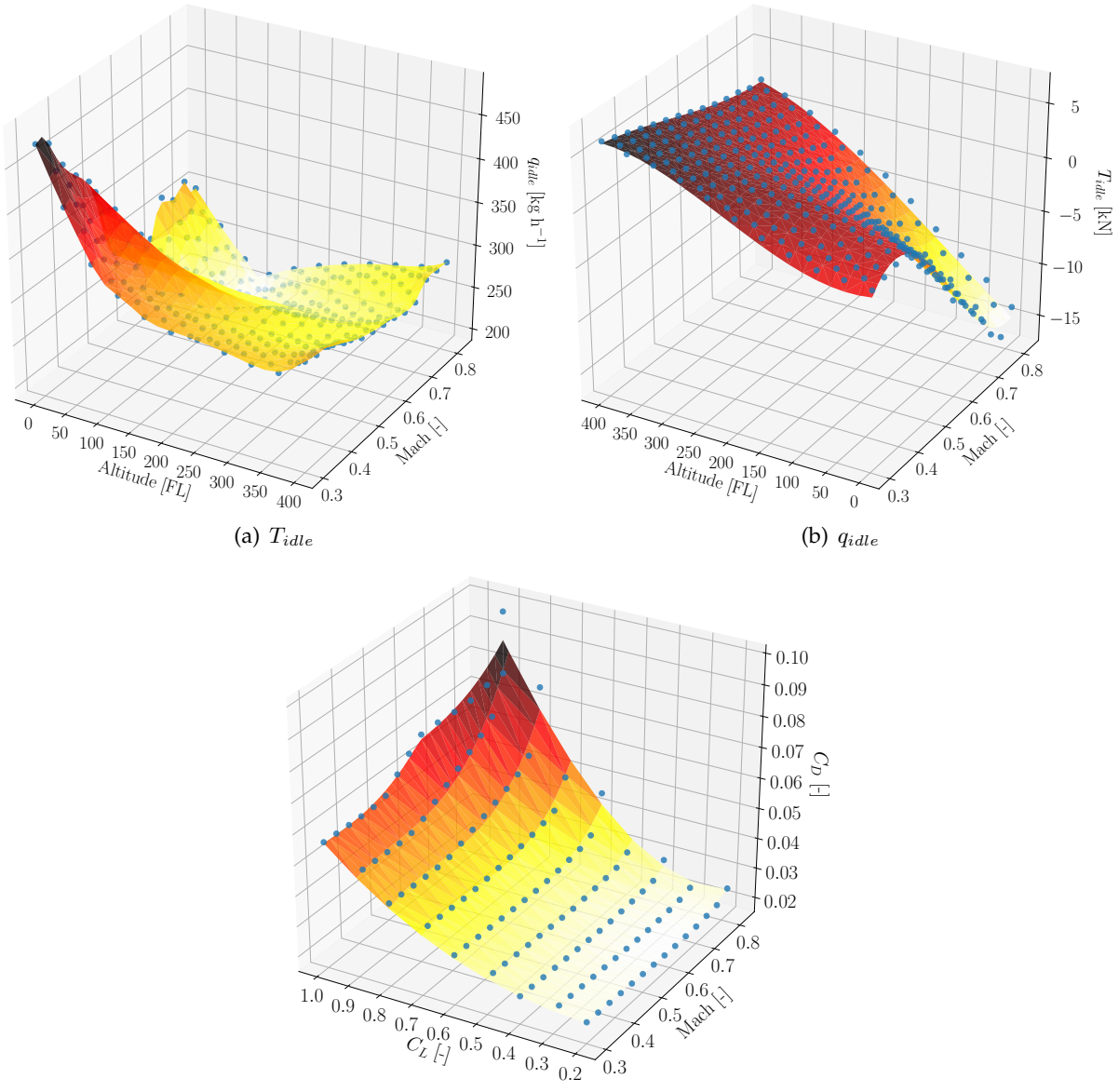

(a) T_{idle}

(b) q_{idle}

(c) C_D (for $h = 0$)

Figure III-2: *Smoothing spline approximating aircraft performance data obtained from PEP*

III.2.2.3 Weather model

This study aimed to be as generic as possible. Accordingly, the international standard atmosphere (ISA) model, established to provide a common reference for temperature and pressure, was considered to represent the normalised temperature θ and pressure δ as a function of h through Eqs. (II.4) and (II.5), respectively. Then, the normalised density was computed assuming the perfect gas law relationship with Eq. (II.6).

With the same rationale, the empirical Hellman model defined by Eq. (II.7) was used to represent the wind speed as a function of h. The parameters of this empirical model were particularised as follows: $\alpha = 1/7$, which is the typical value for neutral stability conditions; h_r was set to 36,000 ft; and different values of w_r were analysed to assess the sensitivity of the feasible time window to the longitudinal wind speed (see Section III.2.4 for the detailed list of case studies). In addition, the wind vector was assumed to point in the direction of the aircraft track (i.e., $w_s = |\vec{w}|$).

III.2.3 Optimal control problem formulation

The optimisation process adopted to generate earliest and latest trajectories at the metering fix is a constrained, multi-phase and nonlinear optimal control problem, as described in Section II.2.1. This section particularises the cost function and constraints of the generic multi-phase optimal control problem Eq. (II.10) for each one of the phases composing the flight profile of an energy-neutral CDO.

The differential constraints ($\vec{f}$) were particularised by the γ-*command* model given by Eq. (III.2):

$$\vec{f}_j = \begin{bmatrix} \frac{T_{idle}(v,h) - D(v,h,\gamma,\zeta_j)}{m} - g\sin\gamma \\ v\cos\gamma + w_s(h) \\ v\sin\gamma \end{bmatrix}; j = 0, \ldots, P-1, \tag{III.7}$$

where ζ_j is the flaps/slats configuration of the j^{th} phase. In this experiment, ζ_j was set to *clean* (i.e., no flaps/slats deployed) for all phases except for the last one, which modelled the approach.

In order to mimic a representative yet generic operation, the descent was split into $P = 4$ phases, where different phase-dependent path, algebraic and interior-point constraints may apply. Table III-1 wraps up the different phases and their constraints. This table is illustrated in Fig. III-3.

Table III-1: *Definition of the phases and constraints for an energy-neutral descent*

Phase (j)	Description	$\vec{b}_j^{in}$	$\vec{b}_j^{eq}$	$\vec{\vartheta}_j^{in}$	$\vec{\vartheta}_j^{eq}$
0	Descent above FL100	$\begin{bmatrix} v_{CAS}(v,h) - \text{VMO} \\ \text{GD} - v_{CAS}(v,h) \end{bmatrix}$	-	-	$\begin{bmatrix} h - 10{,}000\,\text{ft} \end{bmatrix}$
1	Descent below FL100	$\begin{bmatrix} \text{GD} - v_{CAS}(v,h) \\ v_{CAS}(v,h) - 250\,\text{kt} \end{bmatrix}$	-	-	$\begin{bmatrix} s - s_{\text{IAF}} \end{bmatrix}$
2	Approach	$\begin{bmatrix} \text{GD} - v_{CAS}(v,h) \\ v_{CAS}(v,h) - 250\,\text{kt} \end{bmatrix}$	-	-	$\begin{bmatrix} v_{CAS}(v,h) - \text{GD} \\ h - h_{\text{FAP}} \end{bmatrix}$
3	Levelled deceleration	$\begin{bmatrix} v_{\text{FAP}} - v_{CAS}(v,h) \\ v_{CAS}(v,h) - \text{GD} \end{bmatrix}$	$\begin{bmatrix} \dot{h} \end{bmatrix}$	-	-
All	Entire descent	$\begin{bmatrix} M(v,h) - \text{MMO} \\ \gamma \\ \gamma_{min} - \gamma \end{bmatrix}$	-	-	-

Several path constraints applying all along the descent were also considered in order to ensure that the Mach number remains within operational limits and that the maximum descent gradient is not exceeded. The maximum operative CAS (VMO) and the maximum operative Mach (MMO) are constant parameters that depend on the aircraft type. In this study, MMO and VMO were set to 0.80 and 340 kt, respectively, according to Airbus (1993). Furthermore, v_{FAP} corresponds to the CAS that the aircraft should have when intercepting the ILS glide slope at the FAP, and was computed as a fraction of the stall speed, which is a function of both m and ζ (Airbus, 1993). The maximum descent gradient (γ_{min}) was set to -15°.

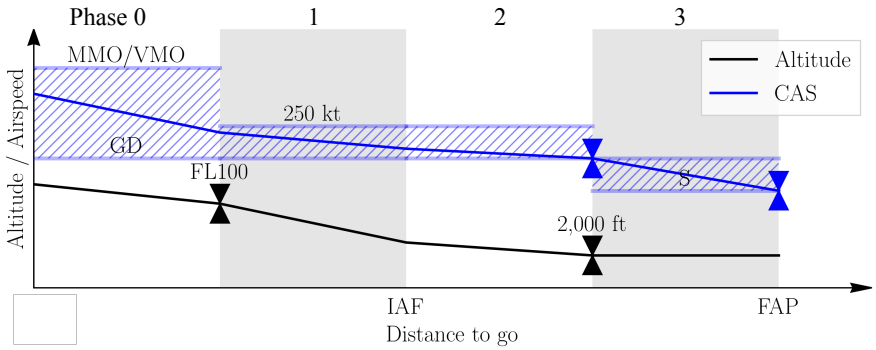

Figure III-3: *Definition of the phases and constraints for an energy-neutral descent*

According to Table III-1, the first phase starts at the current state of the aircraft ($\vec{X}$) and ends at FL100. Note that since the goal of this study was to quantify the CTA window for different initial conditions, the optimal control problem was solved for several values of $\vec{X}$. Below FL100, ATC procedures typically restrict the CAS to 250 kt. Afterwards, the aircraft heads towards the IAF, where the approach procedure begins. Few nautical miles before the FAP, the aircraft decelerates to the green dot speed (GD)[1] and starts configuring with flaps at constant altitude (still at idle thrust), in order to intercept the ILS glide slope at the FAP. Therefore, terminal constraints were:

$$\vec{\psi} = \begin{bmatrix} v_{CAS}(v,h) - v_{\text{FAP}} \\ h - h_{\text{FAP}} \\ s - s_{\text{FAP}} \end{bmatrix}, \tag{III.8}$$

where h_{FAP} is the altitude at which the FAP has to be intercepted, which value was set to 2,000 ft; and the distance of the FAP (s_{FAP}) was fixed at 6 NM from the runway threshold (see Fig. III-1).

The objective of this study was to compute trajectories minimising and maximising the time of arrival at a given metering fix, which was assumed to be the IAF of an hypothetical straight-line procedure. Accordingly, the running cost function was defined as:

$$\pi_j = \begin{cases} \pm \frac{1}{v\cos\gamma + w_s(h)} & \text{if } j = 0, 1 \\ 0 & \text{otherwise,} \end{cases} \tag{III.9}$$

where the $+$ sign applied when computing the earliest trajectory, and $-$ when computing the latest. The end cost for each phase was not considered, that is $\phi_j = 0$ for $j = 0, \ldots, P-1$. Furthermore, since the duration of the time horizon, t_F, was not fixed but had to be optimised, t_{j+1} for $j = 0, \ldots, P-1$ were additional decision variables of the optimal control problem.

The optimal control particularised above was transformed to a parametric NLP optimisation problem as described in Section II.2.3. Then, the resulting parametric NLP optimisation problem was formulated in the general algebraic modelling system (GAMS) software suit, and solved with CONOPT as NLP solver, which uses active-set methods. In this experiment, the trapezoidal integration scheme was adopted to obtain $\vec{F}_j$ and Π_j from $\vec{f}_j$ and π_j, respectively. In addition, techniques to recover from infeasibility were not used, i.e., all the constraints shown in Table III-1 are *hard* constraints.

Last but not least, the profile shown in Table III-1 and Fig. III-3 does not include speed and altitude constraints throughout the descent (excepting the typical speed limit at FL100), aiming to be as generic as possible. Consequently, it is rather optimistic and the obtained results correspond to a best-case scenario. In current operations, aircraft may encounter additional altitude and speed constraints, which negative effect on the feasible CTA window would depend on their location and severity. It might even be the case that it would not be longer possible to reach the metering fix using neither additional thrust nor speed brakes. Nevertheless, it is expected that future procedures will trade altitude and speed constraints for CTAs, giving more flexibility to FMSs for planning the optimal trajectory provided that time CTAs are satisfied.

[1]For the Airbus A320, the green dot speed is the minimum operating speed in managed mode and clean configuration, being approximately the best lift-to-drag ratio speed.

III.2.4 Case studies

Taking into account all the possible combinations of initial altitude, distance to go and speed would lead to highly combinatorial problem, extremely difficult to visualise and analyse. In order to overcome this issue and present the results in an intuitive way, the feasible time window is shown as a function of the distance to go and altitude, either fixing the initial speed to a certain value or leaving it free (as an additional decision variable) during the optimisation process.

For a given initial altitude and distance to go, and assuming the constraints presented in Table III-1, the earliest and latest times of arrival at the metering fix (and therefore the feasible CTA window) could be affected by the aircraft mass, the longitudinal wind, the exact location of the metering fix along the arrival route, and the initial speed of aircraft.

A case study with intermediate values for these parameters was taken as baseline. For each one of these parameters, negative and positive variations were considered, aiming at investigating the parametric sensitivity of the feasible CTA window. As a result, 14 representative case studies were chosen for this study, which are summarised in Table III-2.

Table III-2: *List of case studies for the energy-neutral feasible time window assessment*

Parameter	Negative variation	Baseline	Positive variation
m [% MLM]	80	90	100
s_{IAF} [NM]	15	25	50
w_s [kt]	$-60,\ -40,\ -20$	0	$20,\ 40,\ 60$
Initial speed (v)	Minimum (GD)	Medium	Maximum (MMO/VMO/250 kt)

The baseline case study assumed a typical landing mass corresponding to 90% of the maximum landing mass (MLM), an IAF located at 25 NM from the runway threshold and calm wind conditions. It was also assumed that the aircraft received the CTA when flying at a speed corresponding to a kinetic energy in the middle of the feasible kinetic energy range, which depends on the current altitude. Above the cross-over altitude (h_{CO}) the maximum airspeed (v_{max}) is limited by MMO, between the cross-over altitude and FL100 by VMO, and below FL100 by 250 kt in terms of CAS:

$$v_{max}(h) = \begin{cases} v\,(\text{MMO}, h) & \text{if } h_{\text{CO}}(M, v_{CAS}) < h \\ v\,(\text{VMO}, h) & \text{if } 10,000\,\text{ft} < h \leq h_{\text{CO}}(M, v_{CAS}) \\ v\,(250\,\text{kt}, h) & \text{if } h \leq 10,000\,\text{ft}, \end{cases} \tag{III.10}$$

where:

$$v(M, h) = M\sqrt{R\gamma_a\tau_{SSL}\theta(h)} \tag{III.11a}$$

$$v(v_{CAS}, h) = \sqrt{\frac{2\gamma_a}{\gamma_a - 1}\frac{\delta(h)p_{SSL}}{\sigma(h)\rho_{SSL}}\left(\left(\frac{A(v_{CAS})}{\delta(h)} + 1\right)^{\frac{\gamma_a - 1}{\gamma_a}} - 1\right)} \tag{III.11b}$$

and

$$A(v_{CAS}) := \left(\frac{1}{2}\frac{\gamma_a - 1}{\gamma_a}v_{CAS}^2\left(\frac{\rho_{SSL}}{p_{SSL}}\right) + 1\right)^{\frac{\gamma_a}{\gamma_a - 1}} - 1. \tag{III.12}$$

The cross-over altitude can be calculated as:

$$h_{\text{CO}}(M, v_{CAS}) = \frac{\tau_{SSL}}{\lambda_\tau}\left(1 - \left(\frac{\left(1 + \left(\frac{\gamma_a - 1}{2}\right)\left(\frac{v_{CAS}}{a_{SSL}}\right)^2\right)^{\frac{\gamma_a - 1}{\gamma_a}} - 1}{\left(1 + \frac{\gamma_a - 1}{2}M^2\right)^{\frac{\gamma_a - 1}{\gamma_a}} - 1}\right)^{-\frac{\lambda_\tau R}{g}}\right). \tag{III.13}$$

Regardless of the initial altitude, the minimum kinetic energy before the IAF is always limited by GD, which is also given in terms of CAS and is computed as a function of m (Airbus, 1993):

$$v_{min}(h,m) = v\left(\mathrm{GD}(m), h\right). \tag{III.14}$$

As seen above, the maximum and minimum operational speeds are given in terms of CAS or Mach, thus they were converted to true airspeed (TAS) by using Eqs. (III.11b) and (III.11a), respectively. Then, the maximum and minimum kinetic energies were computed and the speed corresponding to their average was used to set the initial speed of the descent in $\vec{X}$:

$$v_0(h,m) = \sqrt{2\frac{\frac{1}{2}mv_{max}^2(h) + \frac{1}{2}mv_{min}^2(h,m)}{m}} = \sqrt{v_{max}^2(h) + v_{min}^2(h,m)}. \tag{III.15}$$

Three additional case studies were considered to assess the sensitivity of the feasible time window to the initial speed: for the first case study, the aircraft received the CTA update when flying at the maximum speed (either MMO, VMO or 250 kt, depending on the altitude); for the second case study, the initial airspeed was fixed to that corresponding to GD; for the third case study, the initial airspeed was left free, assuming that the transition from any airspeed to that chosen by the optimiser would be quick enough in practice by using the elevator, and neglecting the thrust or drag required to reach such energy level.

For each case study shown in Table III-2, the earliest and latest trajectories at the IAF were computed at all possible combinations of initial altitude and distance to go in the selected ranges. Initial altitudes between FL100 and FL360 and distances to go ranging from $s_{\mathrm{IAF}} + 5$NM to 120 NM were considered.

It should be noted that, for each initial aircraft state, there exist many energy-neutral trajectories that satisfy the constraints listed in Table III-1. Only one of them, however, is optimal in terms of fuel consumption. In order to quantify the extra fuel consumption that earliest and latest trajectories would entail, the minimum fuel trajectory was also computed for each initial condition of the baseline case study. When computing the minimum fuel trajectory, the running cost in Eq. (III.9) was set to:

$$\pi_j = q_{idle}(v,h);\ j = 0,\ldots,P-1. \tag{III.16}$$

III.3 Results

This section presents the results obtained after computing the earliest and latest trajectories at the IAF, starting at different initial altitudes and distances to go, for the case studies listed in Table III-2. First, Section III.3.1 shows and analyses examples of earliest and latest trajectories for illustrative purposes. Then, the results for the baseline case study are thoroughly discussed in Section III.3.2. Finally, the results for the remaining case studies are shown in Section III.3.3.

III.3.1 Earliest and latest trajectory examples

Figure III-4 shows four examples of optimal energy-neutral trajectories computed for an Airbus A320 located at 70 NM from the runway threshold, and with an initial speed corresponding to the middle of the feasible kinetic energy range (i.e., for the baseline case study).

Figures III-4(a) and III-4(b) show, respectively, the earliest and latest trajectories at the IAF for a situation where the aircraft has excess of energy. In both cases, the aircraft aims at increasing the aerodynamic drag in order to release enough energy so that all the constraints are satisfied. This requirement penalises the latest trajectory, which would like to fly at a lower speed. Initially, altitude is exchanged by speed at the maximum descent gradient until VMO is reached. Thereafter, the descent is performed at this speed down to FL100, where the aircraft levels-off (but maintaining thrust idle) in order to decelerate as quick as possible. Below this altitude, the earliest and latest trajectories keep, respectively, the maximum and minimum allowed speed until the IAF. What happens after the IAF has no impact on the cost function. Yet, all the constraints in Table III-1 must still be satisfied and it does impact on the shape of the whole trajectory. For this flight conditions, the time window is around 20 seconds.

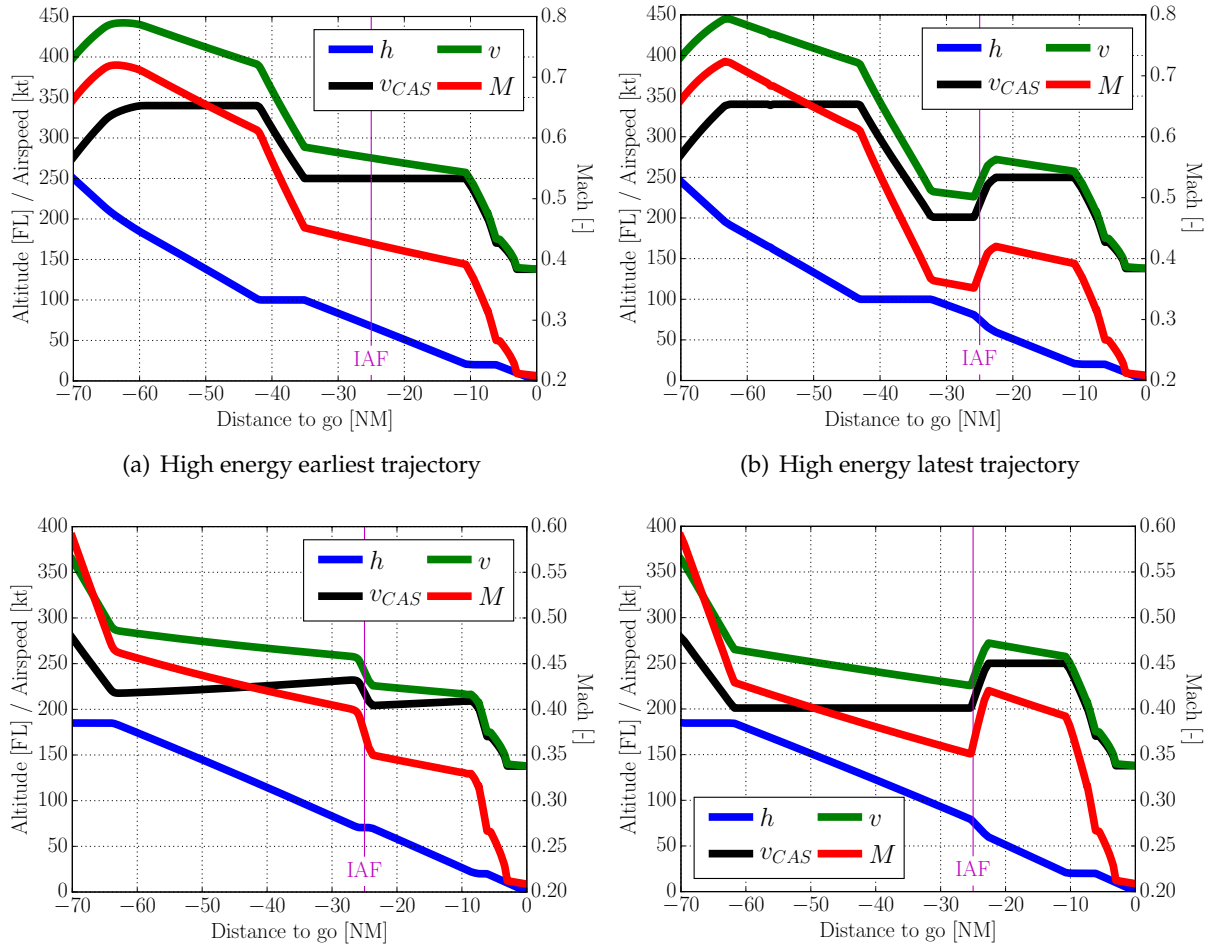

(a) High energy earliest trajectory

(b) High energy latest trajectory

(c) Low energy earliest trajectory

(d) Low energy latest trajectory

Figure III-4: *Examples of earliest and latest energy-neutral trajectories*

By contrast, Figs. III-4(c) and III-4(d) show, respectively, the earliest and latest trajectories for a situation where the aircraft lacks of energy. Obviously, the earliest trajectory would like to accelerate and arrive as soon as possible. However, the higher the speed the more drag and, consequently, the more energy loss rate. Since the aircraft lacks of energy and it is not allowed to apply thrust, it has to settle for preserving the spare energy and fly slower. The latest trajectory is not penalised in this case, and executes the descent by gliding at GD. Then, the speed is increased after the metering fix aiming at releasing energy to satisfy the terminal constraints. For this flight conditions, the time window is also around 20 seconds.

III.3.2 Baseline scenario results

This section thoroughly discuses the results obtained for the baseline case study, whose parameters were presented in Table III-2. Figures III-5(a) and III-5(b) show, respectively, the earliest and latest times of arrival at the IAF as a function of the initial altitude and distance to go of the aircraft. It is worthy to remember that, for the baseline scenario, the initial speed is fixed to that corresponding to a kinetic energy in the middle of the feasible kinetic energy range.

Figure III-6 shows the feasible energy-neutral time window, consisting on the difference between Figs. III-5(b) and III-5(a), at the IAF, as a function of the altitude and distance to go. The black dashed line represents the trajectory that maximises the feasible time window throughout the descent. An aircraft starting the descent in the lower or upper white region would need to apply additional thrust or to deploy speed brakes to satisfy all the constraints, respectively. In other words, energy-neutral trajectories are not possible in the white region.

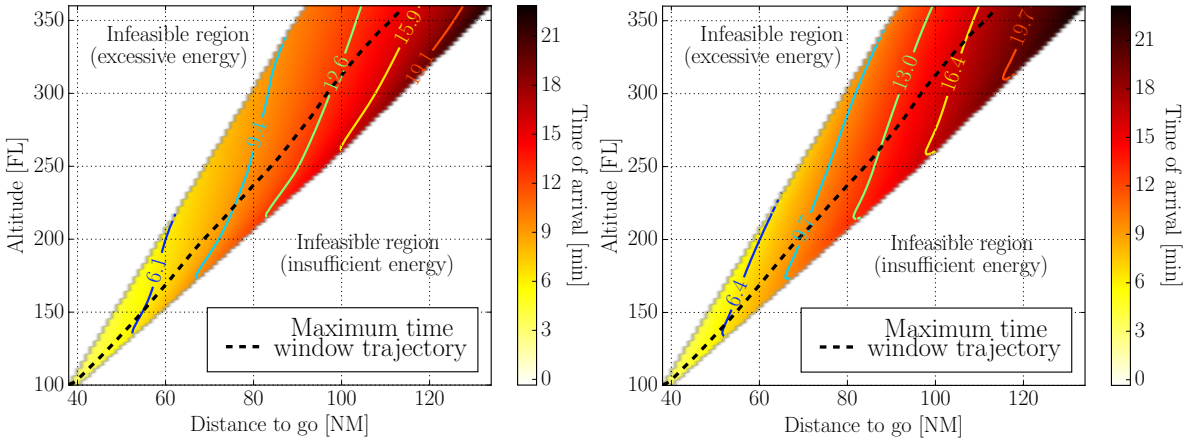

(a) Earliest time of arrival (b) Latest time of arrival

Figure III-5: *Baseline scenario: earliest and latest times of arrival at the metering fix*

For a given distance, at the highest feasible altitudes the aerodynamic drag needs to be increased in order to release the excessive energy. Since speed brakes use is not allowed, the most appealing option is to accelerate and generate more drag, thus penalising the latest trajectories. Conversely, at the lower feasible altitudes, the energy is limited and needs to be preserved. Since additional thrust is not permitted, the best practise is to decrease the energy loss rate by decelerating, thus penalising the earliest trajectories. Consequently, at a given distance to go, the maximum time window is expected to be achieved at intermediate altitudes, where neither the earliest nor the latest trajectory is penalised.

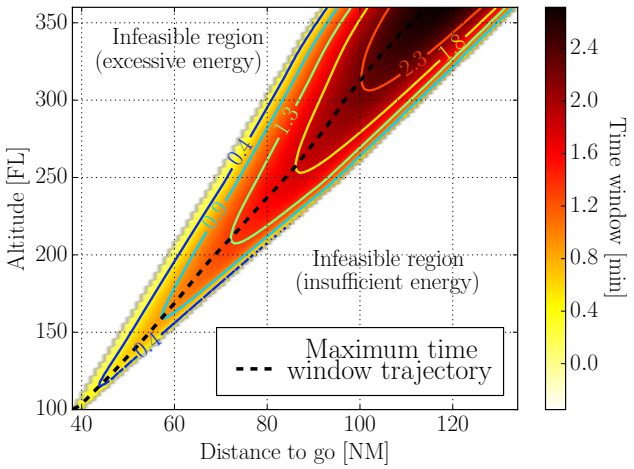

Figure III-6: *Baseline scenario: feasible time window at the metering fix*

According to Figs. III-5 and III-6, there exist only a feasible region of initial distances to go and altitudes such that an aircraft could satisfy all the constraints without requiring neither additional thrust nor drag devices during the descent. If the aircraft is close to the lower border of this feasible region, the energy needs to be sustained by means of a shallower flight path angle and almost no margin is left to increase the aircraft speed using elevator control. As the aircraft position approaches the trajectory of maximum time window (black-dashed line), it has more freedom either to accelerate or decelerate by means of elevator control, and the time window increases until it reaches its maximum. However, if the aircraft is close to the upper border of the feasible region, potential energy needs to be exchanged by kinetic energy by descending with a steeper gradient and almost no margin is left to decrease the aircraft speed.

For this baseline scenario, the maximum time window is approximately 2.8 min, and is reached at the highest altitude (FL360) and at 110 NM. It can be also observed that the time window decreases about 9 s per NM or 30 s per 50 FL.

The vertical trajectory plan of the aircraft is a function of many factors such as the cost index (CI), the mass of the aircraft, the scheduled speed profile, the wind field or even a previous CTA assigned in cruise. For instance, depending on the CI values the location of the TOD will *move* towards or away the metering fix. Too high or too low CI values will narrow the feasible time window while intermediate CI values will place the TOD in such a way that a wider feasible time window could be achieved. Accordingly, there might exist a trade-off between airline preferences and robustness of the CDO facing late changes of the CTA during the descent.

Even if keeping the engines at idle throughout the descent, the resulting fuel consumption depends on the aircraft altitude and (to a lesser extent) on the speed profile. Figures III-7(a) and III-7(b) show, respectively, the fuel consumption of the energy-neutral earliest and latest trajectories at the IAF, as a function of the altitude and distance to go of the aircraft when computing them. As expected, the fuel consumption and the time of arrival at the IAF are strongly correlated. In Fig. III-7 significant differences in fuel consumption, between the earliest and latest trajectories, are observed, even though both are performed with the engines at idle. Interestingly, it can be observed that earliest trajectories are more fuel-efficient than latest trajectories.

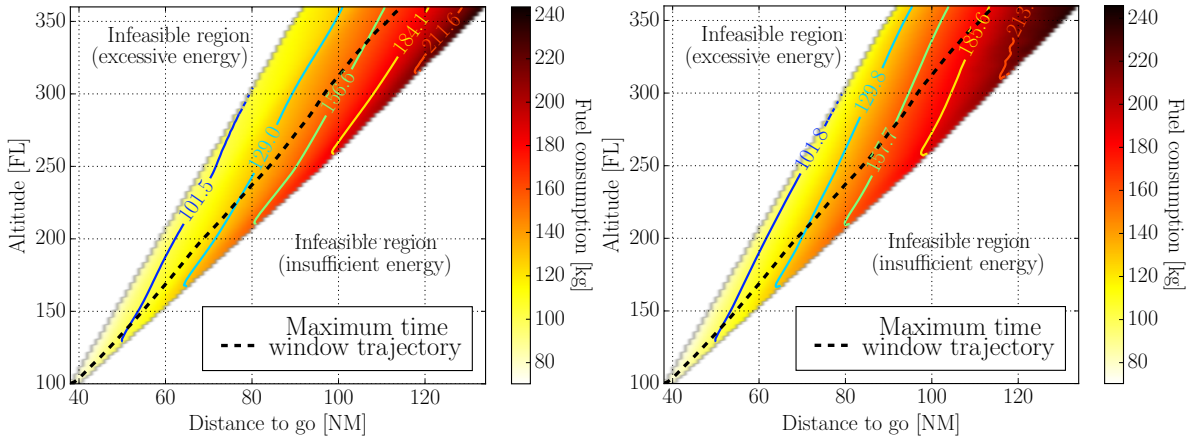

(a) Earliest time of arrival

(b) Latest time of arrival

Figure III-7: *Baseline scenario: fuel consumption at the metering fix*

A priori, this could be seen as a paradox, since one might think that the higher the aircraft speed, the higher the fuel consumption. If the CTA were updated in cruise, earliest trajectories would select a later TOD, leading to higher fuel consumption due to the larger amount of time spent in the cruise phase. In the scenario discussed herein, however, the aircraft is already descending when the CTA is updated and only elevator control is allowed to gain or release time. The idle fuel flow depends mainly on altitude, being lower at high altitudes. The latest trajectories tend to release as much energy as possible at the beginning of the descent, then flying at low speeds and low altitudes. On the other hand, earliest trajectories attempt to keep the faster speeds at the higher altitudes where the density (and the drag) are lower in order to maintain the total energy level as long as possible, then releasing this energy close to the time-constrained metering fix. Therefore, earliest trajectories operate at more fuel-efficient altitudes.

Among all the possible energy-neutral trajectories starting at a given flight conditions, there exist only one that minimises fuel consumption. Figures III-8(a) and III-8(b) show, respectively, the extra fuel consumption of the earliest and latest trajectories at the IAF with respect to those of minimum fuel consumption, as a function of the distance to and altitude of the aircraft.

According to Fig. III-8(a) the most fuel-efficient trajectories at the IAF are very close to those of minimum time, since both select similar altitude and speed profiles. Interestingly, the trajectory that maximises the feasible time window throughout the descent also entails the maximum extra fuel consumption with respect to the minimum fuel trajectory for the same initial conditions. Consequently, it can be concluded that there is a trade-off between maximising the probability to achieve the whole descent at thrust idle (i.e., following the maximum time window trajectory) and minimising the fuel consumption.

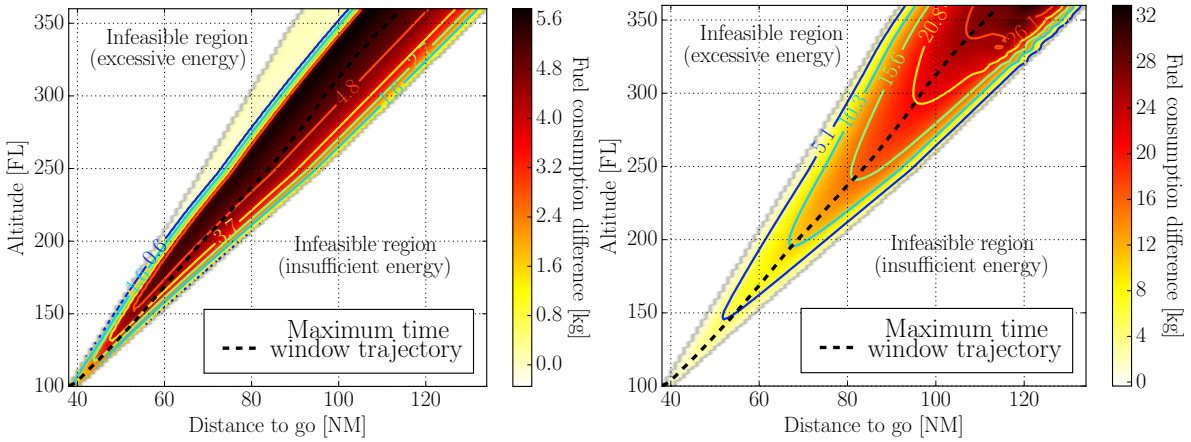

(a) Earliest time of arrival

(b) Latest time of arrival

Figure III-8: *Baseline scenario: extra fuel consumption with respect to the minimum fuel*

III.3.3 Sensitivity study results

This section sums up the main results obtained from the sensitivity study. Results have been classified according to the parameter subject of analysis.

III.3.3.1 Effect of the aircraft mass

Figure III-9 shows the effect of aircraft mass on the feasible time window. According to Fig. III-9, the set of possible initial conditions (i.e., combinations of altitude and distance enabling an energy-neutral descent) is larger and the feasible energy-neutral time window (i.e., difference between the latest and earliest times of arrival) is wider for lighter aircraft.

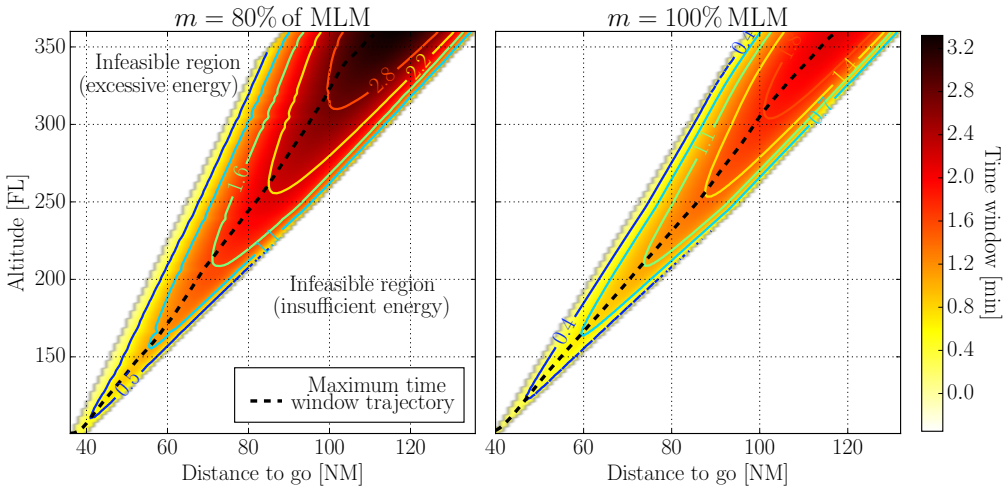

Figure III-9: *Effects of aircraft mass on the feasible time window at the metering fix*

The best glide speed of an aircraft (i.e., the speed that gives the most distance forward for each increment of altitude lost) is found at the maximum lift-to-drag ratio, which only depends on the aerodynamic characteristics of the aircraft (Roskam & Lan, 1997). However, the speed at which the maximum lift-to-drag ratio occurs (approximately the GD speed) is a function of the aircraft mass. For a given altitude, the heavier the aircraft, the higher the GD speed.

When the involved aircraft is in clean configuration, fully automated and flying the trajectory plan as determined by the FMS, the CAS is not allowed to drop below GD (Airbus, 1993). Therefore, while the earliest times of arrival keep almost unchanged with the aircraft mass (since MMO and VMO are independent

of the mass), slower descents can be achieved with lighter weights because of the lower GD speeds. Consequently, there is a trade-off between maximising the feasible time window and maximising the amount of payload carried on-board the aircraft.

It is worth noting that the difference of feasible time window between two different aircraft masses becomes more significant at farthest distances from the runway threshold. For instance, for an increment of the aircraft mass from 80% to 100% of MLM, at 60 NM from the runway threshold the maximum time window decreases 30 s, while at 100 NM the detriment is about 1 min.

III.3.3.2 Effect of the longitudinal wind

Figure III-10 shows the effect of the longitudinal wind on the CTA window in a matrix form. Each column represents a different magnitude of the wind speed. The first row shows the results for the simulations with head wind, while the second row for those with tail wind. It is important to recall that the wind speed is not constant, but changes with the altitude according to Eq. (II.7). Therefore, the values of wind speed shown in Fig. III-10 correspond to w_r, not to w_s.

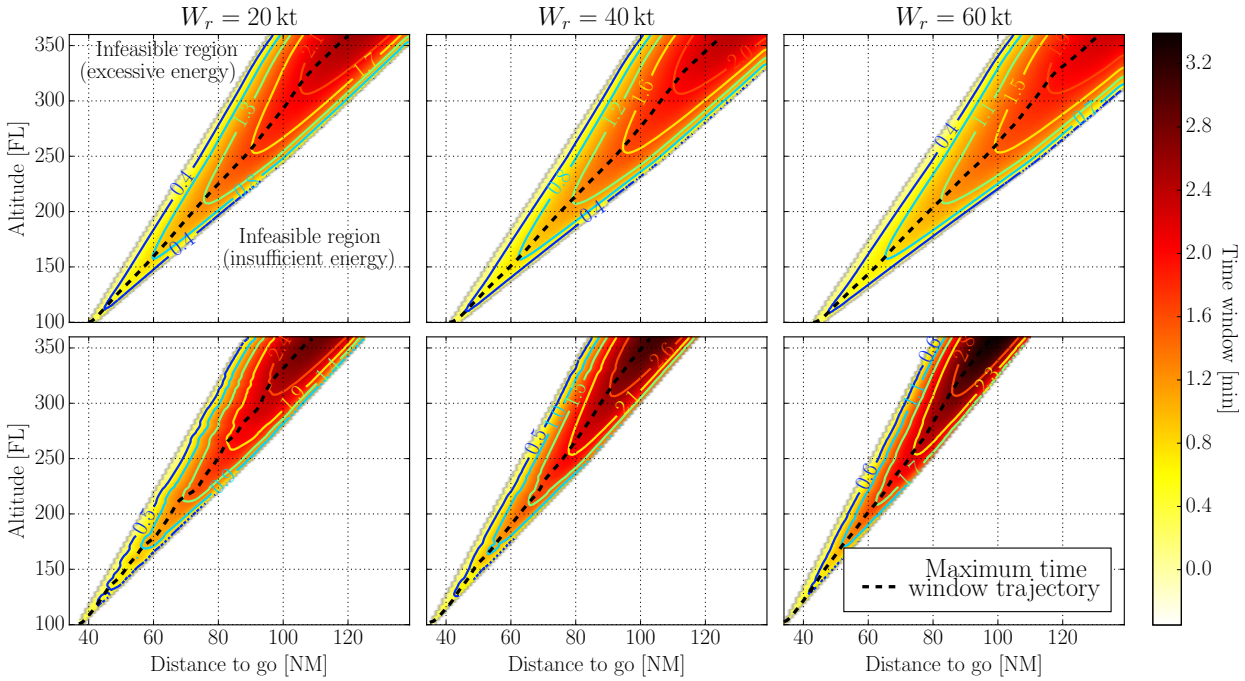

Figure III-10: *Effects of longitudinal wind on the feasible time window at the metering fix*

According to Fig. III-10, in presence of head wind the feasible range of initial aircraft states *moves* towards the time-constrained metering fix and becomes narrower, but the feasible energy-neutral time window at the IAF increases, if compared with calm wind conditions (see Fig. III-6). The opposite behaviour applies in presence of tail wind.

This observation is easy to understand by analysing the impact of the w_s on the total energy lost per unit length, which expression can be deducted by combining Eqs. (III.2) and (II.29):

$$\frac{\mathrm{d}E_t}{\mathrm{d}s} = \frac{\mathrm{d}E_t}{\mathrm{d}t}\frac{\mathrm{d}t}{\mathrm{d}s} = \frac{\dot{E}_t}{\dot{s}} = \frac{v\,(T_{idle} - D)}{v\cos\gamma + w_s}. \tag{III.17}$$

Equation (III.17) leads to the following inequalities for a given weight, altitude and speed:

$$\left.\frac{\mathrm{d}E_t}{\mathrm{d}s}\right|_{w_s>0} < \left.\frac{\mathrm{d}E_t}{\mathrm{d}s}\right|_{w_s=0} < \left.\frac{\mathrm{d}E_t}{\mathrm{d}s}\right|_{w_s<0}. \tag{III.18}$$

According to Eq. (III.18), in presence of head (resp. tail) wind, less (resp. more) distance is needed to release the same amount of energy if compared with calm winds condition. Namely, for a given initial

energy, in presence of head wind the descent must start closer to the metering fix to satisfy all the constraints. Equation (III.18) explains why, for a given altitude, the set of initial states *moves* towards the IAF and becomes narrower for head wind conditions.

Generally speaking, for the earliest trajectories it would be desirable to maintain the maximum allowed speed (either MMO/VMO or 250 kt, depending on the altitude) down to the IAF. Similarly, for the latest trajectories, the deceleration to GD should be performed as soon as possible. In practice, however, the capability to release energy once the IAF is overflown constrains the altitude and speed at which this fix can be reached, and the ideal conditions cannot always be met. For instance, for the earliest energy-neutral trajectories in the case studies with head wind, the optimal solution consists of reaching FL100 at VMO and decelerating to 250 kt just before the IAF, since the aircraft is capable of releasing such amount of energy in the remaining descent distance. In presence of tail wind, however, the energy at the IAF cannot be as high because of the lower $|\mathrm{d}E_t/\mathrm{d}s|$, and the deceleration to 250 kt must be performed well before the metering fix.

III.3.3.3 Effect of the IAF position

Figure III-11 shows the effect of the position of the metering fix on the feasible CTA window.

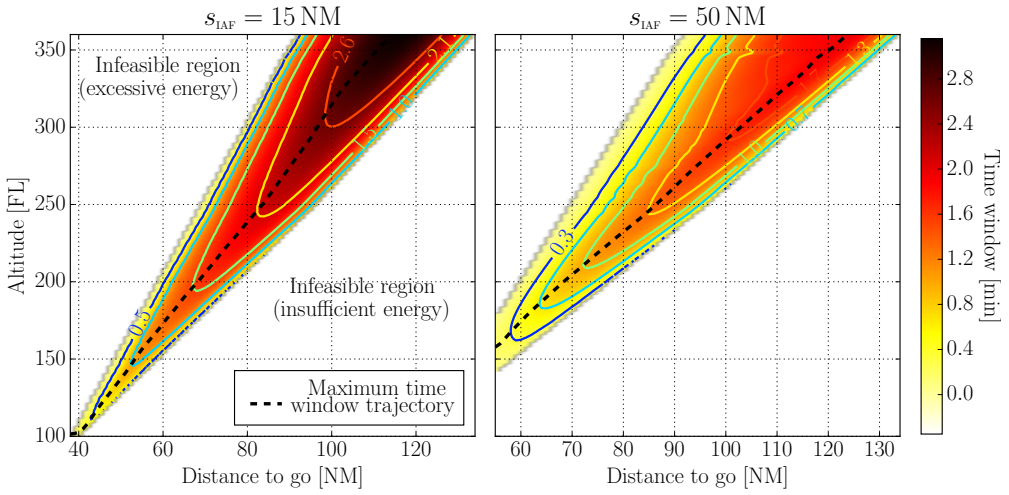

Figure III-11: *Effects of the position of the metering fix on the feasible time window*

As expected, the closer the metering fix to the runway threshold, the wider the CTA window because more distance is left to gain or lose time. It is interesting to note that, even if the time window is significantly affected by the position of the metering fix, the set of feasible initial conditions remains unchanged. This is because of the particularities of the selected scenario, in which neither speed nor altitude constraints have been considered. As a result, the set of feasible initial conditions is not affected by the IAF location, but only the value of the cost function.

III.3.3.4 Effect of the initial speed

Results shown in the preceding sections were computed fixing the initial speed of the aircraft to that corresponding to a kinetic energy in the middle of the feasible kinetic energy range. However, the initial kinetic energy of the aircraft plays an important role in the feasible time window, which must be also investigated. For instance, if the CTA update forces the aircraft to arrive earlier than initially planned while flying very slow, it might be not possible to accelerate enough without adding energy by means of thrust. Conversely, if the aircraft is forced to arrive later than initially planned while flying at a very high speed, it might be infeasible to decelerate (thus decrease the drag) and at the same time release the required energy without using speed brakes

Figure III-12 shows the effects of the initial speed on the feasible energy-neutral time window.

According to this Fig. III-12, flying at a very high speed when receiving a CTA update is typically preferred. For a given altitude and distance to go, the higher the speed, the higher the total energy. A high energy level leads to more freedom to either release or retain it by increasing (provided that the aircraft is not flying

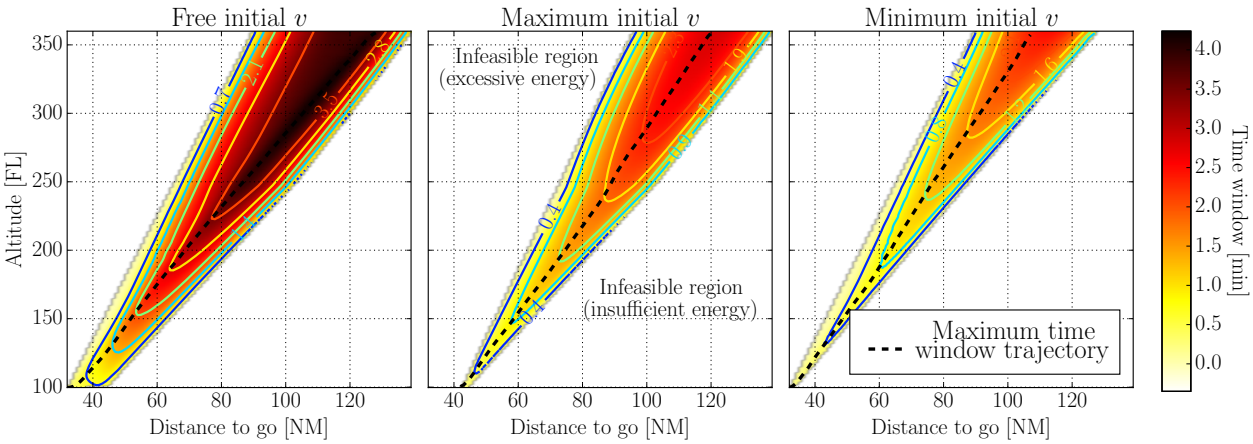

Figure III-12: *Effects of the initial speed on the feasible time window at the metering fix*

at VMO/MMO/250 kt) or decreasing the speed, respectively. If the initial energy is limited, however, the only choice left consists of preserving it as long as possible to satisfy the terminal condition, not being able to fly faster and, consequently, highly penalising the earliest energy-neutral time of arrival.

Results for the case with a free initial airspeed (i.e., allowing the aircraft to change its initial speed instantaneously) show feasible energy-neutral time windows up to 4 min, in contrast to the 2.8 min shown for the baseline case study. However, changing the initial speed implies adding or removing energy from the system by means of additional thrust or drag, respectively, leading to extra fuel consumption and/or noise nuisance.

III.4 Discussion

An efficient assignment of CTAs when sequencing and merging traffic could enable the introduction of CDOs in the TMA, where conflictive trade-offs exist between airspace capacity and environmental objectives. For this purpose, future ground automation systems will require a good knowledge of the feasible CTA windows for each inbound aircraft. This study quantified this feasible time window at the IAF for an Airbus A320 performing a CDO such that the speed profile is only adjusted by means of elevator control along the descent, and assuming the descent has been already initiated.

Results for a baseline case study show that CTA windows up to 2.8 min at the IAF could be achieved for certain flight conditions. Another important remark that arises from this study is that a previously assigned CTA or even the CI could have a significant impact on the CTA window. Interestingly, it has been observed that minimum time (i.e., faster) trajectories are very similar to those of minimum fuel, provided that the optimisation takes place once in the descent (i.e., the top of descent has been overflown) and neither additional thrust nor drag devices usage are allowed.

It has been also found that there is a trade-off between maximising the robustness of facing late CTA updates throughout the descent (i.e., adapting the time of arrival) and minimising the fuel consumption. Therefore, for robust and optimal CDOs in the presence of uncertainties, it would be more interesting to fly a higher extra fuel consumption if compared to that minimum achievable.

Moreover, it has been observed that the lighter the aircraft, the wider the feasible time window. In addition, in presence of head wind, the set of feasible flight conditions such that an energy-neutral trajectory can be accomplished, narrows and moves towards the time-constrained metering fix, but the magnitude of the feasible time window increases. Results also show that receiving the CTA update while flying at a high speed is typically preferred. Finally, and as expected, the closer the aircraft to the metering fix when receiving the CTA update, the narrower the feasible time window

The most important conclusion of this chapter is that CTAs can be updated after overflying the TOD, and that large energy-neutral time windows could still be attainable depending on the flight conditions.

He who is not satisfied with a little, is satisfied with nothing.

— Epicurus

The aim of science is not to open the door to infinite wisdom, but to set a limit to infinite error.

— Bertolt Brecht

IV

Comparison of guidance strategies to meet time constraints in optimal descents

In Chapter I, the assignment of time constraints to each inbound aircraft at some strategic fixes for separation, sequencing and merging tasks was identified as a potential approach to enable continuous descent operations (CDOs) in dense traffic scenarios. With this type of flight operations, air traffic control (ATC) would assign (using data-link, for instance) at least one controlled time of arrival (CTA) to each aircraft, ideally before they reach the top of descent (TOD). Chapter III quantified the feasible time windows of energy-neutral CDOs that have overflown their TOD, showing that time windows up to 2.8 minutes could still be achieved for certain flight conditions.

After receiving the CTA from the ATC, either before of after the TOD, the time instruction would be entered as a required time of arrival (RTA) by the aircraft crew into the flight management system (FMS). Right after, the on-board trajectory planner would compute the optimal trajectory plan for the descent satisfying the RTA and other applicable operational constraints.

In practise, however, because of modelling errors and uncertainties encountered during the execution of the trajectory plan, aircraft may deviate from the planned altitude and/or speed profile, and may also be delayed or advanced with respect to the planned time schedule. In order to safely execute the trajectory plan as well as to accurately comply with the entered RTA in such uncertain environment, corrective actions must be taken by the on-board guidance system of the aircraft.

Several guidance strategies were proposed as a part of the time and energy managed operations (TEMO) concept for this purpose, as mentioned in Section I.4.2.2. The aim of this chapter is to compare the performance of the three existing TEMO guidance strategies described in Section II.3 (i.e., strategic, tactical and hybrid), in terms of noise nuisance, energy error at the metering fix, fuel consumption, speed-brakes use, as well as their ability to satisfy time constraints in presence of modelling errors. Furthermore, a new TEMO guidance strategy called nonlinear model predictive control (NMPC), which is one of the major contributions of this PhD thesis, will also take part of this comparison.

IV.1 State of the art

Various guidance strategies have been proposed to comply with a CTA during a CDO, which essentially differ on how the aircraft actuators are used to nullify the time deviations with respect to the trajectory plan, and whether this trajectory plan is dynamically adjusted or not.

For instance, the speed profile could be continuously modified to tactically nullify a time error signal by using throttle and speed-brakes commands, while remaining on the vertical flight path with the elevator, as suggested by Rumbo *et al.* (2002). At present, however, the automatic control of speed brakes is seldom, implying that an additional margin must be available to control the throttle. This margin may be acquired, for instance, by generating a trajectory plan at idle thrust plus some arbitrary increment. For constant speed segments, the resulting flight path angle will be less steep, while for constant flight path angle decelerations, the resulting decelerations will be slower. The continuous action on thrust required by this guidance strategy, however, has a negative effect on noise nuisance, gaseous emissions, fuel usage and engine wear and tear.

A more appealing guidance strategy, in terms of environmental impact, consists of actively controlling the speed with the elevator (speed-on-elevator) in order to tactically nullify time deviations, then using near-idle thrust variations to recover the initially planned path only when the vertical deviation exceeds a predefined threshold (Garrido-López *et al.*, 2009).

A set of additional guidance strategies were proposed as a part of the TEMO concept (De Jong *et al.*, 2017, 2015). These strategies have in common to manage the total energy of the aircraft (altitude and speed) such that time constraints are satisfied in the most environmentally friendly way. For instance, if the aircraft is late with respect to the CTA but exceeds the planned energy, the guidance system could command a steeper descent angle to accelerate, which would result in an increased energy loss rate while simultaneously reducing the time error. These guidances were described in Section II.3, and will be summarised below for the sake of completeness.

One guidance option in TEMO is to use speed-on-elevator to nullify time errors, while throttle and speed brakes are continuously used to correct energy deviations (tactical guidance). Differently, the strategic guidance approach consists of strictly follow the trajectory plan using speed-on-elevator while allowing certain energy and time deviations during the execution, as long as some predefined thresholds are not exceeded. Whenever time and/or energy errors exceed these thresholds, a new trajectory plan can be computed from the current aircraft state in such a way that corrective actions are taken to satisfy all operational constraints with minimum fuel usage (De Jong *et al.*, 2017). In previous work, this guidance technique was compared with the guidance strategy of a typical FMS that does not correct time errors, showing superior performances in terms of fuel consumption and RTA compliance in presence of wind errors (Dalmau *et al.*, 2016). The combination of the strategic and tactical guidance variants leads to the hybrid strategy, where only the thrust plan is followed and a tactical controller is in charge to nullify time errors by using speed-on-elevator (De Jong *et al.*, 2015). Energy deviations exceeding the allowed threshold are corrected by means of strategic updates of the trajectory plan. Finally, with NMPC (Diehl *et al.*, 2008), the remaining descent trajectory to the metering fix is frequently updated by solving an optimal control problem, setting the current state of the aircraft as initial conditions. Different from the previous guidances strategies, the NMPC does not wait for energy and time deviations to exceed a certain threshold, nor nullifies them to strictly follow the initial trajectory plan. Thus, it could be seen as the limit of the strategic guidance, with energy and time deviation thresholds tending to zero, in which the optimal plan is tactically updated.

Recent research demonstrated the feasibility of using NMPC guidance strategies to achieve precise spacing between aircraft, the main objective of interval management operations (Weitz & Bai, 2018). However, due to limitations in the execution time of the trajectory optimisation algorithm, previous work implemented a receding NMPC that did not update the remaining descent trajectory at each time sample, but only computed the optimal controls over a relatively short future horizon such that the initial trajectory plan was closely followed in the most optimal way. Other relevant contributions of NMPC in the aerospace field have been performed, for instance, by Arrieta-Camacho & Biegler (2005), Gibbens & B. Medagoda (2011) and Eren *et al.* (2017).

IV.2 Setup of the experiment

The comparison of the four TEMO strategies was performed by simulating 123 descents per guidance strategy (a total of 492) in the avionics prototyping environment for research and operations (APERO), a flight simulator located at the Netherlands Aerospace Centre (NLR). The APERO is composed by a research FMS, which allows the development testing of modules targeting applications for the optimisation of trajectories, and a high-fidelity simulator of the aircraft dynamics, which implements a six-degree-of-freedom model fed with accurate aircraft performance data.

A trajectory management software developed at the Technical University of Catalonia (UPC) as a result of this PhD thesis was connected to the research FMS of the APERO, as illustrated in Fig. IV-1. This trajectory management software is composed by a trajectory planner and a variety of guidance algorithms build on time and energy management concepts.

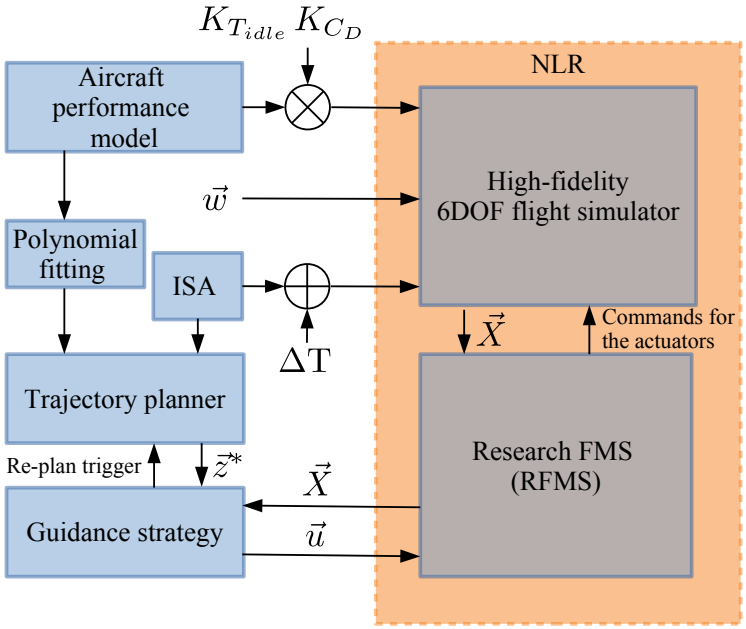

Figure IV-1: *Setup of the experiment to compare guidance strategies*

Basically, the trajectory planner was in charge of computing the initial trajectory plan complying with a CTA at a certain metering fix of a realistic procedure. The optimisation of the aircraft trajectory was formulated as an optimal control problem (see Section II.2.1), and solved by using the optimisation techniques described in Section II.2.3. Thereafter, the trajectory plan was executed with the specific guidance strategy subject of study. Using its particular logics, the guidance system provided the optimal controls to the research FMS, which was in charge of computing the commands for the actuators. The trajectory planner updated the optimal trajectory plan when requested by the guidance system, based on the state observations provided by the research FMS.

As shown in Fig. IV-1, the simulations were performed by introducing intentional discrepancies between the weather forecast and aircraft performance models implemented in the trajectory planner, and the corresponding models implemented in the simulation environment. The detailed list of case studies and their respective modelling errors will be presented in IV.2.4.

Fuel consumption, time and energy deviations at the metering fix, the number of speed brakes deployments, and area affected by the aircraft noise were selected as metrics for this comparison. Noise contours were calculated using the model described by Van der Wal *et al.* (2001).

This section describes the setup of the experiment performed in this study. First, the scenario is presented in Section IV.2.1. Then, the generic models introduced in Section II.1 are particularised in Section IV.2.2. Analogously, the generic optimal control problem stated in Section II.2.1 is particularised in Section IV.2.3 with specific cost function and constraints. The case studies of the experiment are listed in Section IV.2.4, and the workflow of a single descent simulation is summarised in Section IV.2.5.

IV.2.1 Scenario

All simulations assumed the following scenario: an Airbus A320 was cruising at a certain altitude when the ATC requested a CTA at a metering fix. Right after entering the RTA in the FMS, the on-board trajectory planner computed the optimal trajectory plan and executed it by implementing any of the guidance strategies considered in the experiment. However, the trajectory plan was computed under certain weather forecast and aircraft performance modelling errors, and the guidance system reacted to correct energy and time using its specific mechanisms.

All the simulations were performed to Barcelona-El Prat airport (LEBL), using four realistic standard arrival procedures (STARs) published for runway 25L. As can be observed in Fig. IV-2, each STAR ends at one of the four initial approach fixs (IAFs) of LEBL and then, all the approaches finally merge into a single intermediate fix (SOTIL). The instrumental landing system (ILS) glide slope is intercepted at the final approach point (FAP) few nautical miles later.

For this experiment, SOTIL (the intermediate fix) was selected as the metering fix where CTAs were assigned by an hypothetical ATC for sequencing and merging tasks.

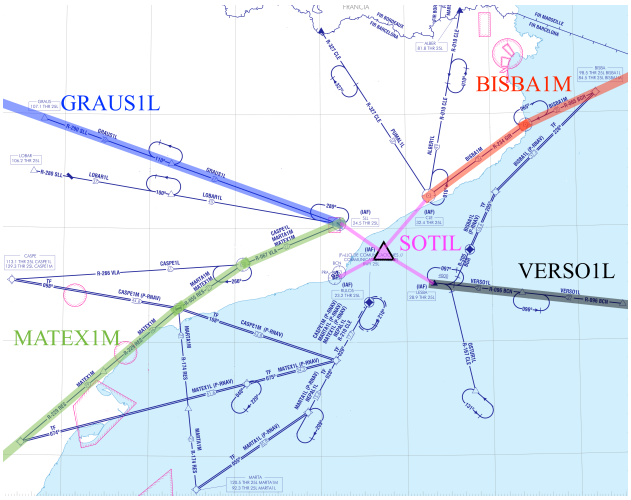

Figure IV-2: *Routes at Barcelona-El Prat chosen to compare guidance strategies (Source: Spanish AIP)*

IV.2.2 Models

The models presented in Section II.1 are particularised below for the experiment conducted in this chapter.

IV.2.2.1 Aircraft dynamics model

The point-mass model described by Eq. (II.1) was implemented in the trajectory planner of this experiment. The control vector, however, was modified in the following way: the lift coefficient was exchanged for the load factor (n_z), and the thrust for the throttle setting (κ); that is: $\vec{u} = [\kappa, n_z, \beta]^T$ instead of $\vec{u} = [T, C_L, \beta]^T$. This also implies the following change in Eq. (II.1b):

$$\frac{\mathrm{d}\gamma}{\mathrm{d}t} = \dot{\gamma} = \frac{g}{v}\left(n_z - \cos\gamma\right), \tag{IV.1}$$

where the load factor is defined as the ratio of the aerodynamic lift of an aircraft to its weigh:

$$n_z = \frac{L}{mg}, \tag{IV.2}$$

which represents a measure of the stress to which the structure of the aircraft is subject. According to Eq. (IV.2), a load factor of one corresponds to straight and level flight, where the lift is equal to the weight. Load factors different from one (or even negative) are the result of manoeuvres.

The throttle was assumed to control the revolutions of the engine fan ($N1$) using a linear relationship:

$$N1(v,h,\kappa) = N1_{idle}(v,h) + \kappa\left(N1_{max}(v,h) - N1_{idle}(v,h)\right), \tag{IV.3}$$

where $N1_{idle}$ and $N1_{max}$ represent, respectively, the minimum and maximum revolutions of the engine fan, which are both function of the altitude and airspeed of the aircraft. In this model, the thrust force and fuel flow were described as a function of N_1, the altitude and the speed:

$$T(v,h,\kappa) = T(v,h,N1(v,h,\kappa)) \tag{IV.4a}$$
$$q(v,h,\kappa) = q(v,h,N1(v,h,\kappa)). \tag{IV.4b}$$

The differential equations of Eq. (II.1) for the remaining states kept unchanged.

IV.2.2.2 Aircraft performance model

The aircraft performance model (APM) used in this experiment was based on the performance data provided in tabular form by NLR for the Airbus A320. Since the nonlinear programming (NLP) solver used in this study required first and second-order differentiability of the cost function and constraints, the drag coefficient was modelled as the following drag polar:

$$C_D(\eta,\zeta,\beta,C_L) = C_{D0}(\eta,\zeta) + C_{D2}(\eta,\zeta)C_L^2 + C_{D\beta}(\eta,\zeta)\beta, \tag{IV.5}$$

which neglects the compressibility effects and consider the effects of the speed brakes deflection as an additional linear term. In Eq. (IV.5), $C_{D\beta}$ is a coefficient that represents the increase in drag coefficient when the speed brakes are deployed, and C_L can be computed by combining Eq. (IV.2) with Eq. (II.2a):

$$C_L(n_z,v,h,m) = \frac{2n_z\sigma(h)\rho_{SSL}Sv^2}{mg}. \tag{IV.6}$$

Figure IV-3 shows the drag coefficient as a function of C_L, for different aerodynamic configurations.

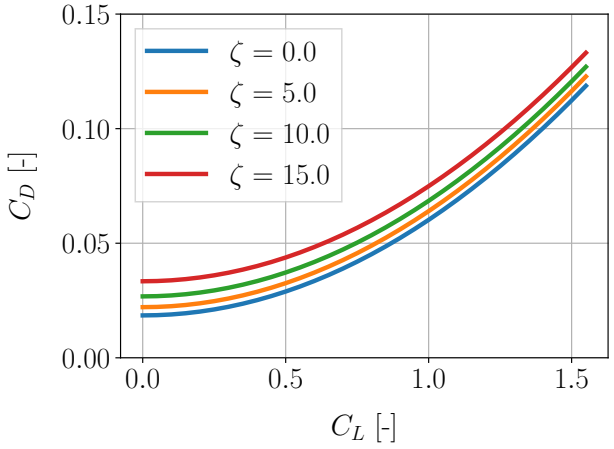

Figure IV-3: *Drag polars approximating aerodynamic data for the A320*

The maximum revolutions of the engine fan were set to a constant value, and the normalised revolutions of the engine at idle thrust were modelled as fifth order polynomial:

$$N1_{max} = 87 \tag{IV.7a}$$
$$\frac{N1_{idle}(v,h)}{\sqrt{\theta(h)}} = \sum_{i=0}^{3}\sum_{j=0}^{3} c_{i,j}\theta^i(h)M^j(v,h). \tag{IV.7b}$$

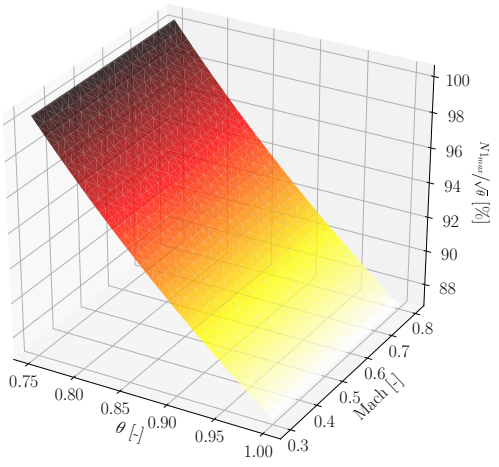

(a) Normalised max. revolutions of the engine fan

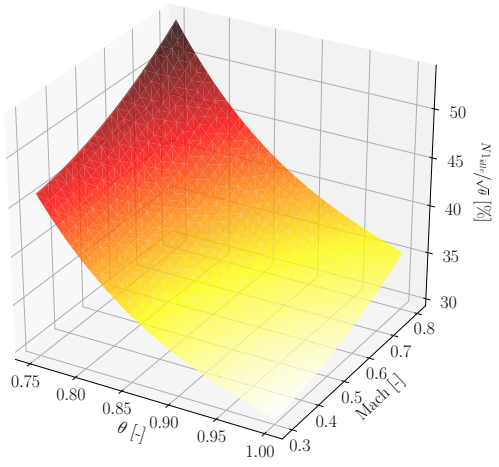

(b) Normalised min. revolutions of the engine fan

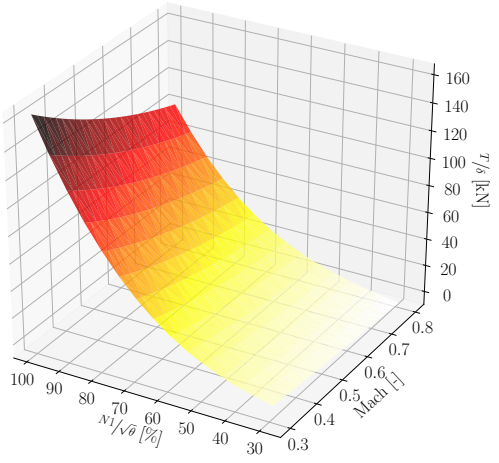

(c) Normalised thrust

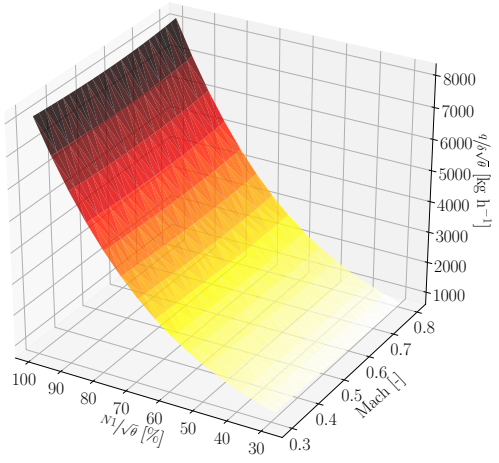

(d) Normalised fuel flow

Figure IV-4: *Polynomials approximating propulsive data for the A320*

The same methodology was used to model the normalised fuel flow and the normalised thrust as a function of the normalised revolutions of the engine fan:

$$\frac{q(v,h)}{\delta(h)\sqrt{\theta(h)}} = \sum_{i=0}^{3}\sum_{j=0}^{3} c_{i,j}\left(\frac{N1}{\sqrt{\theta(h)}}\right)^{i} M^{j}(v,h) \tag{IV.8a}$$

$$\frac{T}{\delta(h)} = \sum_{i=0}^{3}\sum_{j=0}^{3} c_{i,j}\left(\frac{N1}{\sqrt{\theta(h)}}\right)^{i} M^{j}(v,h). \tag{IV.8b}$$

The coefficients of the polynomials functions appearing in Eqs. (IV.5), (IV.7) and (IV.8) where obtained as a result of a least-squares fitting process with the aerodynamic and propulsive tabular data used in the flight simulator, respectively. Figure IV-4 shows the polynomial approximation of the propulsive data.

It should be noted that even if both flight simulator and trajectory planner draw upon the same aircraft type (i.e., an Airbus A320), the dynamics and performance models used by these components were sightly different. The flight simulator used as a high fidelity six-degree-of-freedom model to represent the aircraft dynamics, and very accurate look-up tables for the aircraft performance. Moreover, the trajectory planner

represented the aircraft as a three-degree-of-freedom point-mass model (similar to Eq. (II.1)), and approximated the aircraft performance data included in the look-up tables of the flight simulator with polynomial functions, aiming at achieving the continuity and second-order differentiability required by the embedded NLP solvers.

IV.2.2.3 Weather model

The trajectory planner used in this experiment assumed international standard atmosphere (ISA) conditions and calm winds. Accordingly, the normalised temperature θ and pressure δ were modelled as a function of h through Eqs. (II.4) and (II.5), respectively; the normalised density was computed assuming the perfect gas law relationship with Eq. (II.6); and $w_s = w_x = 0$.

IV.2.3 Optimal control problem formulation

The trajectory planner used in this experiment generated the optimal descent trajectory subject to a RTA by solving a multi-phase, constrained and nonlinear optimal control problem, as described in Section II.2.1. This section particularises the cost function and the dynamic, path, algebraic and interior-point constraints for each one of the phases composing the flight profile.

The differential constraints on the dynamics of the aircraft ($\vec{f}$) were particularised by the following point-mass model, independently of the phase:

$$\vec{f_j} = \begin{bmatrix} \frac{T(v,h,\kappa) - D(v,h,m,n_z,\beta)}{m} - g\sin\gamma \\ \frac{g}{v}\left(n_z - \cos\gamma\right) \\ v\sin\gamma \\ v\cos\gamma \\ -q(v,h,\kappa) \end{bmatrix}; \; j = 0, \ldots, P-1. \tag{IV.9}$$

The descent was divided into $P = 4$ different phases, where several phase-dependent path, algebraic and interior-point constraints may apply. Table IV-1 wraps up the different phases and their associated constraints. This table is also illustrated in Fig. IV-5.

Table IV-1: *Definition of the phases and constraints for the comparison of guidance strategies*

Phase (j)	Description	$\vec{b}_j^{in}$	$\vec{b}_j^{eq}$	$\vec{\vartheta}_j^{in}$	$\vec{\vartheta}_j^{eq}$
0	Cruise phase	$\begin{bmatrix} \text{GD} - v_{CAS}(h,v) \\ v_{CAS}(h,v) - \text{VMO} \end{bmatrix}$	$\begin{bmatrix} \dot{h}(v,\gamma) \\ \dot{M}(h,v) \end{bmatrix}$	-	-
1	Cruise deceleration	$\begin{bmatrix} \text{GD} - v_{CAS}(h,v) \\ v_{CAS}(h,v) - \text{VMO} \end{bmatrix}$	$\begin{bmatrix} \dot{h}(v,\gamma) \end{bmatrix}$	-	-
2	Descent	$\begin{bmatrix} \text{GD} - v_{CAS}(h,v) \\ v_{CAS}(h,v) - \text{VMO} \end{bmatrix}$	-	-	$\begin{bmatrix} v_{CAS}(h,v) - \text{GD} \end{bmatrix}$
3	Approach	$\begin{bmatrix} v_{\text{IF}} - v_{CAS}(h,v) \\ v_{CAS}(h,v) - \text{GD} \end{bmatrix}$	-	-	-
All	Entire descent	$\begin{bmatrix} M(h,v) - \text{MMO} \\ \kappa \\ \kappa - 1.0 \\ \beta \\ \beta - 1.0 \\ n_z - 1.15 \\ 0.85 - n_z \end{bmatrix}$	-	-	-

Phase-independent path constraints (i.e., applying all along the descent) as a function of the state and control vectors were also considered, which ensured that the Mach number remains within operational limits all along the descent, and that the bounds on the controls are not exceeded.

The bounds on n_z were chosen to provide good passengers comfort (Pratt, 2000). Maximum operative CAS (VMO) and maximum operative Mach (MMO) are constant parameters that depend on the aircraft type. In this study, MMO and VMO were set to 0.80 and 340 kt, respectively. Finally, v_{IF} was the callibrated airspeed (CAS) that the aircraft must have when arriving at SOTIL.

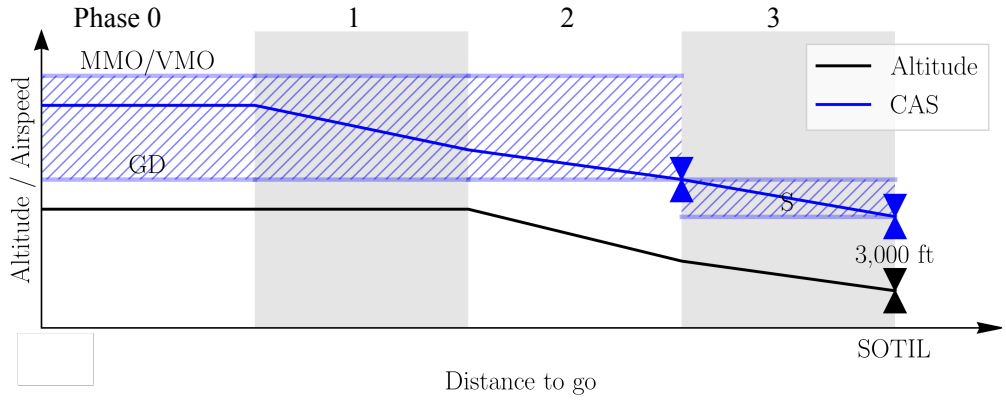

Figure IV-5: *Definition of the phases and constraints for the comparison of guidance strategies*

The cruise phase, starting at the current position of the aircraft ($\vec{X}$) and performed at constant Mach and altitude, was followed by a cruise speed adjustment phase (still at constant altitude) that ended at the TOD (which was a variable of the optimisation problem). There, the aircraft started the descent towards SOTIL. Before reaching this fix, the aircraft configured with flaps at the green dot speed (GD). The last phase of the profile ended with the aircraft at SOTIL and the following terminal constraints:

$$\psi = \begin{bmatrix} v_{CAS}(h,v) - v_{\text{IF}} \\ s - s_{\text{IF}} \\ h - h_{\text{IF}} \end{bmatrix}, \tag{IV.10}$$

where h_{IF} is the altitude at which the intermediate fix (IF) has to be intercepted, which value was set to 3,000 ft; the distance of the IF (s_{IF}) was fixed at 11 NM from the runway threshold; and the GD was computed according to Airbus (1993), as a function of the mass and the altitude.

The CTA was imposed by fixing the final time of the last phase. Therefore, the final times of each phase were additional decision variables to be optimised subject to the following constraint:

$$t_3 - \text{CTA} = 0. \tag{IV.11}$$

Aiming at reducing the environmental impact, the running cost of the optimal control problem was a compound function of fuel flow and speed brakes use:

$$\pi_j = q(v,h,\kappa) + K_\beta \beta;\ j = 0,\ldots,P-1, \tag{IV.12}$$

where K_β is a weighting parameter that determines how much the use of speed brakes is penalised if compared to the fuel flow. In this particular experiment $K_\beta = 1$, and no terminal costs were considered (i.e., $\phi_j = 0$ for $j = 0,\ldots,P-1$).

The optimal control particularised above was transformed to a parametric NLP optimisation problem as described in Section II.2.3. Then, the resulting parametric NLP optimisation problem was formulated in the general algebraic modelling system (GAMS) software suit, and solved with CONOPT as NLP solver, which uses active-set methods. In this experiment, the trapezoidal integration scheme was adopted to obtain $\vec{F}_j$ and Π_j from $\vec{f}_j$ and π_j, respectively. Finally, the constraint relaxation method described in Section II.2.4.1 was implemented to recover from infeasibility.

IV.2.4 Case studies

The aim of this experiment was to compare the performance of the following guidance strategies when the target is to comply with time constraints during an optimal descent: tactical, strategic, hybrid (time tactical and energy strategic), and ideal NMPC (see Section II.3). For each one of these guidance strategies, a set of 123 descents were simulated, which correspond to the case studies shown in Table IV-2.

For each arrival route shown in Fig. IV-2, three different CTAs were considered, enforcing to arrive at SOTIL after 21, 22 and 23 minutes from the start of the simulation. It should be noted that for this particular scenario, the earliest trajectory plan keeping the engines at idle during the entire descent (but allowing to modify the position of the TOD) in ISA conditions, calm winds and nominal aircraft performance models could bring the aircraft to the metering fix in 19 minutes, and the latest trajectory in 27 minutes.

Independently of the guidance strategy, the trajectory planner computed the optimal trajectory plan assuming ISA conditions, calm winds and nominal aircraft performance models (i.e., the polynomials approximating the performance data used in the flight simulator). Then, either wind or non-standard atmospheric conditions were incorporated during the execution of the descent, in the flight simulator, in order to mimic mismatches between the models used by the trajectory planner and the *reality*. Similarly, the aircraft performance models of the flight simulator were sightly modified by adding variations with respect to those used by the trajectory planner.

Several combinations of CTAs and arrival routes with either wind, temperature or aircraft performance modelling errors composed the complete set of case studies shown in Table IV-2. Note that not all possible combinations were considered in this study. In fact, the effects of the different sources of modelling error were assessed separately. The case studies considered to capture the effects of each particular source of modelling error are listed in the following sections.

Table IV-2: *List of case studies per each of the four guidance strategies assessed*

Route	CTA [min]	ΔT [K]	$K_{T_{idle}}$ [%]	K_{C_D} error [%]	Wind speed [kt]	Wind direction [◦]	Total
BISBA1M [1]	21,22,23	-10,-5,5,10	-5,5	-5,5	5,10	0,90,180,270	$3 \cdot (4+2+2+2 \cdot 4+1) = 51$
VERSO1L	21,22,23	-	-	-	5,10	0,90,180,270	$3 \cdot 2 \cdot 4 = 24$
MATEX1M	21,22,23	-	-	-	5,10	0,90,180,270	$3 \cdot 2 \cdot 4 = 24$
GRAUS1L	21,22,23	-	-	-	5,10	0,90,180,270	$3 \cdot 2 \cdot 4 = 24$

IV.2.4.1 Weather forecast errors

The accuracy of the plan computed by the trajectory planner, and especially the computation of the estimated time of arrival, critically depends on the quality of the weather model.

Wind and temperature accuracy requirements for the future air traffic management system have been assessed before. According to Robert & De Smedt (2013), standard deviations of 5 kt and 2.5 K for the along track wind and temperature, respectively, were considered as a requirement to compute accurate trajectory plans. In this experiment, positive and negative temperature forecast errors of 5 and 10 K and wind speed forecast errors of 5 and 10 kt were considered. It is important to remember that the trajectory planner computed the plan considering ISA and calm winds. As a result, the temperature forecast errors were translated to ISA deviations during the execution of the simulation. Similarly, wind forecast errors were accomplished by simply adding winds in the simulation that were not considered during the planning.

The two wind speeds chosen for this experiment were combined with the four main compass wind directions (north, south, east and west), leading to a total of eight case studies with wind forecast errors for each CTA. That is, $8 \cdot 3 = 24$ simulations per guidance strategy and lateral route.

Regarding the temperature forecast errors, a single STAR (BISBA1M) was considered because results are independent of the route, provided that the ISA deviation is not a function of the distance to go, leading to a total of four case studies with temperature forecast errors per CTA. That is, $4 \cdot 3 = 12$ simulations,

Finally, an additional case study with neither wind nor temperature forecast errors was also considered for each CTA, but only for BISBA1M arrival route. It should be noted that the simulations corresponding to the case studies with either wind or temperature forecast errors were performed by using the nominal aircraft performance model (i.e., $K_{T_{idle}} = K_{C_D} = 0$).

[1] An additional case study without modelling errors was considered for each CTA value

IV.2.4.2 Aircraft performance modelling errors

Inaccuracies in the aircraft performance models are also a source of error when generating trajectory plans. In this experiment, the effects of errors in the drag coefficient (see Eq. (IV.5)) and idle thrust models were analysed. In order to accomplish that, either the drag coefficient or the idle thrust of the flight simulator were increased by some percentage as follows:

$$\begin{aligned} T'_{idle,sim} &= K_{T_{idle}} T_{idle,sim} \\ C'_{D,sim} &= K_{C_D} C_{D,sim}, \end{aligned} \tag{IV.13}$$

where $T_{idle,sim}$ and $T'_{idle,sim}$ are, respectively, the generic thrust idle of the simulator and the thrust of the simulator increased by a factor of $K_{T_{idle}}$. Similarly, $C_{D,sim}$ and $C'_{D,sim}$ are , respectively, the generic drag coefficient of the simulator and the drag coefficient of the simulator increased by a factor of K_{C_D}. Overestimations and underestimations of 5% in the magnitude of these two aircraft parameters were considered in this experiment. Therefore, a total of four case studies with aircraft performance model errors were executed for each CTA. As for the case with temperature errors, a single STAR (BISBA1M) was considered for this analysis, because results are independent of the lateral route. That is, $4 \cdot 3 = 12$ simulations per guidance strategy.

It should be noted that the simulations corresponding to the case studies with aircraft performance modelling errors were performed in ISA and calm wind conditions (i.e., $\Delta\mathrm{T} = \|\vec{w}\| = 0$).

IV.2.5 Workflow of a simulation

All simulations started at a distance to go of 140 NM from the landing runway threshold, cruising at FL360 and Mach 0.78, and with a mass corresponding to the 90% of the maximum landing mass (MLM). Immediately, a CTA at SOTIL was received from an hypothetical ATC, and a re-plan was triggered to generate an optimal trajectory plan satisfying the entered RTA at this waypoint.

Right after configuring with flaps at the GD, the pseudo-pilot implemented in the simulator pressed the approach button (this was achieved few nautical miles before SOTIL), disabling the guidance under testing and engaging the ILS guidance modes. Consequently, all the simulations finished at SOTIL, and all the metrics used for the comparison were computed at this fix.

The tactical guidance logic was configured to continuously adjust the commanded CAS such that time deviations were nullified using speed-on-elevator. Regarding the specific energy (E_s)[2], a maximum allowed deviation of 50 ft was set. In the case of being above this threshold, speed brakes were deployed; in the case of falling below, the throttle acted to recover the planned energy level by commanding small amounts of thrust. It is important to remark that under no circumstances the trajectory was updated during the execution of the descent when implementing this guidance mode.

The specific energy deviation bounds for the strategic and hybrid guidances were set to 500 ft in the cruise phase until the TOD and 100 ft at the metering fix, while time deviation bounds for the strategic guidance were set to 10 and 3 seconds at these two points, respectively. Between these two points, specific energy and time deviation bounds were linearly interpolated as a function of the distance to go.

Finally, the NMPC guidance strategy updated the plan every 30 seconds, independently of the energy and time deviations present at the moment of updating the trajectory. This strategy was activated at the beginning of the descent, in order to avoid a continuous shift of the TOD.

IV.3 Results

Section IV.3.1 shows the working principle of the four guidance strategies presented in Section II.3 by means of an illustrative example taken from the batch study. Then, Section IV.3.2 compares the performance of the guidance strategies subject to weather forecast and aircraft performance modelling errors. Finally, the sensitivity of the performance metrics to the mean longitudinal wind error experienced during the descent is discussed in Section IV.3.3.

[2]The specific energy is defined as the total energy divided by the weight of the aircraft

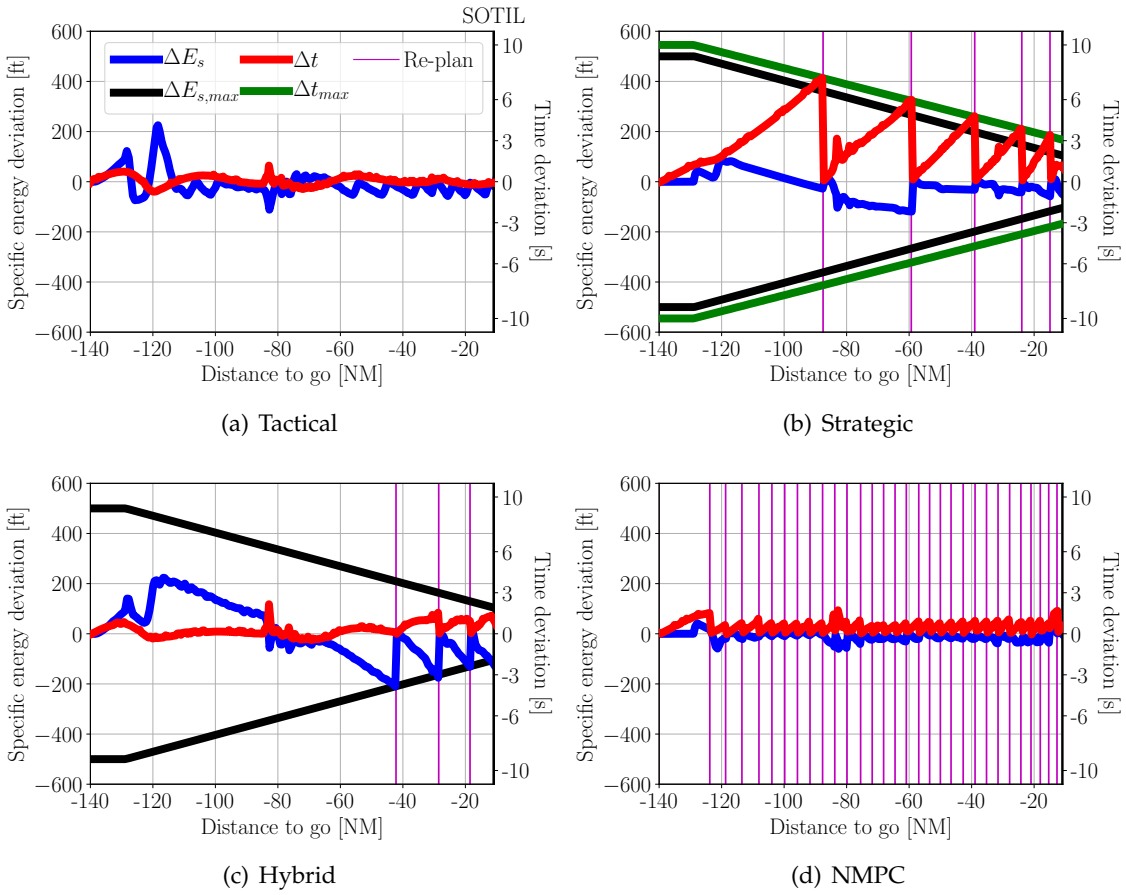

(a) Tactical

(b) Strategic

(c) Hybrid

(d) NMPC

Figure IV-6: *Specific energy and time deviations per guidance strategy*

IV.3.1 Guidance examples

The simulation chosen for this illustrative example corresponds to that executed by following the BISBA1M STAR (see Fig. IV-2), subject to a CTA requiring to arrive 23 minutes after the start of the simulation, with approximately 10 kt of unexpected head wind, in ISA conditions, and without aircraft performance modelling errors. That is, in this particular case study the same temperature profile and aircraft performance model were used in both simulation and trajectory planner, but with a different wind.

Figure IV-6 shows, for each guidance strategy, the time and specific energy deviations along with their associated thresholds (if any), as a function of the distance to go. Figures IV-7 and IV-8 show the planned and executed states and controls, respectively, for these four guidance strategies.

As seen in Fig. IV-6(a), with tactical guidance the time error caused by the unexpected head wind is continuously nullified by using speed-on-elevator, while energy deviations are corrected by either deploying speed brakes or by adding minimum amounts of thrust whenever these deviations exceed 50 ft. Figure IV-7(a) illustrates that using this guidance strategy the initial plan computed before the TOD is never updated. Figure IV-8(a) shows that the throttle acted twelve times to correct a negative energy deviation, while speed brakes were deployed two times right after the TOD.

Remember that in strategic guidance, the CAS and thrust plans are executed by the elevator and throttle, respectively, and neither time nor energy deviations are corrected as long as they remain within the allowed thresholds. If the energy and/or time error exceeds the threshold, the optimal trajectory plan is re-calculated starting at the current aircraft position. Figure IV-6(b) shows that five re-plans were triggered by a time error exceeding the upper threshold (i.e., the aircraft was late with respect to the CTA due to the unexpected head wind). Whenever a re-plan is triggered, the current state and time are enforced as the initial conditions for the subsequent optimal control problem, thus both energy and time deviations are nullified at the moment the new plan becomes active. According to Fig. IV-7(b), all re-plans required a noticeable faster speed profile if compared with what was initially planned, aiming to correct the accu-

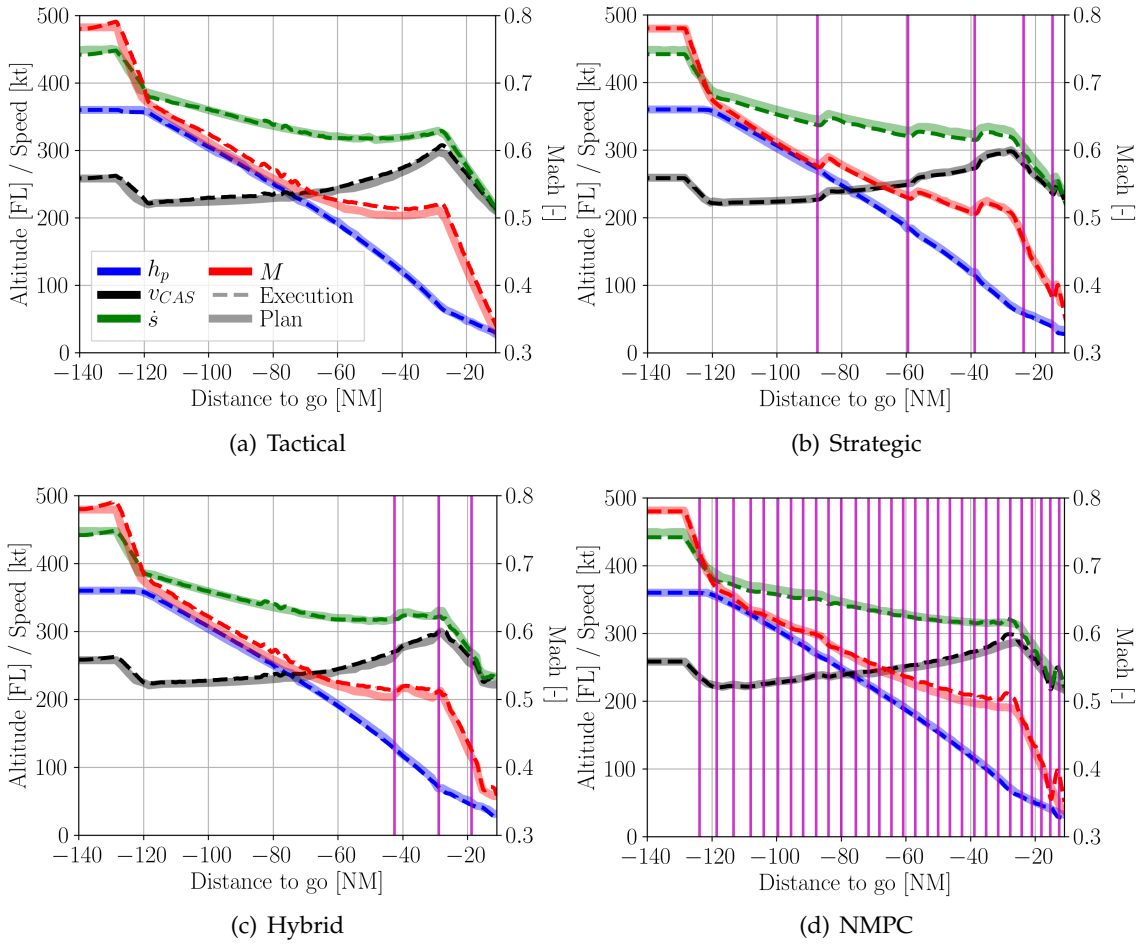

(a) Tactical (b) Strategic

(c) Hybrid (d) NMPC

Figure IV-7: *Planned and executed states per guidance strategy*

mulated time deviations, which could be as high as the maximum allowed threshold at the distance to go where the re-plan is triggered. Figure IV-8(b) shows that for none of the re-plans energy modulation with the elevator was sufficient to correct the accumulated time and energy deviations. All re-plans required to add a relatively small amount of energy to increase the kinetic energy and arrive on time.

In hybrid guidance, a tactical controller nullifies time deviations with the elevator while following the thrust plan with the throttle, and energy deviations are corrected by re-planning the trajectory plan in a strategic way whenever the maximum energy deviation is exceeded. According to Fig. IV-7(c), the tactical controller systematically increased the speed above that planned in order to nullify the time deviations caused by the unexpected head wind. This higher speed led to an increase of the aerodynamic drag and, consequently, to the energy loss rate. As a result, three re-plans were triggered in the last 40 NM by an excessive energy deviation reaching the lower threshold (i.e., the aircraft lacked of energy). All re-plans required additional thrust. Since this guidance strategy does not correct energy deviations as long as they remain within the allowed threshold, the metering fix was achieved almost 100 ft below the planned specific energy level. This missing energy would need to be recovered afterwards by means of additional thrust, leading to more fuel consumption as well as noise nuisance at low altitudes.

In NMPC guidance, energy and time deviations are neither tactically nor strategically corrected during the course of the descent (see Fig. IV-6(d)). Instead, the trajectory is frequently updated by solving an optimal control problem over the remaining descent. The aim of this guidance strategy is to obtain the optimal control vector that, at each plan update, corrects the deviations while optimising the remaining descent for fuel consumption and speed brakes use. In this particular example, the plan was updated 30 times, reaching SOTIL at the planned time and energy level. According to Fig IV-8(d), energy modulation was sufficient to correct energy and time deviations until 90 NM from the runway threshold. Thereafter, small yet optimal amounts of energy were added to the system after each re-plan, aiming to correct energy

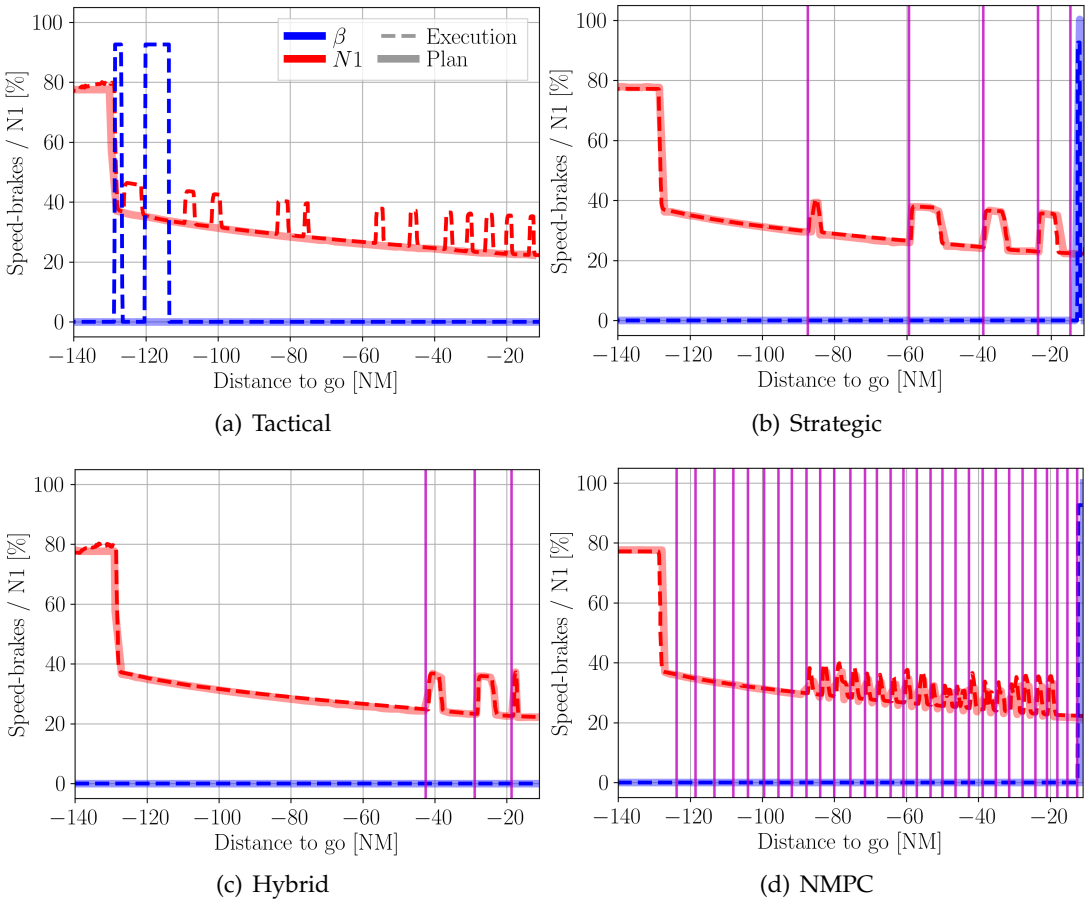

Figure IV-8: *Planned and executed controls per guidance strategy*

deviations and adjust the speed plan. If compared with the hybrid and strategic re-plans, NMPC re-plans led to less modifications of the active plan, thus requiring less throttle and speed brakes use. The reason behind this fact is that time and energy deviations at the moment the re-plan is triggered are smaller, because they are continuously corrected rather than waiting them to reach a certain threshold.

IV.3.2 Comparison of guidance strategies

The comparison of the four guidance strategies is illustrated using spider charts (Fig. IV-9), which allow to easily identify the trade-offs of each guidance strategy relative to the others, as well as violin plots (Fig. IV-10), which show the distribution of the data at different values. Figure IV-9(a) gathers the average results from all simulations. For the remaining subfigures, the set of case studies subject to either wind, temperature or aircraft performance modelling errors were selected separately to isolate their effects.

According to Fig. IV-9(a), the average time deviation at the metering fix is lower than two seconds for all the guidance strategies investigated herein, and less than one second for all those different from the strategic. The reason behind this fact is that, in strategic guidance, time deviations are allowed as long as they remain within the allowed bounds. The remaining guidance strategies show better time deviation figures because their logics continuously correct sustained time deviations, either tactically (in hybrid and tactical) or by means of a continuous re-plan of the optimal descent trajectory (in NMPC). These results demonstrate the excellent performance of time and energy management concepts to satisfy time constraints in uncertain environments.

Regarding the environmental impact, the tactical strategy shows the worst figures in terms of fuel consumption and noise nuisance, due to the continuous (and not optimal) use of thrust and speed brakes to correct energy deviations from the initial (static) trajectory plan. It should be noted that the mechanisms used by the NMPC are similar to those used by the tactical strategy: energy and time deviations are not

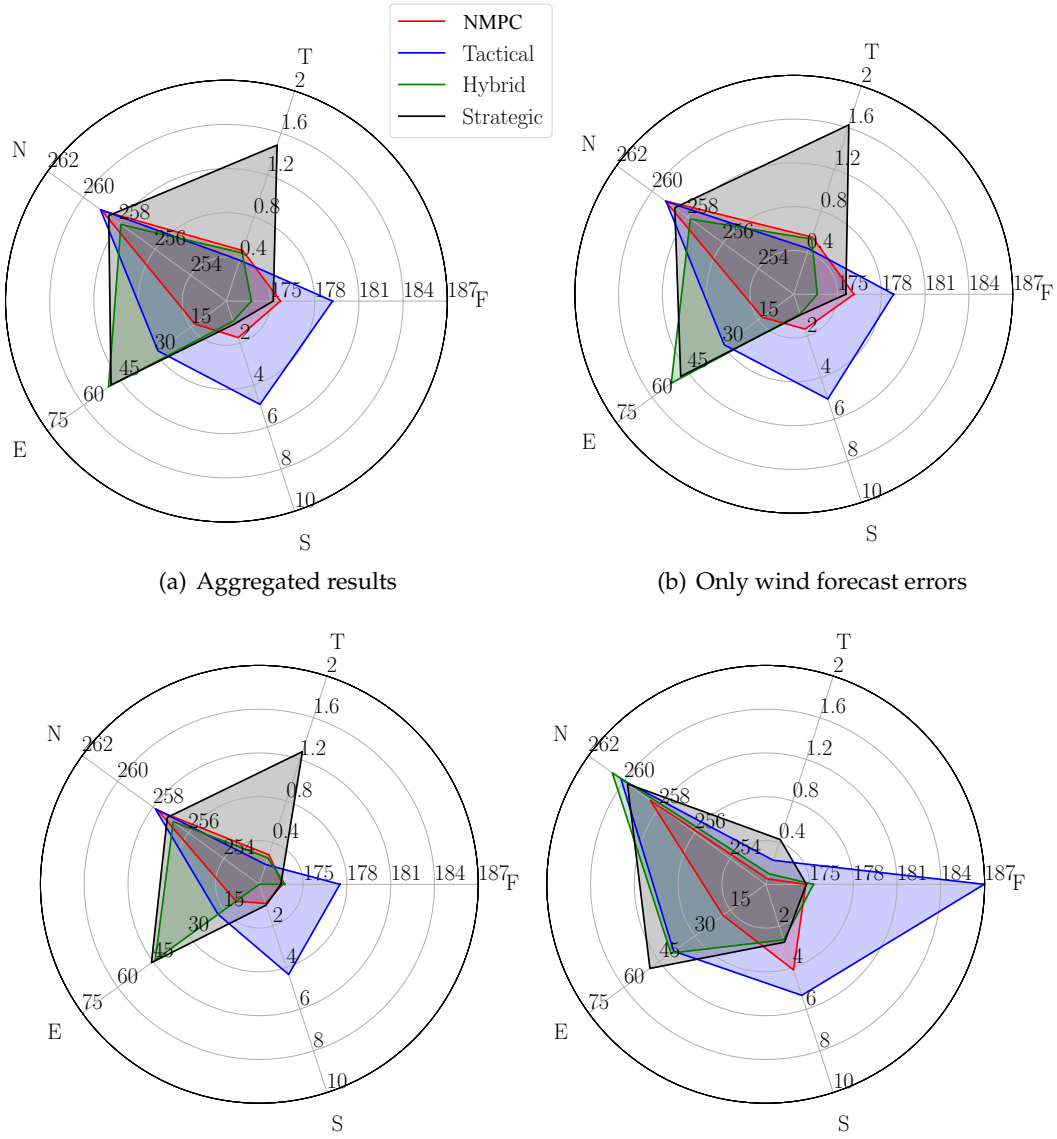

(a) Aggregated results

(b) Only wind forecast errors

(c) Only temperature forecast errors

(d) Only aircraft performance modelling errors

Figure IV-9: *Mean metrics per guidance strategy. E: Specific energy deviation [ft]; F: Fuel consumption [kg]; N: Area affected by aircraft noise [NM^2]; S: Number of speed brakes deployments; T: Time deviation [s].*

monitored, but the elevator, throttle and speed brakes continuously act together to nullify them. Yet, the corrective actions performed by the NMPC are mathematically optimal and take into account the remaining descent trajectory, which is dynamically adjusted. For this reason, the noise nuisance, fuel consumption and speed brakes use for the NMPC strategy are comparable with those of the strategic and hybrid strategies.

The hybrid strategy show the best results in terms of environmental impact mitigation and speed brakes use, proving to exploit the advantages of the strategic and tactical mechanisms. However, the differences with respect to the strategic and NMPC strategies are not significant enough to conclude that the hybrid guidance could be preferred over the others.

As expected, the specific energy deviation at the metering fix is higher for the strategic and hybrid strategies, which allow deviations up to 100 ft at this fix before triggering a re-plan. Similarly, the tactical strategy permits specific energy deviations up to 50 ft before applying throttle or deploying speed brakes. The NMPC shows the best results in terms of energy deviation, because every 30 seconds the energy deviation is nullified when activating the new trajectory plan.

The fuel consumption shown in Fig. IV-9 does not consider the phases after the metering fix. If this fix

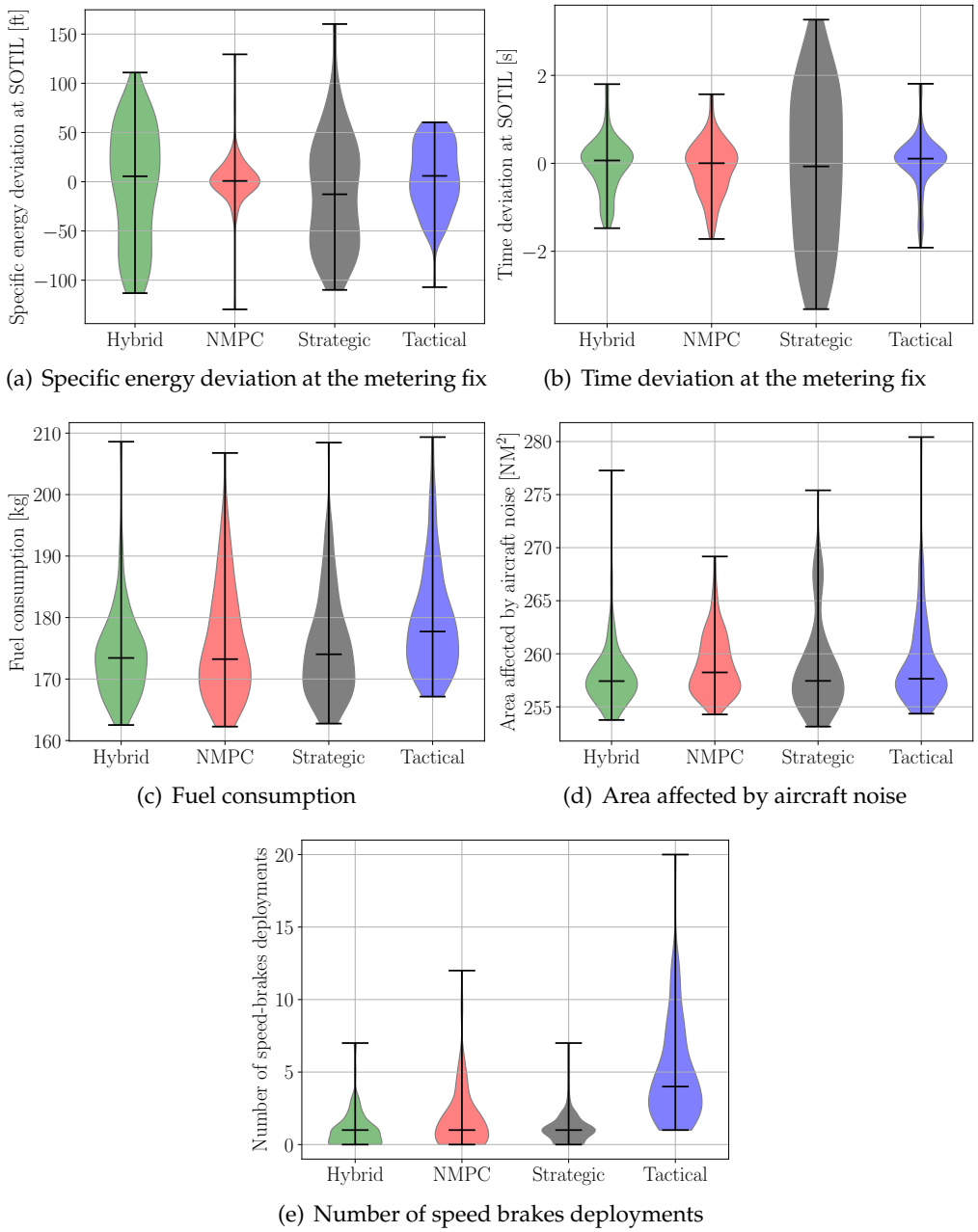

(a) Specific energy deviation at the metering fix

(b) Time deviation at the metering fix

(c) Fuel consumption

(d) Area affected by aircraft noise

(e) Number of speed brakes deployments

Figure IV-10: *Metrics distribution per guidance strategy*

were reached with a certain energy deviation, the missing or excessive energy would need to be added by means of additional thrust (leading to more fuel consumption and noise) or released by deploying speed brakes (leading to more airframe noise), respectively, at low altitudes and near populated areas. With NMPC guidance, the aircraft typically reaches the metering fix with negligible energy deviations. Consequently, the NMPC does not require the addition nor subtraction of energy after the metering fix.

As expected, and according to Fig. IV-9(b), wind errors have the effect of increasing both absolute time and energy deviations. It is also worth to note that, at aggregated level (and considering the same number of case studies with prevalent head wind than with tail wind), the fuel consumption, noise nuisance and speed brakes use are similar to those observed in Fig. IV-9(a). In addition, Fig. IV-9(c) shows that temperature deviations also lead to significant time and energy deviations. On the one hand, all the guidance strategies considered herein execute the CAS plan, leading to true airspeed (TAS) errors in presence of temperature deviations. On the other hand, the aircraft performance strongly depends on the air temperature (see Eq. (IV.8b)). Finally, according to Fig. IV-9(d), errors in the aircraft performance models are not penalising

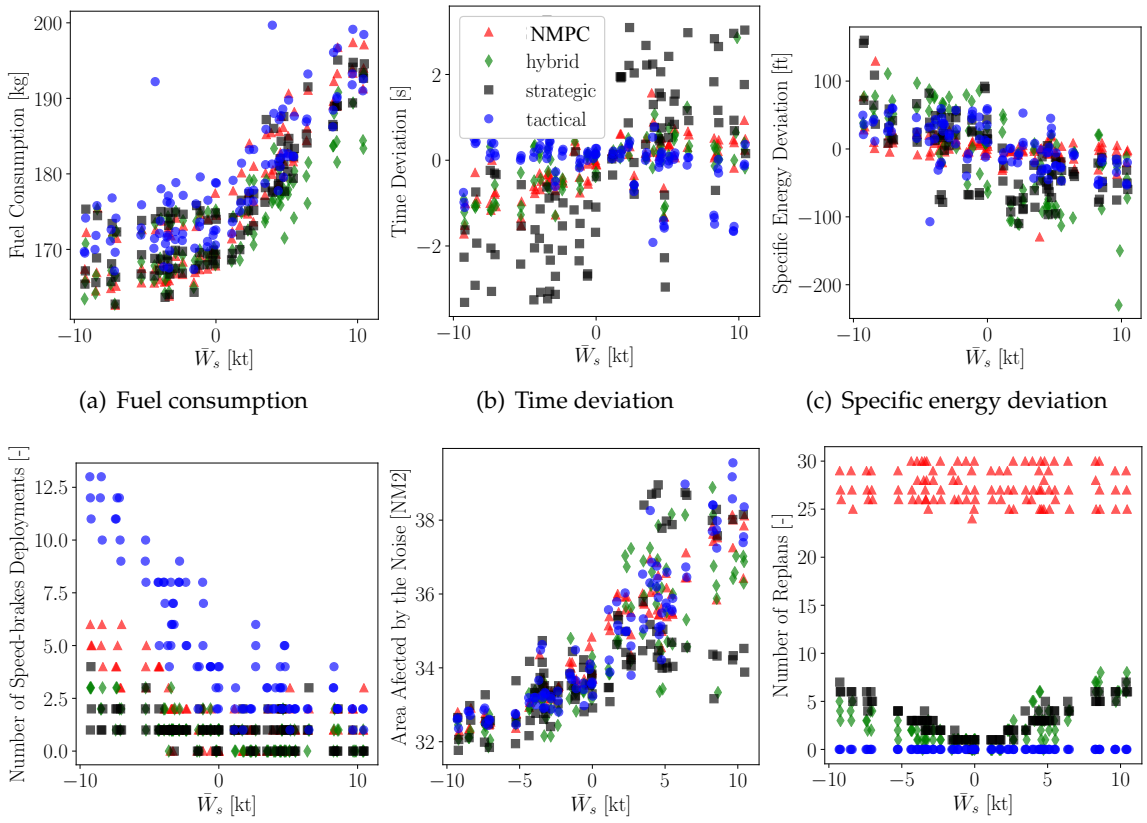

(a) Fuel consumption (b) Time deviation (c) Specific energy deviation

(d) speed brakes use (e) Area affected by the noise (f) Number of re-plans

Figure IV-11: *Correlation between metrics and longitudinal wind speed error*

the capability to satisfy CTAs, but have a major impact on the environment.

Figure IV-9 showed only the mean of the different metrics per guidance strategy. Figure IV-10 shows the complete distribution for each metric and guidance strategy. Essentially, the conclusions remain the same than stated before. Namely, the strategic and hybrid show the larger dispersion of energy deviations at the metering fix, due to their passive behaviour with respect to the energy deviation as long as it remains within the allowed threshold; the tactical hybrid and NMPC show excellent figures in terms of time error at the metering fix, while the time error for the strategic approach shows larger dispersion; and the tactical strategy is the one leading to more fuel consumption, noise nuisance and speed-brakes use.

IV.3.3 Sensitivity to the wind error

Figure IV-11 shows, for each guidance strategy, the dependence of each particular metric with respect to the average longitudinal wind speed error encountered druing the descent. Each point in the scatter plot shows the result of a single simulation. Positive (resp. negative) values of longitudinal wind speed error represent unexpected head (resp. tail) wind encountered during the execution of the descent.

According to Fig. IV-11, and as expected, the higher the unexpected head wind, the larger the fuel consumption and noise nuisance. In contrast, the number of speed brakes deployments typically increases with the unexpected tail wind. The rationale behind these results was already discussed in Section III.3.3.2: the head wind leads to an increase of the energy loss rate per unit distance, while the tail wind reduces the amount of energy lost per unit distance. During the execution of the descent, the guidance system will add more energy (directly related to fuel consumption and noise) or will release it by deploying speed brakes to safely and efficiently guide the aircraft along the planned trajectory.

According to Fig. IV-11(c), for the tactical and NMPC guidance strategies, the energy deviation at the metering fix is always close to zero, independently of the wind speed error. However, in strategic and hybrid guidance more dispersion is found for large wind speed errors. The same conclusion applies for the

time deviation (see Fig. IV-11(b)). In this case, however, the tactical, hybrid and NMPC guidance strategies show excellent figures of CTA adherence, while the time deviation for the strategic guidance shows a linear correlation with the longitudinal wind speed error.

Figure IV-11(f) shows that the number of re-plans for the strategic and hybrid guidance strategies strongly depends on the absolute value of the longitudinal wind error. However, the number of re-plans of these guidance strategies is still much lower than that of the NMPC strategy, which generates a new descent plan starting at the current aircraft state every 30 seconds.

IV.4 Discussion

This chapter compared the performance of four guidance strategies based on time and energy management concepts: tactical, strategic, hybrid and NMPC. Results from a batch study demonstrated that the four guidance variants can safely accomplish a CTA during a CDO with negligible time and energy deviations, even in presence of significant weather and aircraft performance modelling errors.

The tactical guidance strategy requires continuous actions on the throttle and speed brakes to remain on the planned energy level and arrive on time, leading to more fuel consumption and noise nuisance if compared with other strategies. The hybrid strategy shows the best results in terms of environmental impact mitigation, and also requires less pilot actions to deploy speed brakes. However, due to its strategic behaviour with respect to specific energy deviations, the metering fix is reached with larger specific energy deviations than for other strategies. In this context, the NMPC strategy demonstrated to be the most robust in terms of specific energy and time deviations at the metering fix, while simultaneously showing environmental impact figures comparable to those of the hybrid and strategic.

The main conclusion of this study is that these four guidance strategies provide very similar performance. However, even these small differences could be significant at aggregated level. Since all the guidance strategies showed similar results in terms of fuel consumption and time and energy error at the metering fix, the additional robustness of the NMPC guidance strategy promotes its use for this application. Compared to the other guidance strategies investigated herein, NMPC provides more situation awareness for the pilot, since deviations from the (dynamic) trajectory plan are lower than for strategic and hybrid. Also for this reason, the NMPC reduces the chances of obtaining infeasible solution as a result of a trajectory update. Note that when the strategic and hybrid strategies update the trajectory plan due to an excessive time and/or energy error reaching the threshold, it might be too late to react and satisfy all the constraints. In such cases, any of the strategies discussed in Section II.2.4.1 could be used to recover feasibility as long as the operational limits of the aircraft are not overpassed, yet degrading the performance of the operation. Last but not least, another advantage of the NMPC is that, if at certain moment during execution of the descent up-to-date and accurate wind data is obtained from, e.g., the leading aircraft in the procedure, re-planning the trajectory plan may be beneficial in both environmental impact and constraints compliance terms. The combination of NMPC and wind networking concept will be further investigated in Chapter VI.

A limitation of the experiment presented herein is that the remaining descent after the metering fix was not taken into account. If the energy of the aircraft at this fix were too low, additional thrust would be needed after overflying it. Similarly, if the energy were too high, it would be required to use speed brakes and/or to deploy high-lifting devices or the landing gear earlier. After the metering fix, however, the approach procedure is heavy constrained, since the aircraft has to intercept the ILS glide slope in few nautical miles and thereafter follow a constant ground flight path angle (not allowing for energy management).

Last but not least, in this chapter the guidance strategies were not optimised for noise explicitly, even if noise nuisance was used as metric for comparison. In future research, descents will be optimised for noise (and emissions) explicitly, and even better results may be obtained in terms of these metrics.

A complex system that works is invariably found to have evolved from a simple system that works.

— John Gaule

Any sufficiently advanced technology is indistinguishable from magic.

— Arthur C. Clarke

V

Model predictive control to meet time constraints in optimal descents

In Chapter IV, the performance of various guidance strategies build on the time and energy managed operations (TEMO) concept (De Jong *et al.*, 2015) were compared using a high-fidelity flight simulator located at Netherlands Aerospace Centre (NLR), focusing in the environmental impact mitigation of these guidance strategies as well as their ability to comply with operational constraints (of particular interest, time constraints). Hundreds of optimal descents to Barcelona-El Prat airport subject to controlled time of arrival (CTA) at a metering fix were simulated by introducing errors in the weather and aircraft performance models implemented in a research flight management system (FMS). Results showed that nonlinear model predictive control (NMPC) (Diehl *et al.*, 2008), a guidance strategy based on a frequent update of the optimal trajectory plan during the execution of the descent (e.g., every 30 seconds), could be very robust in terms of correcting energy (speed and altitude) and time deviations at the metering fix, providing at the same time acceptable fuel consumption and noise nuisance figures, if compared to existing TEMO strategies. Another advantage of NMPC is that deviations from the (continuously adjusted) trajectory plan are always small, thus providing more situational awareness for the pilot and being less prone to infeasible solutions as a result of a trajectory plan update. Based on these conclusions, NMPC was identified as a very attractive guidance strategy to enable continuous descent operations (CDOs) in high traffic demand scenarios.

A practical limitation of the basic NMPC for *real-life* applications, however, was that each trajectory update could take up to 10 seconds. The main reason of this excessive computation time was that the trajectory planner formulated the optimal control problem in the remaining time horizon from scratch, without taking advantage of the nonlinear programming (NLP) structure, parametric sensitivity or primal-dual solution of a similar optimisation problem computed at a previous time sample (see Section II.2.4.3).

In this chapter, two additional variants of the basic NMPC will be investigated, which take advantage of parametric sensitivities to update the optimal trajectory plan quasi-instantaneously. The hypothesis is that sensitivity-based strategies will provide considerable reduction in execution time (thus allowing to updated the trajectory plan more often), simplification of the optimisation algorithm (thus improving convergence and robustness), at the expense of a small reduction on the accuracy of the solution.

In order to accomplish that, more than 4,000 descents per guidance strategy were simulated at the National Aeronautics and Space Administration (NASA), supported by their expertise in trajectory operations and, in particular, CDOs and interval management. Errors in the parameters used by the FMS to describe the wind profile were intentionally introduced in the simulations. The *open-loop* fuel consumption as well as time and energy errors at the metering fix, obtained by applying the initial optimal control plan (computed at the TOD) in open-loop subject to these modelling errors, were compared with those of the pure sensitivity-based NMPC (SbNMPC), which uses only parametric sensitivities to update the optimal trajectory plan at each time sample; the ideal NMPC (INMPC) (Suwartadi *et al.*, 2017), which ideally updates the optimal trajectory plan at each time sample by solving a rigorous NLP optimisation problem without delay (i.e., zero execution time); and the advanced-step NMPC (AsNMPC), which combines an early rigorous re-calculation of the trajectory plan based on the predicted state at the next time sample, with a sensitivity-based update to correct perturbations after measuring the actual state of the aircraft and parameters. Last but not least, the sensitivity of the performance metrics to the mean longitudinal wind error experienced during the descent was also investigated for the INMPC, if compared to the open-loop execution.

It should be noted that the flight simulator used in this experiment was simpler than that used in Chapter IV. In particular, the simulator consisted on a set of accurate ordinary differential equation (ODE) integrators that, given the controls of the aircraft and its current state, calculated the future position at the next time sample using CVODES, a solver for stiff and nonstiff ODE systems bundled into the SUite of Nonlinear and DIfferential/ALgebraic Equation Solvers (SUNDIALS) (Hindmarsh *et al.*, 2005).

V.1 State of the art

Generic NMPC implementations, such as that used in Chapter IV, frequently update the optimal trajectory plan by solving a rigorous NLP optimisation problem. Ideally, the trajectory should be updated without delay at each time sample, right after measuring the current state of the aircraft ($\vec{X}$) and estimating the parameters of the model ($\vec{d}$). In practical real-time applications, however, solving the rigorous NLP optimisation problem may take a significant amount of time, leading to potential stability issues and/or degrading the overall performance of the descent operation (Suwartadi *et al.*, 2017).

In order to reduce the execution time, educated simplifications in the models used by the FMS have been used, for instance by Kim & Hull (1995), at the expense of compromising the accuracy of the solution. Other NMPC implementations compensate for computational delay by starting the optimisation process in advance, setting the initial conditions of the new trajectory plan to the predicted state of the aircraft at the next time sample (Zavala & Biegler, 2009), or at a look-ahead time equal to the estimated execution time. In the later case, the unpredictability of the execution time remains a critical issue (Wetzel, 1996).

An alternative method widely used in process industries consists of computing fast trajectory updates in the neighbourhood of the last optimal solution using the theory of neighbouring extremals (Pesch, 1979). Using this approach, parametric sensitivities are obtained by linearisation of the necessary conditions of optimality, also known as Karush-Kuhn-Tucker conditions (KKT) conditions, along the (optimal) active trajectory plan to rapidly update it for small perturbations in the parameters of the model. This strategy, known as SbNMPC, has shown important benefits in terms of execution time (Würth *et al.*, 2008b, 2009; Wolf & Marquardt, 2016). For more technical details about this strategy the reader is referred to Section II.3.4.2.

V.2 Setup of the experiment

In the experiment performed in this chapter, 4,143 descents per guidance strategy were simulated to asses the performance of the INMPC, SbNMPC and AsNMPC guidance strategies in the presence of errors in the wind forecast model used by the trajectory planner. All the descents were subject to CTA at a metering fix, and to several altitude and speed constraints of a realistic flight procedure.

First, Section V.2.1 presents the scenario. Then, the generic models introduced in Section II.1 are particularised in Section V.2.2. Analogously, the generic optimal control problem stated in Section II.2.1 is particularised in Section V.2.3 with specific cost function and constraints. The selected case studies are listed in Section V.2.4, and the workflow of a single simulation is summarised in Section V.2.5.

V.2.1 Scenario

The Denver international airport (DEN) was selected as the scenario for the experiment performed in this chapter. Fig. V-1 shows the BOSSS TWO standard arrival procedure at DEN, which was the starting point to define the route and the vertical profile used in this study. The metering fix where CTA were assigned by an hypothetical air traffic control (ATC) during the simulations was the final approach point (DYMON in Fig. V-1). The aircraft type used for the assessment was an Airbus A320-214.

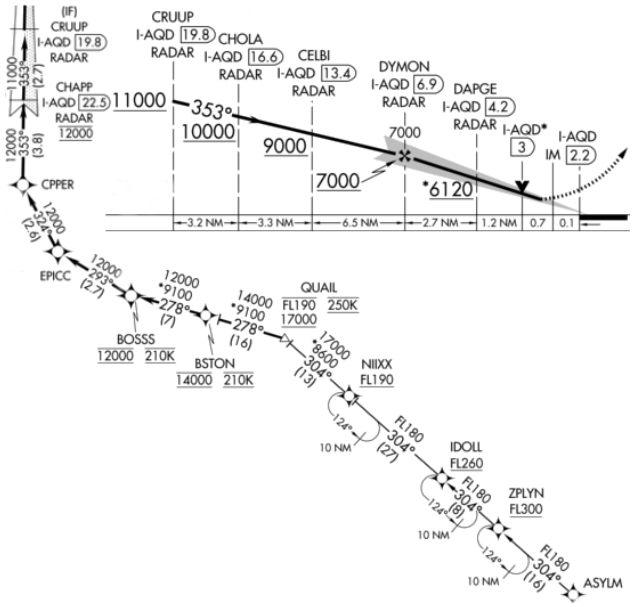

Figure V-1: *BOSSS TWO standard arrival procedure (source: US AIP)*

V.2.2 Models

The models required to formulate the optimisation of the aircraft trajectory, which were presented in Section II.1, are particularised below for the experiment conducted in this chapter.

V.2.2.1 Aircraft dynamics model

A variant of the γ-*command* model described by Eq. (III.2) was implemented in the trajectory planner. Different from typical approaches, the independent variable of this variant is the distance to go (s) and not the time. The selection of s as the independent variable was driven by the fact that during an ideal CDO, with no intervention from the ATC except for the negotiation of the CTA, the aircraft will follow a *closed-loop* route and the remaining distance to go will be known. In addition, this formulation replicates how constraints are defined in the current operational environment, thereby enabling more precise modelling.

In the distance-based γ-*command* model, the state vector is $\vec{x} = [t, v, h]^T$, and the control vector is $\vec{u} = [\gamma, T, \beta]^T$. The dynamics of $\vec{x}$ are expressed by the following system of ODEs:

$$\begin{aligned}
\frac{\mathrm{d}t}{\mathrm{d}s} &= t' = \frac{1}{v\cos\gamma + w_s(h)} \\
\frac{\mathrm{d}v}{\mathrm{d}s} &= v' = \left(\frac{T - D(v,h,\gamma)}{m} - g\sin\gamma\right)\frac{1}{v\cos\gamma + w_s(h)} \\
\frac{\mathrm{d}h}{\mathrm{d}s} &= h' = \frac{v\sin\gamma}{v\cos\gamma + w_s(h)}.
\end{aligned} \tag{V.1}$$

Note that w_x was neglected for the sake of simplicity.

V.2.2.2 Aircraft performance model

Different alternatives can be used to model T_{idle}, T_{max}, C_D, q, q_{idle}, as mentioned in Section II.1.2. In this experiment, the base of aircraft data (BADA) v4 model was adopted (Poles *et al.*, 2010). Unfortunately, BADA v4 still does not include a model for the effects of the speed brakes on the drag coefficient. As a workaround, the contribution of the speed brakes was modelled as an extra linear term in the generic BADA v4 drag coefficient model ($C_{D,BADA}$). A similar approach was adopted in the study performed in Chapter IV:

$$C_D(C_L, M, \beta) = C_{D,BADA}(C_L, M) + C_{D\beta}\beta. \tag{V.2}$$

Figure V-2 show the propulsive functions of the BADA v4 performance model for the A320-214 used in this study. Analogously, Fig. V-3 shows the drag coefficient.

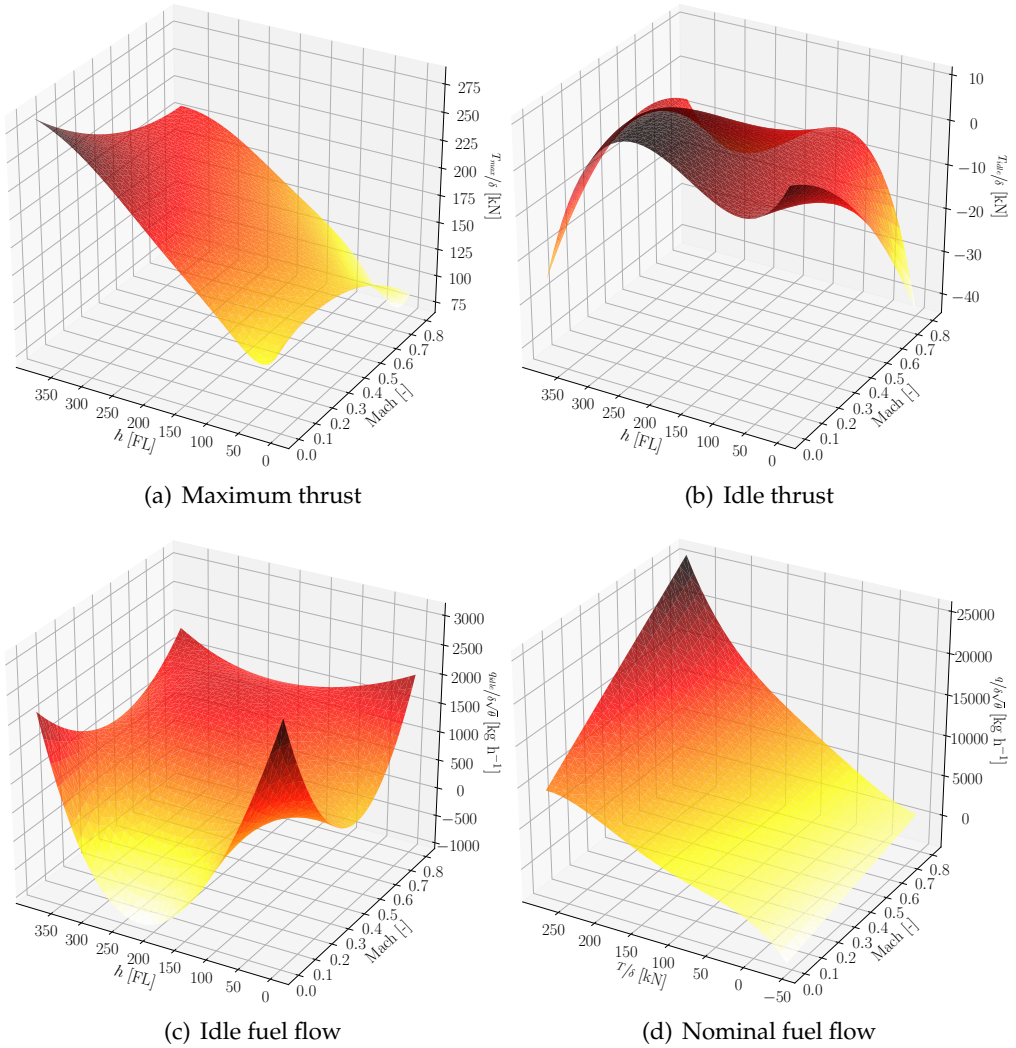

(a) Maximum thrust

(b) Idle thrust

(c) Idle fuel flow

(d) Nominal fuel flow

Figure V-2: *BADA 4 propulsive model for the A320-214*

V.2.2.3 Atmosphere model

In this experiment, the international standard atmosphere (ISA) model, established to provide a common reference for temperature and pressure, was considered to represent the normalised temperature θ and pressure δ as a function of h through Eqs. (II.4) and (II.5), respectively. Then, the normalised density was computed assuming the perfect gas law relationship with Eq. (II.6). The longitudinal component of the wind (w_s) was modelled by a smoothing spline of the form:

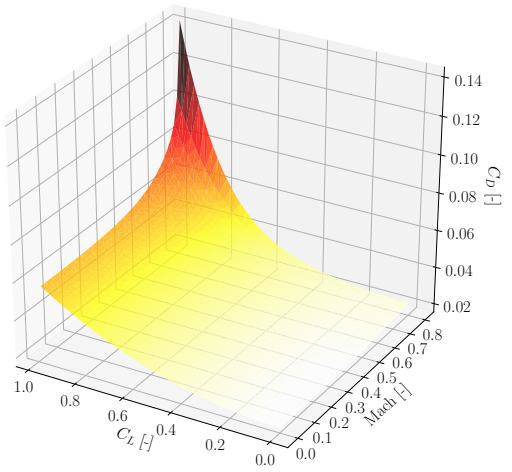

Figure V-3: *BADA 4 aerodynamic model for the A320-214*

$$w_s(h) = \sum_{i=1}^{n_c} c_i B_i(h), \tag{V.3}$$

where B_i, $i = 1, \ldots, n_c$, are B-spline basis functions and $\vec{c} = [c_1, \ldots, c_{n_c}]$ are control points of the spline (de Boor, 1972). It should be noted that the longitudinal wind was modelled as a function of the altitude only, as done in similar works (De Jong *et al.*, 2015). Yet, it would be straightforward to consider dependence also on the distance to go, which is the independent variable of the model.

V.2.3 Optimal control problem formulation

The trajectory planner used in this experiment generates the optimal plan trajectory subject to a CTA by solving a multi-phase, constrained and nonlinear optimal control problem, as described in Section II.2.1. This section particularises the cost function and the dynamic, path, algebraic and/or interior-point constraints for each one of the phases composing the flight profile of the procedure illustrated in Fig. V-1.

The differential constraints that enforce the dynamics of the aircraft ($\vec{f}$) were particularised by the following distance-based γ-*command* model, independently of the phase:

$$\vec{f_j} = \begin{bmatrix} 1 \\ \frac{T - D(v,h,\gamma)}{m} - g\sin\gamma \\ v\sin\gamma \end{bmatrix} \frac{1}{v\cos\gamma + w_s(h)}; \; j = 0, \ldots, P-1. \tag{V.4}$$

From all the waypoints of the route, only the altitude and speed constraints at QUAIL, BOSSS, CHAPP and DYMON were modelled. In order to accomplish that, the descent was divided into $P = 4$ different phases, with associated phase-dependent path, algebraic and/or interior-point constraints. It should be noted, however, that the fact of modelling few constraints of the real procedure is not a shortcoming nor a limitation of the model. The model proposed in this study could handle an unlimited number of phases and associated constraints, yet few constraints were selected aiming to represent a futuristic and less restricted procedure facilitating CDOs, as well as to ease the interpretation of the results. Table V-1 wraps up the different phases and their associated constraints. This table is also illustrated in Fig. V-4.

Note that the last row of Table V-1 includes phase-independent path constraints (i.e., applying all along the descent), which ensure that the aircraft airspeed remains within operational limits, and that the maximum and minimum descent gradients, thrust and speed brakes are not exceeded.

In Table V-1, $\beta = 0$ and $\beta = 1$ indicate that speed brakes are retracted and fully extended, respectively; the minimum descent gradient was set to $\gamma_{min} = -7°$; and the values for maximum operative CAS (VMO) and maximum operative Mach (MMO) were obtained from the BADA v4 performance model.

In addition, the following terminal constraints were set at the metering fix DYMON:

Table V-1: *Definition of the phases and constraints for the comparison of NMPC strategies*

Phase (j)	Description	$\vec{b}_j^{eq}$	$\vec{b}_j^{in}$	$\vec{\vartheta}_j^{in}$	$\vec{\vartheta}_j^{eq}$
0	TOD-QUAIL	$\begin{bmatrix} v_{CAS}(v,h) - \text{VMO} \\ 250\,\text{kt} - v_{CAS}(v,h) \end{bmatrix}$	-	$\begin{bmatrix} \text{FL170} - h \\ h - \text{FL190} \end{bmatrix}$	$\begin{bmatrix} v_{CAS}(v,h) - 250\,\text{kt} \end{bmatrix}$
1	QUAIL-BOSSS	$\begin{bmatrix} v_{CAS}(v,h) - 250\,\text{kt} \\ 210\,\text{kt} - v_{CAS}(v,h) \end{bmatrix}$	-	-	$\begin{bmatrix} v_{CAS}(v,h) - 210\,\text{kt} \\ h - 12,000\,\text{ft} \end{bmatrix}$
2	BOSSS-CHAPP	$\begin{bmatrix} v_{CAS}(v,h) - 210\,\text{kt} \\ \text{GD} - v_{CAS}(v,h) \end{bmatrix}$	$\begin{bmatrix} \dot{h} \end{bmatrix}$	-	-
3	CHAPP-DYMON	$\begin{bmatrix} v_{CAS}(v,h) - 210\,\text{kt} \\ \text{GD} - v_{CAS}(v,h) \end{bmatrix}$	-	-	
All	Entire descent	$\begin{bmatrix} M(v,h) - \text{MMO} \\ \gamma \\ \gamma_{min} - \gamma \\ T_{min}(v,h) - T \\ T - T_{max}(v,h) \\ \beta \\ \beta - 1.0 \end{bmatrix}$	-	-	-

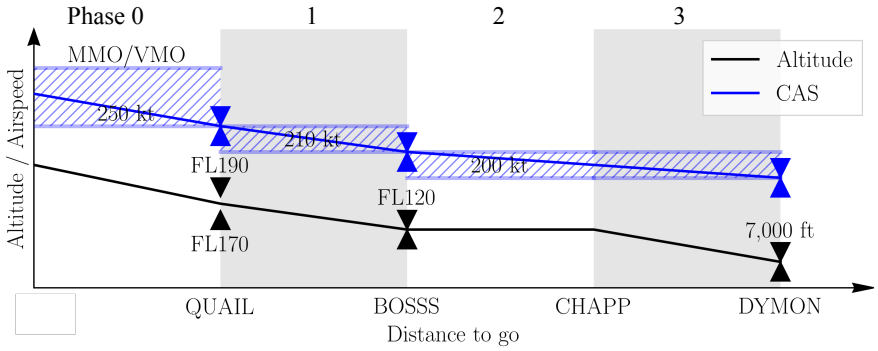

Figure V-4: *Definition of the phases and constraints for the assessment of NMPC strategies*

$$\vec{\psi} = \begin{bmatrix} v_{CAS}(v,h) - \text{GD} \\ h - 7,000\,\text{ft} \\ t - \text{CTA} \end{bmatrix}. \tag{V.5}$$

According to Eq. (V.5), the CTA was imposed by fixing the final time (which was considered a state) of the last phase. Since the flight time was fixed by the CTA, the goal was to minimise a weighted sum of fuel consumption and speed brakes use for the remaining descent. Therefore, the stage cost was:

$$\pi_j = \frac{q(v,h,T) + K_\beta \beta}{(v\cos\gamma + w_s(h))};\ j = 0,\ldots,P-1. \tag{V.6}$$

In this particular experiment $K_\beta = 1$, and a fourth-order Runge-Kutta scheme was used to obtain $\vec{F}_j$ and Π_j from $\vec{f}_j$ and π_j, respectively. Moreover, no terminal costs were considered (i.e., $\phi_j = 0$ for $j = 0,\ldots,P-1$).

It should be noted that the vector of model parameters included the control points of the spline approximating the longitudinal wind and the CTA, i.e., $\vec{d} = [\vec{c}, \text{CTA}]^T$. This definition allowed the optimal trajectory to be updated whenever an improved wind forecast was available or the CTA was modified.

Finally, the soft-constraint method was implemented to recover feasibility (see Section II.2.4.1).

V.2.4 Case studies

Accurate wind data can be obtained from the rapid refresh (RAP) forecast/analysis system of the National Oceanic and Atmospheric Administration (NOAA). This system generates numerical weather forecasts hourly for look-ahead times up to +18 hours in a 13 km resolution grid covering North America and for 50 vertical levels extending up to 10 hPa. Sightly different, RAP analyses, which reproduce the actual weather conditions, are generated hourly by using weather observations gathered from commercial aircraft, balloons, radars and satellites.

For each case study of this experiment, a different wind forecast generated by RAP was used to initialise the wind profile spline of the FMS (see Eq. (V.3)). Then, during the execution of the descent in the simulator, the actual wind encountered by the aircraft was obtained from the corresponding RAP analysis. Historical wind forecasts generated by RAP at 00:00, 06:00, 12:00 and 18:00 for look-ahead times of +1, +3 and +6 hours during one year (from June 2017 to June 2018) and actual wind data as reported by the corresponding RAP analysis were used to configure a total of 4,143 case studies per guidance strategy.

Figure V-5 shows the distribution of root-mean-square error (RMSE) for the RAP forecast from June 2017 to June 2018, as a function of the forecast look-ahead time. It is interesting to observe that the three distributions are centred at 1.5, 2.5, and 3 kt, approximately, and that the tail of the distribution increases with the wind forecast look-ahead time, as does the uncertainty of the wind prediction.

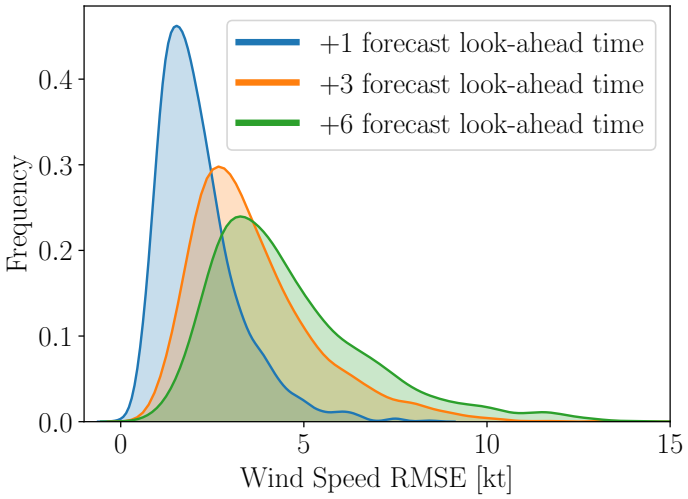

Figure V-5: *RAP wind forecast RMSE distribution from June 2017 to June 2018*

V.2.5 Workflow of a simulation

The experiment simulated an aircraft cruising at FL360 and Mach 0.78. Well before starting the descent to DEN, the FMS computed the optimal descent trajectory plan to DYMON considering a typical cost index (CI) of $30\,\text{kg}\,\text{min}^{-1}$ (Airbus, 1998), and discretising the continuous optimal control problem into $N = 60$ time samples. Note that the more the number of time samples, the more accurate the solution will be, but the higher the computational burden. The initial trajectory plan was computed considering a spline for the longitudinal wind profile[1] that approximated wind data from the RAP forecast.

As a result of this optimisation, the best distance to go of the top of descent (TOD) and the optimal time of arrival at DYMON, for a CI of $30\,\text{kg}\,\text{min}^{-1}$, were obtained. In addition, the energy-neutral time window [2] from the TOD to DYMON was also computed and sent to the hypothetically ATC, who replied with a random CTA at DYMON within this energy-neutral time window.

[1] It should be noted that the longitudinal wind profile was computed assuming a constant track of 304° all along the route for the sake of simplicity.

[2] The energy-neutral time window from a state to a metering fix is defined as the difference between the latest and earliest time of arrival that could be achieved without requiring neither thrust nor speed brakes usage throughout the whole descent. Results from Chapter III showed that energy-neutral time windows up to 2.8 minutes can be obtained for certain flight conditions.

Right after, the FMS set the CTA as a terminal constraint for the time state in Eq. (V.5), and calculated the optimal descent trajectory from the current state to DYMON by solving $\mathcal{P}_N$. All simulations started with the aircraft located at the TOD obtained by solving $\mathcal{P}_N$ subject to the CTA, ready to start the execution of the optimal descent trajectory using either of the NMPC strategies.

During the execution of the descent, the aircraft encountered the actual wind profile (obtained from a RAP analysis), which was different from the forecast used by the FMS (obtained from a RAP forecast). The initial forecast, however, progressively converged to the actual wind profile as the aircraft descended. At each time sample, the actual wind at the current altitude was sensed by the ownship, the pair of altitude and wind speed was appended to the set of available wind observations, and the control points of the spline that approximated the wind profile were updated based on the ownship observations collected so far.

Given a set $\mathcal{O}$ composed by n_o wind observations with associated time stamps, $(\hat{h}_k, \hat{w}_k, \tau_k)$ for $k = 1, \ldots, n_o$, and a vector of fixed knots, the optimal locations of the control points $\vec{c}$, that minimise the curvature of the smoothing spline while bounding the approximation error was obtained by solving a weighted least-squares fitting problem:

$$\begin{aligned} \min_{\vec{c}} \quad & \int w''(h, \vec{c})^2 \mathrm{d}h \\ \text{s.t} \quad & \sum_{k=1}^{n_o} \omega_k \left(w(\hat{h}_k, \vec{c}) - \hat{w}_k \right)^2 \leq \varepsilon, \end{aligned} \tag{V.7}$$

where ε is the smoothing factor, which specifies the trade-off between smoothness and accuracy of the approximation. The weights associated with the observations can be defined in many different ways. In this chapter, all the weights are updated at each time sample τ_i according to $\omega_k = \Lambda^{\tau_k - \tau_i}$, where τ_k is the time sample when the observation at $\hat{h}_k$ was obtained. The forgetting factor $\Lambda \in [0, 1]$ weights the more recent measurements so that old observations are discounted at an exponential rate.

Right after updating the control points of the wind profile, the trajectory was updated either by solving $\mathcal{P}_{N-i}$ or $\mathcal{Q}_{N-i}$ (see Chapter II.3), depending on the guidance strategy considered during the simulation.

In this chapter, $\mathcal{P}_{N-i}$ and $\mathcal{Q}_{N-i}$ were formulated in CasADi (Andersson *et al.*, 2018)[3], a symbolic framework for automatic differentiation and numeric non-linear optimisation, and were solved by using the sequential quadratic programming (SQP) algorithm implemented by the sparse nonlinear optimiser (SNOPT) NLP solver (Gill *et al.*, 2005).

Figure V-6 shows the main components of this experiment and their interactions.

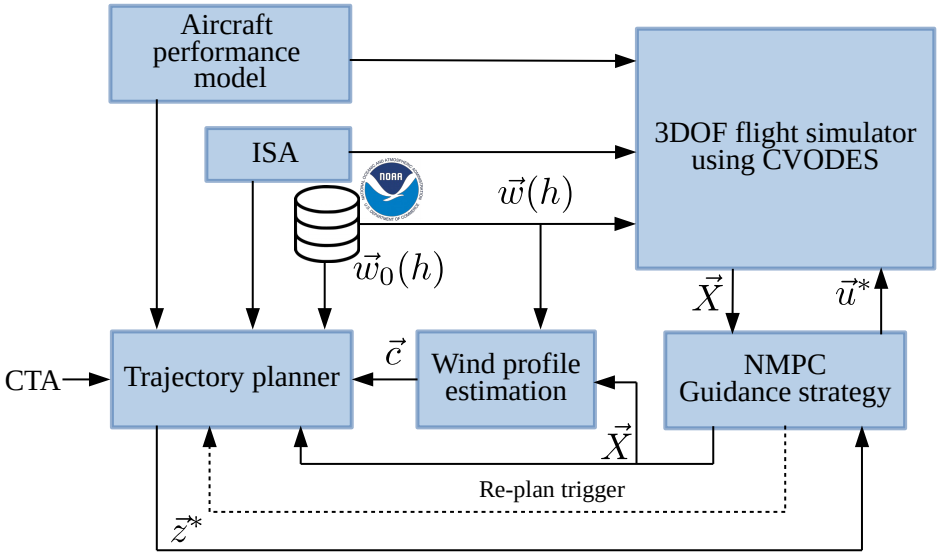

Figure V-6: *Setup of the experiment to compare NMPC guidance strategies*

[3] https://github.com/casadi/casadi/wiki

V.3 Results

The results of the experiment described above are presented in this section. Section V.3.1 shows illustrative examples of trajectory updates, which were generated after intentionally perturbing different elements of the parameters vector at the first time sample. Then, Section V.3.2 shows examples of descent execution, aiming to illustrate the distinctive traits of the different NMPC alternatives. From the 4,143 wind forecasts and associated wind analysis considered in this experiment, those corresponding to the 2018-04-21 at 00:00 with a look-ahead time of +1 hour were selected for the illustrative examples in Sections V.3.1 and V.3.2. Figure V-7 shows the forecast and the actual wind profile for this particular date and look-ahead time. Finally, the aggregated results for the 16,572 simulations are presented and discussed in Section V.3.3.

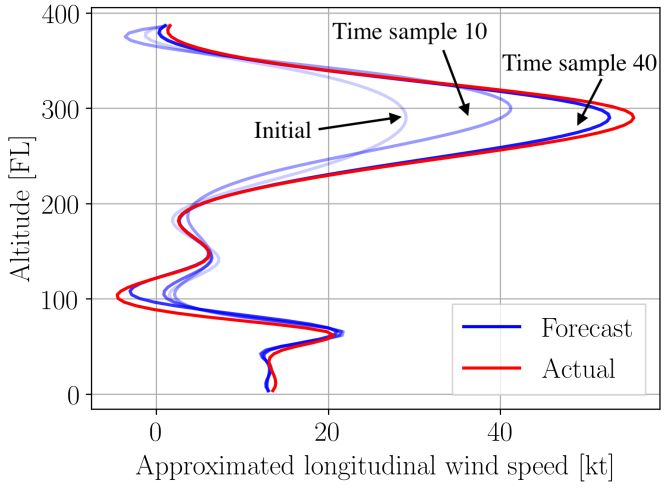

Figure V-7: *RAP wind forecast and analysis (2018-04-21 00:00 for a look-ahead time of +1 hour)*

V.3.1 Illustrative examples: trajectory updates

The three NMPC guidance strategies presented in Section II.3.4 update the optimal trajectory at each time sample τ_i, $i = 1, \ldots, N-1$ according to the vector of NLP parameters $\vec{p}$. By definition, any perturbation in one of the elements of $\vec{p}$ will entail a new optimal trajectory plan. Remember that for the model proposed in Section V.2.3, the vector of NLP parameters at time sample τ_i is composed by the current state of the aircraft ($\vec{X}$) and the parameters of the model ($\vec{d}$). In turn, $\vec{d}$ includes the control points of a spline approximating the longitudinal wind profile ($\vec{c}$) and the CTA to be satisfied. That is:

$$\vec{p} = \begin{bmatrix} \vec{X} \\ \vec{d} \end{bmatrix} = \begin{bmatrix} \vec{X} \\ \vec{c} \\ \text{CTA} \end{bmatrix}. \tag{V.8}$$

The initial (unperturbed) trajectory plan computed at the TOD for this illustrative example is shown in all three panels of Fig. V-8. The vector of parameters used to generate this trajectory plan was composed by the control points of the spline approximating the wind forecast data obtained from RAP, the nominal initial state exposed and the CTA corresponding to the simulation for the same wind forecast and analysis. Figure V-8 also shows the trajectories that would result from solving the rigorous NLP and a sensitivity-based update with perturbations in the different elements of the parameters vector. Each panel of this figure corresponds to a different element of $\vec{p}$. The state perturbation ($\delta\vec{X}$) was an altitude deviation of 1,000 ft below the unperturbed trajectory, the wind perturbation ($\delta\vec{c}$) was the difference between the control points of the splines approximating the RAP forecast and analysis data, and the CTA perturbation (δCTA) was ATC requesting the aircraft to arrive 30 seconds earlier. It should be noted that each panel of Fig. V-8 shows only the results of a single trajectory update performed at τ_0, after intentionally perturbing one element of the parameters vector. Accordingly, results are independent of the guidance strategy.

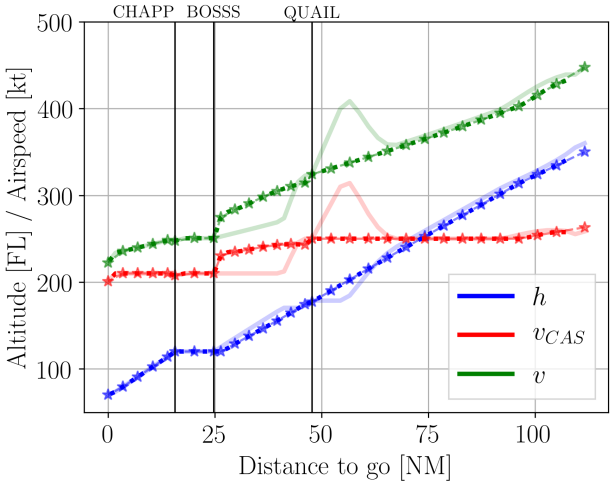

(a) $\delta\vec{X} = [0, 0, -1000\,\text{ft}]$ at τ_0

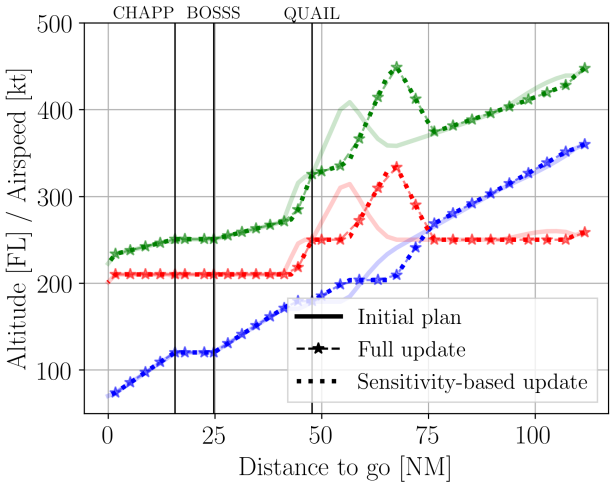

(b) $\delta\vec{c}$ (actual minus forecast of Fig. V-7) at τ_0

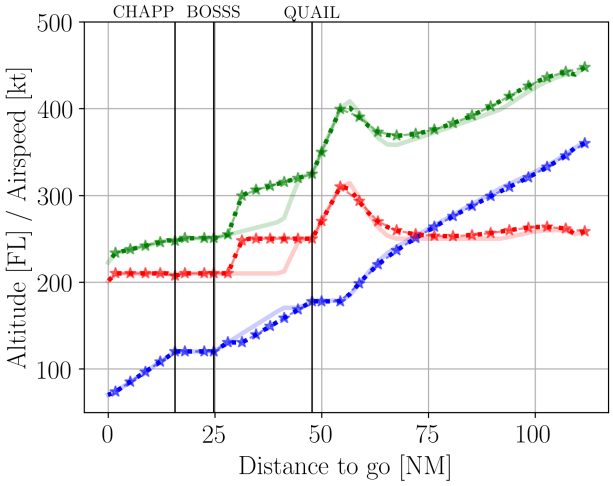

(c) $\delta\text{CTA} = -30\,\text{s}$ at τ_0

Figure V-8: *Optimal trajectory updates for perturbations in the parameters vector (2018-04-21 00:00, look-ahead time of +1 hour)*

Generally speaking, Fig. V-8 shows that the optimal trajectories resulting from sensitivity-based updates (solving $\mathcal{Q}_N$) are almost identical to those obtained from solving a rigorous NLP optimisation problem ($\mathcal{P}_N$), even for large perturbations in the elements composing the parameters vector. This conclusion is very important, and demonstrates that the trajectories updated by means of parametric sensitivities are accurate enough while reducing the execution time, provided that the perturbation in $\vec{p}$ is relatively small. In addition, it should be noted that for the three examples presented in this figure, the trajectories resulting from any of the trajectory updates reached DYMON at the enforced time and energy using only energy modulation by means of elevator control, thus requiring neither additional thrust nor speed brakes use.

According to Fig. V-8(a), when the actual altitude of the aircraft was 1,000 ft below that initially planned (lacking of energy), the energy loss rate needed to be reduced in order to satisfy the altitude and speed constraints enforced at QUAIL (see Table V-1). The most fuel efficient method to accomplish that consisted on reducing the airspeed and consequently the aerodynamic drag, which is the main cause of energy loss. Applying this strategy, the updated trajectory reached QUAIL at a feasible altitude and airspeed without using speed brakes. However, this sustained reduction in airspeed delayed the aircraft with respect to the enforced CTA. The time error was compensated by flying at a higher speed from QUAIL to BOSSS, yet releasing the same energy than initially planned by following a different energy profile.

Figure V-8(b) shows trajectory updates in case of changes in the control points of the spline approximating the wind profile, while keeping the initial CTA. This means that the aircraft needed to adjust the altitude and speed profile to comply with the initial CTA but subject to a different wind profile. According to Fig. V-7, during the first part of the descent (from FL360 to FL200) the actual tail wind was significantly heavier than that reported by the initial wind forecast. Consequently, the updated trajectory at τ_0 avoided the altitude interval from FL260 to FL200 as much as possible, where the tail wind was drastically higher than initially planned. In order to accomplish that, potential energy (altitude) was exchanged for kinetic energy (airspeed) at the maximum descent gradient using the elevator. This process was only applied down to FL200, since the extra kinetic energy would bring the aircraft to DYMON earlier than the imposed CTA. The extra kinetic energy was rapidly released by means of a level-off at idle thrust at FL200.

Finally, according to Fig. V-8(c) the optimal way to arrive 30 seconds earlier than the initially enforced CTA (which was 21 minutes and was received just at the TOD), subject to the same wind profile and for the original initial state, consisted of flying at the maximum allowed airspeed from QUAIL to BOSSS (250 kt) to gain time, and then releasing the excess of kinetic energy by executing a level-off at idle thrust just before BOSSS, in order to satisfy its associated hard altitude and speed constraints.

V.3.2 Illustrative examples: guidance strategies

Using the same RAP wind forecast and analysis as in the previous section, this section will describe the behaviour of the three NMPC guidance strategies considered in this experiment.

Figure V-9 shows the initially planned trajectory (computed at the TOD) and the executed trajectory, for the INMPC variant and for the open-loop guidance (OL) execution. For the OL execution, the optimal control of the initial plan was implemented throughout the descent, without neither monitoring state deviations nor updating the trajectory plan. Results for the remaining NMPC strategies are not shown in this figure because the differences with respect to the INMPC are difficult to appreciate at first sight. This statement agrees with the results presented in Section V.3.1, which showed little differences in the trajectories generated by solving the rigorous NLP optimisation problem and by using parametric sensitivities.

The light solid lines in Fig. V-8 and in Fig. V-9 are identical to each other, i.e., the initial trajectory plan computed at the TOD. Then, the slightly darker solid lines in Fig. V-9(b) represent the plans resulting from trajectory updates at two of the sixty time samples. These time samples, which were selected only for illustrative purposes, are τ_{10} and τ_{40}. The plans generated at the remaining time samples are not shown for the sake of clarity of the figure, even if being computed when implementing the NMPC strategies.

Before updating the trajectory plan at each time sample, the NMPC guidance system recalculated the control points of the spline that approximates the wind profile, based on the wind sensed at the current and previous altitudes. As a result, the wind profile used by the NMPC trajectory optimiser converged to the actual wind profile as wind measurements were collected by the ownship during the execution of the descent. This can be observed in Fig. V-7, which shows the initial wind profile, the wind profile at the time samples τ_{10} and τ_{40}, and the actual wind profile encountered by the aircraft during the descent.

The plan resulting from the trajectory update performed at time sample τ_{10} aimed to start an energy

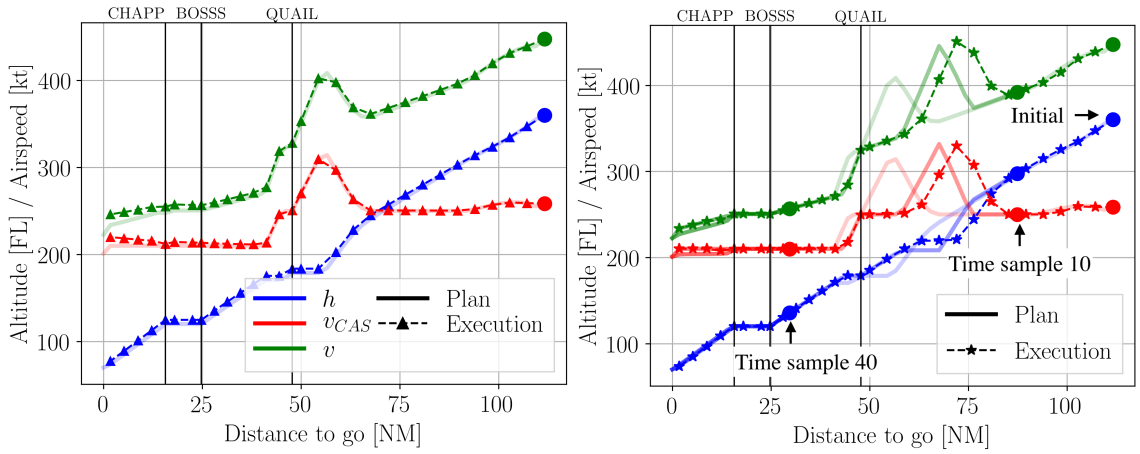

(a) Open-loop (b) INMPC

Figure V-9: *Planned and executed trajectories by guidance strategy (2018-04-21 00:00 with a look-ahead time of +1 hour)*

modulation process around FL260 to avoid the altitude interval with extreme and unexpected tail wind, given the best available wind profile estimation at that time sample (see Fig. V-7). However, according to the executed trajectory, a later trajectory update (not shown in Fig. V-9(b)) which had more accurate information of the actual wind profile requested to start exchanging potential for kinetic energy around 1,000 ft earlier. After QUAIL, the updated trajectory demanded a sightly lower speed than that of the initial plan, in order to compensate the unexpected head wind in the altitude interval FL170–7,000 ft.

It should be noted that, using NMPC, the optimal control applied at each time sample was based on the best estimation of the wind profile at the current altitude. The actual wind conditions that the aircraft would encounter at lower altitudes, however, were still unknown. Even if the control applied at each time sample was optimal for the estimated wind, it was sub-optimal for the actual (unknown) wind conditions (provided, of course, that the estimation of the wind downstream was not *perfect*). This can be observed by comparing Figs. V-9(b) and V-8(b): the executed trajectory (resulting from applying the optimal control for the best estimated wind profile at each time sample), and the trajectory update computed at the TOD with accurate information of the actual wind for the entire descent, are similar yet not identical.

For the wind forecast error of this illustrative example, the open-loop trajectory arrived at DYMON 27 seconds earlier than the CTA and 600 ft above the enforced specific energy level. For any of the NMPC strategies investigated in this chapter, the aircraft arrived at DYMON with negligible time and specific energy error, while simultaneously using the minimum required fuel consumption and speed brakes.

V.3.3 Aggregated results

This section presents the aggregated performance metrics for the 4,143 case studies per guidance strategy. Figure V-10 shows the time error at the metering fix (DYMON) with respect to the enforced CTA for the INMPC, AsNMPC and SbNMPC guidance strategies. The time error that would be achieved by applying the optimal control resulting from the initial trajectory plan in open-loop is also shown in Fig. V-10(d). Analogously, Fig. V-11 shows the specific energy (E_s)[4] error at DYMON. This kind of plots visualise the distribution of the data. The red horizontal line represents the average value, the central black horizontal line represents the median value, and the whiskers extend out to the minimum and maximum values.

According to Fig. V-10, the more the look-ahead time of the wind forecast, the more time error (in absolute value) is observed, independently of the guidance strategy. The maximum time error at the metering fix (115 s) was realised when executing a trajectory plan computed with a wind forecast of +6 h in open-loop (note that the scale of Fig. V-10(d) is different from the other subfigures). The median time error at the metering fix when considering a wind forecast of +6 h is around 15 s for the open-loop execution. For

[4]The specific energy is defined as the total energy of the aircraft divided by the aircraft weight. By definition, the units of the specific energy are ft.

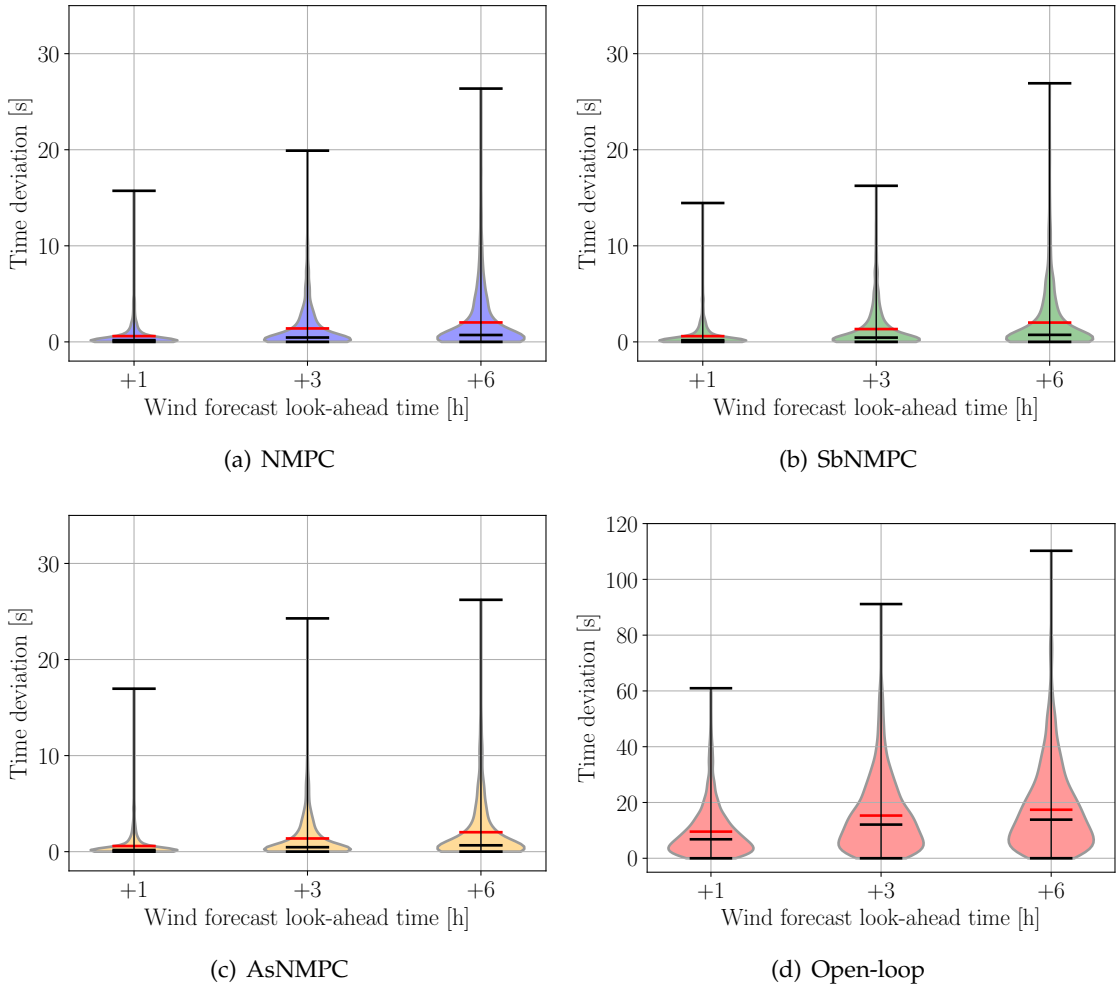

(a) NMPC (b) SbNMPC

(c) AsNMPC (d) Open-loop

Figure V-10: *Time deviation at the metering fix for different NMPC variants*

a wind forecast of +1 h, this value is reduced to 8 s. For the set of descents simulated with a wind forecast of +6 h, the distribution of time errors is concentrated in the range 0-60 s. When using strategies build on NMPC concepts, the time error is drastically reduced if compared to the open-loop execution of the initial trajectory plan. In particular, for all case studies analysed herein (one year of descent operations at DEN using the BOSSS TWO procedure) the time error is always lower than 27 s. The median time error for any of the NMPC guidance strategies is lower than 2 s for the set of descents simulated with a wind forecast of +6 h. In addition, the distribution of time errors is always concentrated below 10 s.

Similar results can be observed for the specific energy error. According to Fig. V-11(d), the metering fix could be achieved with specific energy errors up to 1,800 ft by implementing the control of the initial trajectory plan computed at the TOD in open-loop. Conversely, guidance strategies build on NMPC concepts achieve the metering fix with negligible specific energy error, always lower than 150 ft and with a median value around 10 ft for a wind forecast of +6 h. In addition, the distribution of specific energy errors for the open-loop execution extends up to 1,000 ft, while for any of the NMPC strategies it extends up to 100 ft.

Figures V-10 and V-11 show that the performance of the SbNMPC and AsNMPC, in terms of energy and time errors, is equivalent to that of INMPC. Results agree with those shown in Section V.3.1, where the trajectory updates based on parametric sensitivities were similar to those obtained by solving the rigorous NLP optimisation problem, considering relatively small perturbations in the vector of NLP parameters.

In the model proposed in this chapter, the optimal control computed at each time sample could demand to modulate energy with the elevator or to add/remove energy to/from the system by means of additional thrust or speed brakes. Ideally, the NMPC optimiser will attempt to obtain an energy-neutral trajectory. In certain conditions with significant errors in the model parameters, however, energy modu-

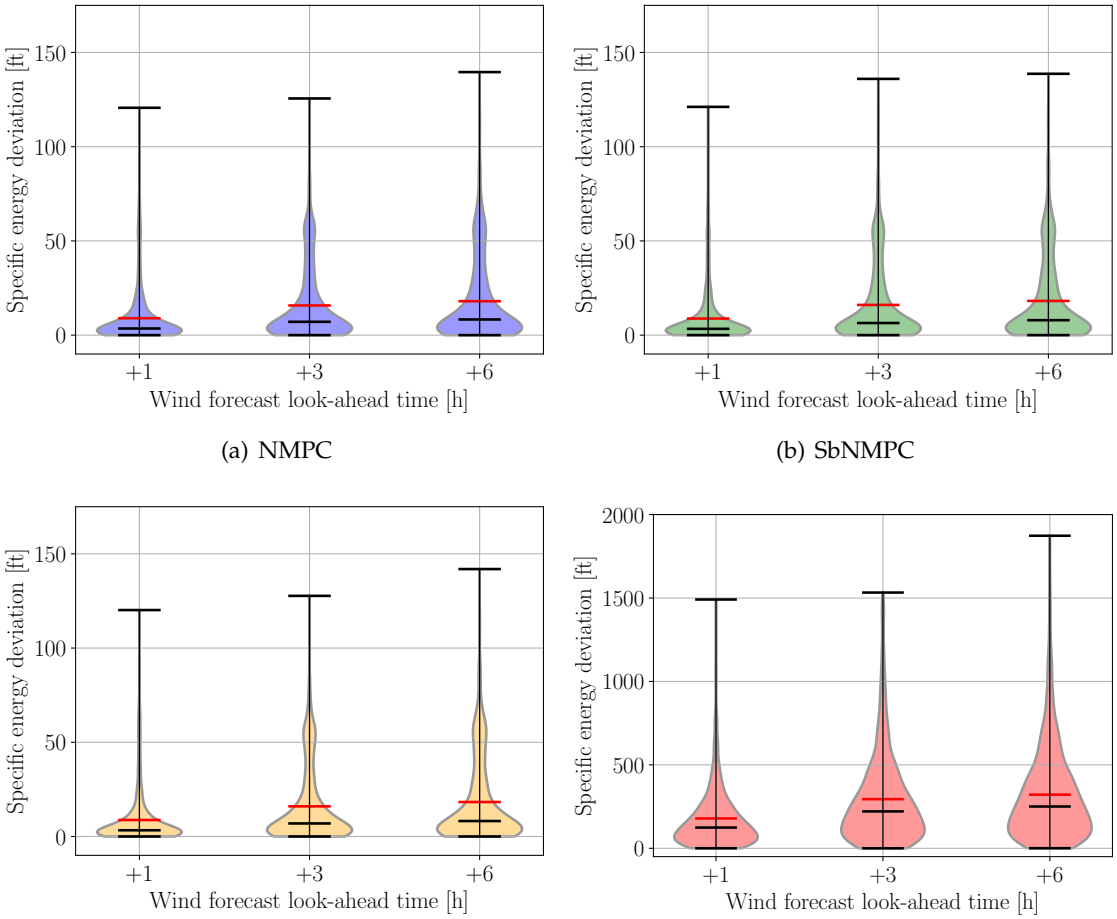

(a) NMPC (b) SbNMPC

(c) AsNMPC (d) Open-loop

Figure V-11: *Specific energy deviation at the metering fix for different NMPC variants*

lation by means of elevator control may not be sufficient to obtain a solution satisfying all the constraints. In this case, the NMPC trajectory optimiser would calculate the optimal amount of energy to be added or removed in terms of fuel consumption and use of speed brakes such that all constraints are satisfied.

Table V-2 shows the mean, maximum and standard deviation of the specific energy removed by using speed brakes. For each case study, this metric was computed as follows:

$$\Delta E_{s_\beta} = \frac{1}{2}\frac{S}{mg}\int_{t_I}^{t_F} v^3(t)\sigma(t)\rho_{SSL}C_{D\beta}\beta(t)\mathrm{d}t \tag{V.9}$$

For each guidance strategy and forecast lookahead times, the metrics shown in Table V-2 aggregate the results of the corresponding 1,381 case studies. Note that results for the open-loop execution are not shown in Table V-2 because the initial plan was always computed without speed brakes (i.e., $\beta(t) = 0$).

Table V-2: *Metrics of energy removed by using speed brakes for the different NMPC variants and wind forecast lookahead times*

Guidance strategy	Mean [ft]			Standard deviation [ft]			Maximum [ft]		
	+1 h	+3 h	+6 h	+1 h	+3 h	+6 h	+1 h	+3 h	+6 h
INMPC	2	7	13	12	34	45	187	780	641
SbNMPC	2	8	14	16	41	52	340	977	668
AsNMPC	2	8	14	11	40	55	113	914	904

According to Table V-2, and independently of the guidance strategy, the more the look-ahead time of

the wind forecast, the more the mean and standard deviation of energy removed by using speed brakes. Interestingly, the maximum value of ΔE_{s_β} corresponds to a case study with a +3 h wind forecast look-ahead time. The sensitivity of the energy removed by using speed brakes with respect to the mean longitudinal wind error encountered during the execution of the descent will be presented in Section V.3.4.

Table V-2 also shows very similar results for the three strategies based on NMPC, meaning that updating the trajectory by solving a rigorous NLP or by using parametric sensitivities would result in almost identical number of speed brakes deployments during the descent, at aggregated level. Not surprisingly, the worst figures correspond to the SbNMPC, followed by the AsNMPC. These two NMPC strategies update the trajectory plan by using an approximated method, which in some cases could be sub-optimal. The INMPC show the best results, yet the differences with the other strategies are very small.

It is also interesting to remark the significant drop in the three metrics when comparing the results for a wind forecast look-ahead time of +3 hours with those for a wind forecast look-ahead time of +1 hour. For example, for the AsNMPC the maximum specific energy removed by using speed brakes decreases from 914 ft to 113 ft, the mean value from 14 ft to 2 ft, and the standard deviation from 40 ft to 14 ft.

Analogously, Fig. V-12 shows the difference between the executed trajectory and the open-loop execution of the initial plan, in terms of specific energy added by means of thrust above idle during the descent. For each case study, this metric was computed according to the following formula:

$$\Delta E_{s_T} = \frac{1}{mg}\left(\int_{t_I}^{t_F} \left(T(t) - T_{idle}(v(t),h(t))\right)\,\mathrm{d}t\Big|_{\text{NMPC}} - \int_{t_I}^{t_F} \left(T(t) - T_{idle}(v(t),h(t))\right)\,\mathrm{d}t\Big|_{\text{OL}}\right). \tag{V.10}$$

Due to the particular altitude and speed constraints of the BOSSS TWO procedure (see Table V-1), the initial trajectory plan was not computed assuming a complete engine-idle descent, but included some segments with additional thrust above idle. For instance, additional thrust was typically required in the 2nd phase, in order to keep the speed within the allowed bounds while flying at constant altitude.

Note that, since the wind encountered during the execution was different from that used to generate the trajectory plan, the aircraft may deviate from the altitude and speed plan. Accordingly, the idle thrust for the actual flight conditions (which depends on the altitude and speed) may be different from that of the initial plan at the same time sample. In other words, altitude and speed deviations may lead to an actual T_{idle} different from that assumed in the plan. It is also important to remark that, during the execution of the descent, the thrust of the aircraft was not allowed to be lower than T_{idle} for the actual flight conditions:

$$T(t)\Big|_{\text{actual}} = \begin{cases} T(t)\Big|_{\text{plan}} & \text{if } T(t)\Big|_{\text{plan}} \geq T_{idle}(v(t),h(t))\Big|_{\text{actual}} \\ T_{idle}(v(t),h(t))\Big|_{\text{actual}} & \text{otherwhise.} \end{cases} \tag{V.11}$$

Results shown in Fig. V-12(a) demonstrate that, in most of the case studies, the specific energy added to the aircraft by means of thrust when implementing any NMPC variant is identical to that of the open-loop execution (since the median and mean values are close to zero). In addition, even if the maximum value for each combination of guidance strategy and wind forecast look-ahead time is higher than the minim value (in absolute terms), the main distribution is almost symmetric, meaning that the NMPC guidance strategies have similar chances to demand additional specific energy than to remove it by reducing the thrust, if compared to the open-loop execution. These results indicate that the NMPC strategies could take advantage of the reiterated re-planning of the trajectory plan, based on the actual state of the aircraft and a continuously improving estimation of the parameters that describe the model, to execute the descent with the same thrust than initially planned. Taking into consideration the results shown in Figs. V-10 and V-11, it can be concluded the NMPC strategies are able to satisfy operational constraints and to accurately comply with the CTA without requiring extra energy, at aggregated level.

In order to further analyse this interesting conclusion, Table V-3 shows, for each NMPC variant, the percentage of case studies not requiring speed-brakes or additional thrust during the entire descent. In addition, the percentage of case studies that performed an energy-neutral trajectory while complying with the CTA are also shown (i.e., uncertainties in the execution were cancelled by energy modulation).

Not surprisingly, the higher the look-ahead time of the wind forecast, the lower the percentage of case studies not requiring use of speed brakes and/or additional thrust during the descent. An interesting result of Table V-3 is that the figures for the three NMPC variants are almost identical. Another striking result is

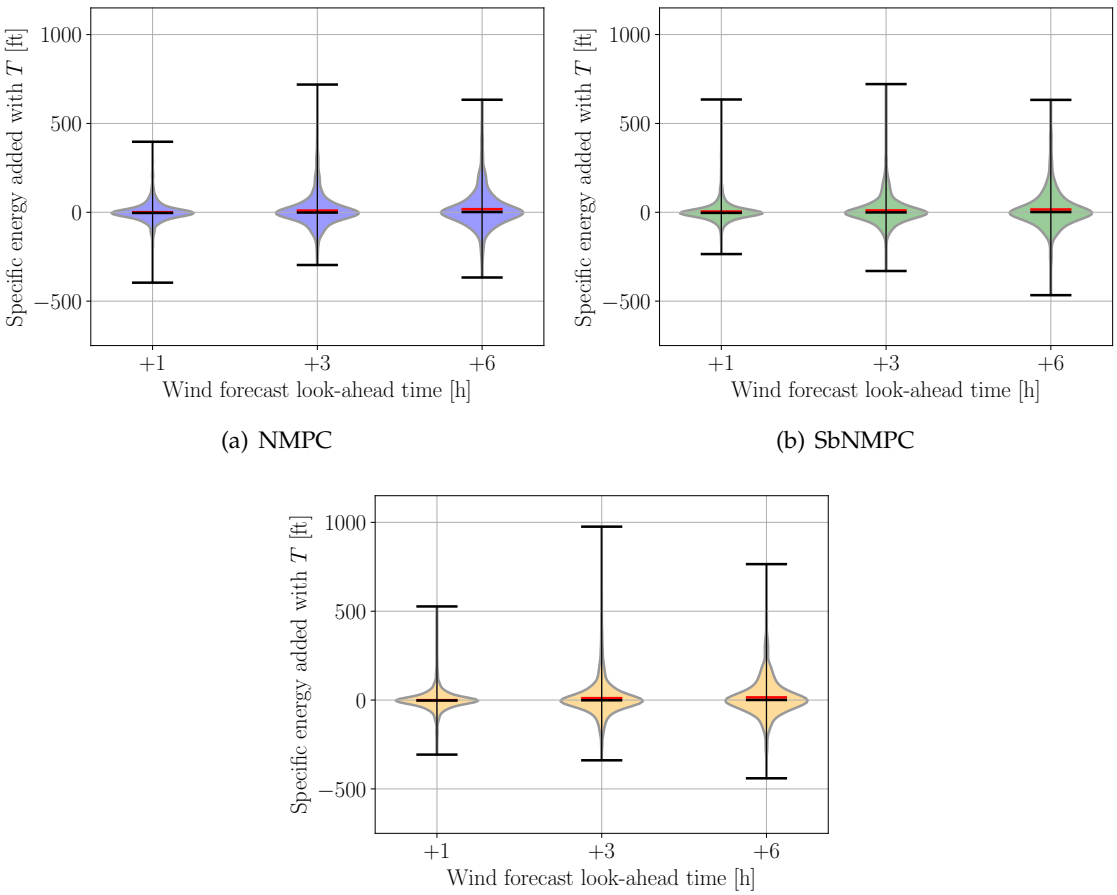

(a) NMPC

(b) SbNMPC

(c) AsNMPC

Figure V-12: *Additional specific energy difference with respect to the open-loop execution for the different NMPC variants*

Table V-3: *Percentage of energy neutral trajectories for the different NMPC variants and forecast look-ahead times*

Guidance strategy	Without speed brakes			Without additional thrust			Energy-neutral		
	+1 h	+3 h	+6 h	+1 h	+3 h	+6 h	+1 h	+3 h	+6 h
INMPC	98.3	93.7	90.0	82.1	75.6	75.5	80.6	70.3	67.0
SbNMPC	98.3	93.2	89.2	81.9	77.4	76.6	80.5	71.3	67.4
AsNMPC	98.6	93.2	89.9	82.0	76.3	76.7	80.9	70.5	68.4

that, even for look-ahead times of +6 h, around 70% of the descents could be performed without requiring neither additional thrust nor speed-brakes use during a whole year of operations at DEN airport following the BOSSS TWO procedure, provided that the sequencing and merging tasks were performed by means of CTAs and without any kind of tactical intervention (e.g., vectoring) from ATC after the TOD.

Finally, Fig. V-13 shows the fuel consumption difference with respect to the open-loop execution for the different NMPC variants. Negative values indicate fuel savings, positive values extra fuel.

Results shown in Fig. V-13 agree with those of Fig. V-12: the more the additional specific energy if compared to the open-loop execution, the more the extra fuel consumption. Interestingly, Fig. V-13 shows that using NMPC guidance strategies the fuel burned during the execution of the descent is typically the same than that burned by implementing the initial trajectory plan in open-loop (the median and mean values are close to zero). In addition, the distribution of fuel consumption difference is almost symmetrical, meaning that the NMPC strategies have similar chances to burn more fuel than to save it, if compared to the open-loop execution. The maximum extra fuel for each combination of guidance strategy and look-ahead

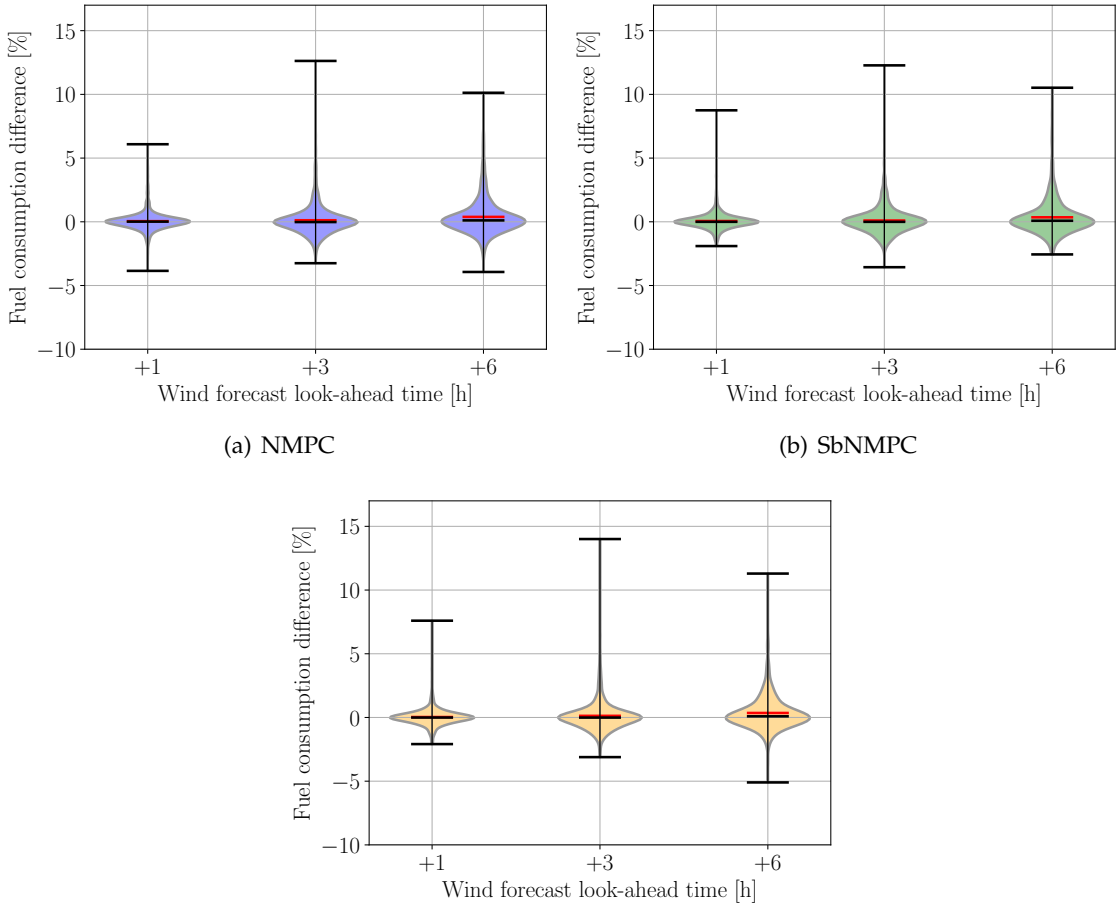

(a) NMPC

(b) SbNMPC

(c) AsNMPC

Figure V-13: *Fuel consumption difference with respect to the open-loop execution for the different NMPC variants*

time of the wind forecast, however, is considerable larger than the corresponding maximum fuel saving. However, the maximum value was observed for a very particular scenario (out of 4,131 case studies) with severe differences between the initial wind forecast and the actual wind. In fact, the distribution of fuel consumption differences is concentrated in the range $[-5\%, 5\%]$. Taking into account that these results include simulations for one year of wind forecasts at DEN, it can be concluded that the dispersion of fuel consumption differences is relatively small, independently of the NMPC variant.

The open-loop execution implements the control plan that is optimal only for the initial wind forecast assumed at the TOD. In contrast, NMPC strategies could take advantage of the frequent update of the optimal trajectory plan based on a continuously improving wind forecast to save fuel. Again, taking into consideration the results shown in Figs. V-10 and V-11, it can be concluded the NMPC strategies assessed herein are able to satisfy altitude and speed constraints as well as to accurately comply with the enforced CTA without requiring additional fuel consumption, at aggregated level.

Based on the results shown in this section, it can be also concluded that the three NMPC guidance strategies assessed in this PhD thesis show very similar performance at aggregated level, even if the method used to update the optimal trajectory plan is sightly different. Recall that the INMPC solves a rigorous NLP optimisation problem at each time sample; the SbNMPC solves a quadratic programming (QP) optimisation problem to update the optimal trajectory plan; and the AsNMPC updates the trajectory in advance by solving a rigorous NLPoptimisation problem (as the INMPC) and then corrects for potential prediction errors by solving a QP optimisation problem (as the SbNMPC). Figure V-14 shows the normalised distribution of execution times for the two optimisation methods, extracted from the whole set of simulations.

According to Fig. V-14, the maximum execution time for the QP algorithm is one order of magnitude

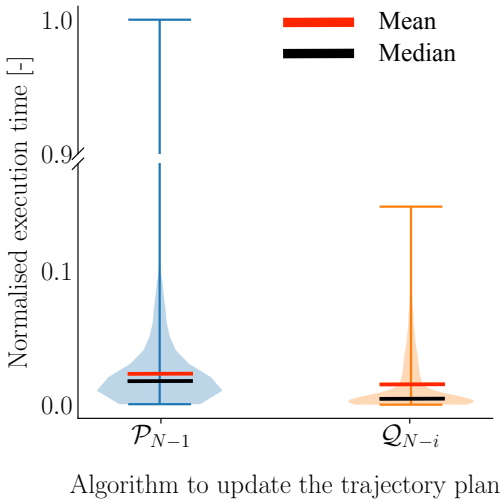

Figure V-14: *Normalised execution time for the NLP and QP algorithms. 1 corresponds to the maximum execution time for all trajectory updates of all simulations, which was 10 seconds*

below that for the NLP algorithm. In addition, the mean and median execution times for the QP algorithm are approximately half of those for the NLP algorithm. The most important conclusion arising from Fig. V-14, however, is that the dispersion of execution times for the QP algorithm is much lower than for the NLP algorithm, thus demonstrating the additional robustness of the QP algorithm.

V.3.4 Sensitivity to the wind error

Previous section assessed the performance of various NMPC guidance strategies in presence of errors in the wind profile forecast, and compared the results with those obtained by executing the initial trajectory plan in open-loop. The time and energy deviations induced by errors in the longitudinal component of the wind are significantly higher than those caused by errors in the cross and vertical components. For this reason, Figs. V-15 to V-17 only show the correlation between the different metrics of the performance assessment and the mean longitudinal wind error. The mean longitudinal wind error for each case study was computed by averaging the longitudinal wind error of all time samples. Positive values indicate more tail wind than initially expected, negative values manifest a stronger head wind if compared to the forecast. Each data point in these figures corresponds to a particular case study. In order to keep this figure simple, only the results for the open-loop execution and the INMPC are shown. Yet, it should be noted that results for the remaining strategies are very similar to those of the INMPC, as shown in previous sections.

According to Fig. V-15(a), when executing the initial trajectory plan in open-loop, the time error at the metering fix shows a strong and negative correlation with the mean longitudinal wind error, i.e., the stronger the unexpected head wind, the later the aircraft will arrive with respect to the CTA. Analogously, the specific energy error at the metering fix (see Fig. V-15(b)) presents a strong, positive correlation with the mean longitudinal error, meaning that the stronger the unexpected head wind, the lower the energy of the aircraft will be when arriving at the metering fix.

For any of the NMPC strategies, the time error appears to be weakly correlated with the mean longitudinal wind error; and the specific energy error is not correlated at all. The differences in the correlation patterns for the OL and NMPC guidance strategies are caused by the corrective actions performed by the later, which repeatedly generates the *best* optimal trajectory plan to satisfy the terminal constraints at the metering fix while simultaneously minimising the fuel consumption and speed brakes usage.

Regarding the extra energy removed by using speed-brakes (see Fig. V-16(b)), it can be observed that for the open-loop execution speed brakes are never used (because the initial trajectory plan is always computed without extra drag). Generally speaking, for the NMPC guidance strategies the stronger the unexpected head wind, the more energy is removed. There exist some particular case studies in which energy is removed for negative mean longitudinal wind error. Even if the mean longitudinal wind error is negative for these case studies, in some regions of the descent more head wind than expected is encountered, which requires the use of speed brakes to satisfy all the constraints.

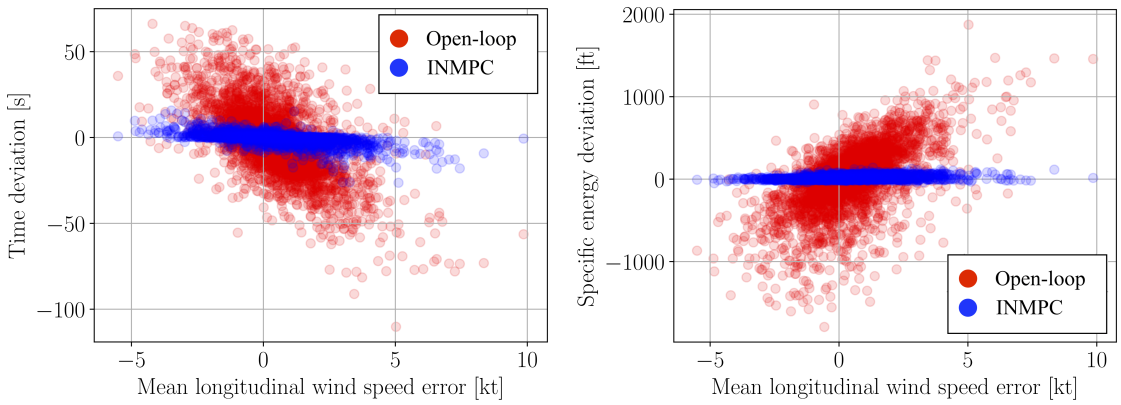

(a) Time error (b) Specific energy error

Figure V-15: *Time and specific energy error at the metering fix as a function of the mean longitudinal wind error*

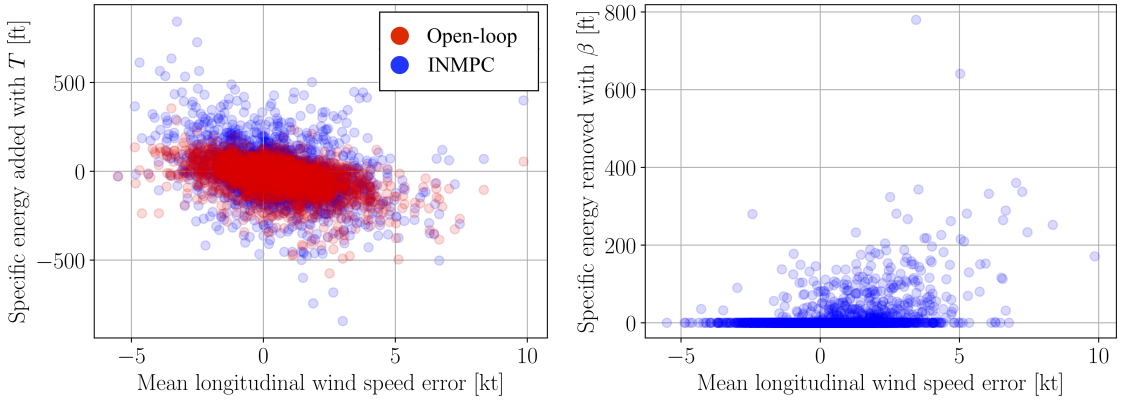

(a) Added by means of T (b) Removed by means of β

Figure V-16: *Specific energy added/removed with respect to the initial plan as a function of the mean longitudinal wind error for the INMPC and OL*

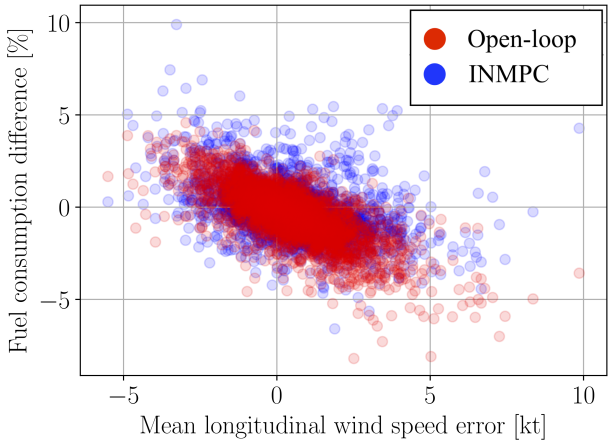

Figure V-17: *Fuel consumption difference with respect to initial plan as a function of the mean longitudinal wind error*

Finally, according to Figs. V-16(a) and V-17 the specific energy difference due to thrust and the fuel consumption difference show very similar patterns. Both performance metrics present a negative correlation with the mean longitudinal wind error, meaning that the stronger the unexpected tail wind, the less thrust and fuel consumption will be required if compared to the initial trajectory plan computed at the TOD. Remember that for the open-loop execution, the differences in fuel consumption and energy added by means of thrust are only caused by altitude and speed deviations from the initial plan (changing therefore the value of the idle thrust). Conversely, for the NMPC guidance strategies, these differences are also caused by trajectory updates that might modify the states and controls plans. For this reason, results for the NMPC strategies show more dispersion than for the open-loop execution.

V.4 Discussion

This chapter described the application of two additional NMPC guidance strategy that use parametric sensitivities to update the optimal trajectory during the descent of an aircraft subject to time constraints.

Results showed that trajectory updates resulting from solving a rigorous NLP optimisation problem are very similar to those obtained by using parametric sensitivities. Yet, the later method to update the optimal trajectory is simpler, faster and more robust in terms of dispersion of execution times and convergence. Accordingly, a guidance strategy that updates the optimal trajectory at each time sample by using parametric sensitivities, called SbNMPC, showed equivalent performance (in terms of fuel consumption, extra thrust, speed brakes use and extra fuel consumption) to the INMPC, which instantaneously updates the optimal trajectory at each time sample by solving a rigorous NLP optimisation problem. A third NMPC variant, which combines an early re-calculation of the optimal trajectory with a sensitivity-based update, also showed similar performance to the INMPC. These results encourage the use of the later strategy.

If compared with the generic NMPC, which solves a rigorous NLP optimisation problem right after measuring the actual state and parameters of the model, the AsNMPC has the advantage of not being affected by computational delay. This is only true, however, if the optimal trajectory plan can be computed in background before reaching the next time sample. Recall that the overall performance, capability to meet constraints and stability of the generic NMPC deteriorate as the execution time increases.

Moreover, if compared to the SbNMPC, the AsNMPC is less affected by large perturbations in the vector of parameters, since the sensitivity-based update is not performed over an approximated trajectory plan but over a very accurate trajectory plan generated recently by solving a rigorous NLP optimisation problem. Any trajectory obtained by using parametric sensitivities is just an approximation to the actual optimal trajectory, and therefore includes some approximation error, which obviously increases with the magnitude of the perturbation. This error would be propagated over time if only sensitivity-based updates were performed (as in the case of the SbNMPC). The rigorous NLP optimisation problem solved by the AsNMPC at each time sample, based on the predicted state and parameters of the model at the next one, acts as a mechanisms to ”reset” these approximation errors. Moreover, since the predictions errors in the state and parameters of the model are expected to be relatively small, provided that the time interval between consecutive time samples is sufficiently small, the subsequent sensitivity-based approximation when measuring the actual state and parameters of the model is expected to be very fast and accurate.

In addition, results showed that using any of the NMPC guidance strategies, energy modulation through elevator control typically suffices to compensate time and energy deviations at the metering fix caused by errors in the wind forecast. In particular, around 70% of the descents at DEN following the BOSSS TWO procedure were able to perform an energy-neutral trajectory for a wind forecast look-ahead time of +6 hours. However, in some circumstances with significant errors in the wind forecast, these guidance strategies could demand to add or remove energy by means of thrust or speed brakes, respectively, to satisfy operational constraints. In this case, the trajectory planner would compute the optimal energy to be added or removed which, at each time sample, minimises the fuel consumption and speed brakes usage while simultaneously satisfying the constraints. In this context, promising results showed that NMPC guidance strategies can accurately comply with CTAs and other operational constraints in presence of significant wind prediction errors at no extra fuel consumption (considering the aggregated results of around 16,000 simulations).

Most common languages used in aviation safety critical systems are *C*, *C++* and *Ada*. In the experiment of this chapter, and taking into account that the developed system was just a prototype, the formulation of

the optimal control problem (i.e., definition of constraints and cost function of the trajectory optimisation problem) was performed in Python, but the resulting NLP optimisation problem was solved by using off-the-shell NLP solvers. Many of these solvers are written in C and could be technically integrated into the avionics systems. Regarding the hardware, modern FMSs provide significant improvements to already highly reliable computers, as well as increased processing power and memory. The computational demand of the proposed algorithm is not extremely high, yet the feasibility of running it using current on-board resources deserves a more comprehensive study.

What drives value in avionics, however, is compliance to mandates, reliability and safety. On-board trajectory planning and guidance algorithms must be simple for the pilot to be easily understood, as well as robust enough to have hundreds of lives depend on them. Accordingly, new features being added into conventional FMSs typically require few extra computational resources, and there is little incentive for the the latest programming paradigms or innovatory technology.

Because the NMPC guidance algorithm uses a NLP solver for the trajectory optimisation process, this trajectory management system can be characterised as an *adaptive system with nondeterministic feature*, which conflicts with current civil aviation certification processes. In particular, NLP solvers lack from determinism and cannot guarantee to always find a solution. In addition, the execution time has a lot of variance and in some unpredictable situations could be unacceptably high. Accordingly, in order to implement any NMPC variant in a real FMS, even if having enough hardware capabilities, operational and certification issues will need to be tackled.

Life can only be understood backwards; but it must be lived forwards.

— Soren Kierkegaard

Prediction is very difficult, especially about the future.

— Niels Bohr

VI

Wind-networking to improve time predictability and fuel efficiency of descents

Several studies investigated the effect of errors in the wind forecast on the performance of continuous descent operation (CDO) subject to controlled time of arrival (CTA), see for instance the excellent works of Klooster *et al.* (2008) and Bronsvoort *et al.* (2011). A common and interesting conclusion of these works was that an accurate knowledge of the actual wind conditions is of utmost importance to accurately comply with CTAs. Supporting this statement, results from flight tests at Denver International Airport (DEN) using conventional wind forecasts indicated that errors in the wind forecast accounted for approximately two-thirds of the mean time error at the metering fix, and nearly all of the standard deviation (Green *et al.*, 2000). Results from flight trials reported by Prats *et al.* (2017) also showed the benefits of using a high-quality wind forecast during the trajectory planing process of time and energy managed operations. However, according to Glina *et al.* (2012), the primary driver of accurate CTA compliance is not only the quality of the wind forecast provided to the flight management system (FMS) to generate the initial trajectory plan, but also the guidance strategy used to follow the plan (or re-plan).

In Chapter V, the nonlinear model predictive control (NMPC) guidance strategy was enhanced to enable the calculation of the trajectory plan using a wind profile based on the original forecast but progressively updated based on the ownship sensed winds. However, that only corrects the wind profile for current and previous positions, not *downstream* positions, that is, from current position to destination. The short coming of using ownship sensed winds is that any time deviation due to an incorrect wind forecast at a downstream waypoint requires a higher and higher change to the aircraft airspeed as the distance to that point becomes shorter and shorter (Glina *et al.*, 2012). Using wind observations from aircraft that have recently crossed downstream fixes at an altitude similar to that planned by the ownship is expected to improve the accuracy of the trajectory prediction that is essential to meeting any constraints and CTAs.

In this chapter, the NMPC guidance strategy is implemented to guide aircraft during CDOs subject to CTAs, and uses the concept of accessing data available in a hypothetical wind networked environment to generate accurate and up-to-date wind predictions on-board and in real-time. Several case studies with mismatches between the wind forecast and the actual wind conditions are simulated at DEN. Results from

simulations are used to assess the benefits of this strategy based on optimisation and estimation techniques, in terms of fuel consumption and time and energy deviations at the metering fix. The sensitivity of the performance metrics to the cadence of wind observations received from nearby aircraft is also investigated.

VI.1 State of the art

Several works already proposed to use wind observations derived from surveillance data to provide enhanced wind predictions for the air traffic management (ATM) community. Most wind estimation methods found in the literature rely on the fact that the wind vector is the difference between the ground speed and the true airspeed (TAS) vectors. For instance, early in the 1980s Hollister *et al.* (1986) was the first to propose a method to estimate the wind vector from ground-based (radar) surveillance observations. The ground speed vectors for every scan of each aircraft track were obtained by taking the difference between the sequential radar positions of aircraft and then dividing by the scan interval. Then, the ground speed vectors from multiple aircraft were used to infer the wind vector by means of Bayesian estimation techniques, assuming constant wind speed and aircraft airspeed during turning manoeuvres. An extension of this algorithm was investigated by Delahaye & Puechmorel (2009).

Aircraft equipped with automatic dependent surveillance-broadcast (ADS-B) autonomously transmit surveillance data including not only aircraft position but also ground speed vector. The wide availability of ADS-B receivers at a relatively low cost and the growing amount of aircraft equipped with this system make ADS-B an attractive source of data for many ATM applications. For instance, De Leege *et al.* (2013) proposed a method to estimate the wind vector from ground speed vector observations. In this case, however, the ground speed vector was directly obtained from the ADS-B surveillance messages. The method was based on a modified extended Kalman filter that estimates the wind recursively from an aircraft in a turn. In addition, a new method to estimate wind using data from multiple aircraft was also proposed.

Mode-S messages emitted by the aircraft surveillance system as a response to a secondary surveillance radar interrogation include information about the ground speed and TAS vectors, from which the wind vector can be easily inferred. The use of Mode-S data for wind networking applications was investigated by Hrastovec & Solina (2013). Recently, Dalmau *et al.* (2017) applied geostatistical techniques to generate a four-dimensional wind model for the terminal maneouvering area (TMA), whilst Sun *et al.* (2017) investigated a novel and relatively fast gas particle model that estimates the wind field in real-time from standard ADS-B and Mode-S messages.

Another work by In 't Veld (2011) proposed a wind prediction algorithm that uses observations broadcast by nearby aircraft to reconstruct, on-board and in real-time, the actual wind profile along the descent route. De Jong *et al.* (2015) used a similar algorithm to update the wind profile before re-planning the trajectory during the descent using guidance strategies based on the time and energy managed operations (TEMO) concept. Other studies investigating aircraft spacing during interval management operations showed that the use of wind predictions generated from observations emitted by nearby aircraft within a *wind networking* concept could reduce the spacing time error if compared with using outdated wind information (Bussink *et al.*, 2012).

Summing up, in a wind networking concept accurate wind data will be available in the FMS as each aircraft equipped with ADS-B and Mode-S will be transmitting information from which the wind vector could be derived, thus acting as a set of airborne wind sensors. Essentially, each aircraft that has completed the descent will have broadcast the complete wind profile, which could be used by nearby aircraft to enhance the wind model and, consequently, the trajectory plan of the ownship.

VI.2 Setup of the experiment

The scenario, models, and formulation of the optimal control problem for the experiment performed in this chapter were identical to those of Chapter V. Furthermore, the same 4,143 case studies presented in Section V.2.4 were selected to assess the benefits of wind networking concepts on the performance of NMPC guidance strategies for CDOs subject to CTAs.

Results from Chapter V showed that the performance of sensitivity-based NMPC strategies are similar

to those of the conventional NMPC, being the former simpler, faster and more robust. Accordingly, results will be shown only for the ideal NMPC (INMPC), yet having in mind that results for the sensitivity-based NMPC (SbNMPC) and advanced-step NMPC (AsNMPC) strategies will be very similar.

In Chapter V, at each time sample, the wind measured by the sensors of the aircraft at the current altitude was appended to the set of available wind observations ($\mathcal{O}$) to re-compute the control points ($\vec{c}$) of the spline approximating the wind profile, right before updating the trajectory by either solving a rigorous nonlinear programming (NLP) optimisation problem or using parametric sensitivities. Here, at each time sample, wind observations emitted by nearby aircraft during the last time interval were also appended to the set of available observations, in addition to ownship wind measurements. The number of wind observations emitted by nearby aircraft during a time interval was modelled as a Poisson probability distribution:

$$p\left(x \mid \mu\right) = \frac{\mu^x}{x!} e^{-\mu}, \tag{VI.1}$$

where μ is a parameter describing the average number of occurrences (here the received wind observations) between two consecutive time samples. Equation (VI.1) expresses the probability of x events occurring in a fixed time interval when the events occur with a known constant rate and independently of the time since the last event. The probability of having x occurrences is shown in Fig. VI-1 for different values of μ. In this chapter, three values of μ were investigated for each one of the 4,143 case studies: 0.0, 0.5 and 1.0. Note that for $\mu = 0.0$ only ownship wind observations are used to update the control points of the spline, since $p\left(x|0\right) = 0 \, \forall x \in \mathbb{N}$, and this essentially corresponds to the results shown in Chapter V. In addition, the reference situation in which the initial wind profile forecast, obtained from rapid refresh (RAP), is never updated during the descent (neither with ownship observations nor wind information broadcast from other aircraft) was also assessed.

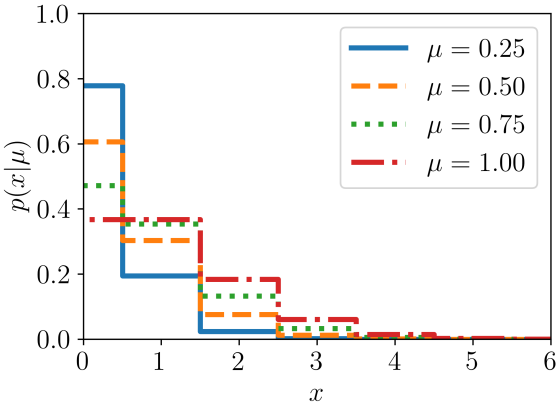

Figure VI-1: *Poisson distribution*

VI.2.1 Workflow of a simulation

The workflow of a simulation was identical to that described in Section V.2.5, with the only difference that, at each time sample, both the wind measured by the ownship sensors at the current altitude and the wind observations received during the last time interval from nearby aircraft were appended to $\mathcal{O}$. Then, the control points of the spline approximating the wind profile were updated by solving Eq. (V.7).

Algorithm VI.1 outlines the steps performed to update $\vec{c}$ at each time sample. First, the wind sensed by the ownship at h_i was appended to the set of wind observations. Then, the number of wind observations received from nearby aircraft between τ_{i-1} and τ_i ($n_{\mathcal{O}}$) was generated from the Poisson probability distribution. For each wind observation $k = 1, \ldots, n_{\mathcal{O}}$, the altitude h_k at which an hypothetical nearby ownship sensed the wind w_k was generated from a uniform distribution in the altitude interval $[0, h_i]$. Each wind observation included a measurement error ϵ_k generated from a normal distribution, which was centred at $\mu_\epsilon = 0$ with a standard deviation of $\sigma_\epsilon = 1\,\text{kt}$. The different wind observations, (h_k, w_k, τ_i) for $k = 1, \ldots, n_{\mathcal{O}}$, were progressively appended to $\mathcal{O}$. Finally, the weights of the wind observations included in $\mathcal{O}$ were updated using the forgetting factor presented in Section V.2.5 and $\vec{c}$ was updated.

Algorithm VI.1: *Update of $\vec{c}$ at each time sample*

$\epsilon_i \leftarrow \mathcal{N}\left(\mu_\epsilon,\, \sigma_\epsilon^2\right)$
$w_i \leftarrow w\left(h_i\right) + \epsilon_i$
$\mathcal{O} \leftarrow \mathcal{O} \cup \left(h_i, w_i, \tau_i\right)$
$n_{\mathcal{O}} \leftarrow \text{Pois}\left(\mu\right)$
for $k = 1, \ldots, n_{\mathcal{O}}$ **do**
    $h_k \leftarrow \mathcal{U}\left(0,\, h_i\right)$
    $\epsilon_k \leftarrow \mathcal{N}\left(\mu_\epsilon,\, \sigma_\epsilon^2\right)$
    $w_k \leftarrow w\left(h_k\right) + \epsilon_k$
    $\mathcal{O} \leftarrow \mathcal{O} \cup \left(h_k, w_k, \tau_i\right)$
Update weights of $\mathcal{O}$
$\vec{c} \leftarrow$ solve Eq. (V.7)

Right after updating $\vec{c}$, the optimal trajectory plan starting at the current state was re-calculated by solving $\mathcal{P}_{N-i}$ according to a more accurate prediction of the actual wind conditions. Note that $\mathcal{P}_{N-i}$ was solved at each time sample τ_i, with $i = 0, \ldots, N-1$. As in Chapter V, $\mathcal{P}_{N-i}$ was formulated in CasADi (Andersson *et al.*, 2018), and solved by using the sequential quadratic programming (SQP) algorithm implemented by sparse nonlinear optimiser (SNOPT) NLP solver (Gill *et al.*, 2005).

VI.3 Results

The results of the experiment described above are presented in this section. Section V.3.2 describes a particular case study for various values of μ, as illustrative example. The aggregated results for all case studies and values of μ are further discussed in Section V.3.3.

VI.3.1 Illustrative examples: wind networking benefits

The case study corresponding to the wind forecast generated the 17-09-2019 at 18:00 with a look-ahead time of +6 hours, was selected as illustrative example. Figure VI-2 shows the planned and executed trajectories, where each panel corresponds to a different rate of wind observations available to update the wind profile during the descent. The lightest solid lines in the three panels of Fig. VI-2 are identical to each other, i.e., the initially planned trajectory computed at the top of descent (TOD). Then, the slightly darker solid lines in Fig. VI-2 represent the plans resulting from trajectory updates at two of the sixty time samples. These time samples, which were selected only for illustrative purposes, are τ_{10} and τ_{40}. Data for the remaining time samples are not shown for the sake of clarity, even if being computed.

Before updating the trajectory plan at each time sample, the NMPC guidance system updates the wind profile according to Algorithm VI.1, provided that networked wind data are available. If this were the case, the forecast wind profile would converge to the actual wind profile. When networked wind data are not available, however, the forecast wind profile remains static and does not converge to the actual wind profile. This can be observed in Fig. VI-3, which shows the initial wind forecast, the wind forecast at the time samples τ_{10} and τ_{40}, and the actual wind profile, for the three values of μ considered herein.

In Fig. VI-3, the initial wind profile forecast (lightest blue line) deviates fairly substantially from the actual wind (red line) in two different portions of the CDO. From FL360 to FL220 the forecast wind profile underestimates the actual headwind (note the negative values of the x-axis), and from FL200 to the surface it overestimates the actual headwind. Therefore, when analysing the error in the forecast wind profile shown in Fig. VI-3, the expectation would be an aircraft would have to increase its airspeed from FL360 to FL220 and decrease its airspeed below FL200 from the initial calculated trajectory. A closer examination of Fig. VI-2 reveals this does in fact happened. In Fig. VI-2(b) for $\mu = 0.5$, the ground speed of the aircraft increased around 15 NM before QUAIL and decreased afterwards, if compared to the initial plan, in order to satisfy the operational constraints enforced at the waypoints of the route. In Fig. VI-2(c) for $\mu = 1.0$, the speed up was performed much earlier (around 25 NM before QUAIL) since a better knowledge of the actual wind conditions downstream was available well in advance (see Figs. VI-3(b) and VI-3(c), respectively). In

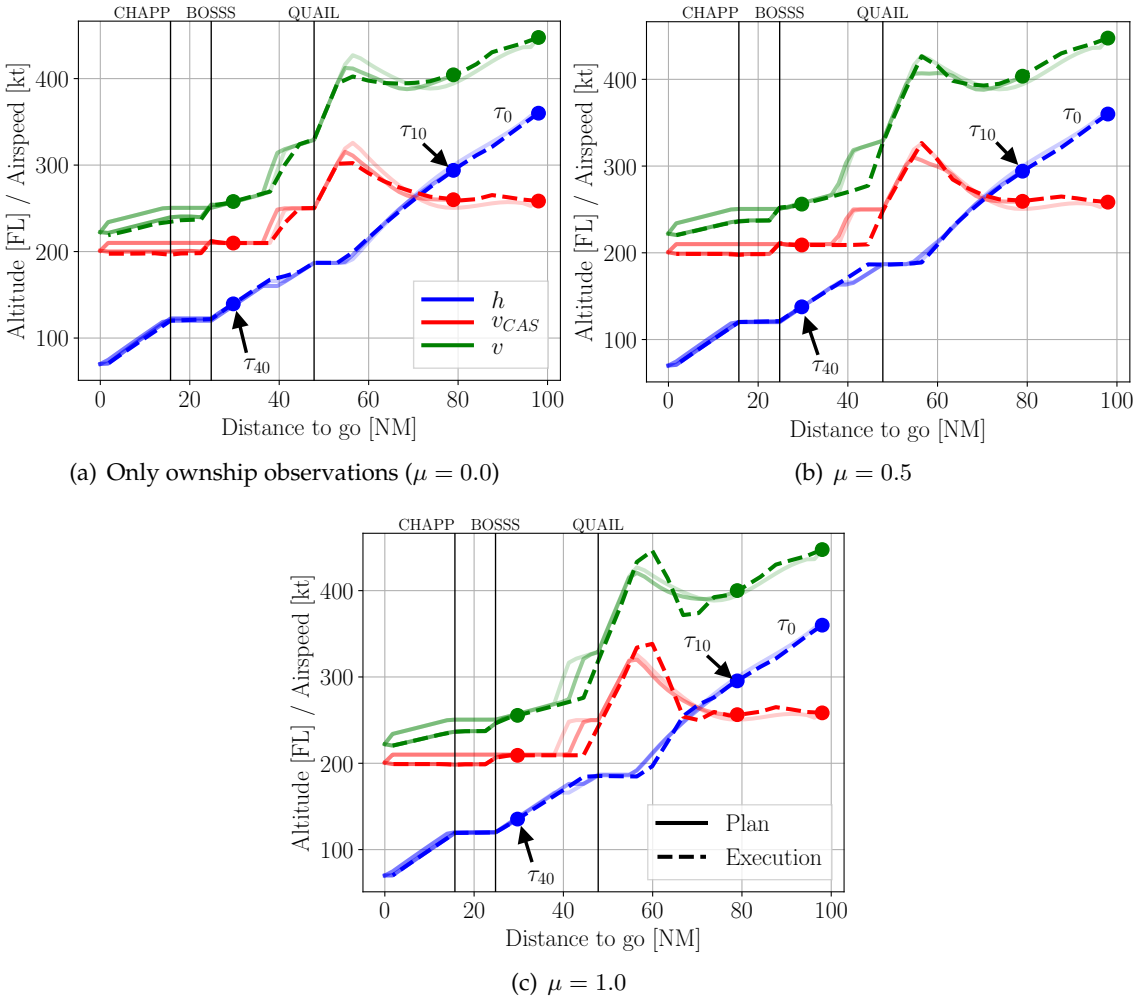

(a) Only ownship observations ($\mu = 0.0$)

(b) $\mu = 0.5$

(c) $\mu = 1.0$

Figure VI-2: *Planned and executed trajectories (17-09-2019 at 18:00 for a look-ahead time of +6 hours)*

all cases, after QUAIL the updated trajectory plan required the aircraft to slow its calibrated airspeed to compensate for the weaker than expected head wind from the initial wind forecast.

Figure VI-3(a) shows that, when only own measurements are used to update the wind forecast, any error in the forecast will not be corrected at downstream waypoints. On the other hand, when wind observations from other aircraft are considered in the estimation of the wind profile, up-to-date wind data in the whole range of altitudes may be accessible. As expected, the wind forecast converges earlier to the actual wind profile as the average number of wind observations received per time interval (μ) increases.

For this particular case study, the time error resulting from executing the optimal control of the initial plan in open-loop (i.e., neither nullifying state deviations nor updating the optimal descent trajectory) was 76 s. When implementing the NMPC guidance strategy, independently of the mechanism selected to manage the wind profile forecast, the time error was reduced to values below 30 s. Using a static wind profile, the time error was 27 s. As expected, the smallest time error (10 s) was achieved for $\mu = 1.0$.

In terms of specific energy error at the metering fix, the deviation with respect to the initial trajectory plan for the open-loop execution was around 1,250 ft. For the NMPC strategy the specific energy error was negligible, being lower than 50 ft independently of the mechanism selected to manage the wind profile forecast during the execution of the descent. Again, the best result was achieved with $\mu = 1.0$.

As a final remark, when a fully wind networked concept concept is implemented (Fig. VI-2(c) with $\mu = 1.0$), the executed trajectory is changed sooner and more profoundly than when less or no updated wind information is available as shown by the larger difference between the light blue and dark red lines.

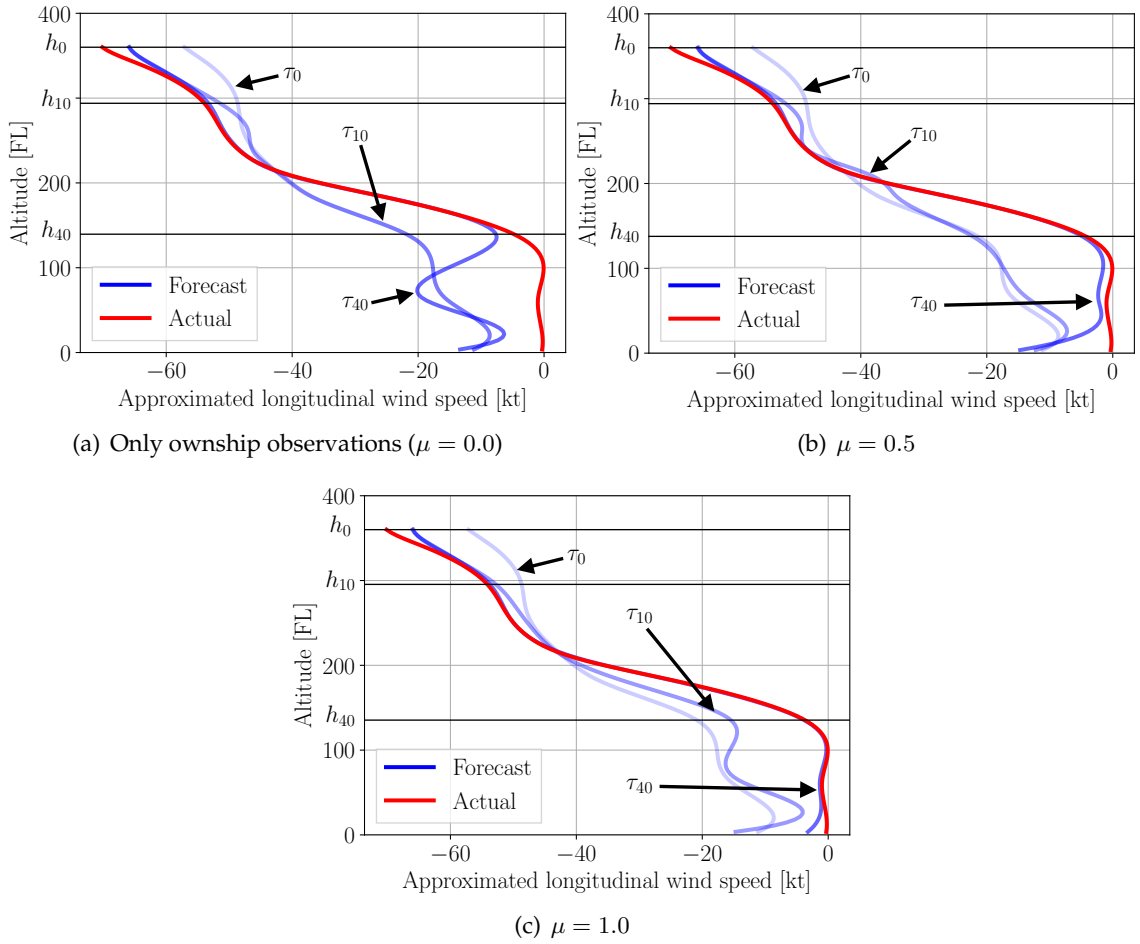

(a) Only ownship observations ($\mu = 0.0$)

(b) $\mu = 0.5$

(c) $\mu = 1.0$

Figure VI-3: *RAP wind forecast and analysis (17-09-2019 at 18:00 for a look-ahead time of +6 hours)*

VI.3.2 Aggregated results

This section presents the performance metrics for all case studies of the experiment. Figure VI-4 shows the time deviation at the metering fix (DYMON) with respect to the enforced CTA for three different values of μ and for the case in which the wind forecast is not updated, i.e., the initial wind forecast obtained from RAP keeps *static* throughout the descent. The time deviation that would result by applying the optimal control of the initial plan in open-loop was already shown in Fig. V-10(d), which could be as high as 110 seconds, with a mean and median value around 20 and 15 seconds for the *worst* forecast look-ahead time (+6 hours), respectively. When using NMPC guidance, both maximum, mean and median time error drastically reduce, independently of the mechanism adopted to update the wind profile (if any).

For instance, when using the static wind profile approach, the time error is lower than 30 seconds for all case studies, and the distribution shows that most of the time deviations are lower than 20 seconds, with a median value of 2.5 seconds and a mean value around 5 seconds for a forecast look-ahead time of +6 hours. Even if at first sight 30 seconds could seem a very large time error, it should be noted that the simulations performed in this chapter considered all the wind forecasts for +1, +3 and +6 h look-ahead time during one year of operations at DEN airport. For the simulations in which the wind forecast is updated with only ownship observations (i.e.,$\mu = 0.0$), the maximum time deviation further reduces to 25 seconds, while most of the case studies show a time deviation lower than 10 seconds. Using only ownship measurements, the time error is approximately halved with respect to that using a static wind forecast. Results show that if additional wind data emitted by aircraft in the neighbourhood were used to update the wind profile, the time error would be negligible for most case studies.

Figure VI-5 show the analogous results for the specific energy deviation at the metering fix. The specific energy deviation at the metering fix that would result by applying the optimal control of the initial plan in open-loop was already shown in Fig. V-11(d), with maximum specific energy errors up to 1,800

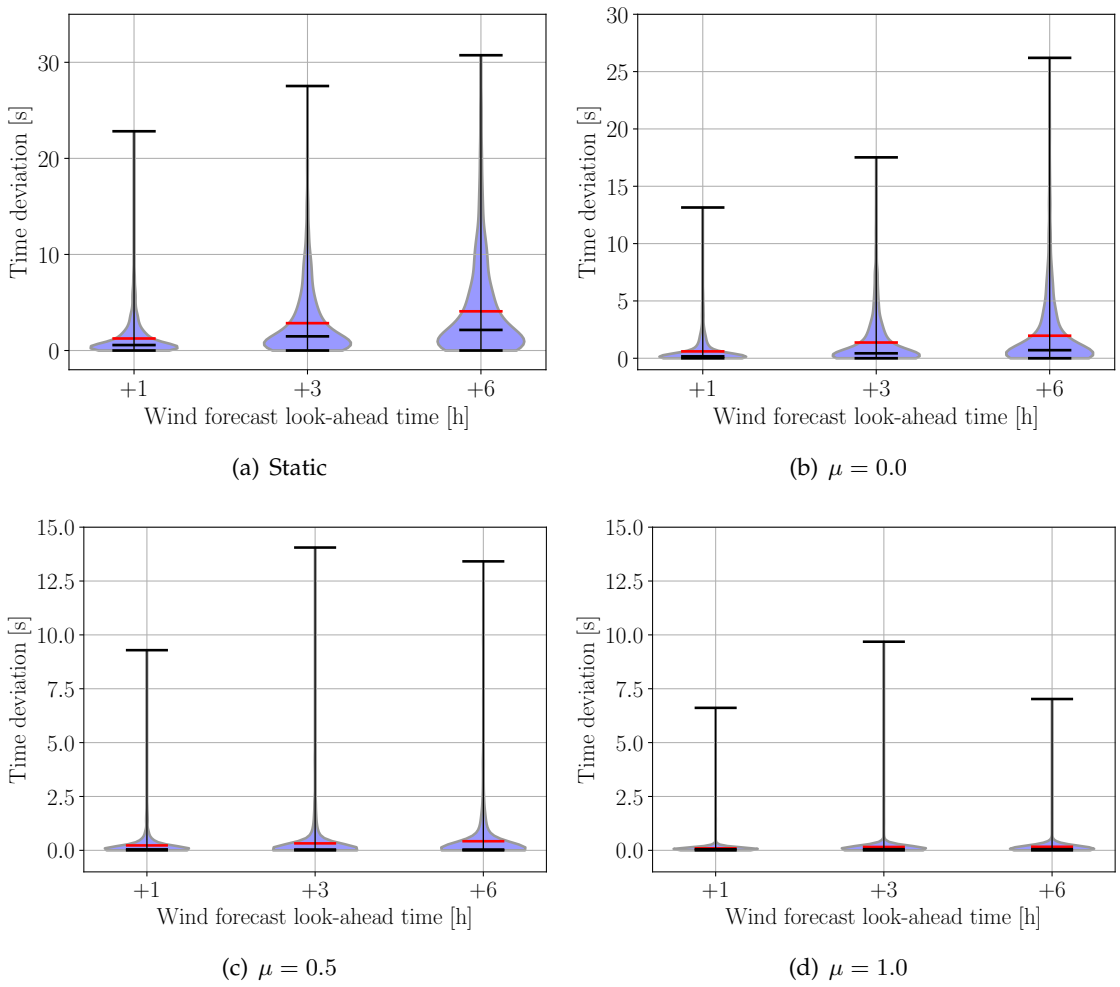

Figure VI-4: *Time deviation at the metering fix for different values fo μ*

ft as well as a mean and median values around 600 ft and 500 ft, respectively, for a wind forecast look-ahead time of +6 hours. Conversely, when executing the descent with NMPC, the metering fix is achieved with much smaller specific energy deviation. In particular, for the static wind profile approach, the specific energy error is lower than 300 ft for all case studies. When the wind profile is updated at each time sample yet using only ownship wind observations, the maximum specific energy error reduces to, approximately, 140 ft. Finally, if additional wind observations from nearby aircraft were used to update the wind profile at each time sample, the specific energy error would be lower than 50 ft for all case studies.

As discussed in Chapter V, the optimal control computed at each time sample could claim to modulate energy with the elevator or to add/remove energy to/from the system by means of additional thrust or speed brakes. Ideally, the NMPC trajectory planner will attempt to obtain an energy-neutral trajectory. In certain conditions, however, energy modulation may not be sufficient to obtain a solution satisfying all the constraints. If this were the case, the trajectory planner would calculate the optimal amount of energy to be added or removed, in terms of fuel consumption and speed brakes use, while satisfying all the constraints.

Table VI-1 shows the mean, maximum and standard deviation of the specific energy removed by using speed brakes. Similarly to Chapter V, for each case study this metric was computed according to Eq. V.9. It should be noted that, for each value of μ and look-ahead time of the wind forecast, results shown in Table V-2 aggregate the results of the corresponding 1,381 case studies.

According to Table V-2, and independently of μ, the more the look-ahead time of the wind forecast, the more the mean energy removed by using speed brakes. For the standard deviation, however, when using wind observations emitted by nearby aircraft to update the wind profile (i.e., $\mu > 0$), the larger values are found for a +3 h wind forecast look-ahead time. As observed in Chapter V, the maximum value of ΔE_{s_β} corresponds to a case study with a +3 h wind forecast look-ahead time.

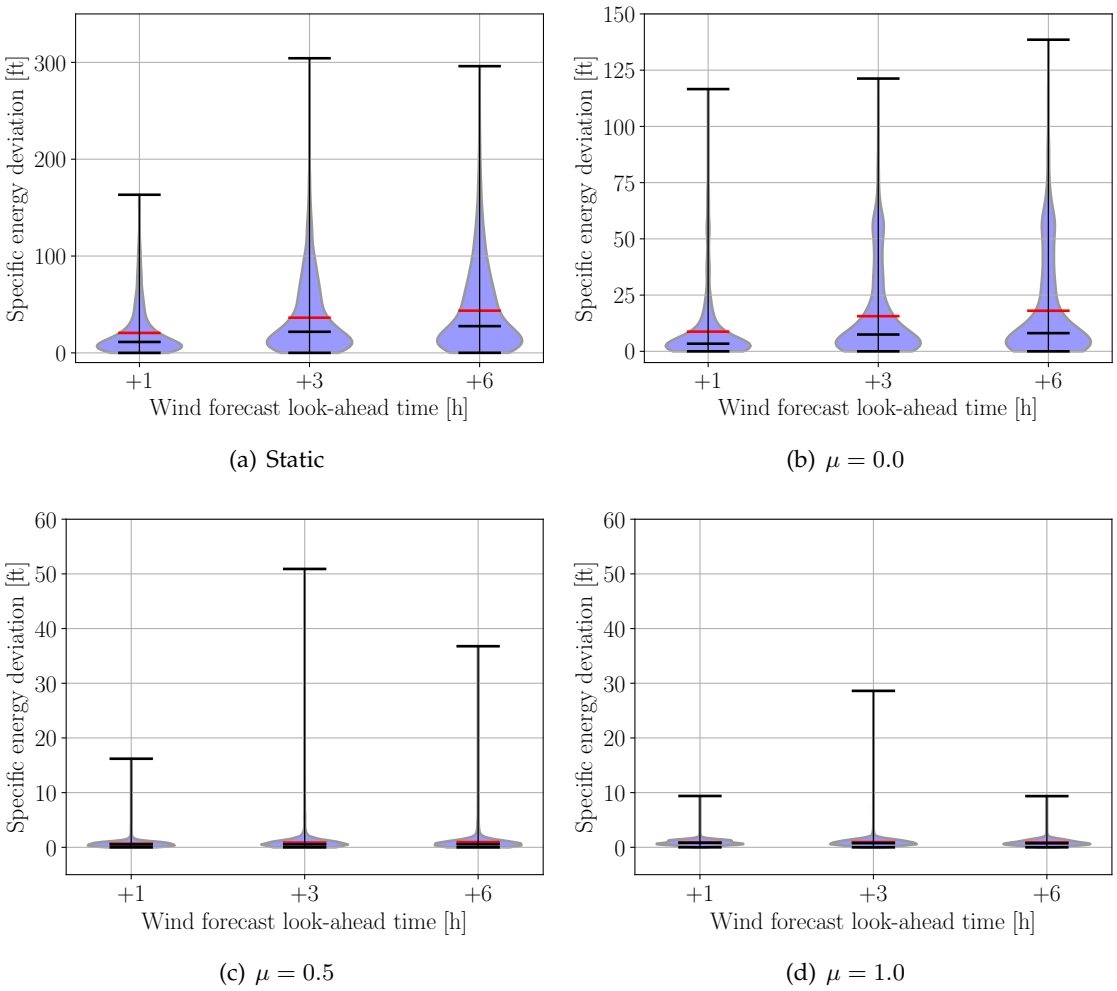

(a) Static

(b) $\mu = 0.0$

(c) $\mu = 0.5$

(d) $\mu = 1.0$

Figure VI-5: *Specific energy deviation at the metering fix for different values of μ*

Table VI-1: *Metrics of energy removed by using speed brakes for different values of μ and wind forecast lookahead times*

Guidance strategy	Mean [ft]			Standard deviation [ft]			Maximum [ft]		
	+1 h	+3 h	+6 h	+1 h	+3 h	+6 h	+1 h	+3 h	+6 h
Static	2	13	22	14	37	49	161	481	453
$\mu = 0.0$	2	7	13	12	34	45	187	780	641
$\mu = 0.5$	1	2	3	24	31	25	586	831	439
$\mu = 1.0$	1	2	3	23	33	29	518	982	421

The largest mean and standard deviation, independently of the wind forecast look-ahead time, correspond to the static wind forecast. These metrics decrease as the value of μ increases. In particular, for $\mu = 1$ the mean energy removed by using speed brakes for a +3 h wind forecast look-ahead time is only 3 ft, with a standard deviation of 29 ft. For the maximum value, however, it is more difficult to determine which value of μ gives the best results. It should be noted that adding wind observations not only reduces the mean and standard deviation of the energy removed by using speed brakes, but simultaneously reduces the time and energy error at the metering fix, if compared to the static wind profile and $\mu = 0$.

Analogously, Fig. VI-6 shows the difference between the executed trajectory and the open-loop execution of the initial plan, in terms of specific energy added by means of thrust above idle during the descent. For each case study, this metric was computed according to Eq. (V.10).

By comparing the distributions of additional thrust for the static wind forecast with those corresponding to $\mu = 0$, it can be concluded that updating the wind profile using only ownship observation does not

have a great impact on the additional thrust used during the descent. Therefore, the time and energy error at the metering fix can be significantly reduced without requiring additional thrust by simply updating the wind profile with ownship observations. When including additional wind observations emitted by nearby aircraft, however, even if the median and mean additional thrust are still close to zero (and even decrease sightly for all wind forecast look-ahead times), the dispersion is larger, as are the maximum and minimum values. Therefore, the huge reduction of time and specific energy deviations observed in Figs. VI-4 and VI-5 for $\mu > 0$ comes at a cost: there is a trade-off between reducing the dispersion of additional thrust and reducing the time and specific energy deviations at the metering fix.

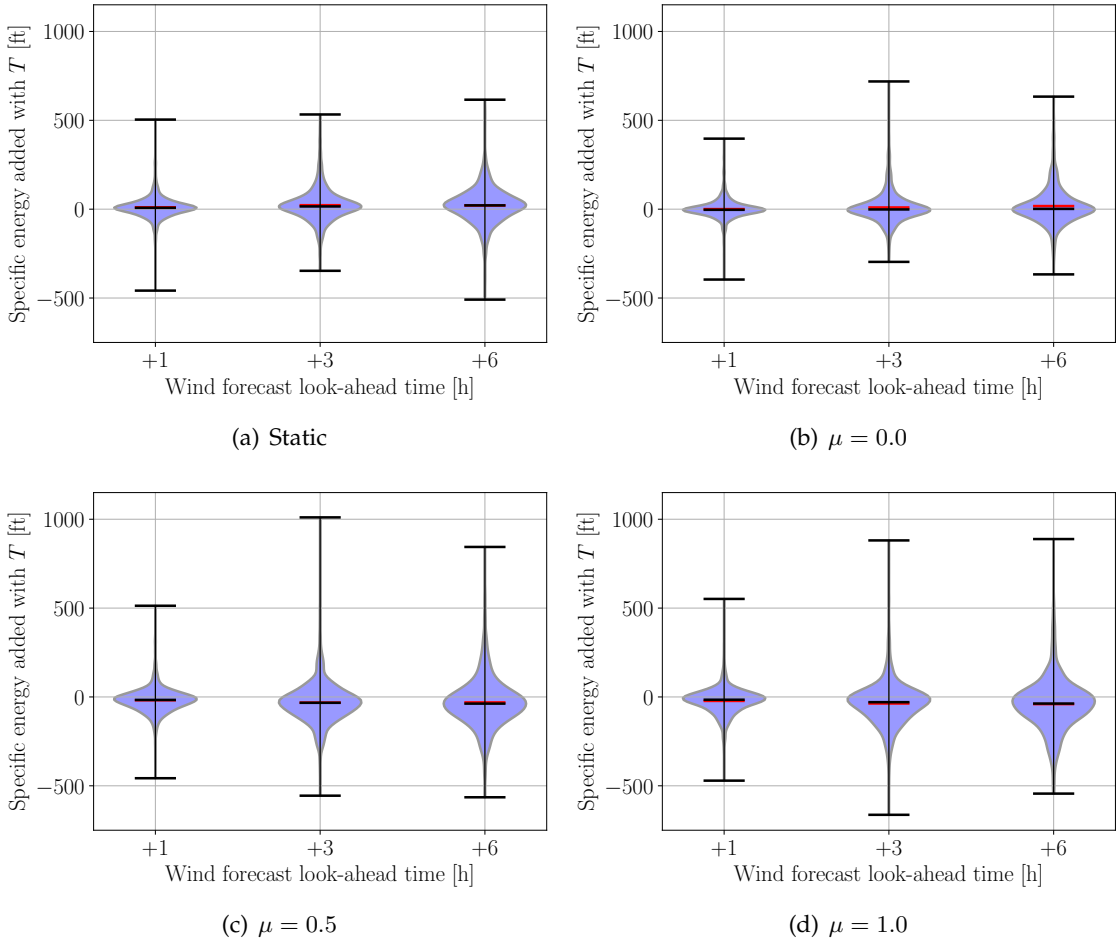

(a) Static (b) $\mu = 0.0$

(c) $\mu = 0.5$ (d) $\mu = 1.0$

Figure VI-6: *Specific energy added by means of T with respect to the initial plan for different values of μ*

Table VI-2 shows, for each strategy to update the wind profile forecast during the descent, the percentage of case studies not requiring speed-brakes or additional thrust during the entire descent. In addition, the percentage of case studies that performed at energy-neutral trajectory while complying with the CTA are also shown in this table.

Table VI-2: *Percentage of energy neutral trajectories for different values of μ and forecast look-ahead times*

Wind forecast update mode	Without speed brakes			Without additional thrust			Energy-neutral		
	+1 h	+3 h	+6 h	+1 h	+3 h	+6 h	+1 h	+3 h	+6 h
Static	97.4	87.8	80.5	76.3	71.9	73.8	74.4	61.5	55.9
$\mu = 0.0$	98.3	93.7	90.0	82.1	75.6	75.5	80.6	70.3	67.0
$\mu = 0.5$	99.2	98.9	97.8	79.9	75.1	74.0	79.6	74.9	73.0
$\mu = 1.0$	99.5	99.0	98.6	80.8	76.2	75.2	80.5	75.9	74.5

According to Table VI-2, and as expected, the more the forecast look-ahead time, the less the per-

centage of case studies not requiring use of speed brakes and/or additional thrust during the descent. For a given forecast look-ahead time, increasing the number of wind observations used to update the wind profile typically reduces the chances of requiring speed brakes. Regarding the use of thrust, it is difficult to determine the probability of executing a descent without additional thrust depending on the number of weather observations used to update the forecast wind profile. Finally, the probability of executing an energy-neutral descent, in which neither additional thrust nor speed brakes use are required to satisfy constraints, typically increases with the amount of wind observations used to update the wind profile forecast. This enhancement becomes even more significant for large forecast look-ahead times. In particular, when using a static wind profile forecast with a look-ahead time of +6 h, only 55.9% of the descents are able to perform an energy-neutral trajectory. Conversely, when updating the wind profile forecast with a cadence of observations corresponding to $\mu = 1.0$, the percentage of energy-neutral trajectories increases to 74.5%.

Finally, Fig. VI-7 shows the difference in fuel consumption between the executed trajectory and the open-loop execution of the initial plan, with negative values indicating fuel savings and positive values indicating that additional fuel was required. Results shown in Fig. VI-7 agree with those of Fig. VI-6: the more specific energy added by means of thrust, the more fuel consumption. As already discussed in Chapter V, when implementing NMPC strategies the fuel burned during the execution of the descent is typically the same than that achieved by implementing the initial trajectory plan in open-loop (the median and mean values are close to zero). In addition, the distribution of fuel consumption difference is almost symmetrical, meaning that the NMPC strategies have the same chances to burn more fuel than to save it, if compared to the open-loop execution. The same conclusions than for the additional specific energy added by means of thrust apply here: there is a trade-off between reducing the dispersion of additional fuel and reducing the time and specific energy deviations at the metering fix.

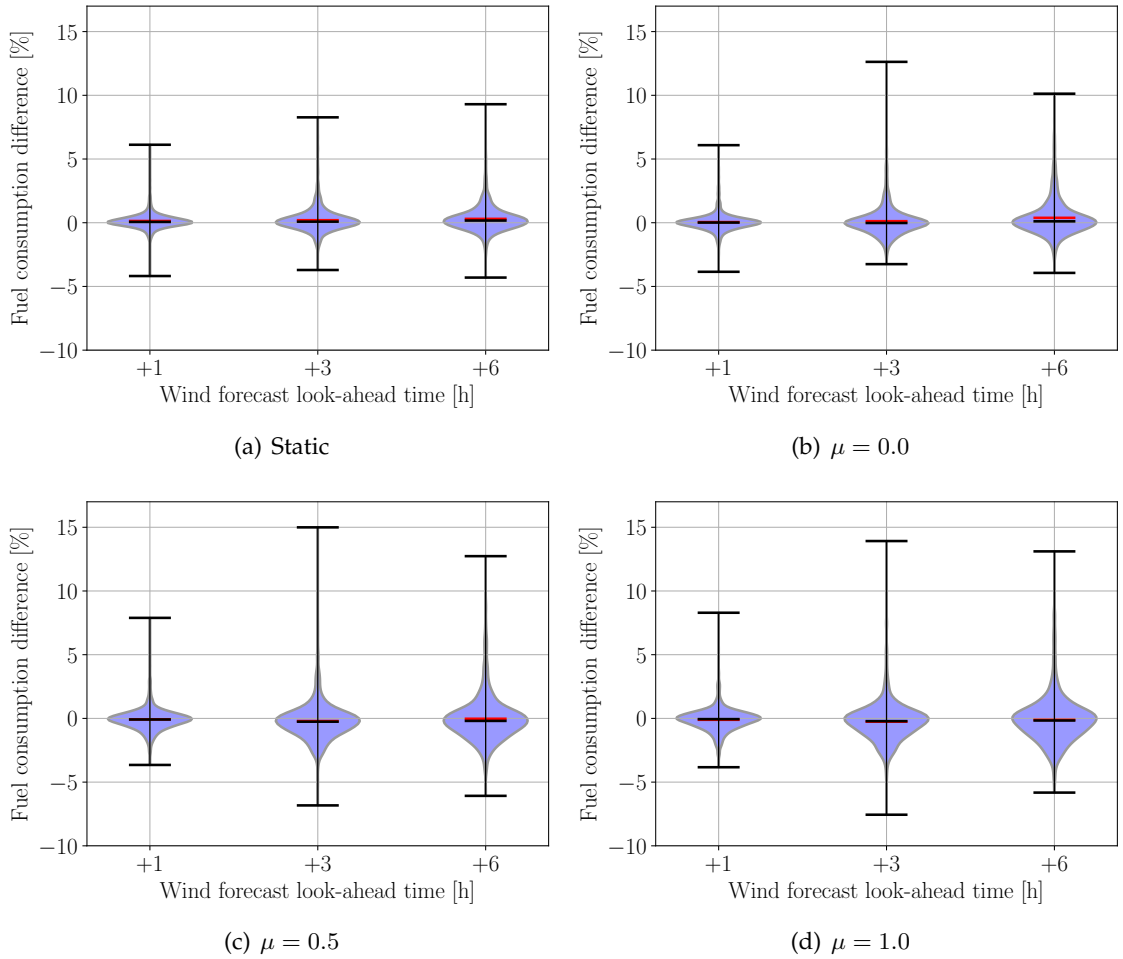

(a) Static (b) $\mu = 0.0$

(c) $\mu = 0.5$ (d) $\mu = 1.0$

Figure VI-7: *Fuel consumption difference with respect to the initial plan for different values of* μ

VI.4 Discussion

In this chapter the NMPC guidance strategy, which repeatedly updates the optimal trajectory of the aircraft, was combined with *wind networking* concepts, in which aircraft collaborate by sharing their wind observations to improve the wind profile forecast on-board and in real-time.

Results show that the performance of the conventional NMPC strategies assessed in Chapter V, which (at most) used ownship wind observations to predict the wind profile just before updating the optimal trajectory plan, could be significantly improved when taking advantage of up-to-date wind observations emitted by nearby aircraft, notably in terms of time and specific energy deviations at the metering fix.

Another interesting conclusion is that there exists a trade-off between reducing the dispersion of additional fuel and thrust and reducing the time and specific energy deviations at the metering fix. Generally speaking, however, increasing the value of μ reduces the mean and median additional fuel and thrust.

It was also observed that by including wind observations emitted by nearby aircraft the number of energy-neutral descents satisfying a CTA at a metering fix could be as high as 75%, considering a wind forecast with a look-ahead time of +6 hours. Without updating the wind profile during the descent, the number of energy-neutral descents satisfying a CTA at a metering fix would be around 55%.

These are very promising results considering that the case studies selected for this experiment correspond to the RAP forecasts generated for +1, +3 and +6 h look-ahead times during one year over the region of Denver. It should be noted that for those case studies in which energy modulation was not sufficient to satisfy operational constraints, the amount of energy added/removed by the NMPC guidance system was optimal in terms of fuel consumption and use of speed brakes.

The integration of CDOs subject to CTAs will require changes in both on-board trajectory management and ground automation systems. In particular, the interaction between aircraft and arrival manager (AMAN) systems on-ground is envisaged to follow the next sequence:

1. the ground system sends via datalink the area navigation (RNAV) route and runway in use to the aircraft, which subsequently computes the most optimal trajectory plan (not subject to time constraints) from its current position to the runway threshold.
2. the ground system requests (also via datalink) the estimated time of arrival for a certain fix along that route.
3. the aircraft sends the estimated time on arrival and possibly the time window (energy-neutral and/or absolute) at the requested fix.
4. the ground system sequences aircraft by assigning CTAs within the time windows transmitted by the aircraft (preferably using their estimated time of arrival, which is supposed to be the most optimal from the airline point of view).

A crucial aspect for the acceptance of the AMAN system in future operations is the accuracy of its trajectory predictions. One of the main factors that directly affect the accuracy of any aircraft trajectory prediction is the wind data that is used in the model. The better the wind data, the closer is to the real wind that the aircraft will encounter, and the more accurate the resulting trajectory prediction (in particular, altitude, speed and time at the different fixes).

Ground systems could also take advantage of wind observations emitted by airborne aircraft to improve their trajectory predictions. Enhanced trajectory predictions would also improve the perceived accuracy of the AMAN system, which will be very important to the overall acceptance by the air traffic controllers.

We can only see a short distance ahead, but we can see plenty there that needs to be done.

— Alan Turing

It's the job that's never started as takes longest to finish.

— J. R. R. Tolkien

VII

Concluding remarks

The growth in traffic implies increased pressure on the environmental sustainability of air transport. The introduction of more fuel-efficient profiles, however, is achieved at the cost of a reduction on capacity due to the more diverse trajectories that the air traffic control (ATC) need to handle. Continuous descent operations (CDOs) with controlled time of arrivals (CTAs) were identified as a potential solution to maintain capacity at acceptable levels, or even increasing it, while simultaneously allowing fuel-efficient descent profiles. The introduction of this kind or flight operations, however, will require the modernisation of both ground and airborne systems. The main objective of this PhD thesis was the development of on-board trajectory management algorithms to comply with time constraints during the descent of an aircraft in an environmentally friendly way, even in presence of uncertainties.

During this work some questions arose that were assessed and some of them are still open and could be topics of further research. A brief summary and conclusions of the achieved results, as well as hints on the possible directions for future work, are presented in what follows.

VII.1 Summary of contributions

The main contributions of this PhD thesis are summarised as follows:

- A trajectory management (planning and guidance) framework for the robust optimisation and execution of aircraft descent trajectories was established in Chapter II. This framework includes the formulation of a generic yet very complete optimal control problem to generate optimal trajectory plans taking into account any aircraft dynamics, performance and weather model as well as any number of flight phases, constraints and cost function. Moreover, several recommendations to face the most common issues that one could encounter when implementing nonlinear optimisation algorithms were also provided in Chapter II. Finally, several guidance strategies to execute the resulting trajectory plan, which take advantage of time and energy management concepts, were are also pro-

posed.

- The potential applicability of these time and energy management concepts was demonstrated in Chapter III by quantifying the feasible time windows at a metering fix for energy-neutral descents. Remember that during an energy-neutral descent the total energy is not increased by means of thrust nor removed by using active drag devices, if compared to the initial trajectory plan. The most important conclusion of this study was that CTAs can be updated even after overflying the top of descent (TOD), and that considerable time windows could be attainable at idle thrust and without using speed brakes depending on the flight conditions. These results should encourage the introduction of time and energy management concepts for CDOs subject to CTAs.
- A comprehensive comparison of guidance strategies build on time and energy management concepts was performed in Chapter IV. The set of guidance strategies compared in this PhD thesis included those already existing in the time and energy managed operations (TEMO) concept (i.e., tactical, strategic and hybrid) and a new guidance strategy called nonlinear model predictive control (NMPC), which has been in use in the process industries in chemical plants and oil refineries since the 1980s. Interestingly, results showed that all these guidance strategies could comply with CTAs with an average time error lower than 2 seconds and very attractive fuel consumption and noise nuisance figures, even in the presence of significant aircraft performance modelling and weather forecast errors. The main conclusion of this study, however, was that the performance of the four guidance strategies assessed are very similar. In spite of that, the NMPC was selected for further research because it demonstrated to be the most robust in terms of time and energy deviations at the metering fix.
- In Chapter V sensitivity-based alternatives to the generic NMPC were proposed to overcome its main limitation: the computational delay. Sensitivity-based NMPC (SbNMPC) and advanced-step NMPC (AsNMPC), which take advantage of parametric sensitivities to update the optimal trajectory plan solving a quadratic programming (QP) optimisation problem at each time sample, were compared to the generic NMPC, which solves a rigorous nonlinear programming (NLP) optimisation problem at each time sample. Fuel consumption, energy added and removed by means of thrust and speed-brakes, respectively, as well as time and energy deviations at the metering fix were the metrics selected for the comparison. Results from 16,000 simulations showed that trajectory updates resulting from solving a rigorous NLP optimisation problem are very similar to those obtained by using parametric sensitivities. Yet, the later method to update the trajectory plan is simpler, faster and more robust. Based on these results, the AsNMPC was the most recommended. Firstly, it has the advantage of not being affected by computational delay, in contrast to the ideal NMPC (INMPC). Secondly, if compared to the SbNMPC, it is less affected by large perturbations in the vector of parameters, since the sensitivity-based update is not performed over an approximated trajectory plan but over a very accurate trajectory generated recently by solving a rigorous NLP optimisation problem. There results shall encourage the integration of AsNMPC into future flight management system (FMS) because it is more robust than INMPC and SbNMPC, thus paving the way to certification processes.
- Finally, the benefits of combining NMPC with wind networking concepts (i.e., sharing wind observations between aircraft) were investigated in Chapter VI, in terms of environmental impact and ability to comply with operational constraints. In addition, the sensitivity of the performance metrics to the rate of wind observations received from nearby aircraft was also quantified. Results showed that the performance of the conventional NMPC could be significantly improved when taking advantage of up-to-date wind observations emitted by nearby aircraft, in terms of time and energy deviations at the metering fix and fuel consumption. In particular, around 75% of the simulated flights were able to execute an energy-neutral descent when taking advantage of wind networking concepts to continuously improve the wind forecast in real-time, in contrast to the 55% observed when using a static wind forecast. Unfortunately, the current and accurate automatic dependent surveillance-broadcast (ADS-B) and Mode-S data being transmitted is not currently being used to update the wind profile used by the FMS to optimise the trajectory plan. Results arising from this work should encourage the aviation community to take advantage of data provided in the wind networked concept to further optimise the trajectory plan and reduce the overall environmental impact of aviation. Ground systems could also take advantage of wind observations emitted by airborne aircraft to improve their trajectory predictions and, consequently, increase the capacity and the safety of the air traffic management (ATM) system.

VII.2 Future Research

During this PhD thesis new questions and research lines arose. Taking advantage of the trajectory optimisation framework that has been developed and for the sake of completeness, the following work items are proposed for the future:

- It is almost impossible to predict how difficult it is to solve a particular model with a particular algorithm, especially for NLP optimisation problems. The only reliable way to find which solver to use for a particular class of models is so far to experiment. A benchmarking of optimal control problem methods, optimisation methods, solvers, and parameters of these components for the particular problem of trajectory optimisation would be very valuable for the aviation community.
- The absolute time windows shown in Chapter III could be extended by allowing the aircraft to apply thrust or speed brakes. It would be interesting to assess the sensitivity of the time window to the amount of energy added or removed by means of thrust or speed brakes, respectively, as well as to quantify the theoretical limits of this time window as a function of the state of the aircraft.
- It would be also interesting to compare the energy-neutral and absolute time windows with a fixed route with that achievable by using path lengthening or stretching, even though pilots and ATC would probably prefer energy management to reduce workload and increase situation awareness.
- The NMPC guidance strategy updates the optimal trajectory plan at regular time intervals; while the strategic and hybrid guidance strategies update the optimal trajectory plan only when the time and/or energy deviations exceed a pre-defined threshold. In the former case, a continuous re-planning of the optimal trajectory plan could be contrapositive if the models used by the FMS are not accurate enough; in the later case, it might be too late to react if the thresholds were not selected properly. In future work, a new guidance strategy based on reinforcement learning could be used to develop a system that "learns" the best time samples to update the optimal trajectory plan, based on the current state of the aircraft and the environment (for instance, procedure being flown and meteorological conditions). The agent (the guidance system) would ought to take actions (re-plan or not re-plan) in an environment so as to maximise some notion of cumulative reward (e.g., the total fuel consumption of the entire descent). A large number of simulations would be required to train this agent.
- All the experiment performed in this PhD thesis were performed from the perspective of a single aircraft. In future work, the potential effectiveness of the CTA window could be tested by a traffic simulation, aiming to assess the effectiveness of the CTA window in the traffic stream management.

Bibliography

AIRBUS. 1993. *Flight Crew Operation Manual (FCOM). A320. Version 1.3.1.* Airbus Training and Flight Operations Support and Services. 17, 46, 49, 53, 64

AIRBUS. 1998 (May). *Getting to grips with the cost index*. Tech. rept. Airbus Flight Operations Support & Line Assistance, Blagnac, France. 4, 81

ALMASSALKHI, M. R. . 2013. *Optimization and Model-predictive Control for Overload Mitigation in Resilient Power Systems*. PhD thesis, The University of Michigan. 36

ANDERSSON, J. . 2013 (October). *A General-Purpose Software Framework for Dynamic Optimization*. PhD Thesis, Arenberg Doctoral School. Faculty of Engineering Science. 24, 25

ANDERSSON, J. , GILLIS, J. , HORN, G. , RAWLINGS, J. B. & DIEHL, M. . 2018. CasADi – A software framework for nonlinear optimization and optimal control. *Mathematical Programming Computation*, july, 1–36. 82, 100

ARRIETA-CAMACHO, J. J. & BIEGLER, L. T. . 2005. Real Time Optimal Guidance of Low-Thrust Spacecraft: An Application of Nonlinear Model Predictive Control. *Annals of the New York Academy of Sciences*, **1065**(December), 174–188. 58

BETTS, J. T. . 2010. *Practical methods for optimal control and estimation using nonlinear programming*. 2nd edn. Society for Industrial and Applied Mathematics (SIAM). 12, 20, 25, 30, 32

BETTS, J. T. & CRAMER, E. J. . 1995. Application of direct transcription to commercial aircraft trajectory optimization. *Journal of Guidance, Control, and Dynamics*, **18**(1), 151–159. 2

BIENERT, N. & FRICKE, H. . 2013. Real-time Wind Uplinks for Prediction of the Arrival Time and Optimization of the Descent Profile. *In: Proceedings of the 3rd ENRI International Workshop on ATM/CNS*. Tokyo, Japan: ENRI. 12

BILIMORIA, K. , SRIDHAR, B. , CHATTERJI, G. , SHETH, K. & GRABBE, S. . 2000. FACET: Future ATM Concepts Evaluation Tool. *In: 3rd USA/Europe Air Traffic Management Research and Development Seminar (ATM2000)*. Napoli, Italy: FAA/EUROCONTROL. 18

BRONSVOORT, J. . 2014. *Contributions to trajectory prediction theory and its application to arrival management for air traffic control*. PhD Thesis, Universidad Politécnica de Madrid (UPM). 41

BRONSVOORT, J. , MCDONALD, G. , POTTS, R. & GUTT, E. . 2011. Enhanced Descent Wind Forecast for Aircraft: Facilitation of Continuous Descent Arrivals with Improved Efficiency and Predictability by the use of Tailored Descent Wind Forecasts. *In: 9th USA/Europe Air Traffic Management Research and Development Seminar (ATM2011)*. Berlin, Germany: FAA/EUROCONTROL. 97

BRYSON, A. E. & HO, Y.-C. . 1975. *Applied optimal control: optimization, estimation, and control*. New York, NY: Taylor and Francis Group. 12, 22, 30

BULIRSCH, R. , NERZ, E. , PESCH, H. J. & VON STRYK, O. . 1993. Combining direct and indirect methods in optimal control: Range maximization of a hang glider. *Pages 273–288 of: Optimal Control*. International Series of Numerical Mathematics, vol. 111. Birkhauser Verlag. 25

BUSSINK, F. J. L. , VAN DER LAAN, J. J. & DE JONG, P. M. A. . 2012. Combining Flight-deck Interval Management with Continuous Descent Approaches in high density traffic and realistic wind conditions. *In: AIAA Guidance, Navigation, and Control Conference*. Guidance, Navigation, and Control and Co-located Conferences. Minneapolis, MN: AIAA. 98

BUSSINK, F. J. L. , VERHOEVEN, R. , MARSMAN, A. , PRATS, X. , BENDRIS, B. , MONTOLIO, J. & DAY, B. . 2016. Optimization of the vertical trajectory through Time and Energy management: A Human in the-Loop Study. *In: AIAA Guidance, Navigation, and Control Conference*. AIAA SciTech Forum. San Diego, CA: AIAA. 11

BYRD, R. , GOULD, N. & NOCEDAL, J. . 2003. An algorithm for nonlinear optimization using linear programming and equality constrained subproblems. *Mathematical Programming*, **100**(1), 27–48. 29

CAO, Y. , JIN, L. , NGUYEN, V. P. , LANDRY, S. , SUN, D. , & POST, J. . 2014. Evaluation of Fuel Benefits Depending on Continuous Descent Approach Procedures. *Air Traffic Control Quarterly*, **22**(3), 251–275. 5, 6

CASADO, E. , GOODCHILD, C. & VILAPLANA, M. . 2013. Sensitivity of Trajectory Prediction Accuracy to Aircraft Performance Uncertainty. *In: AIAA Infotech@Aerospace (I@A) Conference*. Guidance, Navigation, and Control and Co-located Conferences. Boston, MA: AIAA. 20

CHATTERJI, G. , SRIDHAR, B. & BILIMORIA, K. . 1996. En-Route Flight Trajectory Prediction for Conflict Avoidance and Traffic Management. *In: Guidance, Navigation, and Control Conference*. Guidance, Navigation, and Control and Co-located Conferences. San Diego,CA: AIAA. 20

CLARKE, J.-P. B. , HO, N. T. , REN, L. , BROWN, J. A. , ELMER, K. R. , ZOU, K. F. , HUNTING, C. , MCGREGOR, D. L. , SHIVASHANKARA, B. N. , TONG, K. , WARREN, A. W. & WAT, J. K. . 2004. Continuous descent approach: Design and flight test for Louisville international airport. *Journal of Aircraft*, **41**(5), 1054–1066. 3, 44

CLARKE, J.-P. B. , BENNETT, D. , ELMER, K. , FIRTH, J. , HILB, R. , HO, N. , JOHNSON, S. , LAU, S. , REN, L. , SENECHAL, D. , SIZOV, N. , SLATTERY, R. , TONG, K.-O. , WALTON, J. , WILLGRUBER, A. & WILLIAMS, D. . 2006 (January). *Development, Design, and Flight Test Evaluation of a Continuous Descent Approach Procedure for Nighttime Operation at Louisville International Airport*. Tech. rept. FAA PARTNER CDA Development Team. Report No. PARTNER-COE-2006-02. 3

CLARKE, J.-P. B. , BROOKS, J. , REN, L. , NAGLE, G. , MCCLAIN, E. , BOYCE, G. , ALLERDICE, J. , CHAMBERS, T. & ZONDERVAN, D. . 2007. Flight Trials of CDA with Time-Based Metering at Atlanta International Airport. *In: AGIFORS Airline Operations*. 3

CLARKE, J.-P. B. , BROOKS, J. , NAGLE, G. , SCACCHIOLI, A. , WHITE, W. & LIU, S. R. . 2013. Optimized profile descent arrivals at Los Angeles international airport. *Journal of Aircraft*, **50**(2), 360–369. 3

COPPENBARGER, R. A. , LANIER, R. , SWEET, D. N. & DORSKY, S. . 2004. Design and development of the en route descent advisor (EDA) for conflict-free arrival metering. *In: AIAA Guidance, Navigation, and Control Conference and Exhibit*. Guidance, Navigation, and Control and Co-located Conferences. Providence, Rhode Island: AIAA. 7

COPPENBARGER, R. A. , MEAD, R. W. & SWEET, D. N. . 2009. Field Evaluation of the Tailored Arrivals Concept for Datalink-Enabled Continuous Descent Approach. *Journal of Aircraft*, **46**(4), 1200–1209. 8

COPPENBARGER, R. A. , DYER, G. , HAYASHI, M. , LANIER, R. C. , STELL, L. L. & SWEET, D. N. . 2010. Development and testing of automation for efficient arrivals in constrained airspace. *In: 27th international congress of the aeronautical sciences (ICAS)*. ICAS. 7

DALMAU, R. , PÉREZ-BATLLE, M. & PRATS, X. . 2017. Estimation and prediction of weather variables from surveillance data using spatio-temporal kriging. *In: 36th IEEE/AIAA Digital Avionics Systems Conference (DASC)*. St. Petersburg, FL: IEEE. 98

DALMAU, R. & PRATS, X. . 2015. Fuel and time savings by flying continuous cruise climbs. Estimating the benefit pools for maximum range operations. *Transportation Research Part D: Transport and Environment*, **35**(March), 62–71. 2, 20

DALMAU, R. , VERHOEVEN, R. , DE GELDER, N. & PRATS, X. . 2016. Performance comparison between TEMO and a typical FMS in presence of CTA and wind uncertainties. *In: 35th IEEE/AIAA Digital Avionics Systems Conference (DASC)*. Sacramento, CA: IEEE. 58

DALMAU, R. & PRATS, X. . 2017. Assessing the impact of relaxing cruise operations with a reduction of the minimum rate of climb and/or step climb heights. *Aerospace science and technology*, **70**(November), 461–470. 2

DE BOOR, C. . 1972. On calculating with B-splines. *Journal of Approximation Theory*, **6**(1), 50–62. 20, 30, 44, 79

DE JONG, P. M. A. . 2014 (January). *Continuous descent operations using energy principles*. PhD Thesis, Delft University of Technology, Delft, The Netherlands. 10

DE JONG, P. M. A. , DE GELDER, N. , VERHOEVEN, R. , BUSSINK, F. J. L. , KOHRS, R. , VAN PAASSEN, M. M. & MULDER, M. . 2015. Time and Energy Management During Descent and Approach: Batch Simulation Study. *Journal of Aircraft*, **52**(1), 190–203. 10, 11, 58, 75, 79, 98

DE JONG, P. M. A. , BUSSINK, F. J. L. , VERHOEVEN, R. , DE GELDER, N. , VAN PAASSEN, M. M. & MULDER, M. . 2017. Time and Energy Management during Descent and Approach: a human-in-the-loop study. *Journal of Aircraft*, **54**(1), 177–189. 11, 58

DE LEEGE, P. A. M. , IN 'T VELD, A. C. , MULDER, M. & VAN PAASSEN, M. M. . 2009. Three-Degree Decelerating Approaches in High-Density Arrival Streams. *Journal of Aircraft*, **46**(5), 1681–1691. 6

DE LEEGE, P. A. M. , MULDER, M. & VAN PAASSEN, M. M. . 2013. Using Automatic Dependent Surveillance-Broadcast for Meteorological Monitoring. *Journal of Aircraft*, **50**(21), 249–261. 12, 98

DE PRINS, J. L. , SCHIPPERS, F. K. M. , MULDER, M. , VAN PAASSEN, M. M. , IN 'T VELD, A. C. & CLARKE, J.-P. B. . 2007. Enhanced Self-Spacing Algorithm for Three-Degree Decelerating Approaches. *Journal of Guidance, Control, and Dynamics*, **30**(2), 576–590. 6, 9

DELAHAYE, D. & PUECHMOREL, S. . 2009. TAS and wind estimation from radar data. *In: 28th AIAA/IEEE Digital Avionics Systems Conference Proceedings (DASC)*. Orlando, FL: IEEE. 98

DIEHL, M. , FERREAU, H. J. & HAVERBEKE, N. . 2008. Efficient Numerical Methods for Nonlinear MPC and Moving Horizon Estimation Problem Formulation. *In: International Workshop on assessment and future directions on Nonlinear Model Predictive Control (NMPC2018)*. Pavia, Italy: Springer, Berlin, Heidelberg. 58, 75

DIERCKX, P. . 1993. *Curve and Surface Fitting with Splines*. New York, NY: Oxford University Press. 45

DURHAM, M. . 2011. inFlight optimization Services offers Airlines more Fuel-efficient en-route operations. *AERO Magazine*, **42**(2), 21–23. 12

ELMER, K. R. . 2008. Tailored arrivals operations at SFO and expected environmental benefits. *In: 26th International Congres of the Aeronautical Sciences (ICAS) and 8th AIAA Aviation Technology, Integration, and Operations Conference (ATIO)*. Aviation Technology, Integration, and Operations (ATIO) Conferences. Anchorage, AK: AIAA. 8

EREN, U. , PRACH, A. , KOÇER, B. B. , RAKOVIĆ, S. V. , KAYACAN, E. & AÇIKMEŞE, B. . 2017. Model Predictive Control in Aerospace Systems: Current State and Opportunities. *Journal of Guidance, Control, and Dynamics*, **40**(7), 1541–1566. 58

ERKELENS, L. . 2000. Research into new noise abatement procedures for the 21st century. *In: AIAA Guidance, Navigation, and Control Conference and Exhibit*. Guidance, Navigation, and Control and Co-located Conferences. Denver, CO: AIAA. 3

EUROCONTROL. 2013 (June). *Challenges of Growth 2013: Summary report*. 1

FORESTER, D. A. & DHARSSI, I. . 1992. *The improvement of meteorological data for air traffic management purposes - stage 1*. Tech. rept. United Kingdom Meteorological Office, Bracknell, United Kingdom. 20

FRICKE, H. , SEISS, C. & HERRMANN, R. . 2015. Fuel and Energy Benchmark Analysis of Continuous Descent Operations. *Air Traffic Control Quarterly*, **23**(1), 83–108. 6

GARRIDO-LÓPEZ, D. , D'ALTO, L. & GÓMEZ LEDESMA, R. . 2009. A novel four-dimensional guidance for continuous descent approaches. *In: 28th IEEE/AIAA Digital Avionics Systems Conference (DASC)*. Orlando, FL: IEEE. 10, 58

GATH, P. F. . 2002 (November). *CAMTOS - A software suite combining direct and indirect trajectory optimisation methods*. PhD thesis, Insitut für Flugmechanik und Flugregelung. Universität Stuttgart, Stuttgart, Germany. 25

GIBBENS, P. W. & B. MEDAGODA, E. D. . 2011. Efficient Model Predictive Control Algorithm for Aircraft. *Journal of Guidance Control Dynamics*, **34**(November), 1909–1915. 58

GILL, P. E. , MURRAY, W. & SAUNDERS, M. A. . 2005. SNOPT: An SQP algorithm for large-scale constrained optimization. *Society for Industrial and Applied Mathematics (SIAM) Review*, **47**(1), 99–131. 29, 82, 100

GLINA, Y. , TROXEL, S. , REYNOLDS, T. & MCPARTLAND, M. . 2012. Wind Information Requirements to Support Four Dimensional Trajectory-Based Operations. *In: 12th AIAA Aviation Technology, Integration, and Operations Conference (ATIO)*. Aviation Technology, Integration, and Operations (ATIO) Conferences. Indianapolis, IN: AIAA. 97

GREEN, S. M. , GRACE, M. P. & WILLIAMS, D. H. . 2000. Flight Test Results: CTAS and FMS Cruise/Descent Trajectory Prediction Accuracy. *In: 3rd USA/Europe Air Traffic Management Research and Development Seminar (ATM2000)*. Napoli, Italy: FAA/EUROCONTROL. 97

GROS, S. , SRINIVASAN, B. , CHACHUAT, B. & BONVIN, D. . 2009. Neighbouring-extremal control for singular dynamic optimisation problems. Part I: Single-input systems. *International Journal of Control*, **82**(6), 1099–1112. 38

HAAN, S. D. . 2010. *Quality assessment of high resolution wind and temperature observation from ModeS*. Tech. rept. The Royal Netherlands Meteorological Institute (KNMI), The Netherlands. 12

HARTJES, S. & VISSER, H. G. . 2017. Efficient trajectory parameterization for environmental optimization of departure flight paths using a genetic algorithm. *Proceedings of the Institution of Mechanical Engineers, Part G: Journal of Aerospace Engineering*, **231**(6), 1115–1123. 14

HINDMARSH, A. C. , BROWN, P. N. , GRANT, K. E. , LEE, S. L. , SERBAN, R. , SHUMAKER, D. E. & WOODWARD, C. S. . 2005. SUNDIALS: Suite of Nonlinear and Differential/Algebraic Equation Solvers. *ACM Transactions on Mathematical Software*, **31**(3), 363–396. 76

HOEKSTRA, J. . 2016. Aircraft performance models for ATM Research. *In: 7th International Congress on Research in Air Transportation (ICRAT)*. Philadelphia, PA: FAA/EUROCONTROL. 42

HOLLISTER, W. M. , BRADFORD, E. R. & WELCH, J. D. . 1986. Using aircraft radar tracks to Estimate winds aloft. *The Lincoln Laboratory Journal*, **2**(3), 555–565. 12, 98

HRASTOVEC, M. & SOLINA, F. . 2013. Obtaining meteorological data from aircraft with mode-S radars. *IEEE Aerospace and Electronic Systems Magazine*, **28**(12), 12–24. 98

HULL, D. G. . 2007. *Fundamentals of airplane flight mechanics*. 1st edn. Springer-Verlag. 18

ICAO. 1993. *Manual of the ICAO Standard Atmosphere: Extended to 80 Kilometres (262500 Feet)*. Tech. rept. International Civil Aviation Organization (ICAO), Montreal, Canada. 20

ICAO. 2010. *Continuous Descent Operations (CDO) Manual-Doc 9931/AN/476*. Tech. rept. International Civil Aviation Organization (ICAO), Montreal, Quebec, Canada. 6, 7

In 't Veld, A. C. . 2011 (June). *Self-Spacing Algorithms for Continuous Descent Approaches*. PhD thesis, Delft University of Technology, Delft, The Netherlands. 98

Jäschke, J. , Yang, X. & Biegler, L. T. . 2014. Fast economic model predictive control based on NLP-sensitivities. *Journal of Process Control*, **24**(8), 1260–1272. 36, 39

Jin, L. , Cao, Y. & Sun, D. . 2013. Investigation of Potential Fuel Savings Due to Continuous-Descent Approach. *Journal of Aircraft*, **50**(3), 807–816. 3

Johnson, C. M. . 2009. Human-In-The-Loop (HITL) Simulation and Analysis of Optimized Profile Descent (OPD) Operations at Atlanta. *In: 9th AIAA Aviation Technology, Integration, and Operations Conference (ATIO)*. Aviation Technology, Integration, and Operations (ATIO) Conferences. Hilton Head, SC: AIAA. 6, 7

Kadam, J. V. & Marquardt, W. . 2004. Sensitivity-Based Solution Updates in Closed-Loop Dynamic Optimization. *IFAC Proceedings Volumes*, **37**(9), 947–952. 37

Khan, Z. , Idris, H. , Vivona, R. , Woods, S. & Lanier, R. . 2009. Ground automation impact on enabling continuous descent in high density operations. *In: 9th AIAA Aviation Technology, Integration, and Operations Conference (ATIO)*. Aviation Technology, Integration, and Operations (ATIO) Conferences. Hilton Head, SC: AIAA. 6

Kim, T. J. & Hull, D. G. . 1995. Optimal control design that accounts for model mismatch errors. *In: AAS/MAA Space Flight Mechanics Meeting*. 76

Klooster, J. , Wichman, K. & Bleeker, O. . 2008. 4D Trajectory and Time-of-Arrival Control to Enable Continuous Descent Arrivals. *In: AIAA Guidance, Navigation, and Control Conference and Exhibit*. Guidance, Navigation, and Control and Co-located Conferences. Honolulu, Hawaii: AIAA. 97

Kuhn, H. W. & Tucker, A. W. . 1950. Nonlinear programming. *Pages 481–492 of: Proceedings of the Second Berkeley Symposium on Mathematical Statistics and Probability*. University of California Press, Berkeley and Los Angeles. 28

Lee, D. S. , Pitari, G. , Grewe, V. , Gierens, K. , Penner, J. E. , Petzold, A. , Prather, M. J. , Schumann, U. , Bais, A. , Berntsen, T. , Iachetti, D. , Lim, L. L. & Sausen, R. . 2010. Transport impacts on atmosphere and climate: Aviation. *Atmospheric Environment*, **44**(37), 4678 – 4734. Transport Impacts on Atmosphere and Climate: The ATTICA Assessment Report. 1

Lenz, H. & Korn, B. . 2009. Enabling advanced continuous descent approaches - results of the european project OPTIMAL. *In: 28th IEEE/AIAA Digital Avionics Systems Conference (DASC)*. Orlando, FL: IEEE. 9

Liden, S. . 1994. The Evolution of Flight Management Systems. *In: 13th IEEE/AIAA Digital Avionics Systems Conference (DASC)*. Phoenix, AZ: IEEE. 17

Lin, C. & Moré, J. . 1999. Newton's Method for Large Bound-Constrained Optimization Problems. *SIAM Journal on Optimization*, **9**(4), 1100–1127. 29

Lindsay, P. , Ramsay, C. , Vilaplana, M. , Leones, J. L. , Casado, E. & Parks, P. . 2009. Robustness of Idle-Throttle Continuous Descent Approach Trajectories Against Modified Timing Requirements. *In: 9th aiaa aviation technology, integration, and operations conference (atio)*. Aviation Technology, Integration, and Operations (ATIO) Conferences. Hilton Head, SC: AIAA. 42

Liu, J. , Zhang, J. , Dai, X. & Zu, H. . 2018. Research on Trajectory Generation and Optimization in Continuous Descent Operations. *In: 2018 Aviation Technology, Integration, and Operations Conference (ATIO)*. AIAA AVIATION Forum. Atlanta, GA: AIAA. 10

Muynch, R. J. , Bos, T. , Kuenz, A. & Toner, S. . 2012. Implementing time based CDA operations in medium-high density ATM environment. *In: 28th international congress of the aeronautical sciences (ICAS)*. Brisbane, AU: ICAS. 9

Nagle, G. , Sweet, D. N. , Carr, G. , Felipe, V. , Trapani, A. , Coppenbarger, R. A. & Hayashi, M. . 2011. Human-in-the-Loop Simulation of Three-Dimensional Path Arrival Management with Trajectory Error. *In: 11th aiaa aviation technology, integration, and operations (atio) conference*. Virginia Beach, VA: AIAA. 7

Nelson, R. . 1998. *Flight stability and automatic control*. Aerospace Science & Technology. WCB/McGraw Hill. 18

Oberheid, H. , Temme, M.-M. , Kuenz, A. , Mollwitz, V. & Helmke, H. . 2008. Fuel Efficient and Noise-Reduced Approach Procedures. *In: German Aerospace Congress*. Darmstadt, Germany: DLR. 9

Oseguera-Lohr, R. M. , Williams, D. H. & Lewis, E. T. . 2007 (February). *Crew Procedures for Continuous Descent Arrivals Using Conventional Guidance*. Tech. rept. NASA Langley Research Center, Hampton, VA. NASA/TM-2007-214538. 10

Park, S. G. & Clarke, J.-P. B. . 2013. Feasible Time Range Analysis of Wide Fleet for Continuous Descent Arrival. *In: 2013 Aviation Technology, Integration, and Operations Conference (ATIO)*. AIAA AVIATION Forum. Los Angeles, CA: AIAA. 42

Park, S. G. & Clarke, J.-P. B. . 2016. Vertical Trajectory Optimization to Minimize Environmental Impact in the Presence of Wind. *Journal of Aircraft*, **35**(3), 725–737. 42

Park, S. G. , Clarke, J.-P. B. , Feron, E. & Jimenez, H. . 2016. Encounter Rate Estimation of Continuous Descent Arrival Procedures in Terminal Area. *In: AIAA Guidance, Navigation, and Control Conference*. AIAA SciTech Forum. San Diego, CA: AIAA. 6

PENNER, J. , LISTER, D. , GRIGGS, D. , DOKKEN, D. & MCFARLAND, M. . 1999. *Aviation and the global atmosphere*. Cambridge, UK: Cambridge University Press. 1

PESCH, H. J. . 1979. Numerical computation of neighboring optimum feedback control schemes in real-time. *Applied Mathematics & Optimization*, **5**(1), 231–252. 76

PHOENIX, D. , KHODAYARI, A. , WUEBBLES, D. & STEWART, K. . 2019. Aviation impact on air quality present day and mid-century simulated in the Community Atmosphere Model (CAM). *Atmospheric Environment*, **196**, 125 – 132. 1

POLES, D. , NUIC, A. & MOUILLET, V. . 2010. Advanced aircraft performance modelling for ATM: Analysis of BADA model capabilities. *In: 29th IEEE/AIAA Digital Avionics Systems Conference (DASC)*. Salt Lake City, UT: IEEE. 20, 78

PRADEEP, P. & WEI, P. . 2017. Predictability, variability and operational feasibility aspect of CDA. *In: 2017 IEEE Aerospace Conference*. Big Sky, MT: IEEE. 6

PRATS, X. . 2010. *Contributions to the optimisation of aircraft noise abatement procedures*. PhD Thesis, Technical University of Catalonia (UPC), Castelldefels, Catalonia. 24

PRATS, X. , PÉREZ-BATLLE, M. , BARRADO, C. , VILARDAGA, S. , BAS, I. , BIRLING, F. , VERHOEVEN, R. & MARSMAN, A. . 2014. Enhancement of a time and energy management algorithm for continuous descent operations. *In: 14th AIAA Aviation Technology, Integration, and Operations Conference (ATIO)*. AIAA AVIATION Forum. Atlanta, GA: AIAA. 11, 22

PRATS, X. , BUSSINK, F. J. L. , VERHOEVEN, R. & MARSMAN, A. . 2015a. Evaluation of in-Flight Trajectory Optimisation With Time Constraints in a Moving Base Flight Simulator. *In: 34th IEEE/AIAA Digital Avionics Systems Conference (DASC)*. Prague, Czesch Republic: IEEE. 11

PRATS, X. , VILARDAGA, S. , ISANTA, R. , BAS, I. & BIRLING, F. . 2015b. WEMSgen: A real-time weather modelling library for on-board trajectory optimisation and planning. *In: 34th IEEE/AIAA Digital Avionics Systems Conference (DASC)*. Prague, Czesch Republic: IEEE. 11

PRATS, X. , DALMAU, R. , VERHOEVEN, R. & BUSSINK, F. J. L. . 2017. Human-in-the-loop Performance Assessment of Optimized Descents with Time Constraints. *In: Twelfth USA/Europe Air Traffic Management Research and Development Seminar (ATM2017)*. Seattle, WA: FAA/EUROCONTROL. 11, 97

PRATS, X. , BARRADO, C. , NETJASOV, F. , CRNOGORAC, D. , PAVLOVIC, G. , AGUI, I. & VIDOSAVLJEVIC, A. . 2018 (December). Enhanced Indicators to Monitor ATM Performance in Europe: Main findings of the APACHE SESAR Exploratory Research project. *In: 8th SESAR Innovation Days*. 2

PRATT, R. W. . 2000. *Flight Control Systems: practical issues in design and implementation*. Control. Institution of Engineering and Technology. 64

RAMASAMY, S. , SABATINI, R. , GARDI, A. G. & LIU, Y. . 2013. Novel Flight Management System for Real-Time 4-Dimensional Trajectory Based Operations. *In: AIAA Guidance, Navigation, and Control (GNC) Conference*. Boston, MA: AIAA. 10

REN, L. & CLARKE, J.-P. B. . 2007a. Flight demonstration of the separation analysis methodology for continuous descent arrival. *In: 7th USA/Europe Air Traffic Management Research and Development Seminar (ATM2007)*. Barcelona (Spain): FAA/EUROCONTROL. 5

REN, L. & CLARKE, J.-P. B. . 2007b. Separation Analysis Methodology for Designing Area Navigation Arrival Procedures. *Journal of Guidance Control and Dynamics*, **30**(5), 1319–1330. 5

REN, L. & CLARKE, J.-P. B. . 2008. Flight-Test Evaluation of the Tool for Analysis of Separation and Throughput. *Journal of Guidance Control and Dynamics*, **45**(1), 323–332. 5

REYNOLDS, T. , REN, L. , CLARKE, J.-P. B. , BURKE, A. & GREEN, M. . 2005. History, Development and Analysis of Noise Abatement Arrival Procedures for UK Airports. *In: AIAA 5th ATIO and16th Lighter-Than-Air Sys Tech. and Balloon Systems Conferences*. Aviation Technology, Integration, and Operations (ATIO) Conferences. Arlington, VA: AIAA. 3

ROBERT, E. & DE SMEDT, D. . 2013. Comparison of operational wind forecasts with recorded flight data. *In: 10th USA/Europe Air Traffic Management Research and Development Seminar (ATM2013)*. Chicago, IL: FAA/EUROCONTROL. 20, 65

ROBINSON, J. & KAMGARPOUR, M. . 2010. Benefits of Continuous Descent Operations in High-Density Terminal Airspace Considering Scheduling Constraints. *In: 10th AIAA Aviation Technology, Integration, and Operations Conference (ATIO)*. AIAA AVIATION Forum. Fort Worth, TX: AIAA. 3, 4, 6

ROSKAM, J. & LAN, C. T. E. . 1997. *Airplane Aerodynamics and Performance*. Airplane design and analysis. Design, Analysis and Research Corporation. 53

RUMBO, J. R. , JACKSON, M. R. & O'LAUGHLIN, B. E. . 2002. *Aircraft Control System for Reaching a Waypoint at Required Time of Arrival*. Pub. No.: EP1800197B1. 58

SAUSEN, R. , ISAKSEN, I. , GREWE, V. , HAUGLUSTAINE, D. , LEE, D. S. , MYHRE, G. , KÖHLER, M. O. , PITARI, G. , SCHUMANN, U. , STORDAL, F. & ZEREFOS, C. . 2005. Aviation radiative forcing in 2000: An update on IPCC (1999). *Meteorologische Zeitschrift*, **14**(4), 555–561. 1

SCOKAERT, P. O. M. & RAWLINGS, J. B. . 1999. Feasibility issues in linear model predictive control. *Aiche journal*, **45**(8), 1649–1659. 29, 30

SENZIG, D. A. & FLEMING, G. G. . 2009. Fuel consumption modeling in support of ATM environmental decision-making. *In: 8th USA/Europe Air Traffic Management Research and Development Seminar (ATM2009)*. Napa, CA: FAA/EUROCONTROL. 20

SENZIG, D. A. , FLEMING, G. G. & IOVINELLI, R. J. . 2009. Modeling of Terminal-Area Airplane Fuel Consumption. *Journal of Aircraft*, **46**(4), 1089–1093. 20, 42

SERGEEVA, M. , DELAHAYE, D. , MANCEL, C. & VIDOSAVLJEVIC, A. . 2017. Dynamic airspace configuration by genetic algorithm. *Journal of Traffic and Transportation Engineering*, **4**(3), 300 – 314. 1

SESAR. 2015a. *European ATM Master Plan*. Tech. rept. Single European Sky ATM Research (SESAR) Joing Undertaking, Brussels, Belgium. Edition 2015. 1, 2

SESAR. 2015b. *SESAR Concept of Operations Step 1 Final Edition*. Tech. rept. Single European Sky ATM Research (SESAR) Joing Undertaking, Brussels, Belgium. 41

SHRESTA, S. , NESKOVIC, D. , & WILLIAMS, S. S. . 2009. Analysis of Continuous Descent Benefits and Impacts during Daytime Operations. *In: 8th USA/Europe Air Traffic Management Research and Development Seminar (ATM2009)*. Berlin, Germany: FAA/EUROCONTROL. 7

SLATER, G. L. . 2009. Study on variations in vertical profile for CDA descents. *In: 9th AIAA Aviation Technology, Integration, and Operations Conference (ATIO)*. Aviation Technology, Integration, and Operations (ATIO) Conferences. Hilton Head, SC: AIAA. 20

SOLER, M. , OLIVARES, A. , STAFFETTI, E. & ZAPATA, D. . 2012. Framework for Aircraft Trajectory Planning Toward an Efficient Air Traffic Management. *Journal of Aircraft*, **49**(1), 341–348. 2

SOLER, M. , OLIVARES, A. & STAFFETTI, E. . 2015. Multiphase Optimal Control Framework for Commercial Aircraft Four-Dimensional Flight-Planning Problems. *Journal of Aircraft*, **52**(1), 247–286. 22

SOPJES, R. , DE JONG, P. M. A. , BORST, C. , VAN PAASSEN, R. & MULDER, M. . 2011. Continuous Descent Approaches with Variable Flight-Path Angles under Time Constraints. *In: AIAA Guidance, Navigation, and Control Conference*. Guidance, Navigation, and Control and Co-located Conferences. Portland, OR: AIAA. 6

SUN, J. , VU, H. , ELLERBROEK, J. & HOEKSTRA, J. . 2017 (November). Ground-based Wind Field Construction from Mode-S and ADS-B Data with a Novel Gas Particle Model. *In: 7th SESAR Innovation Days*. 98

SUWARTADI, E. , KUNGURTSEV, V. & JÄSCHKE, J. . 2017. Sensitivity-Based Economic NMPC with a Path-Following Approach. *Processes*, **5**(1), 8. 76

TAKEICHI, N. & INAMI, D. . 2010. Arrival-Time Controllability of Tailored Arrival Subjected to Flight-Path Constraints. *Journal of Aircraft*, **47**(6), 2021–2029. 42

TAKEICHI, N. . 2017. Nominal flight time optimization for arrival time scheduling through estimation/resolution of delay accumulation. *Transportation Research Part C: Emerging Technologies*, **77**(April), 433–443. 42

THOMPSON, T. , MILLER, B. , MURPHY, C. , AUGUSTINE, S. , WHITEE, T. & SOUIHI, S. . 2013. Environmental Impacts of Continuous-descent Operations in Paris and New York Regions. *In: 10th USA/Europe Air Traffic Management Research and Development Seminar (ATM2013)*. Chicago, IL: FAA/EUROCONTROL. 3

UEBBING-RUMKE, M. & TEMME, M.-M. . 2011. Controller AIDS for integrating negotiated continuous descent approaches into conventional landing traffic. *In: 9th USA/Europe Air Traffic Management Research and Development Seminar (ATM2011)*. Berlin, Germany: FAA/EUROCONTROL. 9

VADA, J. , SLUPPHAUG, O. , JOHANSEN, T. A. & FOSS, B. A. . 2001. Linear MPC with optimal prioritized infeasibility handling: application, computational issues and stability. *Automatica*, **37**(11), 1835 – 1843. 29

VAN DER WAL, H. , VOGEL, P. & WUBBEN, F. . 2001 (July). *Voorschrift voor de berekening van de lden en lnight geluidbelasting in db(a) ten gevolge van vliegverkeer van en naar de luchtaven*. Tech. rept. National Aerospace Laboratorium (NLR). 59

VERHOEVEN, R. , BUSSINK, F. J. L. , PRATS, X. & DALMAU, R. . 2016. Flight Testing Time and Energy Managed Operations. *In: Society of Flight Test Engineers - European Chapter Symposium*. 11

VIRTANEN, K. , EHTAMO, H. , RAIVIO, T. & HAMALAINEN, R. P. . 1999. VIATO - Visual Interactive Aircraft Trajectory Optimization. *IEEE Transactions of systems, man, and cybernetics - Part C: Applications and reviews*, **29**(3), 409–421. 25

WACHTER, A. & BIEGLER, L. . 2006. On the implementation of an interior-point filter line-search algorithm for large-scale nonlinear programming. *Mathematical Programming*, **106**(1), 25–57. 29

WARREN, A. & TONG, K. . 2002. Development of continuous descent approach concepts for noise abatement. *In: 21st IEEE/AIAA Digital Avionics Systems Conference (DASC)*. Irvine, CA: IEEE. 3

WAT, J. , FOLLET, J. , MEAD, R. , BROWN, J. , KOK, R. , DIJKSTRA, F. & VERMEIJ, J. . 2006. In Service Demonstration of Advanced Arrival Techniques at Schiphol Airport. *In: 6th AIAA Aviation Technology, Integration and Operations Conference (ATIO)*. Aviation Technology, Integration, and Operations (ATIO) Conferences. Wichita, Kansas: AIAA. 3

WEITZ, L. A. & BAI, X. . 2018. Using Model Predictive Control for Trajectory Optimization and to Meet Spacing Objectives. *In: 2018 AIAA Guidance, Navigation, and Control Conference*. AIAA SciTech Forum. Kissimmee, FL: AIAA. 58

WETZEL, T. A. . 1996. *Development of a finite difference neighboring optimal control law and application to the optimal landing of a reusable launch vehicle*. PhD Thesis, Iowa State University. 76

WILSON, I. & HAFNER, F. . 2005. Benefit assessment of using continuous descent approaches at Atlanta. *In: 24th IEEE/AIAA Digital Avionics Systems Conference (DASC)*. Washington, DC: IEEE. 6

WOLF, I. J. & MARQUARDT, W. . 2016. Fast NMPC schemes for regulatory and economic NMPC - A review. *Journal of Process Control*, **44**(August), 162–183. 37, 38, 76

WÜRTH, L. , HANNEMANN, R. & MARQUARDT, W. . 2008a. An Efficient Strategy for Real-Time Dynamic Optimization based on Parametric Sensitivities. *IFAC Proceedings Volumes*, **41**(2), 1928–1933. 38

WÜRTH, L. , HANNEMANN, R. & MARQUARDT, W. . 2008b. An Efficient Strategy for Real-Time Dynamic Optimization based on Parametric Sensitivities. *IFAC Proceedings Volumes*, **41**(2), 1928–1933. 76

WÜRTH, L. , HANNEMANN, R. & MARQUARDT, W. . 2009. Neighboring-extremal updates for nonlinear model-predictive control and dynamic real-time optimization. *Journal of process control*, **19**(8), 1277–1288. 28, 37, 76

ZAVALA, V. M. & BIEGLER, L. T. . 2009. The advanced-step NMPC controller : Optimality , stability and robustness. *Automatica*, **45**(1), 86–93. 39, 76